Architectures de réseaux d'accès hybrides analogique & numérique pour la convergence

Florian Frank

▶ **To cite this version:**

Florian Frank. Architectures de réseaux d'accès hybrides analogique & numérique pour la convergence. Autre. Université Paris-Est, 2011. Français. NNT : 2011PEST1021 . tel-00665650

HAL Id: tel-00665650

https://theses.hal.science/tel-00665650

Submitted on 2 Feb 2012

HAL is a multi-disciplinary open access archive for the deposit and dissemination of scientific research documents, whether they are published or not. The documents may come from teaching and research institutions in France or abroad, or from public or private research centers.

L'archive ouverte pluridisciplinaire **HAL**, est destinée au dépôt et à la diffusion de documents scientifiques de niveau recherche, publiés ou non, émanant des établissements d'enseignement et de recherche français ou étrangers, des laboratoires publics ou privés.

UNIVERSITÉ PARIS-EST

ÉCOLE DOCTORALE UNIVERSITÉ PARIS-EST Mathématiques et STIC

Université Paris-Est

Ecole Doctorale Mathématiques et Sciences et Technologies de l'Information et de la Communication

Thèse de Doctorat de l'Université Paris-Est
mention Électronique, Optronique et Systèmes

Architectures de Réseaux d'Accès Hybrides Analogique & Numérique pour la Convergence Fixe/Mobile des Infrastructures

présentée par

M. Florian Frank

pour obtenir le grade de :

Docteur de l'Université Paris-Est

le 8 juin 2011, CNAM, Paris

devant le Jury composé de :

Mme Christelle Aupetit-Berthelemot	Professeur, XLIM, Limoges	Rapporteur
M. Hong Wu Li	Professeur, IREENA, Nantes	Rapporteur
Mme Frédérique Deshours	Maitre de conférences, UPMC, Paris	Examinateur
M. Yannis Le Guennec	Maitre de conférences, IMEP, Grenoble	Examinateur
M. Thomas Pfeiffer	Ingénieur, Alcatel-Lucent, Stuttgart	Invité
M. Michel Sotom	Ingénieur, Thales Alenia Space, Toulouse	Invité
M. Benoît Charbonnier	Ingénieur, Orange Labs, Lannion	Examinateur/Encadrant
Mme Catherine Algani	Professeur, CNAM, ESYCOM, Paris	Directrice de thèse

A mon père.

Acknowledgments

Mes premiers recemerciements vont au professeur Catherine Algani pour avoir accepté d'être ma directrice de thèse, Anne-Cécile Réau-Thomas et Phillipe Chanclou, responsables successifs de l'unité de R&D NOA devenue ASHA, pour m'avoir accueilli dans les locaux de France Télécom.

Je tiens à remercier vivement Benoît Charbonnier – aussi bien au labo. et en abstrait – pour son encadrement, pour ses explications, discussions, suggestions, sa patience et ses encouragements ... et d'avoir pris le risque de m'encadrer !

J'adresse ma gratitude aux membres du jury, à Christelle Aupetit-Berthelemot et Hong Wu Li pour avoir accepté d'être rapporteurs de ce mémoire de thèse et également à Yannis Le Guennec, Frédérique Deshours, Thomas Pfeiffer, Michel Sotom pour avoir répondu favorablement en qualité d'examinateurs pour l'évaluation de mes travaux de recherche.

Au labo., je remercie Anna Pizzinat pour les premières manips de radio sur fibre, Genay Naveena pour les discussions a propos des APD, Fabienne Saliou pour les discussions sur les ampli. optiques, Laurent Guillo pour la gestion du matériel, Mathieu et Fred pour les discussions non techniques...

Je tiens à remercier Charlotte, Ikram, Lionel, André, Fabia, Qian, avec qui j'ai partagé le bureau pendant trois ans, ainsi que toutes les personnes ayant contribuée à la bonne ambiance générale dans ce couloir du LD.

L'esprit sain dans un corps sain n'étant pas un hasard, je tiens à remercier sportivement et dans l'ordre chronologique :

- les jouers de l'équipe de football de France Télécom (plus particulièrement Harry pour avoir insisté d'y participer et de recommencer!),
- pour leurs accueils chaleureux lors du périple à vélo *DemiTour2France* : Sylvain M. et Hélène à Betton, Nicolas et Samara à Bordeaux, Alexandre et Marie à Toulouse, Corentine à Toulouse, Baptiste à Biot et Mathieu à Paris,
- les joueurs des équipes de football de l'US Ploubezre,
- les cyclos de l'AC Rospez.

Une vie existant en dehors de la thèse je remercie Hugues, Charlotte, Yohan, Qian, Seb, Guillaume, Zineb, Charles, Thomas, Sabrina, Sylvain C., Chi, Nga, Thai, Nguyet,

Cyril, Roman, Ali pour les jeux de mots sans fin & sous toutes leurs formes, les moments agréables passés ensemble, les trucs & astuces des passes de salsa...

Merci à Morgane, pour me supporter avant, pendant et après la rédaction !

Merci à ma famille – en Bretagne et en Allemagne – pour le soutien et l'encouragement apportés avant, pendant et après la thèse, et d'avoir cru à ce que je faisais sans avoir besoin d'expliquer !

Abstract

Hybrid Analog and Digital Access Networks Architectures for Fixed/Mobile Infrastructure Convergence

In order to realize the convergence of the optical infrastructure of fixed and mobile access networks, the objective of this thesis is to study the solutions for distributing native radio carriers through typical optical access networks.

The first Part describes the contexts and the main physical properties of the optical and radio access networks: from nowadays deployed Fiber To The Home (FTTH) systems, and their expected evolutions, to the current radio system Universal Mobile Telecommunications System (UMTS) towards the expected requirements of modern mobile radio systems. This allows to settle the optical environment in which the Radio over Fiber (RoF)-functionalities will have to be integrated, and to know on which radio systems' figures of merits to focus on when implementing it.

The second Part shows the benefit and possibilities of re-using the optical infrastructure of the fixed access networks for distributed radio systems. Then a review of the analog and digital RoF techniques is proposed, and their feasibility of integration into legacy FTTH systems is discussed.

The third part deals with the computing and simulations of an analog RoF-system where the optical link is either passive or optically pre-amplified, and even boosted. The goal is to provide numerical results to the practical lab. results of the second half of the fourth part where the Signal to Noise Ratio (SNR) matters. Therefore successively formal expressions, numerical results for simple 2-tone signals and more realistic UMTS signals are considered.

The fourth and last part deals with the obtained practical results. These can be split into two main categories: Error Vector Magnitude (EVM)-oriented results where an Avalanche Photo-Detector (APD) is used for legacy and extended-reach PON architectures using a direction shared Semiconductor Optical Amplifier (SOA); and an Adjacent/Alternate Channel power Leakage Ratio (ACLR)-driven part where the focus is set on a very critical figure of merit of radio systems, especially in the downlink. The latter part turned out to be mandatory and prevailing over the initially considered EVM concerns. Hence several RoF architectures, compatible with PONs, are introduced in order to overcome the non-linearities undergone by the RoF-signals, induced by the chromatic dispersion of the PON's fiber and the laser chirp, and degrading the ACLR performances.

Key words: PON, Radio over Fiber, UMTS, EVM, ACLR, EDFA

Résumé

Architectures de Réseaux d'Accès Hybrides Digitaux et Analogiques pour la Convergence des Infrastructures fixe/mobile

Afin de réaliser la convergence de l'infrastructure optique des réseaux d'accès fixes et mobiles, l'objectif de cette thèse est d'étudier les solutions pour la distribution de porteuses radio natives à travers des réseaux d'accès optiques typiques.

La première partie décrit les contextes et les principales propriétés physiques des réseaux d'accès optiques et radio : depuis les systèmes Fiber To The Home (FTTH) actuellement déployés et leurs évolutions attendues, en passant par l'actuel système radio Universal Mobile Telecommunications System (UMTS) jusqu'aux exigences des futurs systèmes modernes de téléphonie mobile. Ceci permet de fixer le cadre de l'environnement optique dans lequel les fonctionnalités Radio over Fiber (RoF) devront être intégrées, et d'anticiper les figures de mérite, se rapportant aux systèmes radios, auxquelles une attention particulière devra être protée durant la mise en oeuvre.

La seconde partie montre l'intérêt et les possibilités de réutiliser l'infrastructure optique des réseaux d'accès fixes pour les systèmes de radio distribuée. Ensuite est proposé un inventaire des techniques RoF analogiques et numériques, ainsi qu'une discussion quant à leur intégrabilité dans des systèmes FTTH courants.

La troisième partie traite du calcul formel et de simulations d'un système de transmission RoF analogique, où la liaison optique est soit passive ou optiquement pré-amplifiée, et voire amplifiée à l'émission. L'objectif est de fournir des résultats numériques en complément aux résultats pratiques (seconde moitié de la quatrième partie) pour les lesquels le rapport signal à bruit est le souci majeur. Pour cela nous utilisons successivement des expressions formelles, et des résultats numériques obtenus pour des signaux sinusoïdaux et pour des signaux UMTS plus réalistes.

La quatrième et dernière partie concerne les résultats expérimentaux : d'une part ceux concernant les architectures à base de récepteur APD et à portée étendue grâce à un SOA exploité de manière bidirectionnelle, et ayant pour figure de mérite principale l'EVM ; d'autre part les résultats ayant pour figure de mérite l'ACLR, qui pour les systèmes radio dans le sens descendant, est un paramètre critique, et s'avérant être plus important que l'EVM. C'est pourquoi sont présentées des architectures RoF compatibles avec les budgets PON, permettant de surmonter les non-linéarités d'ordre 3 induites par la dispersion chromatique et le chirp du laser, qui dégradent les performances de ACLR.

Mots clés : PON, radio sur fibre, UMTS, EVM, ACLR, EDFA

Contents

List of Figures

List of Tables

Glossary

2G	Second Generation
3G	Third Generation
ACLR	Adjacent/Alternate Channel power Leakage Ratio
ACS	Adjacent Channel Selectivity
ADC	Analog to Digital Converter
ADSL	Asymmetric DSL
APD	Avalanche Photo-Detector
ARPU	Average Revenue Per User
ASE	Amplified Spontaneous Emission
AWG	Arbitrary Waveform Generator
BER	Bit Error Rate
BPF	Band Pass Filter
BPS	Band Pass Sampling
BS	Base Station
CAPEX	Capital Expenditure
CATV	Cable Access Television
CD	Chromatic Dispersion
CF	Crest Factor
CO	Central Office
CPRI	Common Public Radio Interface
CWDM	Coarse Wave Division Multiplexing
DAS	Distributed Antenna System
DCF	Dispersion Compensating Fiber
DFB	Distributed Feed Back
DL	downlink
DS	downstream
DSL	Digital Subscriber Line
EDFA	Erbium Doped Fiber Amplifier
ER-PON	Extended-Reach PON
EVM	Error Vector Magnitude
FDD	Frequency Division Duplexing
FOM	Figure Of Merit
FP	Fabry-Perot

FTTB	Fiber To The Building
FTTC	Fiber To The Cabinet/Curb
FTTH	Fiber To The Home
G-PON	Gigabit-capable PON
GE-PON	Gigabit Ethernet PON
HSI	High-Speed Internet
HSPA	High-Speed Packet Access
I	In-phase
IEEE	Institute of Electrical and Electronics Engineers
IF	Intermediate-Frequency
IM-DD	Intensity Modulation and Direct Detection
IMD	Inter-Modulation Distortion
IP-TV	Internet Protocol Television
ISI	Inter-Symbol Interferences
ITU	International Telecommunication Unit
LD	Laser Diode
LNA	Low Noise Amplifier
LO	Local Oscillator
LOS	Line-of-Sight
LTE	Long-Term Evolution
MAC	Medium Access Layer
MBD	Mobile Broadband Devices
MMF	Multi-Mode Fiber
NLD	Non-Linear Distortions
NLOS	Non-Line-of-Sight
NRZ	Non Return to Zero
OAM	Operation, Administration, and Management
OBSAI	Open Base Station Architecture Initiative
ODN	Optical Distribution Network
OEO	Optical-Electrical-Optical
OF	optical fiber
OFDM	Orthogonal Frequency Division Multiplexing
OFDMA	Orthogonal Frequency Division Multiple Access
OLT	Optical Line Termination
OMI	Optical Modulation Index
ONT	Optical Network Termination
ONU	Optical Network Unit

PAPR	Peak to Average Power Ratio
PD	Photo-Detector
PON	Passive Optical Network
POTS	Plain Old Telephone System
PRBS	Pseudo Random Bit Sequence
PSD	Power Spectral Density
Pt2MPt	Point to Multi-Point
Pt2Pt	Point to Point
Q	Quadrature phase
QoS	Quality of Service
R-E	Reach-Extender
RAN	Radio Access Network
RAP	Radio Access Point
RAS	Remote Antenna Site
RIN	Relative Intensity Noise
RMS	Root-Mean-Square
RoF	Radio over Fiber
RRC	Root-Raised Cosine
RRU	Remote Radio Unit
S-SMF	Standard Single Mode Fiber
SCM	Sub-Carrier Multiplexing
SEM	Spurious Emissions Mask
SF	Spreading Factor
SNR	Signal to Noise Ratio
SOA	Semiconductor Optical Amplifier
TDM	Time Division Multiplexing
TDMA	Time Division Multiple Access
TIA	Trans Impedance Amplifier
UE	User Equipment
UL	uplink
UMTS	Universal Mobile Telecommunications System
US	upstream
VDSL	Very-high-bitrate DSL
VOA	Variable Optical Attenuator
VoIP	Voice over Internet Protocol
VSA	Vector Signal Analyzer
VSG	Vector Signal Generator
W-CDMA	Wide-Band Code Division Multiple Access

WDM	Wave Division Multiplexing
WiMAX	Wireless Microwave Access
WMAN	Wireless Metropolitan Area Network
WWAN	Wireless Wide Area Network

General Introduction

The expected rise of optical access network deployments in order to cope with the increased bandwidth demand lead by enhanced and new services, in parallel to an increase of the mobile users and offered bit rates requiring an enhanced and more numerous coverage, triggered the idea of re-using the optical access network infrastructures for distributing the radio signal.

Therefore in this thesis the current and near-future optical access networks with their properties and also the used components are exposed.

Then the radio access networks' properties and main figure of merits for radio signals are explained. The introduction of mobile radio's last mile and back haul announces the next part.

The benefits of hybrid access networks and the concept of Distributed Antenna System (DAS), which could be used in optical access network architectures, are then presented.

In order to exhibit the adapted Radio over Fiber (RoF) technique a review of the different analog and digital RoF techniques is proposed. This review is lead by considering the criteria of meeting a given target SNR over the widest optical budget. Also the applicability and integrability in current optical access network architectures of the reviewed RoF techniques are considered. Finally the analog transport of radio carriers looks to be the most promising even if lacking the capability of coping with the relatively wide optical budgets of Passive Optical Networks (PONs).

In a third part the maximum optical budgets for given SNR and OMI criteria are formally exposed for passive and optically amplified links.

Then the *VPItransmissionMaker* simulation tool is introduced to show, for simple sinusoidal signals, the third-order like distortions induced by the interaction of the optical source's chirp and the fiber's chromatic dispersion. Since these distortions are estimated not to be negligible the interest of Dispersion Compensating Fiber (DCF) for lowering them is demonstrated.

The simulation tool is finally used to compute Adjacent/Alternate Channel power Leakage Ratio (ACLR) for more realistic UMTS signals. These simulations confirm the benefit of DCF for approaching the 3GPP specified ACLR specifications. Also the benefit of using an EDFA pre-amplifier for increasing the optical budget, for which the ACLR are compliant with the specifications, is demonstrated.

In the last and fourth part of this thesis, the experimental measurements for several hybrid access network architectures are reported.

The starting idea is to use a legacy APD receiver (intended at 10Gbit/s digital applications) for recovering the radio carriers. The related Error Vector Magnitude (EVM) results are promising, thus the APD is used in combination with an in-line and direction-shared Semiconductor Optical Amplifier (SOA) in order to realize a bi-directional transmission of UMTS carriers through an Extended-Reach PON (ER-PON).

Unfortunately, in the downlink, meeting the EVM criterion is not sufficient. Indeed the ACLR figure of merit and its very stringent 3GPP requirements will make us start almost from scratch.

The new starting point will be an optical receiver made of a PIN and an Erbium Doped Fiber Amplifier (EDFA) pre-amplifier. Then around this composite receiver an adapted framework using DCF and an EDFA-booster, increasingly allows to improve the ACLR performances over typical PON budgets.

Part I.

The Access Networks

1. Introduction: economical & user context

1.1. Context of the fixed access networks

1.1.1. Limits of the current copper access network

Until recently, the Digital Subscriber Lines (DSLs) techniques, using the legacy twisted copper pairs, were the dominating standards (Tab. 1.1) for delivering triple play services (High-Speed Internet (HSI), Voice over Internet Protocol (VoIP), Internet Protocol Television (IP-TV)) in addition to the legacy Plain Old Telephone System (POTS).

Table 1.1.: Broadband deployment in access networks by technology in Q4, 2008 [1]

Broadband Technology	**Deployment share**
DSL	65%
Cable	21%
Fibre	12%
Fixed Wireless	1%
Other	1%

Despite the increase of the bit rates offered by the xDSL standards, and consequently the available services, the reach of the corresponding xDSL standards is limited (Fig. 1.1a) because of the important linear attenuation and the low-pass properties of copper lines.

Indeed at the reference frequency of 300kHz, the linear losses value, for 0.4mm and 0.8mm cable sections, are respectively 15 and 8dB/km. Furthermore, the linear attenuation (in dB/km) against the frequency behaves like the square root function due to the skin effect in copper cables.

Thus the number of customers eligible to the most recent DSL standards (Asymmetric DSL (ADSL) 2(+) and Very-high-bitrate DSL (VDSL) 2) is reduced, and makes these DSL standards, which offer higher bit rates, less attractive for customers and thus less profitable for operators.

1.1.2. Need of an optical access networks

Furthermore the bandwidths requirements in the downlink as well as in the uplink directions, are driven by enhanced services tightly linked to the customers' behavior. The latter depends on the available equipments.

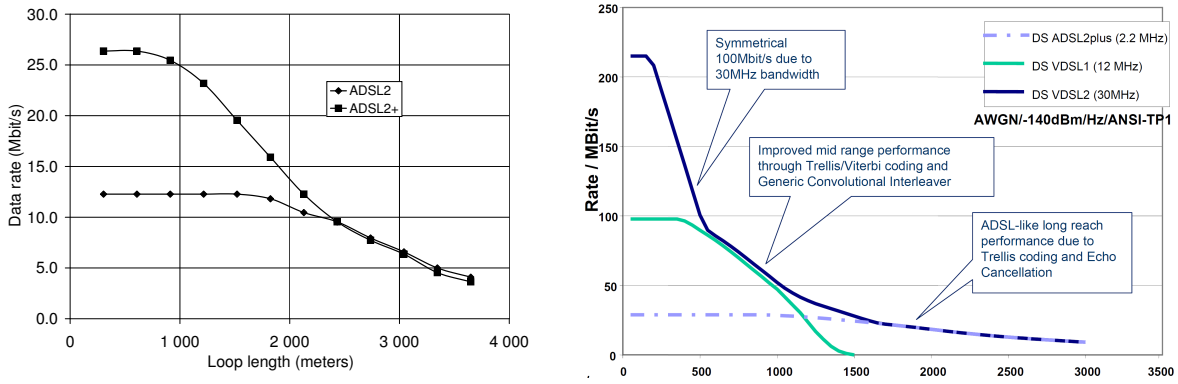

Figure 1.1.: (a)ADSL2 and ADSL2+ maximal data rates vs. loop length (data from [2])
(b)VDSL1 and VDSL2 data rates vs. loop length (meters) (picture from [3])

Equipments

The customer usages and demands are driven by new services and functionalities enabled by technology evolutions and the amount of connected/connectible devices.

Therefore the gateway plays an essential role since recent gateways are no longer *simple* modems, but include home routing and networking oriented functionalities, paving the way for other connected (wired or wireless) equipments such as tablets, several computers per household, and multiple TV sets.

Finally, this leads the customer to spend more time with devices requiring networking functionalities.

Customer behavior

The increasing usage of peer-to-peer services and social sharing sites (personal pictures & videos), made the residential traffic within the access networks become more symmetric with the time.

Furthermore since voice traffic is no more dominating, the traffic has become bursty [4, Chap. 5]. The burstier a traffic is, the more the peak traffic is high compared to average traffic load, and thus requires over-sizing the network through-put in order to avoid congestion.

However the existing DSL standards are not designed for such upstream traffic.

Driving services

In the downlink, as shown in Tab. 1.2, the drivers are 3 dimensional (3D) TV and High Definition IP-TV for multiple TV sets, High Definition telephony, and video telephony.

In the uplink, the main driver is the bandwidth required for the symmetrical HSI connection and video-conference.

The requirements to the upstream bandwidth is furthermore driven by recently appeared centralized services such as:

Table 1.2.: Bandwidth requirements of multimedia services

Service	**Bandwidth (Mbit/s)**	
	Downlink	Uplink
2x HD IP-TV	24	1
HSI	10	10
VoIP	0.5	0.5
Videotelephony	4	4
Online Gaming	1	0.5
Total need	**39.5**	**16**

- infrastructure as a service where computing power (processors), storage, and network capacities can be rented,
- software as a service for terminal-like applications made available to the end users,

These *cloud* type services strengthen the need of a symmetric HSI connection.

Finally, the bandwidth of DSL cannot cope with the bandwidth requirements (Tab.1.2) set by the new and enhanced services.

1.1.3. Costs of optical access networks

In case of new and enhanced services, the adequate bandwidth can be provided by an access network being either partially or end-to-end optical. Fig. 1.2 shows the three main implementation possibilities of such network architectures.

Cost comparison of different access technologies

In the case of Fiber To The Cabinet/Curb (FTTC), fiber is installed up to the street cabinet from whereon the remainder of the access line consists of a copper sub-loop. This solution is less expensive to build than Fiber To The Home (FTTH) architectures as the already installed copper loop is partially reused. Yet it does not achieve the same performance levels.

FTTH networks need to be separated into FTTH-PON and FTTH-P2P (Point-to-Point) solutions. In the first case, several customers share a common feeder fiber between the OLT and the last splitter. In the latter case, a dedicated fiber is installed from the OLT to the user's premises.

Again, FTTH-P2P is more costly than FTTH-PON but delivers better results in terms of available bandwidth [5]. Fiber To The Building (FTTB) is an intermediate case, where only the in-house wiring consists of a copper loop. Since FTTB shares most of its characteristics with FTTH, FTTH-related issues also apply in general to FTTB.

Furthermore whether FTTH networks are deployed in dense urban areas or in rural areas, the dominant cost share is due to the civil engineering as shown in Fig. 1.3.

Other sources converge also show the main share of the costs of deploying a FTTH network to originate from the required civil work of trenching & digging (Tab. 1.3).

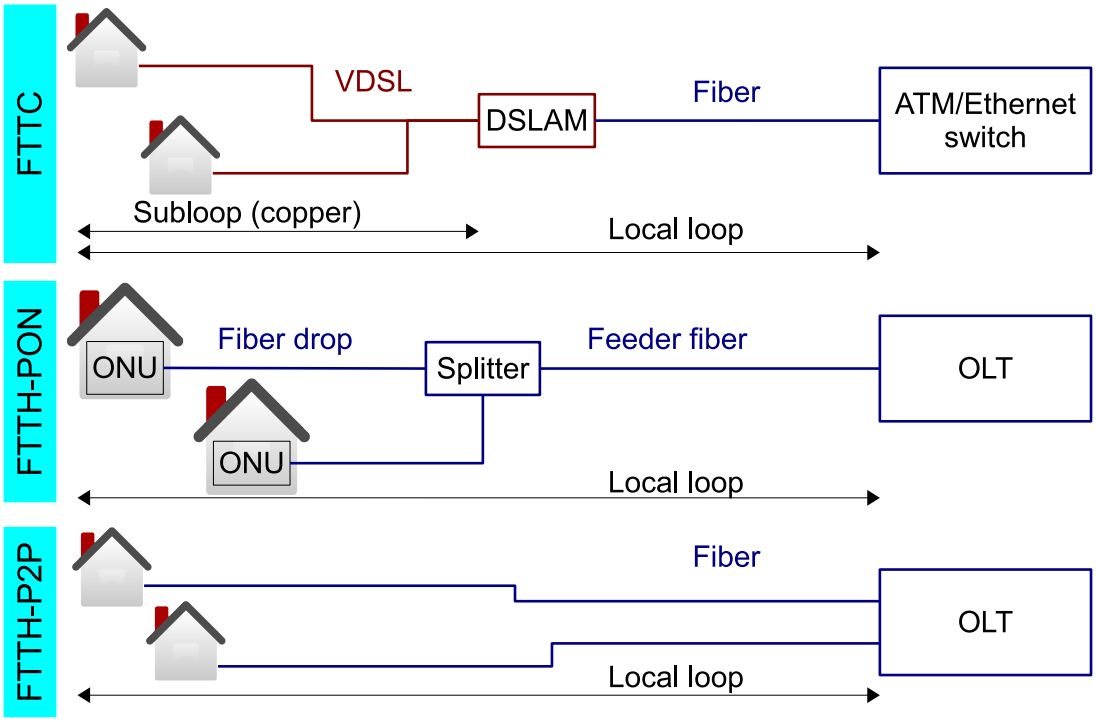

Figure 1.2.: Broadband wireline access technologies

.

Global & individual costs

An example of cost estimation for a country-wide coverage is given by the French ministry of territory. The latter estimates the required Capital Expenditure (CAPEX) for a 100% coverage of the French population by FTTH to value 30 thousand million EUR [6].

According to [7], for a FTTH implementation relying on the PON technology, the lowest in the U.S. reported cost per customer was US$1350 in 2008.

1.1.4. Deployments of FTTH networks

Despite the costs for building FTTH/B networks, the FTTH deployment in Europe is expected to raise sharply (Fig. 1.5). This expected rise can be explained by the fact that the current average penetration of FFTH connections in European households compared to penetration in countries of the Asia/Pacific area, is moderate (Fig. 1.6a).

Furthermore another aspect is that the numbers of connectible and actually connected households differ[1] [8]. For instance in France in June 2010, they differ by a factor 15 (Fig. 1.6b).

[1] feasibility (of infrastructure) vs. effectiveness because no subscribers yet or no planned infrastructure roll-out

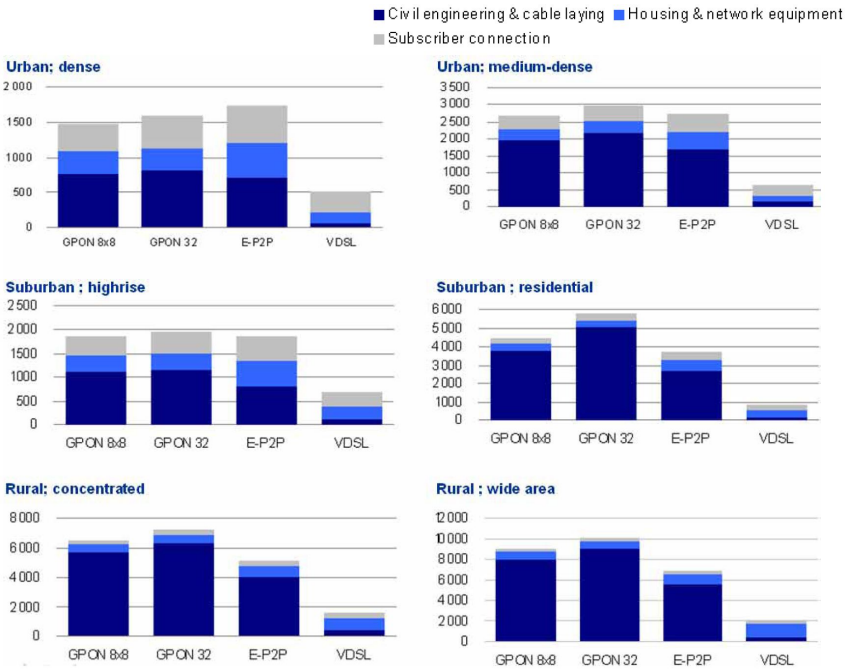

Figure 1.3.: Average investment per subscriber for an incumbent carrier (EUR), (picture from [5], 2010)

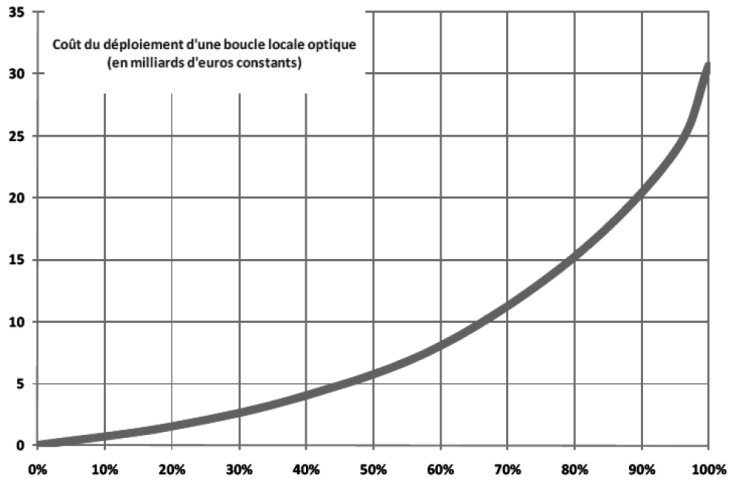

Figure 1.4.: Estimation of the required CAPEX (billions EUR) vs. coverage (percents) of French population by FFTH (picture from [6])

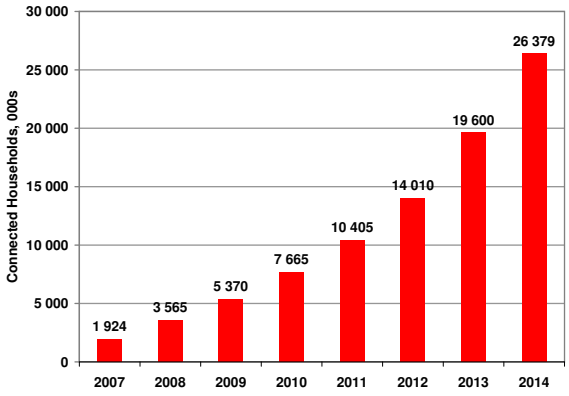

Figure 1.5.: Forecasts of households connected by FTTH in Europe (from Heavy Reading, 24/02/2010 by Graham Finie)

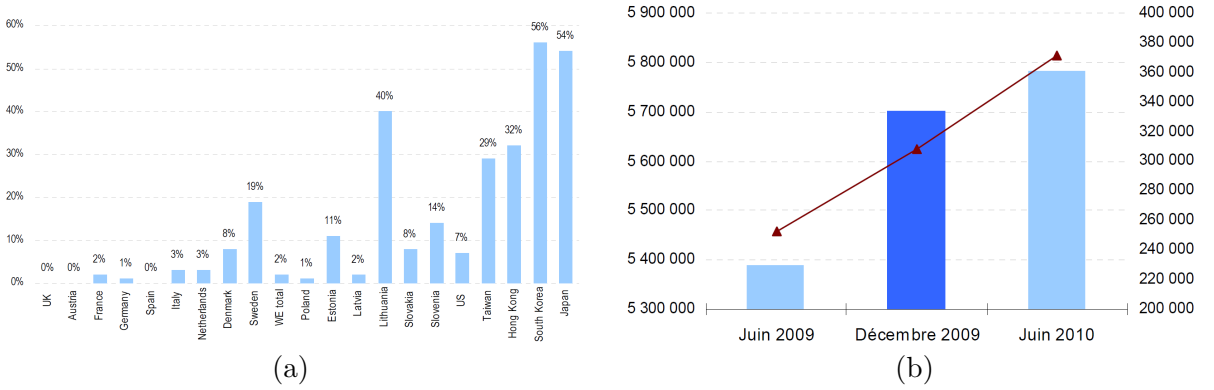

(a) (b)

Figure 1.6.: (a) FTTx share of total broadband lines (Dec. 2009), (picture from [5]);
(b) FTTH/B connectible (bars chart, left axis) and connected (continuous line, right axis) homes in France, (chart from [8])

Table 1.3.: Initial capex distribution for FTTH deployments, Source: Corning&FTTH Council Europe

Type	**Costs**
Civil works	68%
Actives	12%
FO cables	6%
Installation	3%
Hardware	2%
Other services	9%

1.2. Context of the mobile networks

The mobile access networks are usually divided into technological generations. Each technological generation (G) allows new or/and enhanced services, and depend on the appropriate user equipments for transmitting, receiving and rendering.

The number of users can be linked to the number of sold devices since a given technological generation depends on the user equipments. Also the resulting generated traffic is technology dependent.

As for the wired access networks, the customer usages and demands are driven by the evolution of the devices and the offered services.

Table 1.4 gives an overview of the possible services offered by mobile devices and networks.

Table 1.4.: Qualitative overview of mobile services [9]

Class of Service	**Bandwidth**	**Latency**	**QoS Requirement**	**Example**
Conversional	Low-medium	Low	Guaranteed	VoIP/Video calling
Streaming	High	Low	Guaranteed	IPTV, multi-media streaming
Browsing	Low-medium	Normal	Best Effort	Web browser
Background	Medium	Normal	Minimal	Email synchronization
Broadcast	High	Low	Guaranteed	Multi-cast

1.2.1. Mobile broadband devices

The Mobile Broadband Devices (MBD) can be defined as every equipment capable of connecting to a mobile broadband radio network whether regional (Wireless Wide Area Network (WWAN)) or metropolitan (Wireless Metropolitan Area Network (WMAN)).

The devices having only personal or local connecting capabilities are not concerned.

Types and number of devices

The MBD market is segmented in two main parts: the hand-held and the portable devices (Fig. 1.8a).

The portable devices have recently regained of interest with the rise of USB modems or 3G dongles, represent 22% of the MBD sales in 2009. However the hand-held devices are expected to represent 85% of the MBD by 2014, stimulated by the deployments of 3.5G (High-Speed Packet Access (HSPA)), 3.9G (HSPA+), and 4G (Long-Term Evolution (LTE)) networks, and targeting mainly non-professional customers. The main foreseen usages are Internet browsing, up- and download of video sequences, and eventually video telephony.

Figure 1.7.: Mobile Broadband Devices, summer 2010

Hand-held MBD

are devices such as smart-phones with applications inducing data traffic such as e-mail, browsing, file synchronization.

Portable MBD

The portable MBD (notebooks and ultra-portable devices) represented 62 millions of sold units in 2009. By 2014, their shipments are expected to almost double and representing 112 millions of units.

The category of portables MBD, with built-in WWAN interfaces, are expected to represent a stable yet weak share (10%) of the overall sold notebooks and laptops (150 millions in 2009) within the period ranging from 2009 to 2014.

3G cards and dongles Also a new type of external devices, *mobile hot-spots*, which are small transportable boxes having access to the mobile broadband networks and allow to set-up a hot-spot shared by the mean of WLAN or Bluetooth and available to several users.

E-readers In 2009, 5 millions of e-readers having mobile radio connecting capabilities have been sold, whereas in 2010 the total shipments are to almost double yielding 12 millions. However since they are relatively expensive compared to other multi-functional devices offering the same possibility of reading an electronic book by software applications handling the *e-book* file format, the e-reader category is expected to decline in 2013.

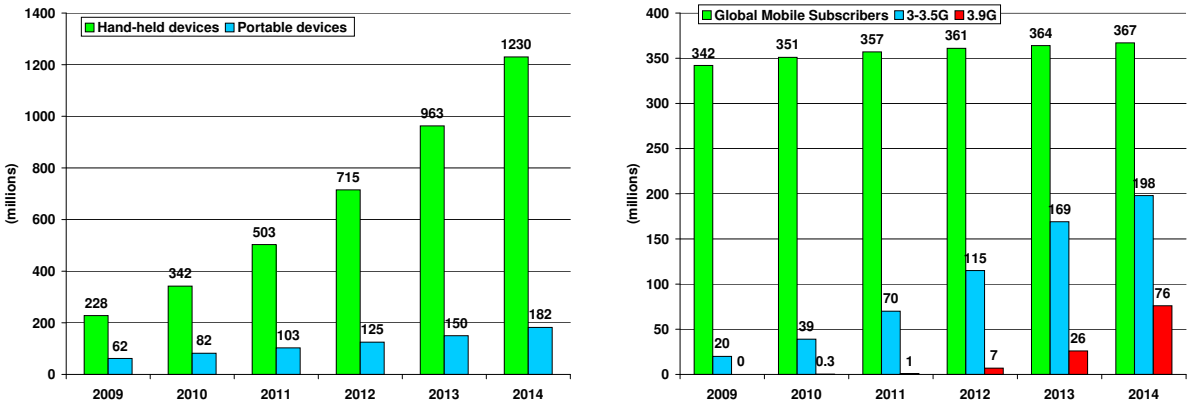

(a) (b)

Figure 1.8.: (a) Worldwide sales of MBD devices. (b) Number of 3.5G and 3.9G subscribers in Western Europe. (Both data sets: *Informa*, April 2010)

1.2.2. Number of subscribers

According to the chart in Fig. 1.8b, in Western Europe subscribers of mobile broadband represented 6% of the overall mobile customers in 2009. By 2014, this figure is expected to rise up to 56% with 390 millions customers. 287 millions of the latter are to use 3.5G (HSPA) connectivities and 95 millions are expected to use evolved standards such as HSPA+ and LTE.

Worldwide, the number of customers using 3.5G and 3.9G connectivities (except WiMAX) should rise from 223 millions in 2009, to 1.65 billions in 2014, corresponding to 25% of the worldwide mobile subscribers.

1.2.3. Traffic evolution and related cost issues

Changes in traffic composition

Currently the world-wide mobile Internet traffic is increasing steadily (Fig. 1.9a). According to [10], between 2006 and 2009, the mobile data traffic is estimated to have been multiplied by 25.

The example of the Singaporean operator *Star Hub* shows that the traffic increase originates from the data traffic while the voice traffic keeps constant. As a consequence of this, in 2010, data is expected to account for 73% of the global mobile network traffic.

According to [12], the two main services behind the mobile data traffic growth are web browsing and IP-TV streaming. This can be partially explained by the enhanced browsing experience: support of full HTML pages, multimedia content, improved network performances for download.

Related cost issues for operators

While from an operator point of view the associated revenue per provided Mega Byte of data is decreasing (Fig. 1.9b), this aspect for customers results in decreasing costs for

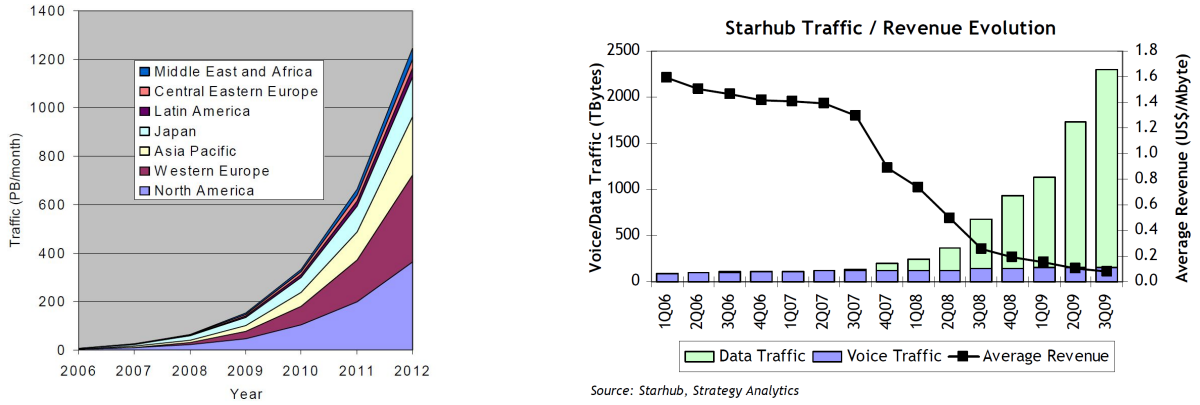

(a) (b)

Figure 1.9.: (a) Forecast of global mobile Internet traffic by region, (picture from [11]); (b) StarHub Singapore Traffic and Revenue Evolution vs. time (quartal, year) (picture from [10])

downloading data and encourages them to consume data and generate traffic.

Yet this evolution is causing a revenue issue (Fig. 1.10b) for mobile operators: as the Average Revenue Per User (ARPU) declines with the time, the provided bit rates to the end users increase. For instance, in 2009 traffic flows over mobile networks from PC account for 41% of the global mobile data traffic but generated only 3% of the mobile service revenues [10].

Currently mobile networks still remain profitable and generate increasing revenues, as it is the case for Germany (Fig. 1.10b). Also according to [10], voice is still making a significant contribution to wireless revenues.

A declining ARPU can be compensated by an increasing number of customers. Yet the more customers there are, the more related infrastructure is required.

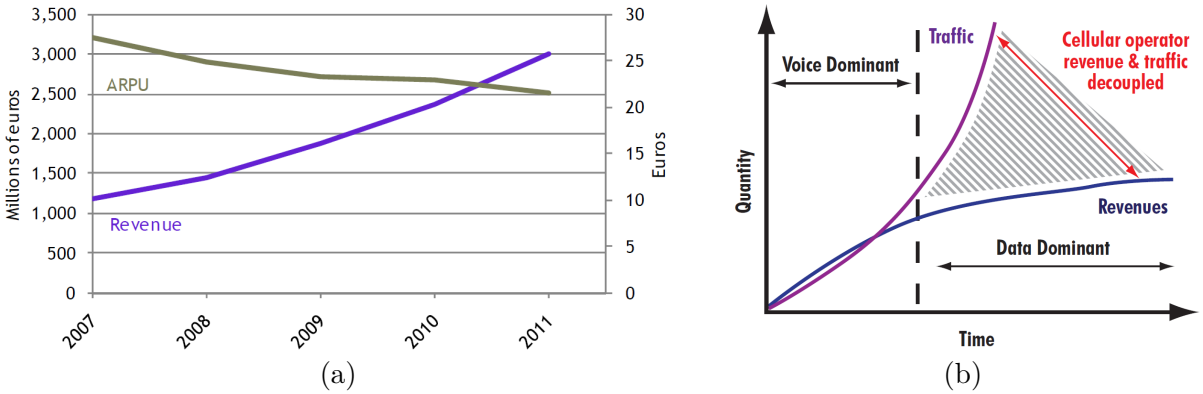

(a) (b)

Figure 1.10.: (a) ARPU decline for Germany (Revenue on the left axis, ARPU on the right axis), (Fig. from [13]) (b) As traffic composition evolves the ARPU declines

Conclusion

Concerning the fixed access networks, we have shown why legacy copper networks cannot cope with the increasing demand for bandwidth in the access networks. Also several access network architectures relying on optical signal distribution have been introduced and their deployment costs compared.

Finally since only *fully* optical access networks architectures offer the possibility of guaranteeing the bandwidth demand in the long term, their deployment can be justified. The properties of a typical FTTH implementation, namely Passive Optical Network (PON), and its physical properties will be discussed in Chapt. 2, and will serve as the framework for a possible convergence of optical infrastructures for fixed and mobile access networks.

Concerning the mobile radio networks, we have shown how devices and their related functionalities drive mobile Internet traffic, and have highlighted the data traffic to be the fastest growing component compared to voice related traffic.

Also we have recalled that in the near future, the increase of mobile Internet traffic is expected to hold on, and thus to become an issue for operators since the related backhaul will have to be strongly reinforced.

Finally the growing importance of mobile Internet traffic and current forecasts have been addressed.

2. The optical wireline access networks

This chapter aims at explaining the different types of existing optical wireline access networks. The latter set the framework in which the different hybrid architectures — exposed in the following chapter— are to evolve.

The optical wire line access networks can be split into two main categories: the Point to Point (Pt2Pt) and the Point to Multi-Point (Pt2MPt) ones (Fig. 2.1).

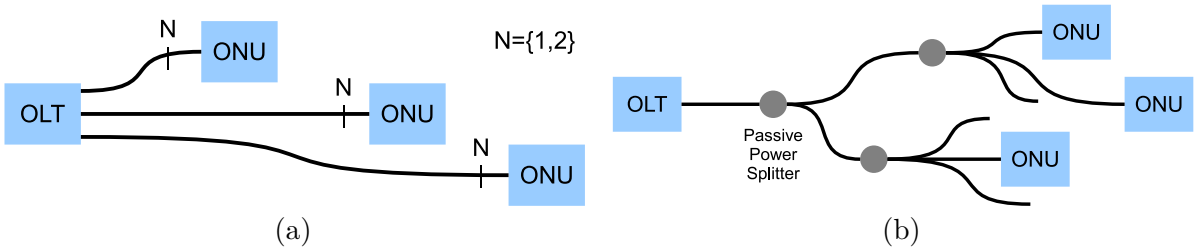

Figure 2.1.: Passive optical architectures: (a) Point-to-point, and (b) point-to-multipoint

The choice of the topology is guided by initial and operative costs, and the operator's strategy in terms of budget or coverage (only dense areas or nation wide). Beyond a certain prove-in distance (Fig. 2.2), the savings for a Pt2MPt topology are attributable to the lower cost of the smaller, shared cable.

For instance, in France, the two types exist: Orange/France Télécom has deployed Pt2MPt networks, whereas Free/Iliad has chosen Pt2Pt. Finally SFR/Neuf Cegetel uses both.

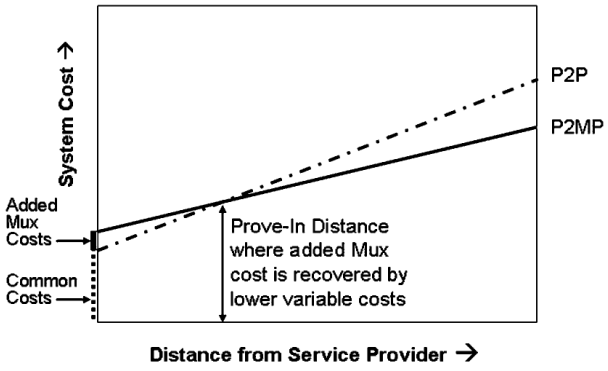

Figure 2.2.: The cost of a Pt2MPt digital-loop-carrier system versus a Pt2Pt system as a function of distance to the customer, picture from [7] 2008

2.1. The point-to-point access networks

The principle of a *point-to-point* network consists of linking individually each customer to the Central Office (CO). This allows a relative ease of evolution and straightforwardness for planification of customer increase. Yet the latter aspect is also one of its weak points since the total amount of fiber at the CO (concentration point) is identical to the number of customers linked to the concerned CO and hence can be several thousands. On such infrastructure, the Ethernet packets are natively transported over the optical signal.

2.2. The passive point-to-multipoint access networks

2.2.1. The concept

The main interest of a *point-to-multipoint* PON is its simplicity. The Optical Line Termination (OLT) is the main element of the network and is usually located at the central office. The Optical Network Units (ONUs) are the interfaces towards the optical network and are located at the customers'. The ONUs are connected to the OLT by the mean of optical fibers and power splitters, the whole building a *passive distribution network* since it contains no energy source to keep the network running.

It is needed to agree upon the notion of *passivity*, given that it can be understood as an electric and/or an optical passivity, or even as a passivity from a protocol point of view[1].

In this way a single ONU can be an access point for a single customer (we then speak of FTTH), or for several customers (we then speak of FTT-Building, -Cabinet, -Curve) where the last tens or hundred of meters of the link between the ONU and the customer rely on DSL or Coax. techniques.

The key element, which distinguishes the PON from other wired networks, is the optical power splitter.

Indeed it allows an architecture (the signal's attenuation due to the splitters put aside) similar to a satellite or mobile network architecture in the sense that the downlink signal is broadcasted to the different ONUs thanks to the different splitters [14].

In the uplink path, the signals of the different ONUs arrive at the splitters, building at the OLT, a signal resulting of the superposition of the signals egressing from the different ONUs. That is why, in order to avoid collisions and related data losses, a mechanism at the level of the communication is required (contrary to the P2P one).

Brief historical

Specified and designed at the end of the 90's, the Broadband-PON (B-PON) [15, §8.3.1], which has a limited total downlink bit rate of 155.52Mbit/s. In case of 64 customers, the bandwidth is shared, and results in individual maximal rough downlink bit rates of 2.4Mbit/s per customer. Finally this bit rate was equivalent to the available bit rates provided by DSL techniques at the time. Thus the deployment of an optical network and its associated systems could not be justified.

[1] see Evolved PONs, 2.5 p. 35

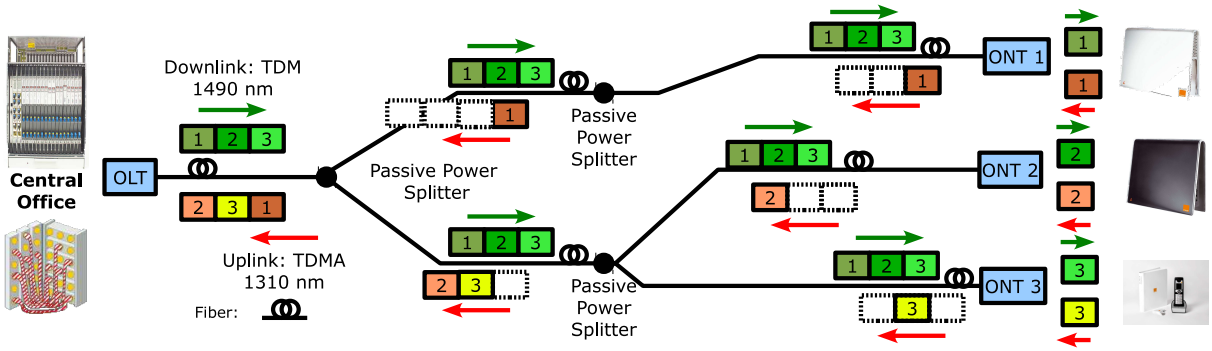

Figure 2.3.: Principle of TDM/TDMA used in nowadays PONs (G-PONs and GE-PONs)

Later, higher capacity versions of the B-PON, known as Gigabit-capable PON (G-PON)[2] and Gigabit Ethernet PON (GE-PON)[3] were developed leading to higher datarates per user.

Regain of interest

Recent bandwidth *hungry* services such as multiple channels of HD Video streams per household cannot be delivered by the capacity and reach limited copper-based DSL techniques.

Thanks to decreasing costs for manufacturing electronics and optics technologies [7], an affordable optical access network technology compatible with mass deployments of fiber – as far as inside the customers' homes – could be developed in the last decade: the FTTH concept.

In this case the trenching for the optical fiber account for the greatest part of the overall network deployment costs [7].

2.2.2. Main properties

Concerning the recently and widely deployed PONs, two normative approaches exist. On the one hand, an approach driven by several main telecommunications operators [16] pushing their concerns, (International Telecommunication Unit (ITU) specifications G.984.x, [17, 18]); and on the other hand an approach dominated by equipment vendors trying to re-use legacy Ethernet technology bricks (Institute of Electrical and Electronics Engineers (IEEE) norms 802.3ah, [19]).

The two approaches are sufficiently different at the MAC layer (data framing[4], synchronization and signalization) to be incompatible with one another [20].

Despite the incompatibility at the protocol layer, both implementations have common properties such as bit rates, line-coding, wavelengths, reach, and optical power budgets.

Thus without loss of generality we can take the G-PON as the PON reference.

[2] standardized by ITU

[3] standardized by IEEE

[4] the ITU flavor uses an evolution of the generic framing procedure (GFP) for encapsulating the payload which can either be native TDM or packet data; while the IEEE flavor exclusively makes use of Ethernet packet encapsulation for the payload

Bitrates and multiplexing

G-PON uses a Non Return to Zero (NRZ) line coding with an extinction ratio of 10dB in the optical domain.

The maximal downlink bit rate in a G-PON tree values 2.5Gbit/s. The bit stream of a PON *tree* is time-shared among the customers by using a Time Division Multiplexing (TDM) protocol.

The typical maximal uplink bit rate in a G-PON tree is 1.25Gbit/s[5], and results of the data streams egressing from the different customers' premises equipments (CPE). In order to avoid collisions a Time Division Multiple Access (TDMA) protocol is implemented, which furthermore includes a *ranging* mechanism allowing to handle the customers having each a different propagation time with respect to the CO.

The PONs, in order to use a single fiber for the two communication directions, make use of wavelength division multiplex (WDM) in a full-duplex mode.

The downlink wavelength (from the CO to the customer) is centered at 1490nm+/-10nm. The uplink wavelength, identical for the different customers, is included within 1260 and 1360nm, and is generally centered at 1310nm.

The optical budget

The optical budget is defined as the difference (*i.e.* attenuation) of the optical power between the optical signal emitted at the OLT and the optical signal received at the ONU, and *vice versa*. The attenuation of a link is the sum of the insertion losses due to the power splitters, the optical fiber, and their splices.

In a PON architecture a minimal and a maximal optical budget are allowed. Their difference is called the *differential* optical budget. The latter, currently set to 15dB for G-PON, is justified by a limited dynamic of the optical receiver at the ONU for maintaining a given QoS/BER: below the minimum budget, saturation of the optical receiver occurs; and beyond the maximal budget, the limit of the receiver's sensitivity is reached.

Typically the minimum and maximum budgets are set to 13dB and 28dB respectively, and correspond to the widely used *B+ Class* of G-PON.[6] The optical power losses mainly results from the overall splitting ratio (typically 1:16, 1:32, 1:64) where the splitting ratio is realized by one or more *splitter stages*. As a consequence of this, a minimum (the customer is located close to the CO after the first splitter stage with a 1:16 ratio) and a maximum (the customer is located the furthest from the CO after the overall splitting ratio of 1:64) optical budget can be observed.

However often, only the maximal budget is mentioned. Other *budget classes* exist for the G-PON: ranging from 20 for *Class A* to 32dB for *Class C+* [21].

The choice of an optical budget is important since it is a compromise of several parameters and necessities being as well financially as technically driven:

- distribution of the customers per PON-*tree* and length of the PON's branches

[5] even if specifications foresee 2.5Gbit/s

[6] The purpose of a *Class* is to organize the various parameters of the physical layer (minimum and maximum of optical budgets, launch and received optical powers, line rates ...) for building a working system. See Tab. 2.2 for examples.

- eligibility ratio of the potential customers for different housing densities of areas
- reusing the sites of presence (CO) already used by copper in order to place the OLTs
- the infrastructures (splitters and fiber) once deployed, and the systems being operating with customers (*production mode*) impose civil works to be done as rarely as possible
- compatibility with future evolutions of PON (§2.5)

2.3. The optical link used in PONs

The optical link is composed of optical fiber, power splitters, and of splices and connectors.

2.3.1. Optical fiber

The G-PON specification of the physical layer [22] foresee a maximum optical fiber length of 20km between the OLT and the ONUs.

In fact, the distance is limited by the maximum differential distance between the ONUs. Indeed, a differential distance greater than 20km disturbs the ranging protocol which synchronizes the ONUs.

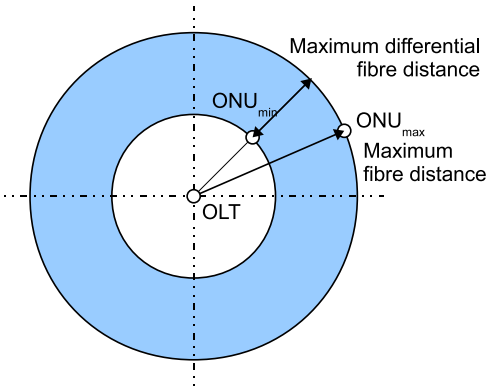

Figure 2.4.: Maximum differential fiber distance between ONUs

However from a pure protocol perspective the maximum distance (called the logical reach) between the OLT and the ONUs is 60km [22].

Furthermore given that the OLT is currently located at the historical CO (copper) used for POTS, the mean distance of the *optical local loop* is, for example in dense inhabited areas of France, within 5 to 7km [23, 24]. It is to be noticed that on-going studies show the possibility of reducing the total number of COs thanks to the possible longer reach of optical access networks compared to copper access networks.

Thus in this thesis we will consider that it is possible to have up to 20km of Standard Single Mode Fiber (S-SMF) between the CO and the customers.

Types

An optical fiber is made of a core surrounded by cladding. The latter has a lower refractive index which causes the light beam to keep inside the core and thus being guided by the internal reflections [25].

For core diameters of 50 to 100μm, up to 200 modes exist [25], and thus the fiber is called Multi-Mode Fiber (MMF), whereas for core diameters of 8 to 10μm the fiber is called Single Mode Fiber (SMF).

For MMF, each path has a slightly different propagation delay, which causes an input pulse to be distorted and spread. This effect is known as modal dispersion and according to [25] 10Gbit/s applications are limited to links of 100 to 300m (typically in-building applications). Thus for telecommunication applications where distance matters (from access to long-haul networks) the single mode fiber is preferred. Henceforth we only consider single mode fiber.

Properties

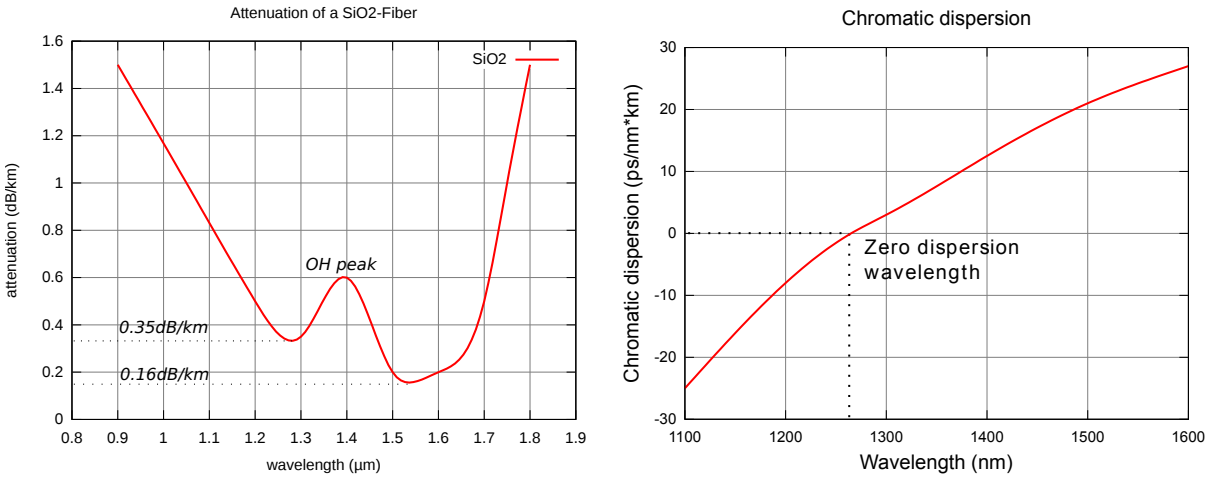

(a) (b)

Figure 2.5.: (a) Attenuation, and (b) dispersion for a SiO2-fiber [26]

Losses The transmission losses in a standard single-mode fiber is wavelength-dependent as shown in Fig. 2.5a. For S-SMF, local wavelength windows around 1.3, 1.5, and 1.6um with minimum transmissions losses exist, and are therefore the preferred transmission windows used in optical networks. The typical insertion losses for a G.652.D S-SMF at 1.5um wavelength values 0.28dB/km typically for a specified maximum of 0.35dB/km.

Recent type of fibers with a flattened OH-peak exist. Yet they are not used in access networks since low cost components are mandatory.

Chromatic dispersion A digitally modulated optical source has a spectral width[7] ($\Delta\lambda$) which depends upon the used modulation format/technique (Fig. 2.6).

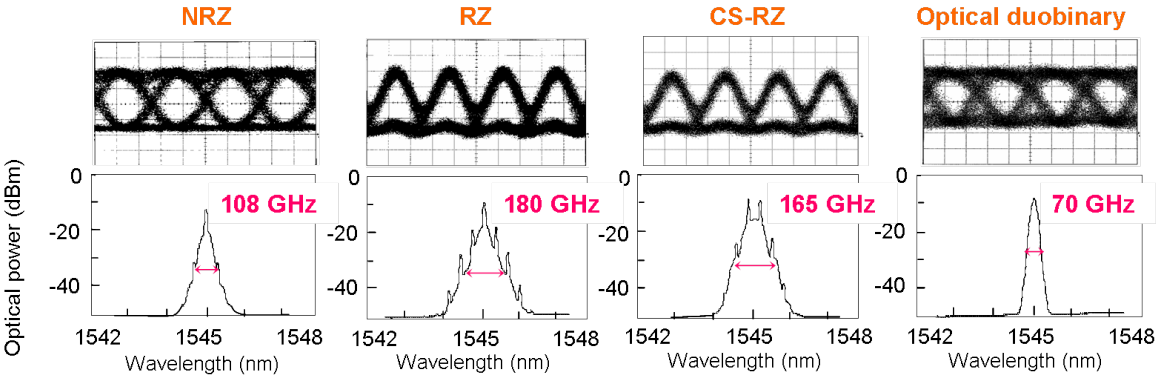

Figure 2.6.: Optical spectra and spectral widths for different modulation formats (40Gbit/s), picture from [27]

Due to the Chromatic Dispersion (CD), when a light pulse is launched into S-SMF, the different frequency components of the pulse's optical spectrum do travel on the same pathway through the fiber but at a different speeds, and arrive at different times at the receiver, and thus the pulse is broadened.

The CD is the superposition of two physical phenomenons: the waveguide dispersion and the material dispersion, the first is relatively small compared to the second.

Consequently broadened pulses may overlap (Fig. 2.7) and result in Inter-Symbol Interferences (ISI), and thus degrade the Bit Error Rate (BER).

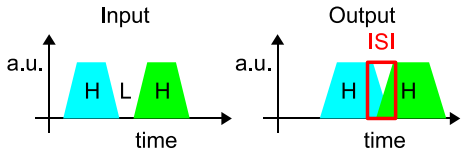

Figure 2.7.: Effect of fiber's chromatic dispersion: the middle-bit cannot be determined

For digital systems, a *simple* relationship between chromatic dispersion and pulse spreading can be established. Assuming an optical source with a spectral width $\Delta\lambda$, chromatic dispersion at the working wavelength D_λ, and the traveled distance L, the light pulse is broadened by [28]:

$$\Delta\tau = \Delta\lambda \cdot D_\lambda \cdot L \tag{2.1}$$

$\Delta\lambda$ can be expressed as the difference of the maximum and minimum wavelengths composing the digital modulated optical spectrum:

$$\Delta\lambda = \lambda_1 - \lambda_2 = c \cdot (1/f_1 - 1/f_2) \tag{2.2}$$

[7] measured at half width

For a NRZ signal $f_2 = f_0 + f_{bit}$ and $f_1 = f_0 - f_{bit}$ where f_0 is the central frequency of the optical laser source, this leads to:

$$\Delta\lambda = c \cdot \frac{f_2 - f_1}{f_2 \cdot f_1} = c \cdot \frac{2f_{bit}}{f_0^2 - f_{bit}^2} \tag{2.3}$$

Since f_{bit} (order of 1 to 10GHz) is negligible compared to f_0 (order of 190THz), $\Delta\lambda$ can finally be approximated by:

$$\Delta\lambda \approx 2c \cdot f_{bit}/f_0^2 = 2\frac{\lambda_0^2 \cdot f_{bit}}{c} \tag{2.4}$$

Injecting the latter approximation into the expression of the pulse broadening, and assuming a maximum pulse broadening of a half bit, the maximal length can be expressed for a NRZ signal as:

$$L_{max} = \frac{c}{4 \cdot f_{bit}^2 \cdot \lambda_0^2 \cdot D_\lambda} \tag{2.5}$$

At an operating wavelength of 1490nm and assuming a chromatic dispersion coefficient of 17ps/nm/km, the maximum link lengths for bit rates of 2.5 and 10Gbit/s —using the afore mentioned formula— are respectively 318 and 20km. These bit rates correspond to the current and next generation downlink bit rates of PON systems.

In the uplink the PON systems (G-PON and GE-PON) operate at 1310nm, which for standard fibers is the central wavelength of the range (1300-1324nm) for which the chromatic dispersion becomes very small.

2.3.2. Splitters

Splitters are bi-directional Y-shaped passive optical power dividers realized in a planar waveguide technology [24], and account from far for the optical budget since their theoretical insertion losses are linked to their splitting ratio following a logarithmic rule:

$$\text{Insertion Loss}_{dB} = -10 \cdot \log\left(\text{Splitting Ratio}\right)$$

However in practice additional losses have to be taken into account (Tab. 2.1): 1 to 2dB for low ratios, and twice this value for ratios higher than eight.

2.3.3. Splices and connectors

are respectively used to couple fiber spools one another, and to connect the fibers spools to the power splitters and equipments. Splicing of a single mode fiber accounts for insertion losses of 0.05 to 0.2dB, whereas connectors have insertion losses of 0.2 to 1dB [30].

2.3.4. Bending losses

Fiber bending losses occurs when the fiber is *excessively* bent causing the light to be no longer confined in the core, but to escape from the fiber. Indeed a tight bend reduces

Table 2.1.: Losses of power splitters, the * annotated losses derive from the computed combination of the measured power splitters

Splitting Ratio	Losses [dB]	
	Theoretical	Measured [29]
2	3	4-5
4	6	7-8
8	9	10-11
16	12	14-16 *
32	15	17-19 *
64	18	20-22 *

the apparent refractive index of the edge of the core to become lower until it equals the refractive index of the cladding [24]. As a consequence of this the light escapes.

As reported by [24] the ITU specifications of the typically used S-SMF G.652.D fiber foresee the bending losses (at 1550nm) to be less than 1dB for 100 turns of the fiber wound on a spool of 7.5cm diameter.

2.3.5. The optical emitters used for direct-modulation

Laser types

Principles A laser diode is a component able of producing radiations by stimulated emissions. In order to maintain alive the stimulation process, a cavity is used, to make the light beam travel several times through an amplifier, and is realized by a feedback loop called *resonator* or *resonating cavity* (Fig. 2.8). When the components of the laser are on a same line the cavity is called *linear* and corresponds to a *Fabry-Pérot*.

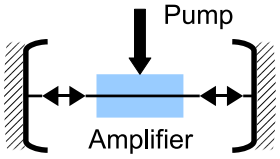

Figure 2.8.: Laser cavity for a Fabry-Pérot

In order to obtain the *laser effect*, a minimum of electrical or optical energy (pumping) has to be brought in the aim that, at each loop, the gain brought by the amplifier exceeds the losses of the mirrors and of the propagation through the cavity. The quantity of energy generating the gain which exactly compensates the losses is called the *laser threshold*.

Once the laser effect has started, it is to be noticed that some favored waves propagate in the cavity, and others are attenuated. The favored waves are called *longitudinal modes*: a longitudinal mode exists each time that the accumulated phase of wave during a round-trip values a multiple of $2 \cdot \pi$. In other words when the optical distance of the cavity round-trip corresponds to an integer multiple of the optical signal's wavelength.

However for systems requiring a single wavelength, a source having a single longitudinal mode is mandatory.

In order to conserve a single mode, the idea is to suppress the undesired modes by using the principle of Bragg reflections, which allows to filter and to let only a single wavelength pass through (Fig. 2.9a).

The using of Bragg gratings in DFB lasers is shown in Fig. 2.9b.

(a) (b)

Figure 2.9.: (a) Bragg grating; (b) DFB structure

Network usage According to [22], Fabry-Perot (FP) and Distributed Feed Back (DFB) lasers can be used at the OLT as well as at the ONUs in optical access networks. While FP lasers exhibit spectral line-width of 3nm, DFB lasers can have line-width as low as 0.001nm at a wavelength of 1500nm [25]. Therefore FP lasers are used primary at the 1300nm wavelength transmission window where the dispersion of S-SMF is low. Thus for bit rates greater than 1.25Gbit/s and distance greater than 10km FP lasers are not recommended in PON networks [22].

Finally cooled DFB laser diodes are preferred. The latter have wavelengths drift due to ambient temperature of 0.1nm degree Celsius. Yet they are more expensive than FP but at the CO, their usage is shared between the users.

Typical launch powers

Tab. 2.2 shows the maximum and minimum specified [17, 21, 31] optical launch powers, with respect to the different optical budget classes, when using a single fiber and bit rates of 2.5 and 1.25Gbit/s respectively in the downstream and in the upstream.

Even if in optical fibers the insertion losses depend upon the working wavelengths, the specified optical budgets apply to the 1490nm central downstream wavelength as well as to the 1310nm central upstream wavelength.

Chirp due to the laser

The chirp can be defined as the instantaneous change of the central frequency $f_0(t)$ in response to variations in the optical power. In other words, for an amplitude modulated optical wave this results in a residual frequency modulation. This frequency *chirp*, Δf, can be expressed as:

Table 2.2.: Specified G-PON network classes and their attenuations (fiber included), launch & receive powers at OLT and ONU

Network Class	**A**	**B**	**C**	**B+**	**C+**
Attenuation min [dB]	5	10	15	13	17
Attenuation max [dB]	20	25	30	28	32
OLT TX power min [dBm]	0	5	3	1.5	3
OLT TX power max [dBm]	4	9	7	5	7
OLT RX power min [dBm]	-23	-28	-29	-28	-32
OLT RX power max [dBm]	-8	-13	-29	-8	-12
ONU TX power min [dBm]	-2	-2	2	0.5	0.5
ONU TX power max [dBm]	3	3	7	5	5
ONU RX power min [dBm]	-21	-21	-28	-27	-30
ONU RX power max [dBm]	-1	-1	-8	-8	-8

$$\Delta f(t) = \frac{1}{2\pi}\frac{d\phi(t)}{dt} = \frac{\alpha}{4\pi}\left(\frac{1}{P(t)}\frac{dP(t)}{dt} + \kappa \cdot P(t)\right) \tag{2.6}$$

where $P(t)$ and $\phi(t)$ are respectively the instantaneous optical magnitude and phase.

The expression of $\Delta f(t)$ can be decomposed in two terms:

1. a transient chirp parameter: it evolves with the time derivate of the optical power and is function of α (called linewidth enhancement factor)

2. an adiabatic chirp term: it produces a frequency shift proportional to the instantaneous optical power and depends upon α and κ.

The analysis of the transient chirp term shows a dependency upon the time variation of the instantaneous optical power, and thus —for digital applications— a dependency upon the rise and fall times of the modulating signal.

When the optical source is intensity modulated (low modulation index m) by a sine wave of frequency f, a residual phase modulation (factor p) of each sidebands can be measured [32].

These factors are related as follows:

$$\frac{2p}{m} = \alpha\sqrt{1 + \left(\frac{f_c}{f}\right)^2} = \alpha\sqrt{1 + \left(I_0\frac{\kappa}{2\pi \cdot f}\right)^2} \tag{2.7}$$

where f_c is the chirp frequency and I_0 the bias current of the laser.

Fig. 2.10a illustrates the previous formula. Indeed, for a constant modulating frequency below 1GHz, the $2p/m$ ratio factor decreases with bias current. Whereas for modulating frequencies beyond 1GHz, the $2p/m$ ratio tends to converge asymptotically, no longer depending upon the bias current.

Finally, Fig. 2.10b shows the evolution of the transient (α) and adiabatic (κ) chirp factors with respect to bias current.

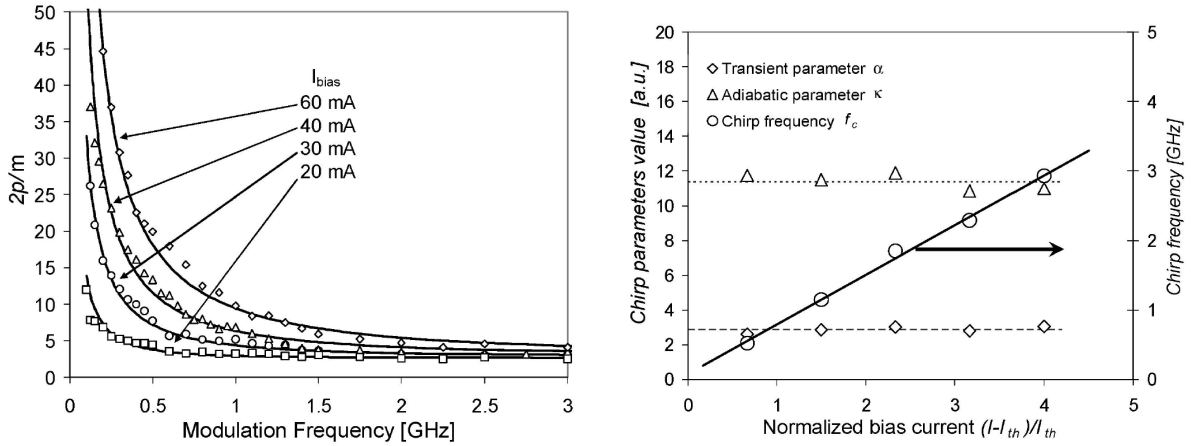

(a) (b)

Figure 2.10.: Example of Laser chirp values for different bias conditions, (pictures from [32]

Modulation bandwidths for a direct modulation

The modulation bandwidth of the lasers determines the maximum bit rate for which the laser can be used. For laser diodes (such as DFB lasers), the small signal modulation bandwidth can be approximated [25] by:

$$BW \propto \sqrt{I_{Bias} - I_{Threshold}} \tag{2.8}$$

Fig. 2.11a illustrates this relationship. Thus in high-speed transmissions, in order to increase the modulation bandwidth, the laser is biased as much above the threshold current as possible, while remaining below the laser's relaxation frequency.

According to [33], at bit rates of 10Gbit/s or higher the frequency chirp imposed by direct modulation (the injected current modulates the optical frequency [25]) becomes large enough that direct modulation of semiconductor lasers is rarely used.

For such high-speed transmitters, the laser is biased at a constant current to provide the CW output, and an optical modulator (such as a Mach Zehnder modulator) placed next to the laser converts the CW light into a data-coded pulse train with the right modulation format.

Relative Intensity Noise (RIN)

The stimulated emission of photons in the laser produces a coherent electromagnetic field. However, occasional spontaneous emissions add amplitude and phase noise to this coherent field, even when the laser is biased at a constant current with negligible current fluctuations [25, 33].

The results are a broadening of the (unmodulated) spectral linewidth and fluctuations in its intensity. The latter effect is known as Relative Intensity Noise (RIN).

Since such fluctuations can affect the performance of light-wave systems (demonstrated in §7.2, p. 112 and 7.3, p. 121), it is important to estimate their magnitude. The fluctuations

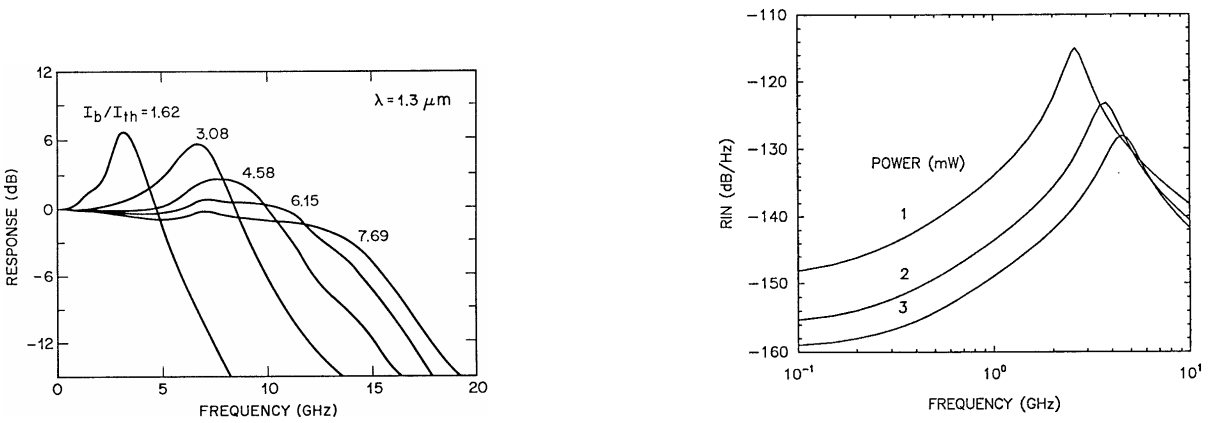

(a) (b)

Figure 2.11.: (a) Measured modulation response of a 1.3um DFB laser as a function of modulation frequency at several bias levels;
(b) RIN spectra at several power levels for a typical 1.55um semiconductor laser, (both pictures from [33])

are translated by the RIN figure of the laser (in dBc/Hz) with respect to the average emitted optical power.

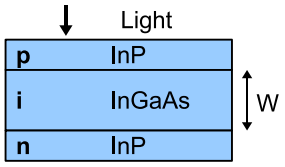

Figure 2.12.: PIN photo-detector (schematically)

2.3.6. The optical receivers

The optical receivers are made of an optical front-end containing the Photo-Detector (PD), which converts the photon-flow into an electrical signal (photo-current), and of an electrical pre-amplifier in order to amplify the detected photo-current.

Additional electrical circuitry filters the pre-amplified signal, and matches the electrical output impedance.

The main characteristics of the PD, in particular its responsivity and noise properties, have a significant impact on the receiver's performances. Furthermore in optical access networks, constraints such as costs, reliability and power consumption have to be taken into account.

The commonly used PDs are the PIN photo-detector and the Avalanche Photo-Detector (APD).

PIN

The simplest detector is the PIN photo-detector. A PIN photo-diode consists of a p-n junction with a layer of intrinsic (undoped) material sandwiched in between the p- and the n-doped material. The sandwiched material depends upon the working wavelength and thus upon the application. For telecommunication applications, InGaAs, which is sensitive in the 1000 to 1650nm range, is a common choice [25].

The junction is reverse biased (5 to 10V) to create an electrical field in the intrinsic material. Incident photons on the i-layer create electron-hole pairs, which under the electrical field are separated. As a result, a photo-current appears at the terminals.

The width W of the i-layer (Fig. 2.12) controls the trade-off between efficiency and speed of the detector. Indeed, the wider W is, the greater is the fraction[8] of incident photons which create electron-hole pairs. However the wider W is, the longer it takes for the electrons and holes to traverse the i-layer, thus making the photo-detector slower.

The responsivity of typical InGaAs PIN photo-detectors is in the range 0.6 to 0.9 A/W.

Noise Additionally to the signal current I_{PIN}, the PIN photo-detector produces a noise current known as *shot noise*. This noise current is a result of the photo-current being composed of a a large number of short pulses that are distributed randomly in time. Each pulse corresponds to an electron-hole pair created by a photon. The shot noise can be approximated to a white spectrum [25] with a mean-square of:

$$\overline{i^2_{n,PIN}} = 2q \cdot I_{PIN} \cdot BW_n \tag{2.9}$$

[8] this ratio is called the *quantum efficiency* and is function of the wavelength

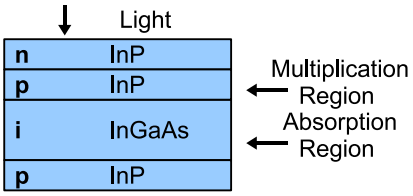

Figure 2.13.: APD photo-detector (schematically)

where I_{PIN} is the signal current, BW_n is the noise bandwidth of the measurement, and q the electron charge.

Dark current The PIN photo-detector produces a small amount of current even when it is not illuminated. This so called *dark current* according to [25] is less than 5nA for high-speed InGaAs photo-detectors, and its effect is often negligible.

SNR expression Finally the SNR at the output of the PIN, taking into account the shot and thermal noise of the receiver, can be expressed as follows:

$$SNR_{PIN} = \frac{I_{PIN}^2}{\overline{i_{n,PIN}^2} + \overline{i_{th}^2}} = \frac{(\eta_{OE} \cdot P_{in})^2}{\left(2q \cdot \eta_{OE} \cdot P_{in} + \overline{i_{th}^2}\right) \cdot BW_n} \tag{2.10}$$

where P_{in} is the received optical power, and η_{OE} the conversion efficiency of the photo-detector.

APD

Like the PIN photo-detector the APD is a reverse biased diode. However in contrast to the PIN photo-detector, it has an additional *multiplication region* (Fig. 2.13). This additional layer provides *gain* through avalanche multiplication of the electron-hole pairs generated in the i-layer (*absorption region*).

The gain of the APD is called *avalanche gain* or *multiplication factor*, and improves the responsivity by a factor M. It is to be noticed that this gain factor fluctuates around the average value M.

For light-wave systems operating in the wavelength range 1300 to 1600nm, Ge or InGaAs APDs must be used. However only the InGaAs APDs have bandwidths ranging from 1 to 10GHz. For such photo-detectors, M is typically limited to 10 because of a relatively low APD gain ($M \approx 10$) that must be used to reduce the noise [33].

These APD photo-detectors, in order for the avalanche process to set in, must be operated at reverse voltage of 20 to 40V [33].

Avalanche noise The SNR should be improved by a factor M^2 if the receiver noise was unaffected by the internal gain mechanism of APDs. Unfortunately this is not the case, and the SNR improvement is considerably reduced [33].

When taking the random nature of the gain process into account, the mean-square noise current from the APD is:

$$\overline{i_{n,APD}^2} = F \cdot M^2 \cdot 2q \cdot I_{PIN} \cdot BW_n \tag{2.11}$$

where F is the *excess noise factor* and I_{PIN} is the primary photo-detector current before avalanche multiplication.

In the ideal case, the excess noise factor is one ($F = 1$). For a conventional InGaAs APD, this excess noise factor is more typically around $F = 6$. The excess noise factor F increases with increasing reverse bias voltage (Fig. 2.14).

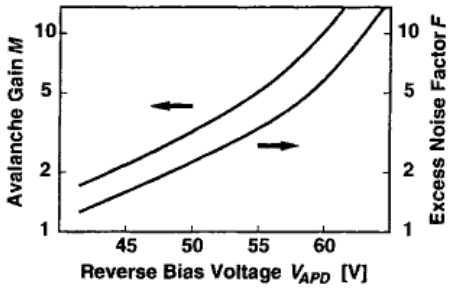

Figure 2.14.: Avalanche gain and excess noise factor of the APD versus the reverse bias voltage, (picture from [25])

F and M are related as follows:

$$F = k_A \cdot M + (1 - k_A) \cdot \left(2 - \frac{1}{M}\right) \tag{2.12}$$

where k_A is the *inonization-coefficient ratio* which depends on the used material. According to [25, 33], for InGaAs APDs, $k_A = 0.5$ to 0.7.

For $M = 10$ and $k_A = 0.5$ to 0.7, F values respectively 6 to 7.6 ($\equiv$ 7.8 to 8.8dB).

Optimum gain Because the avalanche gain can be increased only at the expense of producing more noise in the detector, there is an optimum APD gain at which the receiver becomes most sensitive. When expressing the SNR at the output of the APD and taking into account the shot and thermal noise of the receiver, then the SNR can be expressed as follows:

$$SNR_{APD} = \frac{I_{APD}^2}{\left(\overline{i_{n,APD}^2} + \overline{i_{th}^2}\right) \cdot BW_n} = \frac{(M \cdot \eta_{OE} \cdot P_{in})^2}{(2q \cdot M^2 \cdot F \cdot \eta_{OE} \cdot P_{in} + i_{th}^2) \cdot BW_n} \tag{2.13}$$

From this SNR expression, and the expression of F, a relationship for the optimum APD gain M_{opt} (for which the SNR is maximized), can be derived:

$$k_A \cdot M_{opt}^3 + (1 - k_A) \cdot M_{opt} = \frac{\overline{i_{th}^2}}{q \cdot \eta_{OE} \cdot P_{in}} \tag{2.14}$$

If we assume, $M_{opt} \gg 1$, then the previous relationship becomes:

$$M_{opt} \approx \left(\frac{\overline{i_{th}^2}}{k_A \cdot q \cdot \eta_{OE} \cdot P_{in}}\right)^{1/3} \tag{2.15}$$

The latter expression shows that M_{opt} decreases with an increase in P_{in}.

SNR comparison

From the considerations of the previous paragraphs, the SNRs for two distinct situations can be considered:

For a shot noise dominated situation:

$$SNR_{APD,opt} = \frac{1}{F} \cdot SNR_{PIN} \tag{2.16}$$

where typically $F = 6$ [25]. Then typically the APD's SNR is 7.8dB worse than the PIN's one.

For a thermal noise dominated situation:

$$SNR_{APD,opt} = M_{opt}^2 \cdot SNR_{PIN} \tag{2.17}$$

Assuming M_{opt} to value[9], around 7 to 10 [33], then the APD's SNR is 17 to 20dB better than the PIN's APD.

Conclusion

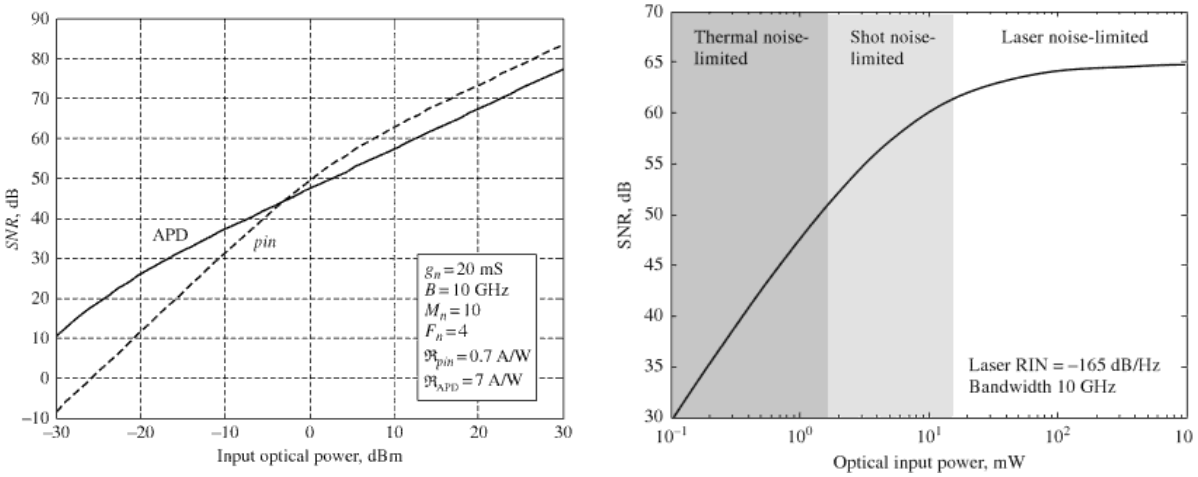

(a) (b)

Figure 2.15.: (a) SNR comparison of PIN and APD receivers with respect to the received optical power, (picture from [34]);
(b) SNR of a link as function of the received power, (picture from [34])

The typical launch powers in PON are around +5dBm, thus after the maximum transmission losses, in the range of 30dB, the received optical power is around -25dBm (3μW). According to Fig. 2.15b, the thermal noise dominates.

Finally it is the dominant thermal noise in practical receivers that makes the APDs attractive for optical communications simply because of their higher sensitivity as shown in Fig 2.15a.

[9] and furthermore assuming this optimal value to be reachable by tuning of the reverse bias voltage

2.4. Short-term evolution of PON architectures

Interest

While keeping the current down- and up-link bit rates of PONs, it is foreseen to increase the optical budget. The increased optical budget can be spent in two ways:

1. either increase the splitting ratio: hence in dense housing areas more customers can be served by a single OLT
2. either increase the reach of the PON: thus in sparsely inhabited areas the numbers of COs can be reduced

Finally in both cases the increased optical budget leads to COs dealing more customers than currently for coper. In order to limit the footprint at the CO, OLT with higher capacity are required.

Realization

The budget increase can be realized by a Reach-Extender (R-E), which may be [35]:

- a Semiconductor Optical Amplifier (SOA)[10],
- an Optical-Electrical-Optical (OEO) re-generator (with or without time synchronization).

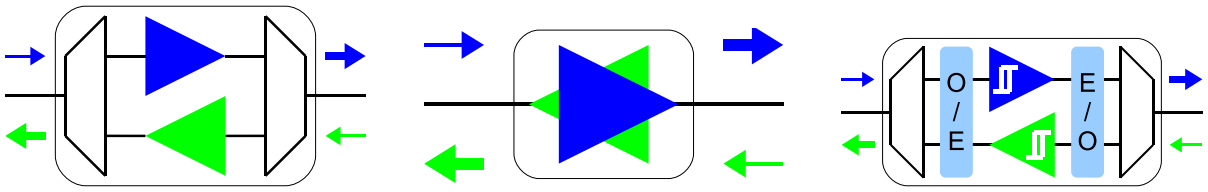

Figure 2.16.: Types of R-E : SOA (a) unidirectional (one per direction), (b) bidirectional, (c) O-E-O re-generator. The blue and green arrows symbolize the propagating wavelengths.

Possible architectural variations

Nevertheless from a pure PON point of view, a R-E allows to implement some of the afore mentioned architectural variants, such as:

- daisy-chaining two PONs thanks to a SOA [36],
- boosting the OLT egressing signal in order to increase the splitting ratio at the CO [23]
- reach-extension up to 135km by placing an in-line O-E-O re-generator [37],

[10]SOA work at the typical PON wavelengths of 1310 and 1490nm, whereas Erbium Doped Fiber Amplifiers (EDFAs) only work in the wavelength region of 1530 to 1570nm

2.5. The *next generation* PONs

The evolution of PONs aims at higher bit rates downstream as well as upstream, but also at higher splitting ratios and/or longer reaches.

The short-term evolutions are regrouped under the label *NGPON1* or *XGPON* which stands for the very next generation of PONs, whereas the label *NGPON2* refers to the on-going work of what the PONs beyond the NGPON1 may be look like beyond 2015.

NGPON1 architectures are developed around a legacy G-PON B+ Class architecture (Tab. 2.3, p. 36). Therefore these architectures have to cope with similar optical budgets, fiber length, splitting ratio, wavelength plan, neutral co-existence with G-PON. Finally *NGPON1* translates the technological improvements of current G-PON systems, while being compatible with.

On the opposite approach, *NGPON2* corresponds to architectures that may not necessarily be compatible with older generation and hence can be developed for *green field* deployment cases. This approach offers more degrees of liberty than *NGPON1*. Indeed the splitting ratio, splitting technique (not exclusively passive power splitters), fiber length, wavelengths, optical budget, and finally the modulation format can be modified.

Henceforth the label *NGPON* stands for both.

2.5.1. Co-existence aspects

One often required feature of *upgraded* telecoms systems is to guarantee co-existence with legacy systems. For PONs the two following aspects account for the most:

Wavelengths plan

The evolution of PONs makes mandatory the co-existence of several generations of systems over the same infrastructure. This transitional phase is called *migration* and leads to have a plan of the currently used and of planned wavelengths.

Currently the ITU [38] standardization body foresees that additionally to the now well established FTTH dedicated 1490+/-10nm and 1310+/-20nm G-PON wavelengths, the *future bands* wavelengths grids from 1360 to 1480nm and from 1565 to 1600nm are reserved for XG-PONs (Fig. 2.5.1), while the *enhancement band* from 1539 to 1565nm being reserved for video distribution (CATV) [39, 40]. The latter band allows RoF applications to exist in access networks and even using several wavelengths.

Optical budgets and infrastructures

To re-use the infrastructures, *NGPONs* must cope with the optical budgets and fiber lengths set by the already deployed infrastructures.

Therefore optical budgets were re-defined taking into account additional losses which can be spent on aggregation (by multiplexers) of legacy and NG-PON systems during a migration phase. This coexistence issu of G-PON and XG-PON on a common optical infrastructure features a class B+ optical budget, which is the *nominal requirement* [41, 42] as shown in Tab. 2.3.

Table 2.3.: Specified XG-PON1 network classes

Network Class	Nominal 1 (N1)	Nominal 2 (N2)	Extended (E)
Attenuation min [dB]	14	16	18
Attenuation max [dB]	29	31	33

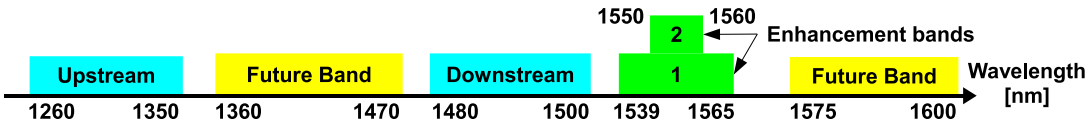

Figure 2.17.: ITU wavelengths plan

2.5.2. NGPON1

The NGPON1 aims at 10Gbit/s downstream bit rates.

The NGPON1 still uses NRZ line coding and is a short term solution given that the IEEE-flavored 10Gbit/s standard (IEEE 802.3av) was normalized in September 2009, whereas its ITU counterpart (ITU G.987.3–4) has been normalized during July 2010 [40].

Even if a compromise between the two standardization bodies could almost be reached on the wavelengths (Fig. 2.19), the two approaches however differ on the upstream bit rates.

Evolution of the upstream bit rates

For instance, the IEEE solution foresees an asymmetric solution with 1Gbit/s for the upstream, which can be extended to symmetric bit rates with 10Gbit/s in the upstream.

The ITU specifies an asymmetric solution (called XGPON1) with a 2.5Gbit/s downstream capacity. The symmetric solution with a 10Gbit/s upstream capability (called XGPON2) remains reserved for further study.

Scope of NGPON1

The IEEE solution's aim is limited at providing the specifications for a 10-Gbit/s physical layer, whereas the ITU approach has a broader scope and discusses more specialized topics such as:

- support of legacy services (POTS),
- native support of IP-TV,
- connectivity to wireless base stations (FTTCell wireless scenario), which itself requires:
  - a time synchronization service between the OLT and ONU
  - symmetric TDM services (Second Generation (2G) cell site backhaul)
  - symmetric and asymmetric packet-based services (3G/4G cell-site backhaul)

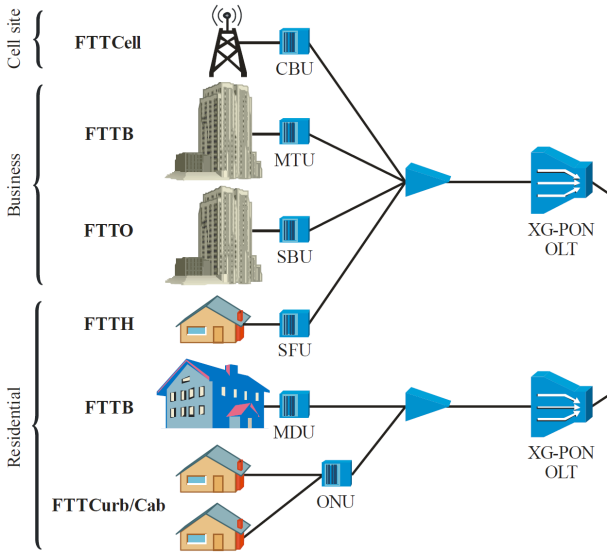

Figure 2.18.: Exemplary scenarios of XG-PON applications, picture from [41]

2.5.3. NGPON2

NGPON2 is a terminology describing what might the next optical access networks look like with a possibility to have a *from scratch* approach not considering any existing systems.

The aim of these architectures is to achieve bit rates of 40Gbit/s minimum in the downstream, where the target is to have 1Gbit/s sustained per user. In the upstream the goal is also to provide 1Gbit/s connection per customer.

Therefore several concepts are currently *discussed*[11]: OFDMA-PON, WDM-PON, and WDM-TDM-PON. These concepts can set the bounds for the fixe/mobile infrastructure convergence.

OFDMA-PON

Technique: The electrical signal which modulates the optical source is modulated (either directly or indirectly) according to an adaptive OFDM-scheme in the electrical domain.

Once the electrical frequency response of the channel is estimated, the bandwidth is sliced into sub-channels. According to the SNR of each sub-channel, the sub-carrier's modulation scheme is individually optimized: the higher the SNR of each sub-channel is, the more complex the modulation scheme is (from 4 to 32-QAM in [43]).

In downstream, this technique allows to use the full bandwidth of the transmission system.

In the upstream, the electrical spectrum is shared among the users, and user emits a portion of the electrical spectrum. If a single wavelength is used by all customers (which is the simplest implementation), the different (and not overlapping portions of electrical spectra) are recombined at the CO. However due to the drift of the lasers' central wavelengths, frequency guard bands have to be introduced.

[11] meaning not standardized yet

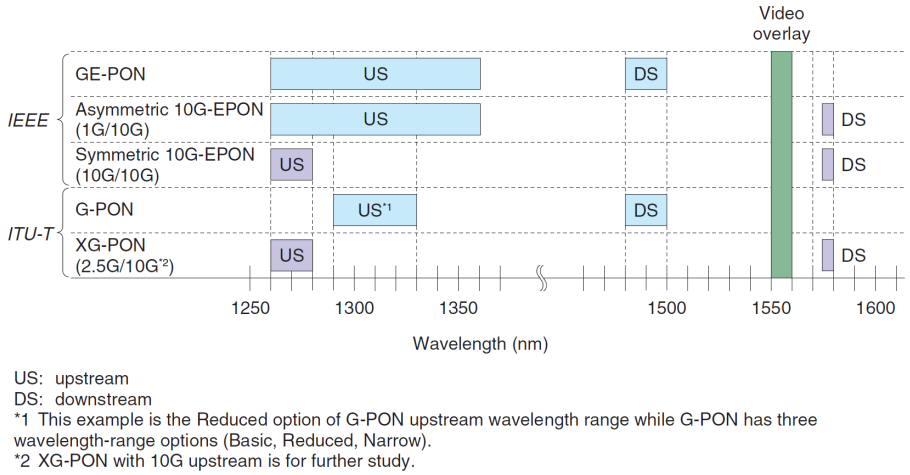

Figure 2.19.: Wavelength allocations of IEEE GE-PON & 10G-EPON and ITU-T G-PON & XG-PON (Picture from [40])

Benefit: The main benefit of this technique is the increased spectral efficiency (from 1/bit/s/Hz for NRZ to 4-5bits/s/Hz for OFDMA [43]), which allows to increase the bit rate while using standard components with limited bandwidth (since designed for NRZ-applications in Intensity Modulation and Direct Detection (IM-DD) systems).

For instance [43] transmitted a 10Gbit/s OFDMA-signal[12] using a DFB laser with a RF frequency bandwidth of 2.1GHz (at -3dB, Fig. 2.20) over a 26dB optical budget including 110km of S-SMF.

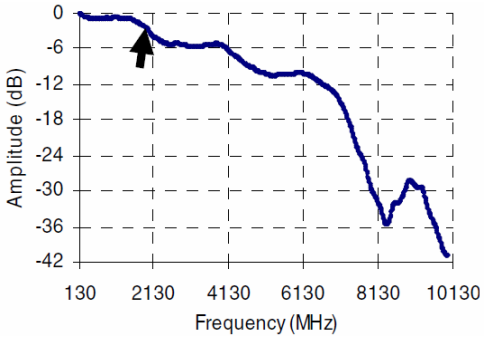

Figure 2.20.: Frequency response of the laser used by [43] for OFDMA modulation

When using standard components designed for 10Gbit/s NRZ applications, then thanks to the electrical OFDM modulation scheme, bit rates of 40Gbit/s are achievable, and this over optical link with an optical budget of 20dB including 100km of fiber. Also 255 users are served per wavelength.

Reach extension The reach or the splitting ratio of a PON-OFDMA can be increased by using a SOA or an Erbium Doped Fiber Amplifier (EDFA) (Fig. 2.21). This was demonstrated by [44] for 10Gbit/s OFDM signals.

[12] 64 sub-carriers, 31 effective data carriers, 15ns symbol length with 17% of cyclic prefix

Maximum Optical Budget (dB)		Electrical BW	No amplifier	SOA	EDFA
Bit rate: 2,5Gbit/s	NRZ	2,5GHz	35dB [1]	45dB [2] 50dB [5]	60dB
	OFDM	2,5GHz	34dB	60dB	71dB
Bit rate : 10Gbit/s	NRZ	10Ghz	30dB [2]	45dB [6]	55dB
	OFDM	2,5GHz	20dB	35dB (8Gbit/s)	45dB

Figure 2.21.: Total optical budget performances (direct modulation) comparison with NRZ or OFDM signals and with and without SOA or EDFA, (picture from [44])

Practical implementations issues: Yet, the afore reported bit rates are off-line performances. The real-time processing results show lower bit rates since the Fast Fourier Transform (FFT) and Inverse FFT (IFFT) operations are very computing intensive, and depend upon the number of processed sub-carriers.

WDM-PON

In a WDM-PON several wavelengths are used in the downstream (DS) as well as in upstream (US) [45], typically 32 to 40 per propagation direction are aimed (Fig. 2.22).

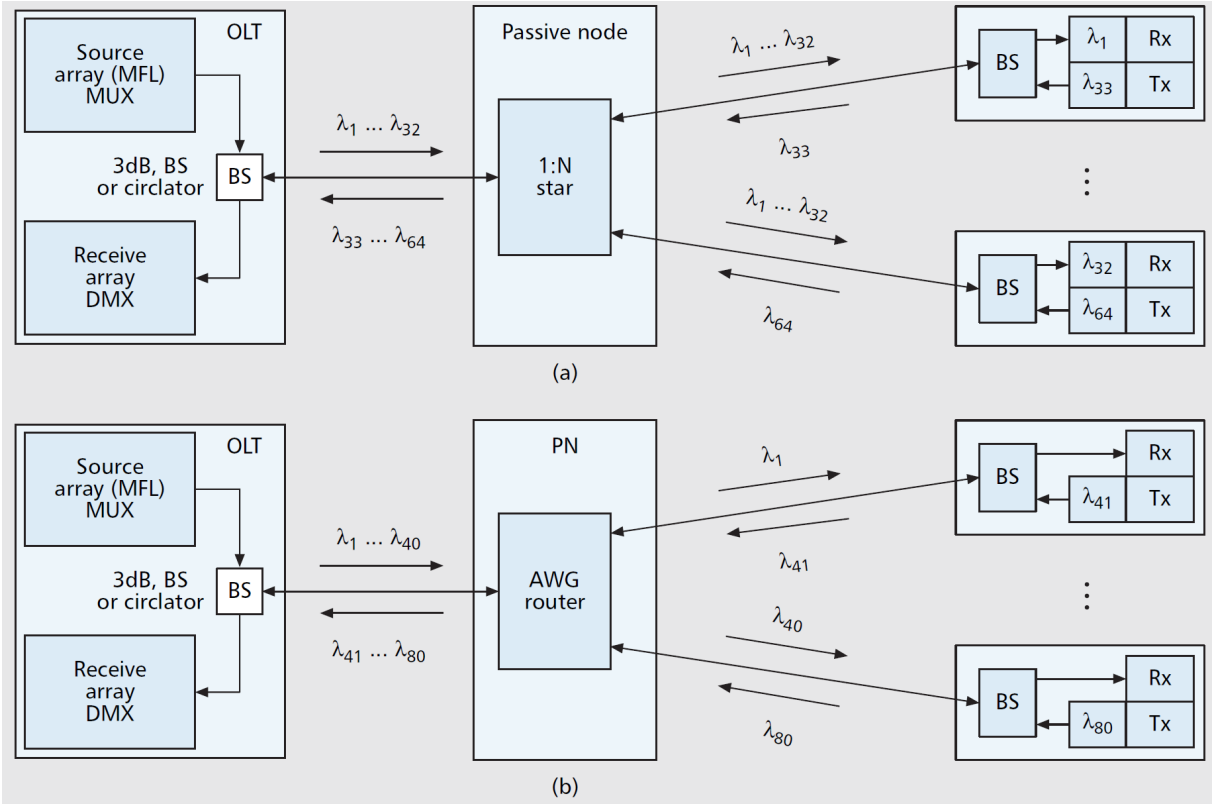

Figure 2.22.: Basic WDM-PON architectures: a) broadcast-and-select (BS) WDM-PON with splitter/combiner in passive node; b) AWG-based, (picture from [45])

Basic WDM-PON architectures , as shown in Fig. 2.22, make use of a fixed-wavelength laser array or a multi-frequency laser (MFL).

For the broadcast-and-select architecture shown in Fig. 2.22a, the OLT broadcasts all wavelengths in the DS through a passive 1:N splitter. Each ONU selects one of the DS wavelengths using an individual filter, and uses another individual wavelength for the US. As in the downstream, the US wavelengths are passively combined in the 1:N coupler. No identical ONUs can be used unless both the receiver filters and transmitters are tunable. The latter aspect is the weakest point of such an architecture [45].

In Fig. 2.22b, an AWG-based (arrayed waveguide grating) wavelength-routing PON is shown. Here, the AWG wavelength router replaces the passive splitter/combiner. This scheme offers lower insertion loss[13] In addition, no wavelength selective (individual) receivers (Rx) are necessary, thus simplifying the ONUs. However the transmitters (Tx) at the ONUs still have to emit at different wavelengths or to be at least tunable.

Whether a 200 or 100GHz array wave grating filter is used for separating the wavelengths, respectively 16 or 32 users can be served. The current state-of-the-art consists in 1.25Gbit/s per wavelength, with one wavelength per user. The typical reach is 20km for an optical budget of 10dB.

Colorless ONUs can resolve the issue of having different ONUs (not emitting at the same wavelength) as well as having ONUs with tunable laser sources.

The combination of a single fiber network and colorless, seed-based ONUs leads to reflective SOAs (RSOAs). Here, one end-facet of the SOA is fully reflective so that input and amplified and modulated output are both coupled to a single fiber at the other end. Alternatives to RSOAs are reflective electro-absorption modulators (REAM).

A block diagram of an PON with RSOA-based colorless ONUs is shown in Fig. 2.23: dedicated seed wavelengths from a multi-frequency laser (MFL) are used as input to the reflective ONU transmitters. The seed signals are not modulated in the OLT and can easily be separated in the ONUs by simple WDM splitters. Since dedicated wavelengths for the seeds are used, the number of ONUs is limited. In Fig. 2.23, transmit and receive signals in the OLT are also amplified (A) for higher maximum reach.

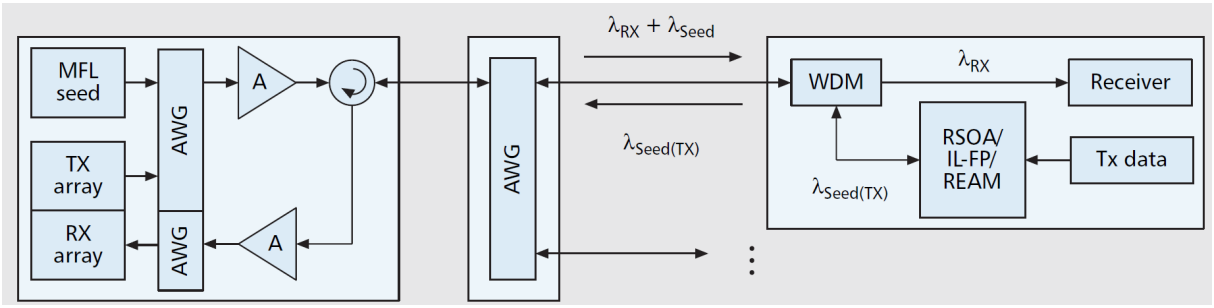

Figure 2.23.: Colorless ONUs for single-fiber working based on RSOAs, REAMs, or (Injection-Locked Fabry Perot Lasers) IL-FP lasers: different seed and DS payload wavelengths, (picture from [45])

[13] AWGs have typical insertion loss of 5 dB, independent of the number of wavelengths.

WDM-PONs can also run at different per wavelength bit rates for DS and US, i.e., 1G, 2.5G, 4G, or 10G, respectively. This provides scalability for both splitting ratio and per-ONU bit rate.

Comparing WDM-PON and 10GPON: according to [46] the 10GPON has more advantages in terms of standardization and maturity, costs and energy consumption than the WDM-PON. Yet the latter offers higher bandwidths and longer reaches.

For these reasons, a tendency according to [46] *would* be to use 10GPON for residential customers, whereas the WDM-PON *could* be envisaged for business and and backhaul applications where higher bandwidths are needed.

WDM-TDM-PON

The idea is reproduce the way a legacy PON works (TDM/TDMA) but for several wavelengths. This results in a wavelength pool shared (statically or dynamically) among all the users of the PON instead of allocating a couple of wavelengths to each ONU [4].

Current state-of-the-art is to have a 2.5Gbit/s bit stream per wavelength. 32 of such channels are aggregated by a 100GHz AWG. Finally this allows to serve 1024 customers for a reach of up to 60km and for a maximal optical budget of 20dB.

Conclusion

We have shown the main architectural variations of current optical access networks.

More specifically the performances (bit rates and optical budgets) and main properties (wavelengths, multiplexing protocol) of PON networks have been discussed. This allows to set the framework within which the discussed (in Part 2) and the proposed (in Part 4) Radio over Fiber (RoF) architectures will have to evolve.

Also the optical properties of the components (emitters, power splitter, optical fiber, and receivers) building the optical link of PONs have been presented and discussed.

Finally the properties of the optical access networks of the close-future and more long-term have been summarized.

3. The mobile radio access networks

3.1. Generalities

This chapter describes the main characteristics of mobile radio systems and signals, and the main Figure Of Merits (FOMs) applying to them. These radio signals' properties will guide the design of the RoF link. Whenever possible the description of the characteristics and FOMs are general, yet some explanations rely on examples for which we will use the Universal Mobile Telecommunications System (UMTS) Frequency Division Duplexing (FDD) standard.

Since the latter is the reference radio standard used in this thesis for simulation and measurements, its properties are described in a second step.

3.1.1. Carrier frequencies

The choice of the frequency range for carriers depends mainly on the following criteria:

the targeted range

According to [47], the attenuation in free space propagation in air (called free-space path loss) is directly proportional to the inverse of the product of the square of the distance and the frequency (Fig. 3.1).

$$\frac{P_r}{P_t} = G_t \cdot G_r \cdot \left(\frac{\lambda}{4\pi d}\right)^2 \tag{3.1}$$

P_t and P_r are respectively the delivered power to the transmit antenna and the available power at the receive antenna. G_t and G_r are respectively the transmitted and the received antenna gains. λ is the wavelength of transmitted electrical signal, and d is the distance between the antennas.

the atmospheric propagation conditions

According to [48], the frequency band below 10GHz does not suffer from attenuation due to the oxygen and water molecules of the atmosphere which absorbs energy beyond 10GHz, and cause an increased path loss.

the availability of spectrum

As a result of these trade-offs, the preferred carrier frequencies for mobile Radio Access Networks (RANs) are ranged within 700MHz and 3.5GHz.

Additionally to the two previous physical considerations, a more practical issue is to be considered for the carrier frequency choice: the availability of free spectrum. Fig. 3.2

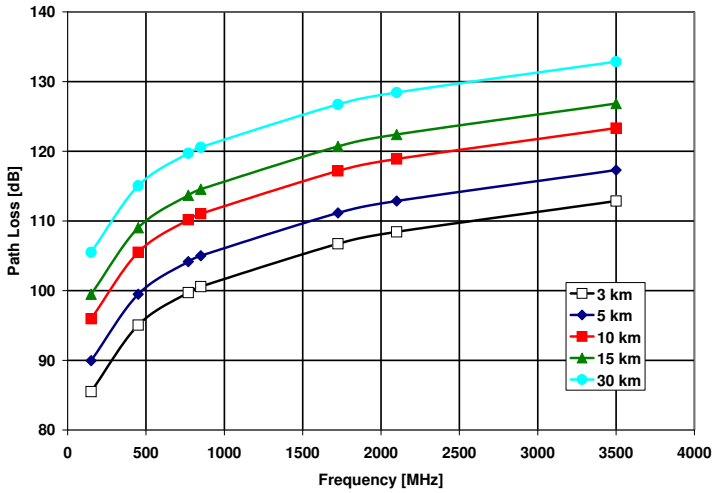

Figure 3.1.: Free-space path loss as a function of the frequency for different link distances for isotropic antennas ($G_{t/r} = 1$)

shows the current available spectrum bandwidth for mobile communications in Western Europe.

The 2G systems traditionally use the *GSM 900* band (890 to 915MHz and 935 to 960MHz) and its contiguous extension band *GSM 900 +* (880 to 890MHz and 925 to 935MHz). Also 2G uses the *GSM 1800 band* (1710 to 1785MHz and 1805 to 1880MHz).

The 3G UMTS systems currently use their initially allocated *core band* (1920 to 1980MHz and 2110 to 2170MHz). Yet recently the spectrum regulation agencies have allowed 3G systems to co-exist in the *GSM 900 band* with legacy 2G systems [49]. This operation is called *refarming* and intends to offer the following advantages:

- better in-building coverage in urban environment
- better range in rural areas with two to three times fewer sites

Fig. 3.3 shows how 900MHz cells can complement the urban coverage achieved with the 2.1GHz band.

Furthermore the 2.6GHz band (2500 to 2570MHz and 2620 to 2690MHz) is currently under discussion for allocation to 3G and up-coming 4G systems.

The 4G systems are expected to benefit from the *digital dividend* in the 800MHz band (790-821MHz and 832-962MHz) thanks to progressive switch-off of analog TV services. Furthermore the 2.6GHz band and the 3.5GHz band[1] (3410 to 3494MHz and 3510 to 3594MHz) offer the possibility of deploying wide radio channels of 20 and even 50MHz.

Finally spectrum of extinct systems are to be granted to 4G.

[1] especially in urban environments

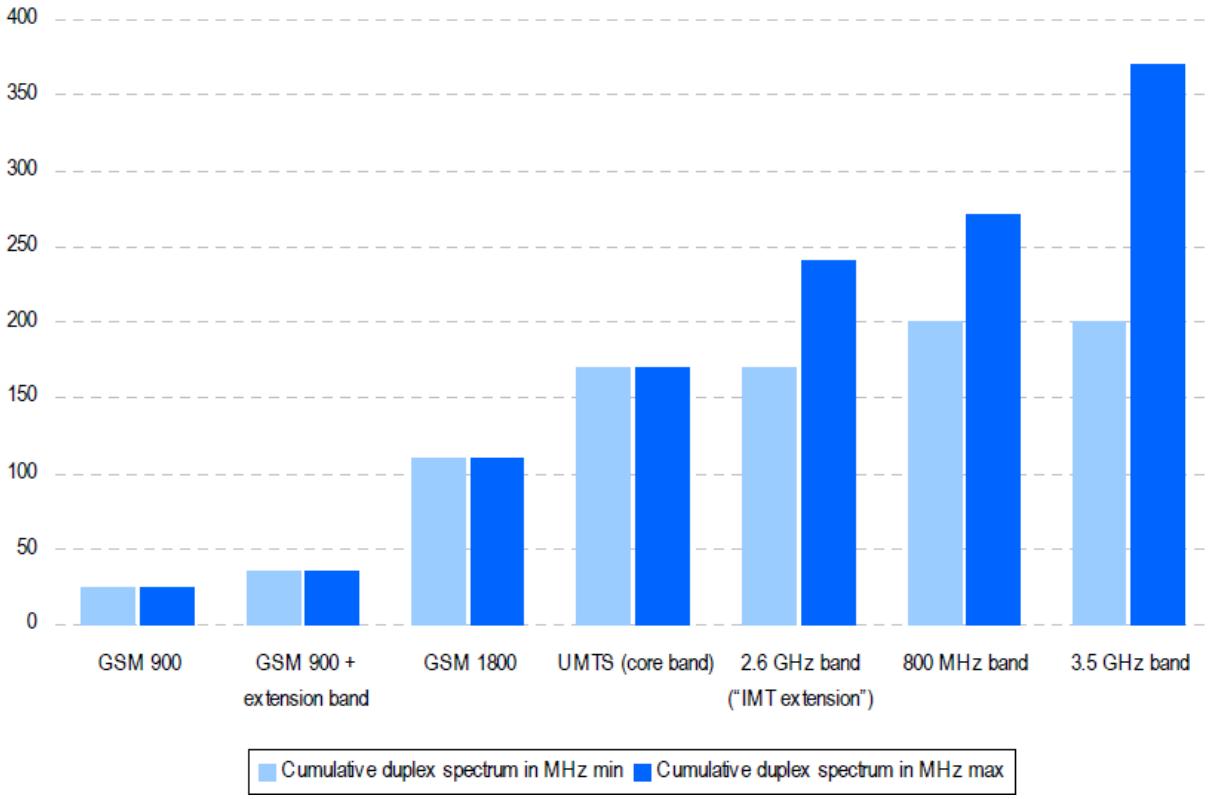

Figure 3.2.: Optimistic and pessimistic cumulative spectrum bandwidth availability in Western Europe (in MHz), (picture from [49])

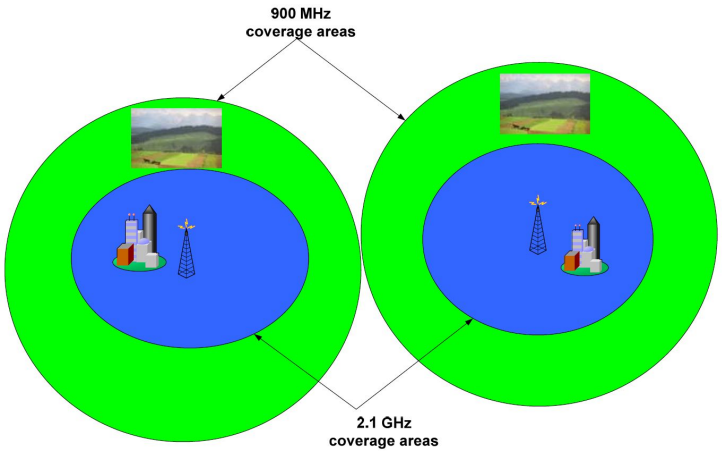

Figure 3.3.: Re-use of the 900MHz band for improved 3G coverage

3.1.2. The targeted bit rate

The rough physical bit rate results from the product of the channel bandwidth and the spectral efficiency:

$$\text{Bit rate [Mbit/s]} = \text{Channel width [MHz]} \cdot \text{Spectral efficiency [bit/s/Hz]}$$

the spectral efficiency

The spectral efficiency itself is linked to the modulation scheme. For instance a BPSK modulation scheme has a rough efficiency of 1bit/s/Hz, while a 16-QAM has a spectral efficiency of 4bit/s/Hz.

Furthermore these rough efficiencies are lowered by redundancy and encoding schemes which make the transmission to become more robust against impairments during the transmissions but at the expense of the overall efficiency.

Thus for a given slice of spectrum (channel), the more complex the modulation scheme is, the higher the spectral efficiency is and thus the higher the bit rate that can be transmitted by the systems is.

Technology	FDD Channel	Spectrum efficiency	Data rate per sector
GSM	200 KHz	<0.1 bps/Hz	
EDGE	200 KHz	<0.1 bps/Hz	
WCDMA	5 MHz	0.15 bps/Hz	
HSPA	5 MHz	0.5-0.9 bps/Hz	3.75 Mbps
LTE	10 MHz	1.5 bps/Hz	15 Mbps
LTE 4 x 4 MIMO	10 MHz	1.8-2.4 bps/Hz	20-30 Mbps

Figure 3.4.: Spectrum efficiency of different radio standards, (picture from [49])

the channel width

As shown in Fig. 3.4, the channel width increases with recent radio standards:

- for 2G systems (GSM and EDGE), the channel width is 200kHz.
- for 3G systems (initial WCDMA, and its evolution HSPA), the channel is 4.68MHz wide. Yet a 5MHz portion of spectrum is allocated.
- for 4G systems (LTE, and its evolution with multiple transmit and receive antennas), the channels widths range from 1.4, 3.5, 5, 10, 15 and 20MHz.

3.1.3. The technological maturity

The realization of systems with increasing complexity such as higher order modulation, higher carrier frequencies, and wider channels depends on the trade-off of between their feasibility, miniaturization, maturity, and costs.

Finally a trade-off of all these considerations has lead the frequency range from 700 to 900MHzto be called the *golden frequencies*.

3.1.4. The air channel

Eq. 3.1 exposed the theoretical free-space path loss. Yet because of the variety of environments (constructions (rural, sub-urban, urban), terrain (hilly, flat), vegetation ...) additional models take into account the experimental path loss measurements.

Ideal two path propagation through reflection

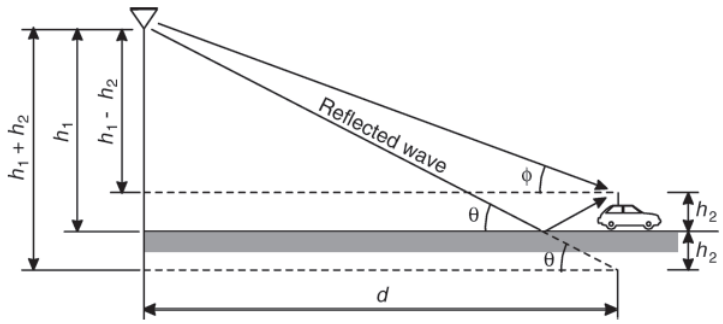

Figure 3.5.: Model for two-path reflection due to reflection, (picture from [50])

Additionally to the losses caused by the distance, a radiated wave also loses energy through reflection, transmission and diffraction due to obstacles. For the relatively simple case scenario of two-path propagation over a reflecting surface (Fig. 3.5), the initial free space loss formula of Eq. 3.1, becomes (for $d \gg h_1, h_2$):

$$\frac{P_r}{P_t} = G_t \cdot G_r \cdot \left(\frac{h_1 h_2}{d^2}\right)^2 \tag{3.2}$$

For this special case, as in shown in Eq. 3.2, the loss is not depending upon the wavelength [51], and the received power decreases propositionally to $1/d^4$ instead of $1/d^2$.

Terrain-adapted propagation through reflection

Finally, the pathloss coefficient γ can be introduced in order to model various terrains:

$$\frac{P_r}{P_t} = G_t \cdot G_r \cdot \left(\frac{\lambda}{4\pi}\right)^2 \cdot \frac{1}{d^\gamma} \tag{3.3}$$

where $\gamma = 2$ corresponds to the initial ideal free space propagation, $\gamma = 5$ is for strong attenuations caused city buildings, and $\gamma = 3.5 \ldots 6$ in buildings [50].

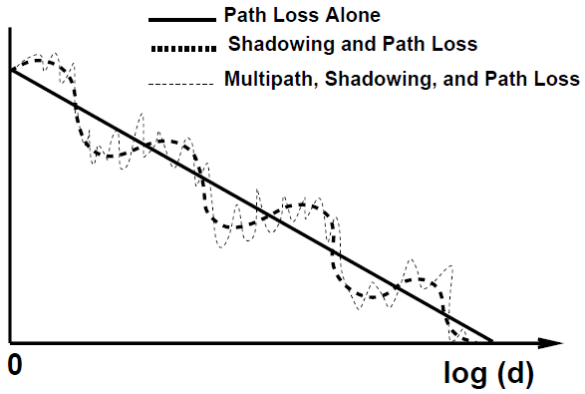

Figure 3.6.: Schematic superposition of path loss, shadowing and fast fading; (figure from [53])

Fadings

Complementing the previous enhanced static model of the path loss, they are statistical models. Fading refers to fluctuations in the amplitude of a received signal that occur leading to propagation related interference.

These models are split into two categories and called the *slow* and *fast fading*, and are schematically summarized in Fig. 3.6. The distinction between slow and fast fading is related to the *coherence time* T_c of the channel, which measures the period of time over which the fading process is correlated.

The fading is said to be slow (10 to 40sec [52]) if the symbol time duration T_s is smaller than the channel's coherence time T_c; otherwise it is considered to be fast.

In slow fading a particular fade level will affect many successive symbols, which leads to burst errors, whereas in fast fading the channel varies from one symbol interval to the next.

Finally, the main interest of fading phenomenon is the standard deviation which allows to design the link budget.

Multipath propagation caused by reflection and the scattering of radio waves lead to a situation in which transmitted signals arrive phase-shifted over paths of different lengths at the receiver and are **randomly** superimposed there (Fig. 3.7). This interference, called multipath fading, can strengthen, distort or even eliminate the received signal.

Furthermore, a typical feature of multipath propagation (frequency-selective with broadband signals) is the existence of drops and boosts in level within the channel bandwidth that sometimes fall below the sensitivity threshold of the receiver or modulate it beyond its linear range [50].

This type of fading is relatively fast and is therefore responsible for the short-term signal variations. Worst case estimations of multipath fading account for 20 to 30dB of the link margin [54].

Slow fading The link quality is also affected by slow variation of the **mean signal level** due to the *shadowing* from a large obstruction such as a hill or large building obscures the main signal path (Line-of-Sight (LOS)) between the transmitter and the receiver. [52].

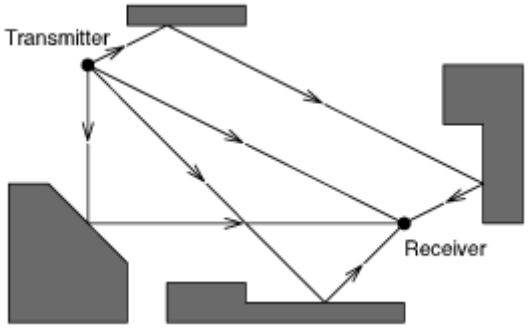

Figure 3.7.: Multipath

The amplitude change caused by shadowing can be modeled (revealed by empirical measurements) by a log-normal distribution with a standard deviation from the theoretical log-distance path loss model [55]. Therefore the expressed path loss is fitted to the following model:

$$PL(d)_{dB} = A + 10 \cdot n \cdot \log(d/d_0) + \chi$$

where A is the theoretical free space path loss.

Then former equation can be expressed as:

$$PL(d)_{dB} = PL_0 + 10 \cdot n \cdot \log(d) + \chi$$

where PL_0 is the free-space path-loss for the reference distance, n the path loss exponent, d the distance between the transmitter and the receiver, d_0 the reference distance, and χ models the shadow effect.

In practical situations the standard deviation of shadow fading does not exceed 9-10dB [52].

An example of the path loss measurement in a suburban environment corresponding to a mixed LOS and Non-Line-of-Sight (NLOS) scenario is given in [56].

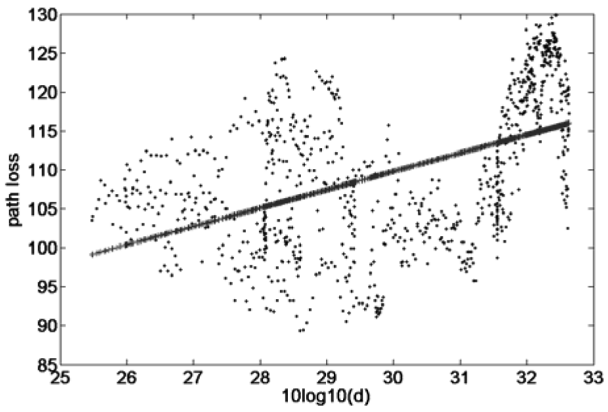

Figure 3.8.: Measured (dots) and modeled (continuous) path loss at 2.3GHz (figure from [56])

For the measured points at 2.3GHz in Fig. 3.8, the path loss is modeled as:

$$PL(d)_{dB} = 43 + 22 \cdot \log(d) \tag{3.4}$$

Thus the pass loss exponent is 2.2, with standard deviation of 9.3dB.

For frequencies of 2.6 and 3.5GHz the reported path loss exponent, increases with respect to the frequency, and values respectively 2.6 and 3.6 —while the standard deviation remains almost unchanged at 9.4 and 9.5dB.

[56] compares the measured path loss to other reported measurements in which for a pure urban scenario the exponent increases by 0.5 to 1 compared to that of a suburban scenario.

3.1.5. Radio link margins

Emission power and receiver noise floor limitations

Given that a Base Station (BS) can emit more power than an User Equipment (UE) —typically 50W for the first, and 5W for the latter— and that the mobile receivers have limited sensitivities, the resulting path loss link budgets have a budget margin (losses allowed between the TX and the RX) within which the communication can be established.

Furthermore, when modelling the TX and RX with *typical* values [48] where the antenna gains[2] are modelled by $G_t = 7$dBi and $G_r = 3$dBi, and additional cable losses are added to each side ($L_t = L_r = 2$dBi), a typical sensitivity of -119dBm can be computed at the two receiving sides.

For given frequency and range, the minimum of the downlink and uplink margins, will be the margin actually limiting the range of the communication for a bidirectional communication scheme.

Fig. 3.9 shows a decreasing link margin as the frequency and the range increase.

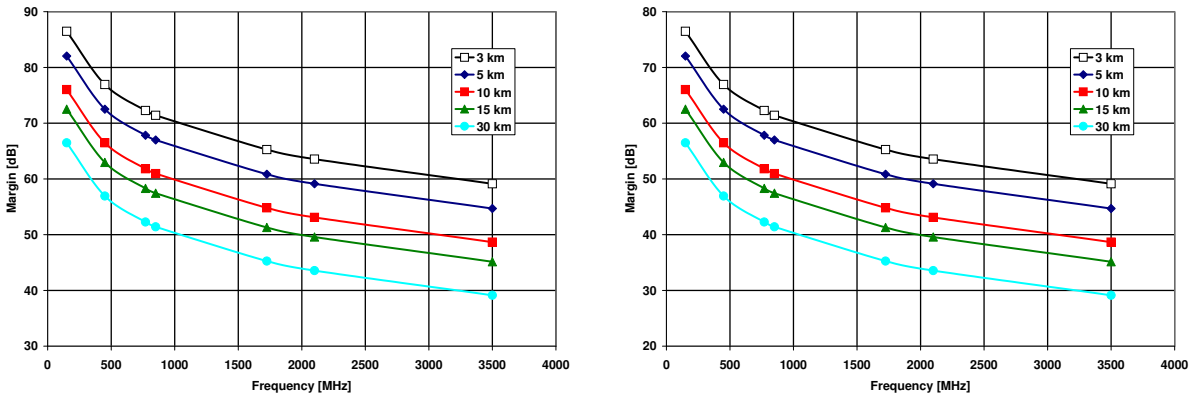

(a) (b)

Figure 3.9.: Path loss link margins for (a) the downlink, and (b) the uplink, as a function of the frequency for different link distances

For instance, Fig. 3.9 shows for a 2.1GHz downlink carrier frequency and target cell ranges of 5 and 15km link margin of respectively 60 and 50dB.

Finally these computed link margins, and are to be spent for SNR and fading issues.

[2]expressed in dBi which is the gain of the considered antenna with respect to an isotropic antenna

Cumulated fading margins

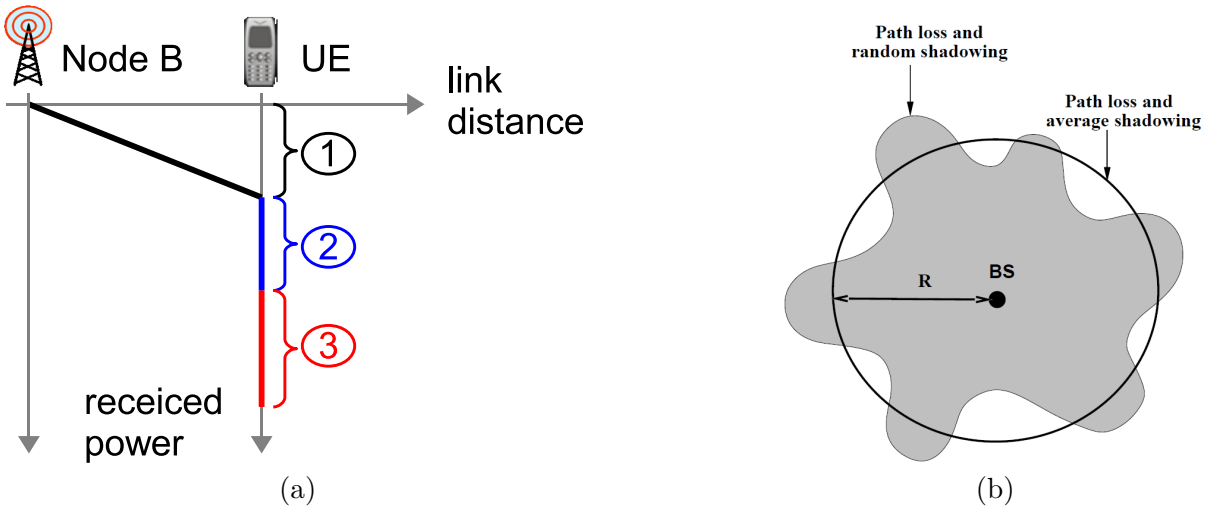

(a) (b)

Figure 3.10.: (a) Cumulated fading **margins** increase the link margin required by free space propagation losses;
(b) Issue of random and average shadowing on the received power, (figure from [53])

As shown in Fig. 3.10a, the different fading issues cumulate and affect the link margin additionally to the loss of the free space model:

- ① is the mean path loss function of the link distance,
- ② is the shadowing margin (worst case: 6 to 10dB),
- ③ is the fast fading margin (worst case: 20 to 30dB)

Finally a conservative link margin budget shows that 26 to 40dB[3] are to be spent for fading issues. The remaining margin is to be spent for SNR requirements, and noise figures of the receiving equipment.

Fading effects on the cell coverage area

Let's consider a base station inside a circular cell of a given radius R. Within the cell, any UE requires a minimum received SNR for acceptable performance. If we assume a reasonable noise and interference level to exist, then from the SNR requirements a minimum received power can be derived. The transmit power at the base station (Node B) is designed to deliver the required average receive power at the cell boundary of radius R. Yet if the shadowing effects cause some locations within the cell to have power levels belows the required minimum, others places may experience excessive received powers.

Fig. 3.10b illustrates the issue of the contour of a constant received power (based on a fixed transmit power at the base station) for path loss with additional average or random shadowing:

[3] to be added to the 50 to 60dB of free-space path loss

- for path loss and average shadowing constant power contours form a circle around the base station, since combined path loss and average shadowing is the same at a uniform distance from the base station.
- for path loss and random shadowing the contours form random variations about the average.

The constant power contours for combined path loss and random shadowing indicate the challenge shadowing poses in cellular system design. Finally it is not possible for all users at the cell boundary to receive the same power level. Thus, the base station must either transmit extra power to insure users affected by shadowing receive their minimum required power , which causes excessive interference to neighboring cells, or some users within the cell will not meet their minimum received power requirement.

3.1.6. Duplexing schemes

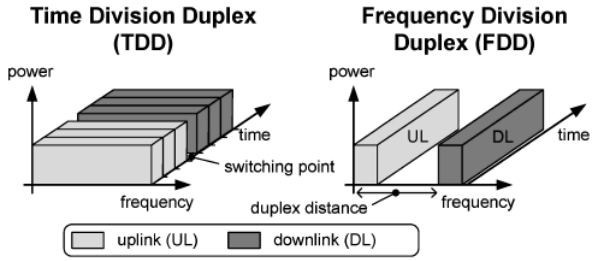

Figure 3.11.: Duplexing schemes, (picture from [50])

Radio communications systems either use a half duplex or full duplex mode. In a half duplex communication scheme only one interlocutor (NodeB or UE) can communicate at the same time, since the transmission medium (carrier frequency) is shared. Whereas in a full duplex communications scheme each interlocutor can communicate at the same time.

Frequency Division Duplexing (FDD)

In the FDD method, the uplink and downlink communications use each different carrier frequencies. Thus a real full duplex communication scheme is possible.

Yet due to the simultaneous transmissions, the transmission must not degrade the reception. Therefore FDD requires spacing between transmit and receive bands and uses paired spectrum. Furthermore stringent duplex RF filters (in order to limit the emitted noise in the receiving band) are required.

In paired spectrum, the upper frequency band is used for downlink (DL) transmissions (from the BS to the UE), while the lower frequency band which suffers less path loss is used for the uplink (UL) transmissions since the UE is designed to transmit less power than the BS (see §3.1.1, p. 42).

Time Division Duplexing (TDD)

In a TDD duplex mode, the same frequency is used alternatively for the uplink and downlink transmissions. Thus a TDD system requires less spectrum.

The transmitted signal carrier does not interfere with the received signal. Hence the RF filter requirements are relaxed.

Since radio signal propagation durations have to be taken into account in order to avoid a partial time overlap and potential interference of data packets originating from different emitters, guard times between transmission and reception are required, and thus larger cells leads to larger guard times. These guard times also lead to a less efficient use of the allocated channel since packets cannot use the full slot for data transmission [50].

Furthermore TDD requires guard bands between operators [49] since according to [57] the produced interferences are sometimes higher than for FDD.

Service approach

For voice services which require symmetric traffic allocation, FDD is the better approach.

However for data services such as Internet browsing, TDD thanks to its asymmetric traffic capability is more efficient since it better adapts data rates (in the downlink as well as in the uplink) to services requirements [49].

UMTS systems

For UMTS systems both duplex schemes are possible. However the FDD is currently the most deployed scheme in the world, except for China [49] which uses a specific variation[4].

As a consequence of these duplex modes, the requirements in terms of radio interferences are more stringent for the FDD mode in order to prevent leakage from the TX path into the RX path and vice versa. Indeed for the downlink, the FDD mode requires high isolation between neighbor channels (see §3.3.2, p. 64). Indeed FDD requires 12dB more of isolation than its TDD counterpart.

3.2. The Universal Mobile Telecommunication System (UMTS) standard

3.2.1. Initial standard

Principle of the code diversity (W-CDMA)

The Wide-Band Code Division Multiple Access (W-CDMA) relies on an base of orthogonal *codes*, for which the inter-correlation tends to have a Power Spectral Density (PSD) of that of *white noise* [58]. The multiple access schemes of UMTS —as well in the downlink as in the uplink— rely on this characteristics of the codes for distinguishing the physical channels and thus the different users. Finally this allows the later to communicate at the same time on the same frequency.

[4]TD-SCDMA: Time Division Synchronous Code Division Multiple Access

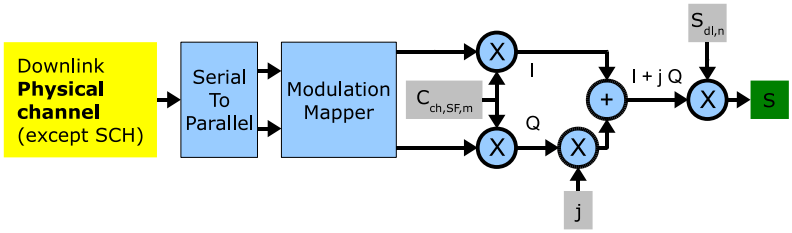

Figure 3.12.: Channelization & Scrambling of a Physical Channel,
where $C_{ch,\ SF,\ m}$ is the channelization sequence of code number m and of spreading length SF; $S_{dl,\ n}$ is the n-th downlink scrambling code. *SCH* refers to the physical synchronization channels

Physical channels

A physical channel exists electrically in opposition to a logical channel, which serves protocol issues. UMTS divides the physical channels into two categories:

- payload and signalization carrying physical channels,
- and, simple physical synchronization channels.

Channel coding

At emission the principle consists in multiplying each data bit of the physical payload & synchronization channels by a constant sequence of N bits called *chips*. N is called the Spreading Factor (SF). This substitution is called *channel coding* or *spreading*, since the spectrum of the signal is broadened by this operation.

For instance a physical channel having a bit rate of 30kbit/s, can be decomposed in I and Q channels of 15kbit/s each. When applying a spreading code of factor 256, the signal will have, after complex recombination, a symbol rate of 3.84Mchip/s for each I and Q channels, and an overall bitrate of 7.68Mbit/s (Fig. 3.12).

It is actually the channel coding (Fig. 3.13) that allows to superimpose electrically the different physical channels (*i.e.* the communications toward/from the different users), without losing information.

Scrambling

The physical channels, once channelized, are *scrambled* by a specific code which *signs* the signal[5]. The scrambling codes **do not** affect the width of the signal's spectrum since this operation *multiplies* the data but keeps the number of symbols constant.

In the downlink this operation allows the terminals to discriminate signals emitted from different base stations (whether from identical or different carrier frequencies as well originating from the same as from different operator(s)) received in a same cell.

In the uplink, this allows the base station to separate the terminals. Furthermore the latter operation allows the hand-over.

[5]Except some *basic* synchronization channels are not scrambled

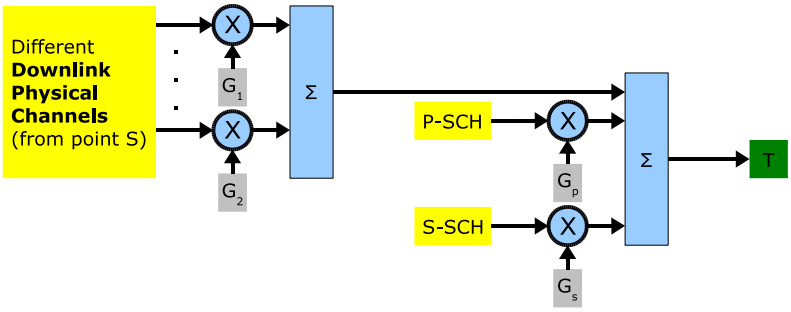

Figure 3.13.: Weighting & Summing of Complex Channels,
where P-SCH and S-SCH refer to physical synchronization channels, and G_1, G_2, G_p, and G_p refer to the gains of the weighting process

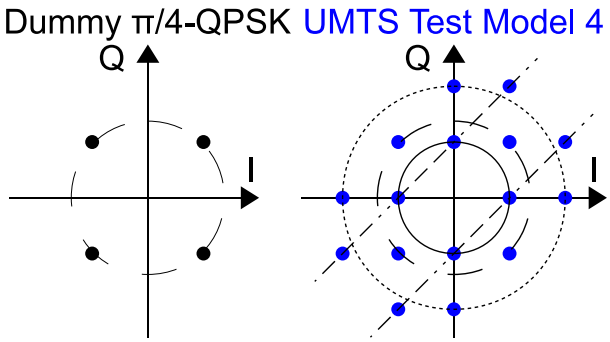

Figure 3.14.: Constellations of (left) a simple $\pi/4$-QPSK, and (right) of an UMTS Test Model 4 signal

After scrambling, the different channels are weighted before being added electrically (Fig. 3.13). The weighting allows to balance the power ratios between the signalization and the payload channels.

Constellation

The summing of the different physical channels with different weights and modulations formats (synchronization channels use BPSK, the other channels use QPSK with different angular offsets) results in a constellation diagram looking like 16-QAM. For instance Fig. 3.14 shows the constellations diagrams of a *simple* QPSK, and constellation of an UMTS test signal (Downlink Test Model 4[6] , [59]) specified for measuring the Composite Error Vector Magnitude (EVM).

Pulse-shaping

Before broad-casting the RF signal and prior to up-mixing, the I and Q parts of the summed channels pass though a pulse-shaping filter (Fig. 3.16). This operation allows to pass from discrete state to continuous signals.

[6]relative powers of the shown example: P-CPICH: 0dB, P-SCH: -3dB, S-SCH: -3dB, P-CCPCH: 0dB

In order to minimize ISI, a raised-cosine-filter (approaching the ideal Nyquist symbol filter) is implemented in UMTS systems by placing, at the emitter and at the receiver, a Root-Raised Cosine (RRC) filter.

The specified pulse-shaping RRC filter (discrete-time finite impulse response, FIR) has a bandwidth of 3.84MHz and a roll-off factor of 0.22. Since the summed UMTS channels have a chip rate of 3.84Mchip/s, the final pulse-shaped UMTS carrier occupies 4.68MHz of spectrum.

Importance of the pulse length The pulse length determines the number of symbols periods over which the filter impulse response is considered in the I/Q calculation. The pulse length has a considerable effect on the modulation accuracy.

For instance, with GSM, a pulse length of 5 bits or greater is required. In order to obtain highly accurate signals, a great impulse length (> 20) is required for UMTS.

Indeed, the impulse length's effect of a RRC filter (with a roll-off factor 0.22) on the out-of-band emission (at transmission) and selectivity (when receiving) is shown in Fig. 3.15. The PSD output levels differ by about 30dB whether the filter is truncated to 8 chip durations (top curve) and 32 chip durations (bottom curve).

In W-CDMA networks, the filter of the receiving UE are truncated to 8 chips in order to lower the computational burden while maintaining an acceptable spectral trade-off. Finally this makes the UE sensitive to in-band emissions of adjacent band operators [60].

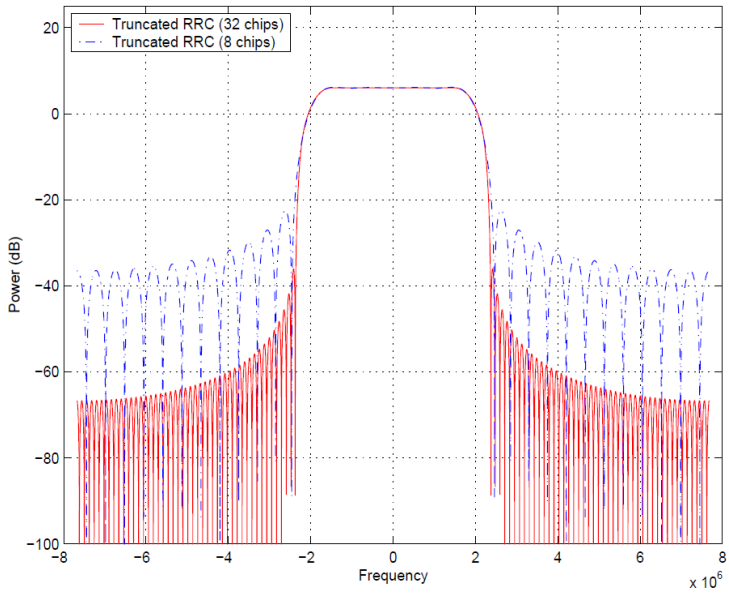

Figure 3.15.: Influence of the RRC truncation chip filter (Fig. from [60])

Frequency shifting

After pulse-shaping, the I and Q components can be up-converted by an local oscillator prior to summation, filtering, amplification and broadcasting (Fig. 3.16).

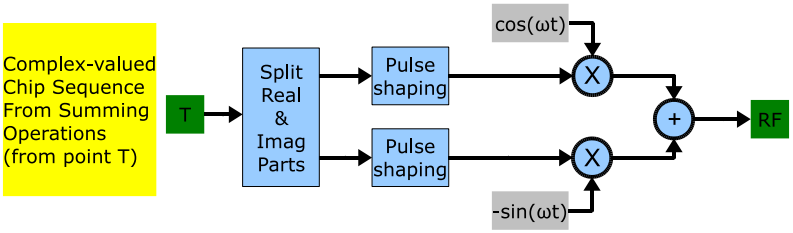

Figure 3.16.: Pulse-shaping & Passing from IF to RF, where $\cos(\omega t)$ and $-\sin(\omega t)$ correspond to the in- and quadrature phase of the local oscillator

At the receiving side, the synchronization channels allows the device or the base station to detect the time slots, recover the cell information by using the signalization channels, and finally recover the transmitted data.

Carrier spacing

As mentioned in the previous section, an UMTS carrier occupies 4.68MHz of spectrum.

However in practice, the UMTS carriers's central frequencies are spaced by 5MHz.

The remaining 0.32MHz gap is kept as a guard band since a closer spacing increases the difficulty of achieving the out-of-band rejection at the reception. For instance, [61] showed the importance of the carrier spacing in terms of interference and power leakage between neighbor channels.

3.2.2. UMTS evolutions

The evolution of UMTS aims at higher bit rates (especially in the downlink) in order to optimize the packet data services.

The terms *High Speed Downlink Packet Access* (HSDPA) and *High Speed Uplink Packet Access* (HSUPA) correspond to the respective standards describing the improvements for the downlink and the uplink. Further improvements are regrouped under the *High Speed Packet Access* (HSPA) term, and its evolution is labeled *HSPA Evolution* (HSPA+).

Currently for the physical layer, three main techniques are used to improve the UMTS data rates: higher order modulation formats, multiple inputs multiple outputs (MIMO), and increased amount of bandwidth available per user by multiplying the number of carriers assigned per user.

Modulation formats

In order to increase the data rate, higher order modulation formats are used in order to increase the spectral efficiency. As the downlink specifications evolved, the downlink channel coding moved from QPSK to the possibility of using 16- and 64-QAM.

However in order to keep the spectral width (see §3.2.1) of an UMTS carrier constant, the overall symbol rate at chip level is kept constant at 3.84Mchip/s. Tab. 3.1 shows the improvement of the bit rate.

Table 3.1.: UMTS downlink higher order modulations. The **figures apply to one physical channel** (up to 15 physical channels can be dedicated to a single user in HSDPA [62])

Modulation format	Bit rate (kbit/s)	Symbol rate (ksymb/s)	SF	Chip Rate (Mchip/s)	Improvement of the bit rate
QPSK	480	240	16	3.84	ref.
16-QAM	960	240	16	3.84	x 2
64-QAM	1440	240	16	3.84	x 3

Multiple Input Multiple Output

Spatial diversity was already foreseen in the initial[7] UMTS FDD standard: a single downlink data stream could be emitted alternately by two different antennas, co-localized and spaced by a few decimeters, at the Node B. The UE has still a single antenna, yet the spacing of the emitting antennas can be sufficient to lower scintillation effects[8], and thus improve the data rates.

A real MIMO scheme with two transmit antennas at the Node BS and at the UE[9], was introduced in the HSPA+ standard including the initial spatial diversity [62–64]. This allows two independent data streams to be transmitted simultaneously over the radio channel over the same W-CDMA channelization codes. Therefore the signals, after spreading (see §3.2.1) and scrambling (see §3.2.1), are precoded (linear combination). The two data streams are summed up prior to transmission on each antenna, so that each antenna transmits a part of each stream.

Performance review Thanks to the complexity which is progressively introduced (higher order modulations schemes and MIMO techniques), the maximum theoretical data rates improve.

UMTS Release 7 introduced MIMO at the UE, for the QPSK and 16-QAM schemes, making possible theoretical data rates between 16 and 28Mbit/s respectively. The introduction of MIMO for QPSK and 16-QAM (but not simultaneously for 64-QAM) yielded theoretical data rates between 18 and 28Mbit/s.

Additionally, Release 8 made possible to use simultaneously 64-QAM and MIMO, thus allowing maximum theoretical data rates between 35 and 42Mbit/s.

Dual carrier transmission

The dual carrier transmission (also known as dual cell), shown in Fig. 3.17a, introduces (Release 8) a second HSDPA carrier usable by a single UE when the radio conditions do not allow to use MIMO [64, 65].

[7] published in 1999

[8] for 2.14GHz frequencies, the wavelength values ≈ 14cm

[9] The corresponding emitting and receiving architectures can be found in [63].

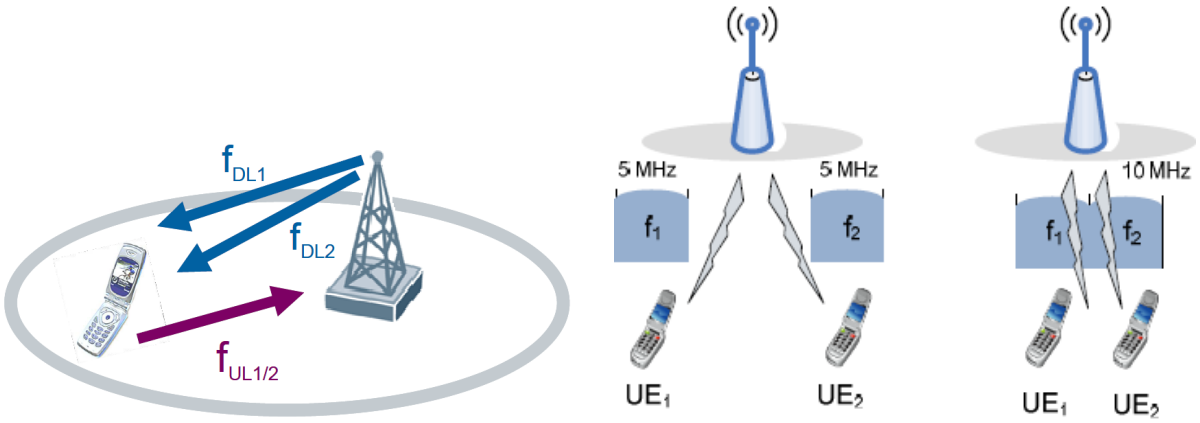

(a) (b)

Figure 3.17.: (a) Dual carrier concept (in the downlink), (figure from [64]) (a) Single (left) carrier and dual carrier (right) transmission, (figure from [66])

According to [64], simulative investigations within 3GPP have shown that Dual Cell HSPA transmission significantly improves the data rates for users experiencing low and moderate SNRs.

Currently the dual carriers transmissions do not use MIMO and have to be applied to adjacent carriers. Furthermore only the downlink is concerned.

Extension to multiple- & non-adjacent carriers According to [66], the previous concept can be extended to aggregate three or four carriers. This multicarrier concept is further supported by the fact that UMTS licenses are often granted as 10 or 15 MHz paired spectrum.

Finally, this carrie aggregation paves the way to LTE[10] where channels can be as wide as 20MHz.

[10]LTE does not uses W-CDMA but OFDM/A

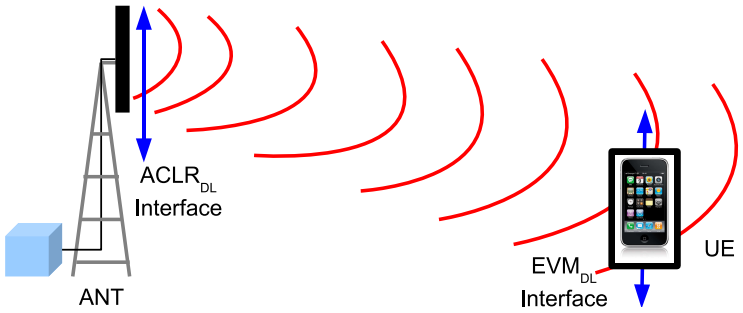

Figure 3.18.: Measurement points for ACLR and EVM for a downlink signal

3.3. Figures of merits for the physical layer

This section presents the figure of merits used in the following chapters to qualify and evaluate the proposed optical access architectures. Thus their importance and impacts are major.

The EVM is a figure of merit intended to quantify the receiver's capability of demodulating the transmitted signal, while the ACLR is a figure of merit intended at quantifying the spectral purity at the transmitter side. Finally the Crest Factor also known as Peak to Average Power Ratio (PAPR) characterizes the power swings of a signal (especially analog ones) over time, and thus allows to anticipate distortion issues whenever amplification or modulating processes are involved.

3.3.1. The Error Vector Magnitude

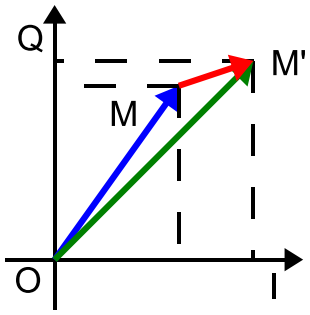

Figure 3.19.: EVM definition: (M) ideal and (M') received constellation points with the (blue) ideal, (green) received and (red) error vectors.

Definitions

The Error Vector Magnitude (EVM) is used to quantify the quality of transmission at the symbol level when analog operations are involved —as the BER is used for digital systems at bit level— and thus translates any distortions at the symbol level.

The EVM is the ratio between the cumulated magnitudes of the error vector ($\overrightarrow{MM'}$ in Fig. 3.19) and an ideal vector ($\overrightarrow{OM}$ in Fig. 3.19). The error vector is the difference of the

coordinates of a received constellation point M' and the coordinates of a ideal constellation point M. The error vector translates the amplitude and/or phase shift undergone by a symbol during transmission or amplification for instance.

The EVM measure requires *apriori* knowledge of the transmitted symbol, or must assume that closest constellation point *is* the transmitted symbol. Therefore the ideal vector can be either the constellations point normalized with respect to the average power or to the maximum power [67]:

$$EVM_{avg\ \%} = \sqrt{\frac{\frac{1}{N}\sum_{k=1}^{N}\left|\overrightarrow{M_kM_k'}\right|^2}{P_{avg}}} \cdot 100 \qquad EVM_{peak\ \%} = \sqrt{\frac{\frac{1}{N}\sum_{k=1}^{N}\left|\overrightarrow{M_kM_k'}\right|^2}{P_{peak}}} \cdot 100 \quad (3.5)$$

The third way is to let the ideal vector be the initially transmitted vector [67]. Hence the ideal vector for a given symbol varies with each symbol to be compared. This dependency is shown in the denominator of the ratio:

$$EVM_{reference} = \sqrt{\frac{\frac{1}{N}\sum_{k=1}^{N}\left|\overrightarrow{M_kM_k'}\right|^2}{\frac{1}{N}\sum_{k=1}^{N}\left|\overrightarrow{OM_k}\right|^2}} \cdot 100 \quad \text{in } \% \tag{3.6}$$

For instance, the UMTS specifications foresee to use the latter method for computing the EVM.

Linking EVM, BER and SNR

According to [68,69], for a Gaussian noise dominated link, the Signal to Noise Ratio (SNR) can be derived from the EVM as follows:

$$SNR_{dB} = -20 \cdot \log\left(\frac{EVM_{\%}}{100}\right) \tag{3.7}$$

This derived SNR is sometimes called the *inverse* EVM (IEVM) [70].

As a consequence of Eq. 3.7, the BER can be plotted as function of the EVM-derived SNR (Fig. 3.20).

Indeed the probability of an error (P_b), *i.e.* the BER, can be linked to the EVM as follows [69]:

$$P_b \approx \frac{2(1-1/L}{\log_2 L} \cdot Q\left[\sqrt{\left(\frac{3\log_2 L}{L^2-1}\right) \cdot \frac{2}{EVM_{RMS}^2 \cdot \log_2 M}}\right] \tag{3.8}$$

where $Q[]$ is the Gaussian co-error function, and where L is the number of levels in each dimension of the M-ary modulation system.

Typical radio communications systems require a conservative target BER of 10^{-4}, and thus according to Fig. 3.20, for the QPSK (= 4-QAM) modulation format, the required SNR is 12dB, and 18dB for a 16-QAM scheme. For the latter SNRs, the equivalent EVMs value then 25.1% (QPSK) and 12.6% (16-QAM).

The UMTS 3GPP specifications set the maximum (worst) acceptable EVM figure (at the receiver) to 17.5% for a QPSK modulation scheme. and corresponding, according to Fig. 3.20, to a SNR of 15dB. For a 16-QAM modulation scheme the EVM upper bound is set to 12.5% corresponding here to a 18dB SNR.

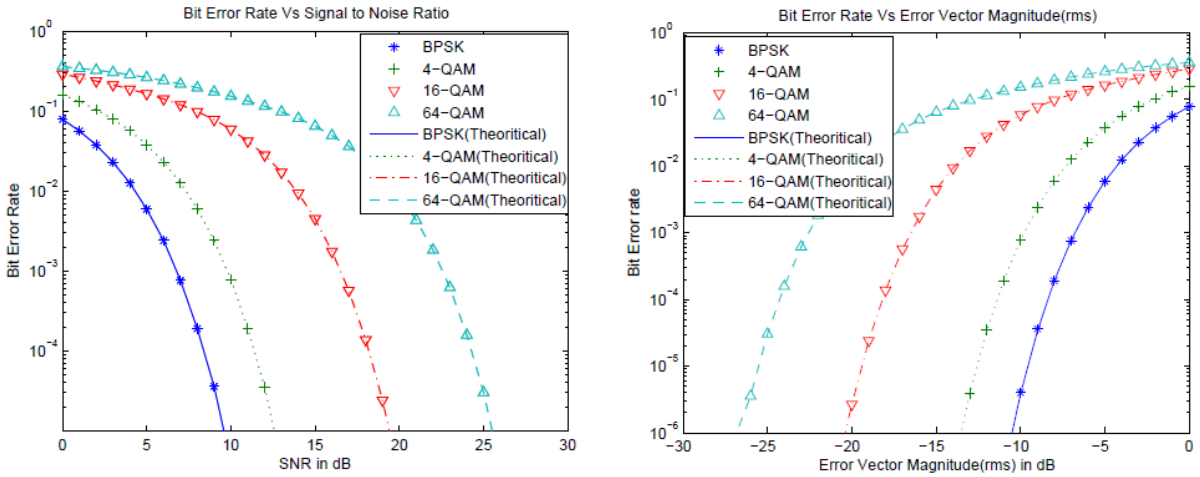

(a) (b)

Figure 3.20.: Theoretical BER as function of SNR and of EVM-derived SNR for different modulation formats, (pictures from [69])

Appreciating the EVM figure

According to [70] the EVM figure is of variable interest whether it is appreciated at the transmitter or at the receiver side.

At the transmitter side, the SNRs are extremely high so that the measured EVM represents eventual transmitter constellation distortion, and not noise-induced signal distortion.

Furthermore measuring high SNRs means that the nearest constellation point is always the transmitted constellation point. Thus for transmitter testing purposes the BER tends towards 0, so does the EVM (Fig. 3.21).

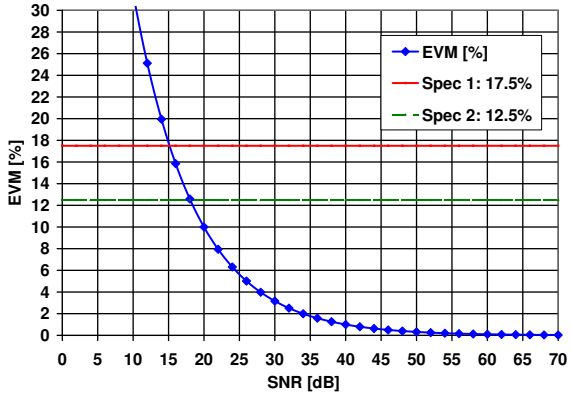

Figure 3.21.: EVM as a function of SNR according to Eq. 3.7

At the receiving side, the characterization of receivers is not limited to high SNRs since receivers are designed for operation in very low SNRs where link distances are stretched to maximum (typically this corresponds to the cell boundary).

However at low SNRs, the processed symbol [I,Q] may cross demodulation decision boundary and lead to demodulation errors. The practical measurement of EVM in receivers has no *apriori* knowledge of transmitted symbol and so must assume closest constellation point. This assumption leads to EVM errors for low SNRs: measured EVM is lower than actual EVM; measured Inverse EVM is higher than actual IEVM.

Conclusion

This section showed that for a given modulation scheme a certain SNR performances can be sufficient for yielding a target EVM (*i.e.* BER).

Yet the next section will show that these SNR requirements, due to specifications for limiting interferences at emission, will actually exceed the SNR requirements set by the EVM.

3.3.2. Output RF spectrum emissions

The previous section mainly addressed issues occuring with and within the (UMTS) channel itself, while this section shows how and why the spectrum properties surrounding the (UMTS) channel import as well.

General definitions

For a given radio standard, the output RF spectrum emissions describe the signal output spectrum with the intention of limiting the interference effects outside of the occupied channel. Even if each radio standard defines individual requirements, the following definitions are used in many standards [65]:

Channel bandwidth: Requirements for channel bandwidth and occupied bandwidth define the frequency range occupied by the wanted signal and ensure that the emission of the transmitter does not occupy an excessive bandwidth. The occupied bandwidth is typically defined as the bandwidth containing 99% of the total integrated mean power of the transmitted spectrum on the assigned channel.

Spectrum emission mask (SEM): The spectrum emission mask limits out-of-band emissions immediately outside the nominal channel resulting from the modulation process and non-linearity in the transmitter. The SEM requirement typically defines limits and associated measurement bandwidths dependent on the frequency offset from the transmit channel. The transmitter's emissions (noise and power) shall not exceed these limits, specified in an ITU recommendation [71].

For the frequency range used in RANs, the maximum noise power level a communication radio system can emit is set to -13dBm/1MHz maximum for the USA (Category A), and to -15dBm/1MHz for the European Union (Category B).

Adjacent Channel Leakage power Ratio (ACLR): The adjacent channel leakage power ratio is defined as the ratio of the filtered mean power centered on the assigned channel frequency to the filtered mean power centered on the adjacent channel frequency.

It is used to verify that the transmitter does not cause (unacceptable) interferences to adjacent channels (Fig. 3.22) by leaking some of its transmitted power into the adjacent channel. This leaking can due to an imperfection: transmit filter, distortions resulting of non-linearities, excessive thermal noise...

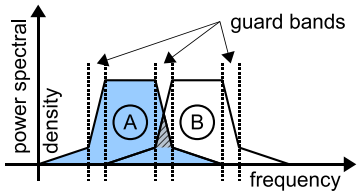

Figure 3.22.: Illustration of interferences between adjacent channels: the dashed area in the channels Ⓐ and Ⓑ are interferences caused by the respective neighbor channel.

UMTS specificities

In order to quantify the interferences and pinpoint their origins, the 3GPP has introduced the terms: adjacent channel leakage power ratio (ACLR), adjacent channel selectivity (ACS), and adjacent channel interference ratio (ACIR) [58].

ACLR: as said, measures the transmitter's performance, and for UMTS FDD signals is specified as follows:

First the *Adjacent-CLR* is defined as the ratio between the power within 3.84MHz of a carrier filtered by a RRC-filter of 3.84MHz bandwidth having a roll-off factor of 0.22, and the power again within 3.84MHz of an adjacent channel located at +/-5MHz from the central frequency of the carrier of interest, and also filtered by a 3.84MHz wide RRC filter with a oll-off factor of 0.22.

The *Alternate-CLR* is defined like *Adjacent-CLR* yet the *adjacent* channels are called *alternate* and their central frequencies are located at +/-10MHz from the central frequency of the carrier of interest.

In the case of multiple carriers the previous definition applies to a chosen carrier (reference), and the relative measurements are done at +/-5MHz and +/-10MHz outside of the multiplex and apply to the lowest and highest carriers' central frequencies of the multiplex.

Whether for a single or for multiple carriers, the 3GPP specifies downlink [59] Adjacent- and Alternate-CLRs of -45dBc and -50dBc maximum respectively (Fig. 3.23a).

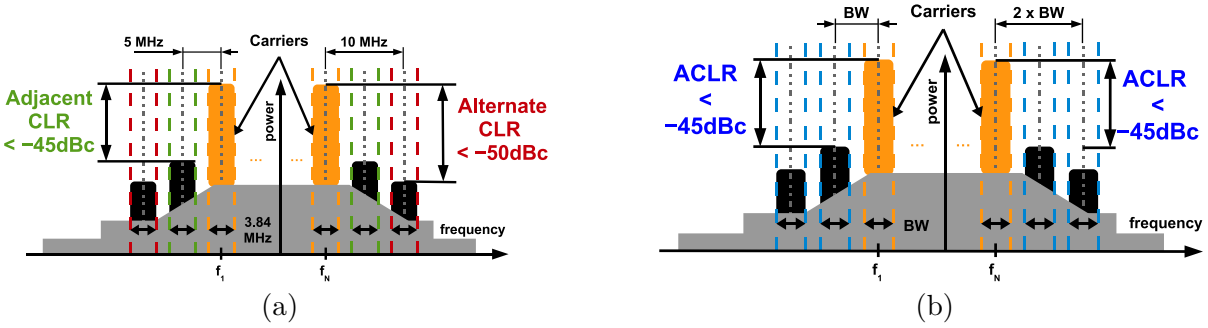

(a) (b)

Figure 3.23.: Definition of ACLR for: (a) UMTS signals, (b) LTE signals

Henceforth the term ACLR describes Adj-CLR and Alt-CLR, unless otherwise stated. Concerning the fourth mobile generation (4G), the ACLR specification (Fig. 3.23b) have similar values, but are expressed as a function of the signal's bandwidth given the tun ability of the channel's bandwidth in such systems (1.5, 3.5, 5, 10, 15, and 20MHz).

ACS: measures the receiver performance's ability of receiving the desired signal while completely rejecting the adjacent carrier signal. Therefore it is defined as the ratio of the receiver filter attenuation on the assigned channel frequency to the receiver filter attenuation on the adjacent channel frequency.

Performances and practical implementations issues can be found in §3.2.1, p. 54.

ACIR: measures the overall system performance. It is defined as the ratio of the total power transmitted from a source (BS or UE) to the total interference power resulting from both transmitter and receiver imperfections affecting a victim receiver.

Thus the ACIR takes into account the two previously defined metrics, and for the downlink is expressed as :

$$ACIR_{DL} = \frac{1}{1/ACLR_{BS} + 1/ACS_{UE}}$$

According to the 3GPP specifications, in the downlink the limiting parameter is set to be the Adjacent Channel Selectivity (ACS) at the UE, since the specifications foresee the BS to bear the main effort for limiting the level of the interferences (see §3.2.1). Thus typically:

$$ACS_{UE} = -33dBc \quad \text{and} \quad ACLR_{BS} = -45dBc$$

Finally ACIR is mainly of interest in network simulation where the total amount of interference, rather than the source of the interference, is the primary concern [58].

Network impact & importance of the ACLR for an operator

According to [72], the performance of the Third Generation (3G) W-CDMA system is limited by interference. The main sources are thermal noise, intra-cell interference from traffic in the same cell, inter-cell interference from traffic in adjacent cells, and inter-operator interference generated from operators using adjacent frequencies.

While a network operator *should* be able to control the interferences generated by its RAN, it has no effective control over interferences generated by third parties.

If the ACLR is sufficiently bad, it can cause the so called *near-far* problem, where a BS simply cannot communicate with a far away UE because of a high ACLR from a nearby adjacent channel BS.

In case of mobility, as the terminal (UE) moves away from its own operator's BS and towards that of a different operator (on an adjacent carrier) the received signal's strength generally diminishes and the interferences signal from the other operator will rise. Inter-cell interferences from the own operator may also rise under these conditions. The inter-cell interference is typically rather strong on the cell edge and considerably weaker closer to the cell center while the opposite is true for the received energy of the intended transmission [63].

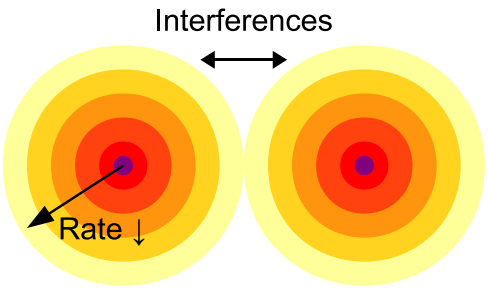

Figure 3.24.: Cell edge located interferences degrade the ACIR

Also the fact that a neighboring cell can use the same carrier frequency makes it difficult to apply higher-order modulation near the cell edge. Thus the service range of high-speed connections (using higher order modulation schemes, see §3.2.2) may be very limited [62].

This affects the region around the other operator's BS creating a potential *dead zone* where, for the worst case, terminals suffer dropped calls due to insufficient link budget to satisfy the required Quality of Service (QoS) (schematically show in Fig. 3.24). Prior to link interruption, if the radio standards uses adaptive modulation schemes, the BS uses simpler and more robust modulation formats, resulting in a lowered bit rate.

Furthermore *dead-zones* and unwanted call drops in the cell, make the concerned part of the network less profitable [72].

Finally the needs are conflicting: from an equipment design perspective a relaxed ACLR specification is attractive, whereas from a network planning perspective, low ACLR is very desirable.

Spurious emission level examples for UMTS Taking into account the channel bandwidth of UMTS carriers (3.84MHz) we have for Category A and B upper limits of respectively -7.16dBm/3.84MHz and -9.16dBm/3.84MHz.

3.3.3. Crest factor of modern mobile signals

Definition The crest factor is defined as the ratio between the peak power (measured in a given time frame) and the average power (rms).

$$\text{Crest Factor}_{lin} = \frac{\max_{t\in[0,T]} |x(t)|^2}{\frac{1}{T}\cdot\int_0^T |x(t)|^2 dt} \qquad \text{Crest Factor}_{dB} = 10\cdot\log\left(\text{Crest Factor}_{lin}\right) \quad (3.9)$$

Cumulative Crest Distribution Function (CCDF) The CCDF allows to visualize the probability within a time frame (distribution over time, fraction of a time frame) of the signal power to be above or below the RMS power. Fig. 3.25 shows the CCDF for UMTS signals.

Historical recall One of the reasons why mobile signals of the second generation (2G) use *Gaussian Minimum Shift Keying* (GMSK) and 8-PSK (EDGE, 2.5G) modulations, is that the latter have constant amplitude over time. Thus regardless of the variation of the modulating signal, the PAPR is low which allows to work closer to the saturation point of the PA increasing the power efficiency [73].

Crest factors of multilevel modulations Recent radio standards are based on multi-level modulations. For instance, UMTS in the downlink, relies on QPSK modulation, known to have a constant module. However as explained in §3.2.1, a real UMTS signal as used in the RAN is a superposition of multiple QPSK modulated signals (Fig. 3.14), resulting in a module no longer constant over time, and in an increased PAPR also known as Crest Factor.

According to [73], for a QPSK signal, when the constellation point I,Q changes simultaneously from [+1, +1] to [−1, −1] the signal trajectory goes through the origin [0, 0]. A value of 0 magnitude indicates that the carrier amplitude is 0 for a moment.

Yet not all transitions in QPSK result in a trajectory that goes through the origin. Therefore some symbol transitions will result in a small amplitude variation, while others will result in a very large amplitude variation.

If the amplifier is perfectly linear, the spectral occupancy of the signal will be unchanged. Yet the problem lies in the circuits' nonlinearities.

Indeed, a signal which changes amplitude over a very large range will exercise these nonlinearities to the fullest extent. These nonlinearities will cause distortion products, and thus spectral regrowth.

Crest Factor of a multi-carrier signal When transmitting multiple carriers which are uncorrelated, the overall crest factor is increased by:

$$10\cdot log\left(\text{Number of carriers}\right)\ \text{dB}$$

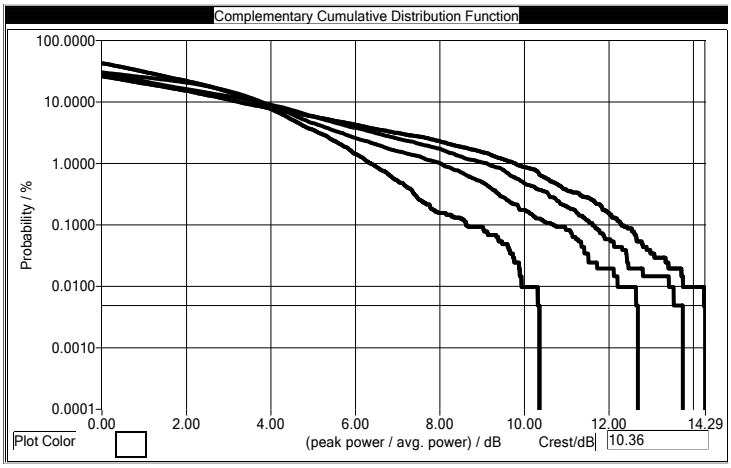

Figure 3.25.: Estimated CCDF for one to four UMTS carriers in Test Model 4 configuration by the *WinIQSim* software

Table 3.2.: Crest Factor as a function of the number of UMTS Test Model 4 numbers

Number of carriers UMTS (TM4)	Crest Factor [dB] for CCDF $< 0.01\%$
1	9,92
2	12,69
3	13,75
4	14,29

Crest factor reduction The issues discussed in the previous paragraph show the interest of reducing the PAPR for *pure* radio applications.

Since in this thesis we aim at transporting multiple radio carriers by using an analog IM-DD scheme, the laser diode can as well benefit from the reduced PAPR of the modulating signals.

Given the importance of PAPR for carriers transported in an analog IM-DD operated optical links, especially when using multiplexes of real radio carriers, reducing the PAPR of the signals can lower the specifications of the electrical linear dynamic of the components.

The simplest technique for reducing the PAPR, is *hard-clipping*, which consists in simply limiting the time-domain magnitude of the signal when the signal crosses predefined thresholds. However the drawbacks are increased EVM due to time-domain distortions and/or degradation of the spectral purity which can be quantified with the ACLR figure of merit.

Another way of reducing the PAPR, and working *on the fly* at Intermediate-Frequency (IF) by over-sampling the symbols, is the *pulse-shaping* technique proposed by [74]. Instead of hard-limiting the time-domain signal, the peaks above a set threshold are attenuated and filtered (Fig. 3.27) gradually by a distortion limited process.

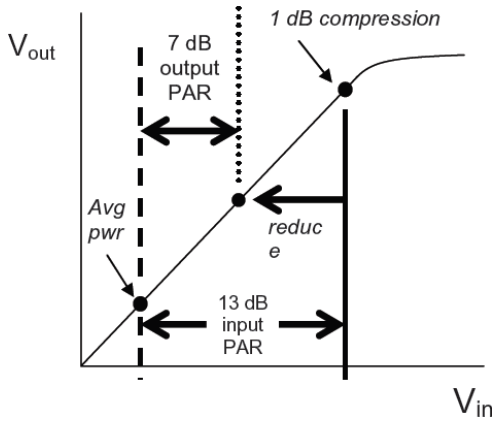

Figure 3.26.: Example of reducing the peak-to-average ratio (PAR) of a W-CDMA signal increases the efficiency: the more the better it is(!), (picture from [74])

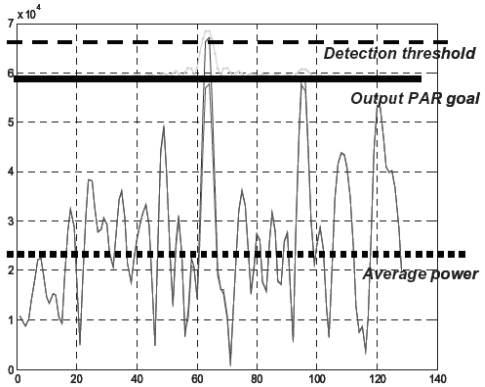

Figure 3.27.: PAPR reduction by a gradual change to each over-threshold peak, (picture from [74])

3.4. The mobile back-hauling

3.4.1. Principle

The mobile back-hauling consists in aggregating and distributing the traffic from and towards the different base stations (called *Node B* for UMTS) and the core network.

Therefore, as shown in Fig. 3.28a (which is a simple and typical UMTS backhaul architecture) the *Iub* interfaces and links consist in the *last mile* back haul. These links concentrate the traffic loads of the Node Bs, and thus of all the concerned radio cells, towards a regional point called Radio Network Controller (RNC).

Compared to the number of Node Bs, the number of RNC aggregation sites is low since a single RNC can handle the traffic of hundreds of Node Bs. In Fig. 3.28b, the yellow dots represent the RNCs while the blue and pink areas correspond to deployed Node Bs for Orange's 3G network in France.

The RNCs themselves are interconnected by the *Iur* links, and to the core network by the *Iu* links, as shown in Fig. 3.28a.

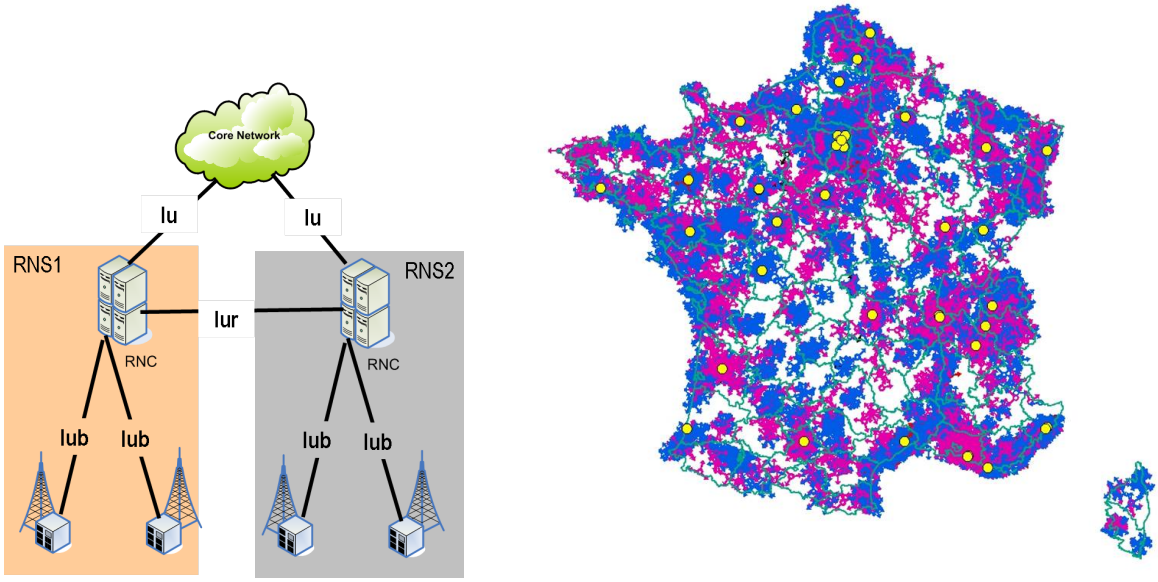

(a) (b)

Figure 3.28.: Mobile backhaul: (a) architecture; (b) map of RNCs and Node Bs

3.4.2. Current backhaul

The afore mentioned *Iub* and *Iu* links currently rely on E-1 circuits (Fig. 3.29). E1 circuits are digital links[11] and have been developed for transmissions of voice services.

These E1 circuits can then be transported by several transmissions techniques natively conserving their switched circuit nature:

[11] 2.048Mbit/s bitrate

- satellite links, which are well adapted for rapid roll-out [75], and is the only realistic solution for remote and isolated areas [11].
- dedicated optical Pt2Pt links using Synchronous Transport Module level-1 (STM-1) links with a bit rate of 155.52Mbit/s.
- xDSL links, in which the E1 circuits are transported by Asynchronous Transfer Mode (ATM) which is an asynchronous TDM protocol
- TDM microwave links using Synchronous Digital Hierarchy (SDH) protocols,
- lines which are leased by third parties

Concentration issue The base station sites are per date usually connected by one or a few 2 Mbit/s links. After aggregation of links from several base station sites, higher capacities are needed.Closest to the base station sites, wireless solutions may remain the most economical ones. However, **after aggregation of tens of radio sites**, (closer to the RNC), gigabit capacity fibre optical solutions will be preferable.

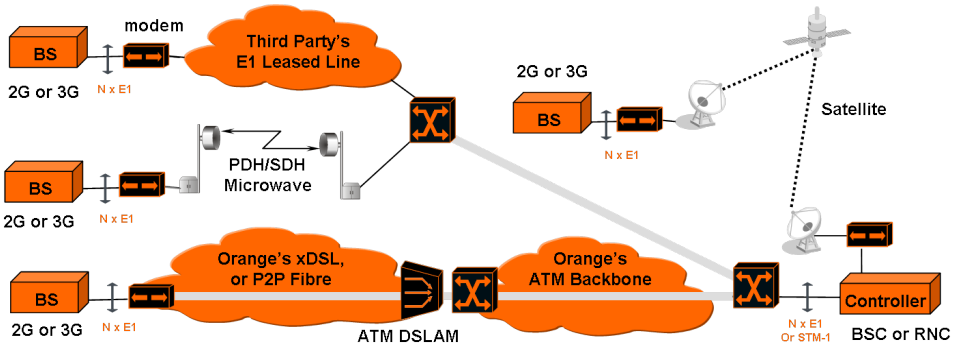

Figure 3.29.: Current mobile back-hauling techniques [76]

3.4.3. Evolved & packet oriented backhaul

Requirements

The requirements to the future back-haul are currently characterized by two mains aspects:

the traffic load: typically delivering streaming video to multiple users per cell site will increase the last-mile backhaul **per radio site** needs from a few Mb/s today, up to 50 or even 100 Mb/s tomorrow. Finally aggregating traffic of multiple BSs will require backhaul network with gigabit links [75].

the traffic type: additionally to the traffic load, the devices and the associated services have made the traffic to be dominated by data instead of voice. Finally this data domination in the payloads imposes a change to a packet-oriented back-haul network with a flatter hierarchy.

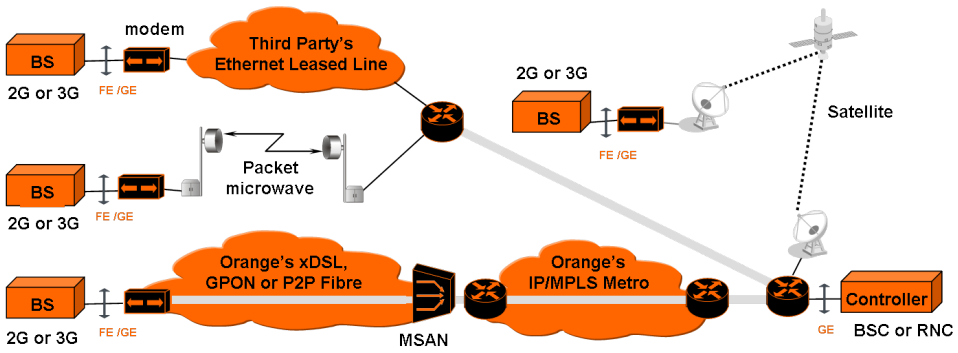

Figure 3.30.: Mobile back-hauling techniques relying on packets, (figure from [76])

Evolved links

As the number of base stations increase, the number of backhaul links is expected to grow accordingly. Depending on the traffic volume, higher capcity links may have to be used to match the bandwidth demand.

As a consequence of these requirements the previous backhaul links are re-used, but their transport protocol is adapted from TDM to packet.

- Optical networks: offer very high capacity, and are used in the backhaul already, primarily close to the core network. As capacity increases, fiber becomes a viable solution in the access part as well, also from a purely economic point of view. The reason for this is that the main cost of the fiber solution stems from leasing/deploying the fibre cable, i.e., the cost is in effect independent of capacity in this case. Thus base stations sites can be fed directly by fibre.

- Microwave packet radio: the data packets are directly delivered over Ethernet connections, and not over TDM based links. Microwave is used to fill in the gaps (providing backhaul to the nearest fibre access point) when no fibre is available [77].

- Third party leased lines and satellite[12] links remain but use Ethernet-based packet transport protocols.

Finally as radio traffic and deployments of FTTH networks are expected to increase significantly, the optical access networks could be used also for the last-mile backhaul of the radio access networks.

Although PONs were originally made for fibre to the home (FTTH) applications, they can be used as a single physical network that serves all segments in a unified way [78]. The carried out work in this thesis will demonstrate this.

For instance, a digital packet connectivity of the radio base stations over FTTH networks is schematically shown in Fig. 3.30.

Yet other techniques do exist, and will be exposed in Part 4.

[12]according to [6] links of 10Mbit/s are already available while up to 200Mbit/s are planned

Conclusion

In a first time we have recalled the main features of radio access networks and the related trade-offs, especially the carrier frequency with respect to propagation losses and spectrum availability, the fadings issues occurring in mobile radio communications and their influence on the link margin, the duplexing schemes with respect to the types of services.

In a second step, we have presented the main properties and construction of the UMTS FDD W-CDMA signals at the physical layer. This understanding is required in order to implement them (detailed in the Appendix) in Matlab for generation by an arbitrary waveform generator (AWG) for the experiments reported in Part 4.

Then general signal quality requirements in radio access networks have been recalled. A focus addressed the quality requirements for transmissions of UMTS signals, and showed that a limited SNR performances can be sufficient for yielding a target EVM (*i.e.* BER). Yet these SNR requirements, due to interference limiting specifications at emission, will exceed the requirements set by the EVM specifications. In Part 4, this latter aspect will be the key argument for justifying the changes in the proposed optical architectures and in the related transmitters and receivers.

Finally this chapter has also dealt with a network related issue by introducing the current and near-future mobile back-hauling architectures. The notion of last-mile backhaul over optical access networks directly introduces the next part: hybrid optical access architectures using radio over fiber.

Part II.

Hybrid Access Networks

4. Mutualizing the optical infrastructures

4.1. Motivation of optical infrastructure re-use

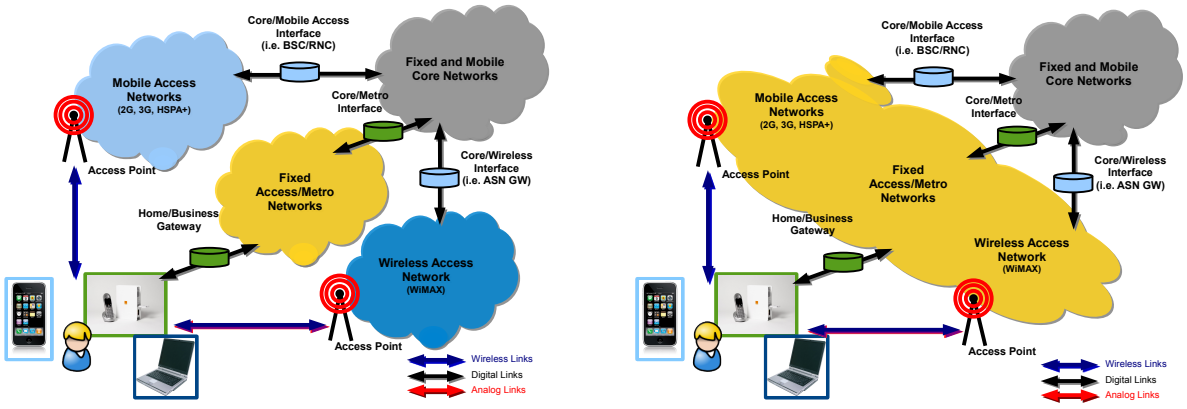

Figure 4.1.: Access networks using optical infrastructures:
(a) separated (currently), (b) converged and shared (future?)

4.1.1. Drivers of the infrastructure mutulization need

Network upgrades and expansion are essential for supporting traffic growth and the need for denser and denser networks. According to [10], a strong focus has to be put on the building out of capacity in high-use locations, achieved either by an increased number of base stations, additional sectors or improved networks speeds. Also additional backhaul capacity to and from the cell sites in order to support peak traffic loads has to be considered. However additional radio sites require additional individual last-mile backhauling links, leading to unavoidable initial and operating costs because of being numerous and wide-spread (Fig. 4.1a).

Given these requirements; a mean to increase the number of radio sites is to re-use the optical infrastructure dedicated to Fiber To The Home (FTTH) for the last-mile backhaul of mobile networks.

Indeed given the foreseen mass deployment of FTTH networks, an operator could take advantage of the FTTH's Central Offices (COs) for distributing the radio carriers over the FTTH networks' fiber infrastructure. In the latter case the last-mile backhauling links are no longer individually dedicated to the base stations but are part of an unified infrastructure architecture (Fig. 4.1b).

Furthermore a welcome side effect, is that the base stations no longer need to be located close to the antennas, but *could* be concentrated in a single location, namely in the FTTH

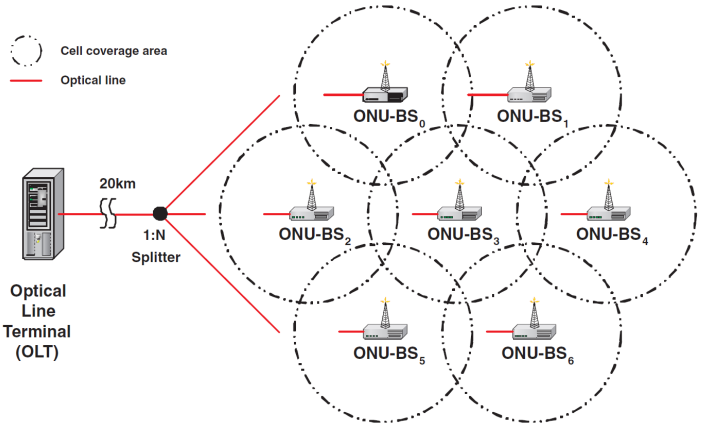

Figure 4.2.: Example of distributed antennas in a PON, (picture from [79])

networks' COs. Indeed, in this hybrid network layout, a significant reduction of the antenna BS complexity can be achieved by moving the routing, switching and processing functionalities to the CO. This strategy also enables the cost and equipment to be shared among all the antenna BSs.

The combination of both aspect leads to the distributed antenna concept extended and adapted to a FTTH network. Therefore we will in a first time define the concepts of distributed antennas systems, and then address the possible analog and digital radio over fiber techniques that could fit this purpose.

4.1.2. Traffic consumption places

According to Fig. 4.3, the prevalent places where the mobile data traffic is consumed, is most of the time, within the reach of an optical access network.

Furthermore if we assume the customer to expect a seamless broadband connection almost everywhere, then we can think of re-using the optical access infrastructures — initially planed for fixed purposes— to address the mobile access as well (Fig. 4.1).

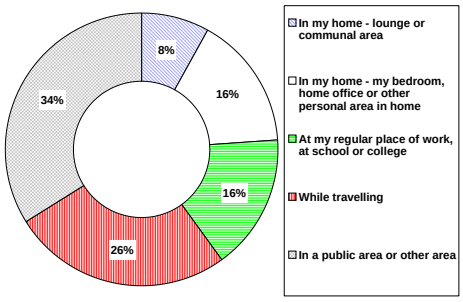

Figure 4.3.: Mobile Data Prevalent in Home (Source: Strategy Analytics US Netbook Owner/Intender Survey, July 2009 in [10])

4.1.3. Opposite point of view

Despite the strong arguments for realizing the hybridization and convergence of optical infrastructures, opposite points of view exist.

According to [46], the plans[1] are to use 10-GPON for residential applications, while the Wave Division Multiplexing (WDM)-Passive Optical Network (PON) technique is to be used for business applications and bandwidth intensive backhaul, even if from a technical point of view WDM-PON is not contradictory with Radio over Fiber (RoF).

[1]The corresponding EU *Gigawam* project can be found at `http://www.gigawam.com`.

4.2. Distributed Antenna Systems

4.2.1. Definition

A Distributed Antenna System (DAS) is a transmission infrastructure that connects one or more base stations at a central location to a number of antennas spread in a given area in order to give a relatively uniform signal coverage.

One of the option for the distribution network is RoF which thanks to the lower attenuation characteristics of optical fiber (OF), can cover larger areas than legacy passive coaxial cables [80].

The splitting and combining network between the Base Stations (BSs) and the DAS central unit defines the distribution of each of the radio channels to the DAS antennas.

4.2.2. Fiber Distributed Antenna Systems

The BS signals are combined and split to the radio inputs of the fiber DAS central unit, which converts them into optical signals, then distributed over an Optical Distribution Network (ODN), towards the different remote antenna units.

At each antenna unit the optical signal is converted back into the electrical domain. The electrical signals are then amplified, filtered and split between one or more antenna connectors.

4.2.3. Switched Fiber Distributed Antenna Systems

A possible evolution of DAS is the switched DAS where a software-controlled switch matrix allows simple configurations changes for coping with capacity requirements.

As ODNs evolve in outdoor environments, they are bound to increased coverage and capacity requirements than in-building scenarii would require. Also for macro-cellular applications the radio environment is more complex.

A switched DAS has the ability to dynamically map the capacity according to the usage demands, and this remotely. This aspect constitutes its main benefit.

Also the switch matrix can reduce the number of required BSs for a given installation, thanks to statistical multiplexing. This reduction is realized by using the switch to drive better base station utilization by enabling the capacity to be shifted to areas of need according to event or time driven requirements.

4.3. The different topologies

The different optical infrastructure topologies impose to the different RoF transmission techniques constraints and degrees of liberty which condition the choice of a transmission technique. These degrees of liberty can be as well the technical complexity, the costs, the upgrade capability, the integration to legacy systems, and the performances.

4.3.1. Simple topologies

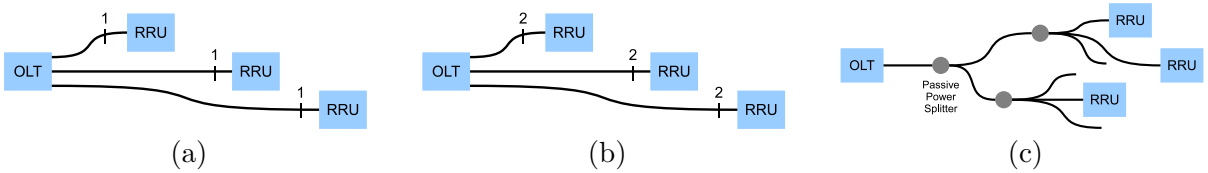

(a) (b) (c)

Figure 4.4.: Simple topologies: (a) mono-fiber Pt2Pt, (b) bi-fiber Pt2Pt, (c) Pt2MPt

The *simple* topologies are schematically summarized in Fig. 4.4. Their pro and cons are as follows:

Pt2Pt

Generally speaking the Point to Point (Pt2Pt) topologies using a pair of optical fibers, offer the following advantages:

- possiblity of re-using the same couple of up- and downstream wavelengths per distant site
- a fibre cut does not impact the other distant sites

and drawbacks:

- in the downlink, there are as much optical emitters as distant sites
- the amount of fibers at the CO can be important and difficult to manage

By using a single fiber per customer two times less optical filters, circulators, (de)multiplexers are required.

Pt2MPt topology

A typical Point to Multi-Point (Pt2MPt) topology using wavelength diplexing offers the following advantages:

- needs only 2 wavelengths for a full-duplex working mode
- at the CO, a single photo-emitter and a single photo-receiver are required

, and drawbacks:

- a cut of a shared link impacts the downstream sites
- necessity of having a multiple access protocol in case of a shared single upstream wavelength

4.3.2. Complex topologies

The ring, daisy-chain and mesh topologies are possible frameworks for RoF applications, and may be well adapted to stadium and large building applications.

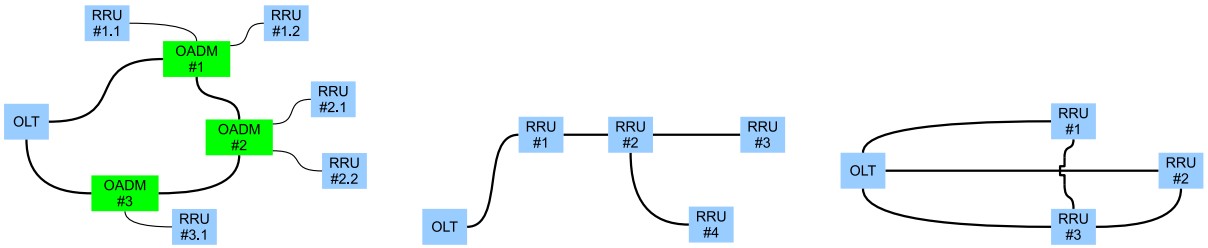

Figure 4.5.: Complex topologies: (a) ring, (b) daisy-chain, (c) meshed

Ring

The ring topology (Fig. 4.5a) requires Optical Add and Drop Multiplexing equipments which allows each Remote Radio Unit (RRU) to receive selected wavelength(s), and eventually a variable number of wavelengths.

This type of topology requires furthermore to define the transmission direction (left or right handed). Especially in case of analog RoF, where the wavelengths cannot be switched, and no token-base sharing scheme can be set-up, a continuous connectivity is mandatory.

To overcome this travel direction issue [81] proposed to use a double fiber ring where each travel direction uses a dedicated fiber.

Daisy-chain & Mesh

The daisy-chain (Fig. 4.5b) and mesh (Fig. 4.5c) topologies are useful for covering sparsely inhabitated areas, and where a drop-off is sufficient for covering an area. Yet due to its structure —more RRUs than links— the links closer to the CO have to bear the traffic from the distant sites. Thus the topology is not adapted to moving crowds (such as in cities) where the traffic load can be varying with day time and social events.

The counter part of a daisy-chain topology is the mesh topology where there are more links than RRUs. The latter aspect allows securing links, and also load balancing between different RRUs. However due to the more numerous links, which are not always fully exploited, their additional costs need to be taken into account.

Limited interest of complex topologies

However since the current FTTH network architectures rely on a simple tree topology, these *complex* RoF network topologies would require to exist in parallel of current and planned FTTH networks. Given that the holing and digging work account from far for the costs of deploying an optical network, the most cost-effective way to use simple RoF networks, is to re-use topologies compliant with PON networks. Then both, as said previously, can be operated together.

4.3.3. Topology and flexibility issue

In most DAS scenarii, the optical infrastructure relies on a star topology with Pt2Pt links. Hence the flexibility is located at the central point of the star.

Yet in a PON context, the optical infrastructure is usually deployed in a Pt2MPt way. Thus the questions are:

- should all the radio traffic be carried by a single wavelength (at the extent of the wavelength's capacity) and then, each remote antenna sites picking up its attributed radio carriers ?
- or should each site be assigned a dedicated wavelength on which the radio traffic is tailored at the CO for the remote antenna sites ?

Thus the switching function in this context can be realized by several wavelengths reserved for RoF purposes, where the radio signals are loaded onto the different wavelengths transporting the radio signals to pre-determined sites. The latter corresponds to an optical Pt2MPt but to a logical Pt2Pt on a wavelength basis.

Furthermore, as we will see, even if optical-wireless integration is able to simplify the backhaul infrastructure and to offer significant benefits to operators, the implementation of hybrid fiber and wireless network is not straightforward [82].

Especially issues regarding wireless signal transport, signal impairments, spectrum allocation, performance optimization and integration with existing infrastructure have to be considered.

4.3.4. Delay issue

Since the Radio Access Networks (RANs) were not designed to have their radio carriers to travel through optical access network architectures, let's briefly evaluate the impact of the additional delay introduced by typical PONs.

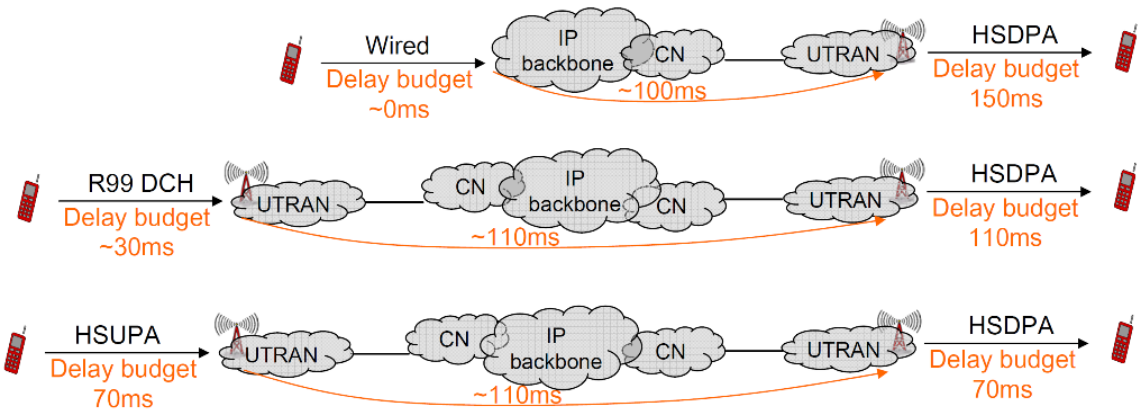

Figure 4.6.: End-to-end delays for mobile communications, (picture from [83])

Therefore let's consider the *worst case* of additional delay when traveling through a PON: 20km of Standard Single Mode Fiber (S-SMF) at a velocity of 200,000m/s cause a delay of 0.10ms. To maximize the upper bound of additional delay, we anticipate the architectures of Part 4 with additional 12.5km of Dispersion Compensating Fiber (DCF), and finally yielding a total one-way additional delay of 0.17ms.

According to [84] when considering the recent HSPA standard (see §3.2.2, p.56), conversational and streaming services, such as VoIP for Video Sharing, have stringent requirements in terms of end-to-end delay (Fig. 4.6), jitter and packet loss.

Delay budget

The considered scenario is a HSUPA User Equipment (UE) to HSDPA UE VoIP call within the same operator's network. For VoIP service, the main constraint concerns the end-to-end delay for a tolerable quality of communication [84]. The different main delay components originate from the sum of the overall delays introduced as shown in Fig. 4.7 and summarized in Tab. 4.1.

The maximum one way delay limit (limit mouth to ear delay) for an acceptable voice quality in terms of delay is 250ms according to [85].

According to [84] in the downlink two different values (50 and 70ms) have been considered for the HSDPA air delay. The latter in turn limit the delay for HSUPA transmission and retransmissions to less than 90 or 70ms (reduced to 40 and 20ms if additional delay for a repetition protocol (HARQ) is considered[2]).

Finally as we can see the total delay introduced by the PON (with eventual DCF) valuing 0.17ms is negligible compared to the down- and uplink delays between the UEs and the Node B. Thus the PON's 20km of S-SMF (and even additional DCF) is not expected to impact the proposed RoF/PON architectures, and further consolidates our proposals.

[2]for LTE the maximum allowable delay drops to 4ms

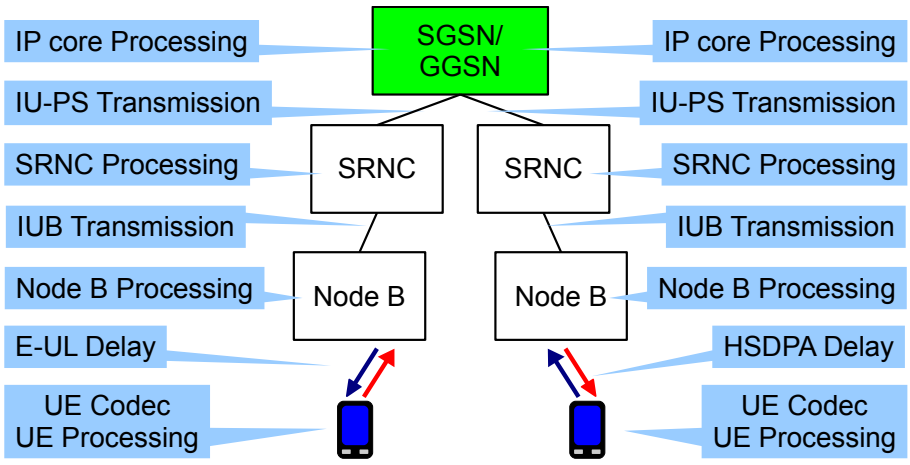

Figure 4.7.: End-to-end delay components, (picture according to [84])

Table 4.1.: Delay repartition in the network for VoIP call between two HSUPA and UE, (from [84])

Entity	**Delay (ms)**	**Delay (ms)**
UE Codec	20	
UE Processing	15	
NodeB Processing	15	
Iub	5	
RNC	5	
Iur	3.6	
Core IP	4	
Iur	3.6	
RNC	5	
Iub	5	
NodeB Processing	2	
HSDPA Delay	50	70
UE De-jitter	20	
UE Decoder	10	
Total (ms)	**163.2**	**183.2**
VoIP E2E Delay for acceptable quality (ms)	**250**	**250**
HSUPA Delay (ms)	**86.8**	**66.8**

5. Analog radio over fiber

5.1. Wavelength shared between radio & fixed broad-band

5.1.1. RF signal electrically added to the NRZ broad-band signal

It is possible to transmit at the same time a fixed broad band Non Return to Zero (NRZ) signal with destination the customers' Optical Network Units (ONUs), and an analog signal such as radio carriers on the same wavelength [86–88].

The main advantage of this technique is that a single optical transceiver is used at emission and at reception. At reception a simple low pass filter allows to recover the fixed broad band signal, while a standard band pass filter allows to recover the radio carrier signals.

As a consequence of this simplicity, in a PON network, a PON termination can be used as a feeder for radio base stations.

Performances in literature

In 2006 [86] used a NRZ signal of 1.25Gbit/s multiplexed with a UMTS radio carrier of 2.1GHz central frequency. [87] in 2008 also used a 1.25Gbit/s PON signal electrically multiplexed with a GSM carrier at 2.0GHz and a Wireless Microwave Access (WiMAX) carrier at 2.5GHz.

In 2009 and 2010, [88, 89] used a NRZ signal at a bit-rate of 2.5Gbit/s combined with a multiplex of radio carriers. For the two latter examples, the multiplex of four WiMAX carriers was 500MHz wide, and centered at 4GHz for the transport in the optical link (instead of 3.5GHz for air broadcasting).

Fig. 5.1 summarizes the different variations [86–89] of Sub-Carrier Multiplexing (SCM) the PON signals of different bit rates with radio carriers.

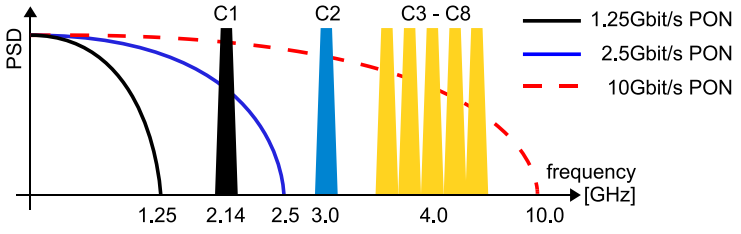

Figure 5.1.: Schematic summary of the different SCM of PON signals with radio carriers [86–89]. C1-C8 represent the different radio carriers.

Despite the novelty and convenience (since published between 2006 and 2010), Fig. 5.1 shows the concept to be limited in case of up-coming 10G-PONs.

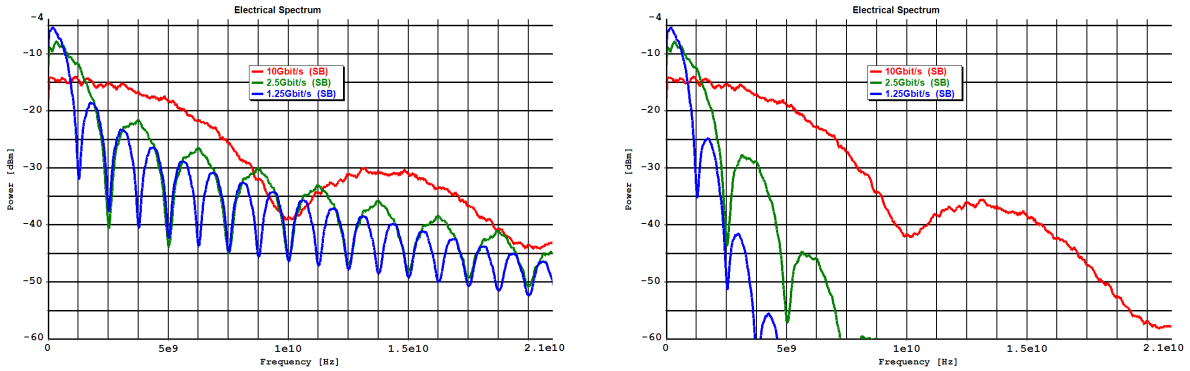

(a) (b)

Figure 5.2.: Electrical spectrum of NRZ signals for different bit rates: (a) unfiltered, (b) low pass filtered by a Bessel of 4th order

Scope of this technique

As we will see, the main drawback of the technique is the spectral occupation of the fixed broad band signal.

Spectral characteristics Current downlink GPON signals (see §2.3, P. 21), egressing from the PON MAC layer, have a NRZ line-coding at a bit rate of 2.5Gbit/s. Given that in the frequency domain, the NRZ signal has a sinus-cardinal envelope, its power spectral density (PSD) occupies the spectrum from 0 to 2.5GHz. This aspect is illustrated for different bit rates in Fig. 5.2a. The occupied spectrum of the low-pass filtered NRZ-signals is shown in Fig. 5.2b.

If we assume the energy contained within the first lobe[1] to be sufficient for yielding BER figures compliant with the PON requirements, then we can deduce that the radio carriers have at least to be frequency multiplexed *beyond* the first transmission zero of the PON's signal (NRZ).

In case of the legacy radio carriers' frequencies to be still too low, then the latter need to be frequency shifted [88, 89]. However this frequency translation would result in more complex RoF emitters' and receivers' architectures due to the additional mixers and filters.

Spectral conflict with legacy radio carriers Furthermore, this multiplexing technique is all the more limited by the fact that next generation PONs targets 10Gbit/s in the downlink (recently normalized) and still uses NRZ line-coded signals, while current (and up-coming) mobile radio legacy carrier frequencies range from 800MHz to 2.6GHz with an additional slot at 3.5GHz.

Indeed, assuming a 10Gbit/s-PON signal electrically superposed to the mobile radio carriers (for instance C1 and C2 in Fig. 5.1), results in a spectral conflict as schematically shown in Fig. 5.1, simply because of the 10Gbit/s-PON signal's spectral occupancy .

[1] 90% of the total energy

A work around would be, as previously, to frequency-shift the radio carriers beyond 10GHz. However this shifting is all the more limited by the typical maximum bandwidth of standard lasers (see §2.3, p. 21). Hence this lowers the possibility of using affordable direct-modulated lasers in Intensity Modulation and Direct Detection (IM-DD) transmissions.

Confined spectrum of PON signals A remedial would be to improve the spectral occupancy (see §2.5.3, p. 37) of the fixed broad band signal by improving its spectral efficiency (by using a DMT[2] or AMOOFDM[3] modulation technique). Generally speaking DMT and AMOOFDM rely on multiplexing several tens to thousands of narrow orthogonal sub-carriers being high-order modulated by taking advantage of the digital FFT and IFFT processes. The total signal rate is spread over the sub-carriers resulting in a low speed modulation per carrier.

Thus the upper bound of the fixed broad-band signal's spectrum is lowered allowing the radio carrier with lower central frequency to be transported. Also improving the spectral efficiency avoids the afore mentioned frequency translations at the extremities of the RoF link.

For instance, let's assume a 10Gbit/s PON signal with a spectral efficiency improved by a factor 4. From now on it has a spectral occupancy reduced to 2.5GHz.

According to §3.1.1, the radio frequency bands at 2.6 and 3.5GHz can then be sub-carrier multiplexed to this improved PON signal. Yet the remaining radio carriers (within the 800, 900, 1800 and 2100 MHz bands) cannot be transported at their native frequencies.

Limited SNR performance However the main limitation of this multiplexing technique appears to be the limited SNR performance.

A typical electrical spectrum capture, for a 21dB optical power budget (link composed of 23.2km of S-SMF and 14dB of splitter losses) in the 1550nm window, is shown in Fig. 5.3.

In this example a 1.25Gbit/s PON signal is electrically multiplexed with four WiMAX carriers: three centered at 3.9GHz and spaced by 25MHz, and a fourth centered at 4GHz.

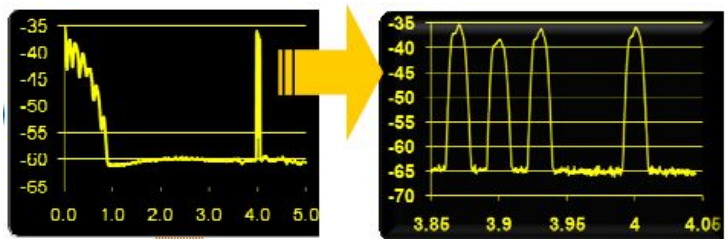

Figure 5.3.: Spectrum capture of a 1.25Gbit/s PON electrically multiplexed with 3 WiMAX carriers, picture from [90]. The horizontal frequency axis is expressed in GHz. The vertical axis corresponds to the power spectral density expressed in dBm.

The shown SNRs for the radio carriers value between 25 and 30dB. This is sufficient for yielding compliant EVM values with respect to the transported radio standard. However

[2]Discrete Multi Tone
[3]Adaptively Modulated Optical Orthogonal Frequency Division Multiplexing

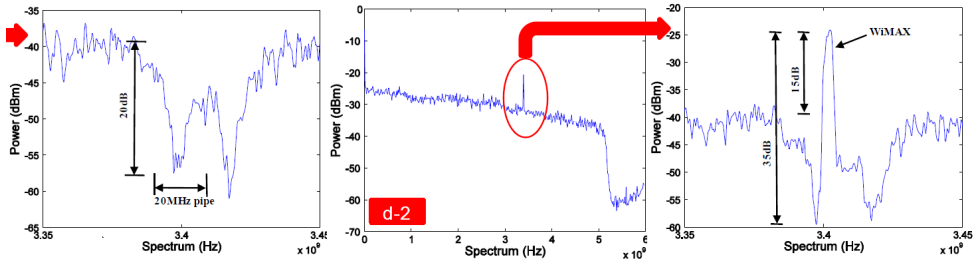

Figure 5.4.: OFDMA detected electrical spectra without and with the WiMAX carrier (from [91])

the SNR value is not compatible with the radio broadcasting in the downlink since the stringent emissions mask, regulating radio emissions, require typical SNRs of 45 to 50dB.

Nevertheless this architecture can fit uplink purposes since no radio broadcast after the RoF transmission is foreseen.

5.1.2. OFDMA-PON with embedded radio carrier

In 2008, [91] proposed an architecture intended collecting uplink optical 10Gbit/s signals and a radio carrier by multiplexing in the electrical domain a WiMAX radio carrier within the fixed broad-band Orthogonal Frequency Division Multiple Access (OFDMA) signals.

The used optical link, is operated around the 1545nm window, and has an optical budget of 20dB including 20km of S-SMF.

The OFDMA signals (5GHz wide) are emitted by different ONUs on different wavelengths (1537 and 1542nm), and are detected by a single PIN photodetector. Furthermore the emitted OFDMA signals have a frequency window of 20MHz (centered on the WiMAX carrier's central frequency) free of OFDM carriers (left inset in Fig. 5.4). The emitted WiMAX signal emitted at 1549nm, has bandwidth of 3.5MHz and the carrier frequency is centered at 3.40175GHz.

After the photo-electrical detection at the Optical Line Termination (OLT), the WiMAX signal can be recovered (middle and right insets in Fig. 5.4). The shown SNR for the WiMAX values 15dB. Yet SNRs up to 22.3 dB are reported, when increasing the received optical power.

From an architectural point of view, this set-up could be as well used for the downlink. Yet the stringent emissions mask regulating radio emissions require at least a SNR of 45 to 50dB. Nevertheless this architecture is suitable for uplink needs where emissions masks are not an issue.

5.1.3. ODFM-PON with chained uplink path

Working principle

[92] suggests to *daisy-chain* (Fig. 5.5a) the ONUs of a PON by the mean of an optical distribution device (ODD) built of a main coupler and several circulators.

In the downlink, the architecture works as a legacy PON —except the circulators.

In the uplink however, the proposed architecture consists of making the uplink wavelength hopping —by the mean of the circulators— from an ONU to the next ONU. The hopping

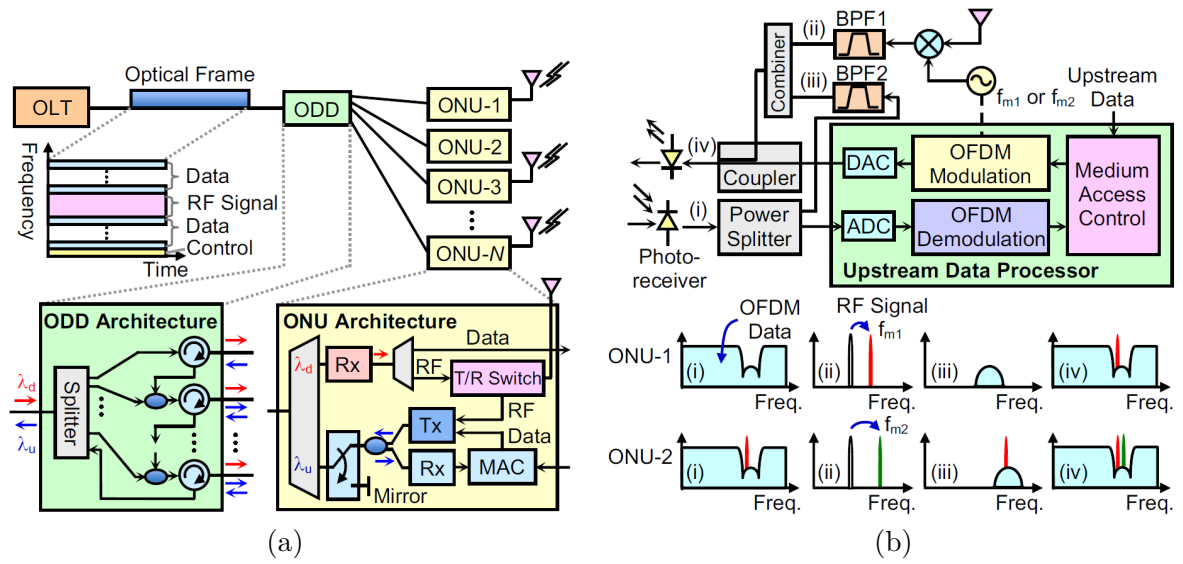

Figure 5.5.: (a) Architecture, (b) superposition of the radio signals with the fixed broad-band; [92].

path is set by the order of the cascaded circulators, and is fix.

Aggregation of the uplink signals

Compared to a standard PON where the aggregation of the uplink signals is done in the optical domain by the optical couplers thanks to a timing/ranging algorithm, in this example the aggregation is done at the Medium Access Layer (MAC) level of each ONU.

At each ONU, the fixed broad-band Orthogonal Frequency Division Multiplexing (OFDM) signal sent by the previous ONU is demodulated and additional information that is to be transmitted, is added to the demodulated OFDM signal. Hence the multiple access scheme takes place at the bit level. Then the resulting data flow is OFDM modulated in order to be transmitted on the uplink wavelength (Fig. 5.5b) towards the next ONU. Finally the uplink signal reaching the OLT has been *enriched* with data from each ONU.

Radio signal

Concerning the uplink radio signal, the approach is similar to the one of the fixed broadband signal, except that the radio signals are not demodulated: the different radio carriers are frequency shifted in order to be placed within a frequency window inside of the broadband signal. A signalization mechanism (carried in some of the OFDM broad-band signal's sub-carriers) allows to allocate the right frequency slot to the different radio carriers.

Interest

The advantage of this architecture is to use only two wavelengths (one per propagation direction), each being used as well for the distributing and collecting the fixed broad-band and mobile radio signals.

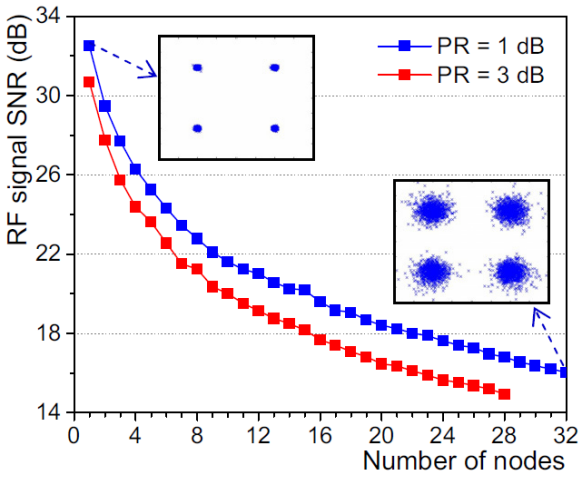

Figure 5.6.: SNR of the uplink RF signal as a function of the number of hops: the optical received power is fixed at -11 dBm, and the term PR is the driving power ratio of the OFDM versus the RF signal, (figure from [92]). N refers to the number of passed ONUs.

Scope of this technique

Yet the main weak point of this architecture comes from its daisy-chain property: the cumulated processing times due to the modulation and demodulation of the fixed broadband OFDM signal at each of the ONUs increase the total round trip time and make the latter become a fixed function of the ONU's position in the chain.

For a downlink application, distributing radio carriers, this technique since similar to the one presented in §5.1.2, necessarily inherits from its drawbacks, namely the limited SNR performance.

For uplink applications, the provided SNRs in Fig.5.6, for the proposed QPSK modulation scheme, are acceptable. However again due to the cascaded structure of this architecture, the SNR decreases (because of the interference from OFDM signal's side-lobes) with the number of ONU-hops.

5.2. Wavelength(s) dedicated to the radio carriers

The main benefit of dedicated wavelengths is the ability to offer a future-proof optical pipe to the radio signals independently of the evolution of the radio standards as well of the evolution of the optical access modulation format. Yet some care has to be brought in terms of optical isolation when (de)multiplexing them [93].

5.2.1. Sub carrier multiplexing of analog RF signals

Generalities

The main advantage of this technique is of course the transparent transport of the radio carriers at their native carrier frequencies. Current lasers (see Part 1) have bandwidths wide enough for carrying radio carriers at their respective broadcast frequencies.

This property lowers the complexity of the up- and down-mixing stages at the remote antenna site as schematically shown in Fig. 5.7. Also at the receiving-side, simple optical detectors are sufficient.

Finally these arguments, make this type of architecture very attractive to use.

Integration of commercial systems

Off-the-shelf systems, as manufactured by Andrew Wireless[4], transparently transport the RF spectrum from 700 to 2500MHz.

These systems typically handle optical links built of S-SMF with lengths up to 3km, and use the 1310nm wavelength to transport the RF signals to and from remote antenna sites. The total optical budget, between the central unit and the remote antenna sites, values around 16dB.

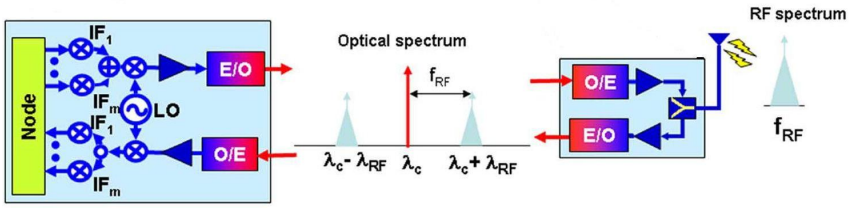

Figure 5.7.: Optical transport scheme for analogue signals at RF frequency, (picture from [82])

Commercial equipments are designed for meeting the Spurious Emissions Mask (SEM) requirements in terms of Signal to Noise Ratio (SNR) and Adjacent/Alternate Channel power Leakage Ratio (ACLR). Yet these systems cannot cope with the budget requirements of PONs which typically range from 13 to 28dB. Furthermore in case of PONs, the 1310nm wavelength is already used. Last but not least, commercial systems in order to get rid of the optical duplexing issues and its related costs, use a single optical fiber per propagation direction. This aspect is not acceptable for integration into PON systems, and may require re-designing the radio distribution system.

[4] http://www.commscope.com/andrew/eng/product/cov_cap/das/index.html

For these reasons, commercial systems unfortunately cannot be directly integrated into PON architectures.

5.2.2. Sub carrier multiplexing of analog IF signals

The main benefit when using SCM of analog IF signals, is that bandwidth limited components can be used. Another advantage of working at IF frequencies is the possibility of re-arranging the spacing of the transported signals.

As the requirements in terms of RF modulation bandwidth of the laser at the transmitter-side can be lowered, the complexity at the receiving-side is increased since down- and up-mixing stages are required at each remote antenna site (Fig. 5.8).

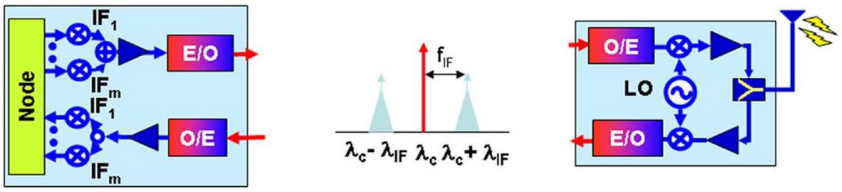

Figure 5.8.: Optical transport scheme for analogue signals at IF frequency, (picture from [82])

Example in literature

In this section, we will briefly present an example of the sub-carrier multiplexing feasibility for different radio signals at Intermediate-Frequency (IF) (several hundreds of MHz) developed by [94]. Again the optical budget is approximately 16dB (11dB spent for splitting, and 5dB for 20km of S-SMF).

The proposed technique relies on frequency translation by transposing the signals which are received and broad-casted at 5.8GHz in the air, to frequencies ranging from 500 to 2000MHz by 250MHz steps for the transmission in the optical link. This allows to aggregate and to broadcast several different radio signals to and from different radio cells using the same frequency in the air link.

In the downlink eight radio channels spaced by 250MHz are packed on a single wavelength.

In the uplink each Remote Radio Unit (RRU) emits at different wavelengths (1510 and 1530nm). For each target RRU four radio channels spaced by 500MHz —non superposing in the electrical domain— are multiplexed per wavelength.

The estimated SNR of the up-mixed carrier values 40dB, which is not sufficient for downlink applications.

6. Digital & Digitized Radio over Fiber

6.1. Digital baseband

As exposed in the *Mobile backhaul* section of the previous part, the base station located at the antenna site can be *fed* with data by an digital link (E1 for instance).

Each base station processes the received data flow to the convenient radio standard protocols before pulse-shaping and up-mixing them in to the radio-frequency domain for broadcast.

In an optical access network, an ONU can play the role of the modem for the base station (Fig. 6.1).

Customer ONU and base station sharing the ONT

Since the ONU and the base station can be connected without any special requirements, this architecture is very intuitive.

However, because the optical access network and the radio network operate independently, the ONU and the BS operate blindly. As a consequence of blindly sharing a same Optical Network Termination (ONT), the available bandwidth is not optimally shared between the competing ONU and BS.

Thus occasional congestion can occur, lowering the benefit of this type of architecture. Furthermore two independent devices, an ONU and a BS, are required at the boundary of the two systems, which is likely to be more costly than using an integrated box as discussed later [95].

Base station with dedicated ONT

Another idea is to dedicate to the base station a single ONT. However again multiple base stations within an optical access network may disturb the customers traffic because of

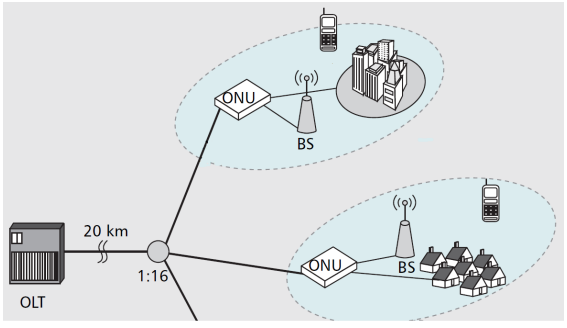

Figure 6.1.: ONU serving as modems for radio base stations, (picture from [95])

their different class of service requirements: several base stations when sending upstream data will be prioritized with respect to the customers' data traffic.

Even if customer are sold *best-effort* connections, too numerous base stations, may again degrade (because of bursty traffic) the connections of customers of the optical access networks.

Finally, both solutions do not take advantage of the distributed antenna concept, and also require a full base station at every antenna.

6.2. Agnostic digitizing of radio signals

The scope of this section is to explain how radio carriers (at intermediate or at broadcasting frequencies) can be digitized in an almost agnostic way to the radio standards.

Once a radio signal is digitized and the samples encapsulated into packets, the final digital flow no longer depends on the transported radio standard. Also the dependency on the radio standard is reduced to the digitizing and reconstruction stages.

6.2.1. Techniques scope

Practical limitations of directly applying the Shannon theorem

A first glance, the Shannon Theorem requires to sample the RF signal at a frequency at least the double of the highest frequency contained in the spectrum of the signal that is to be digitized. The resulting information bandwidth contains all frequencies from DC to half of the sampling frequency. A processor, via software, is then expected to digitally filter, decimate, and operate further baseband functions.

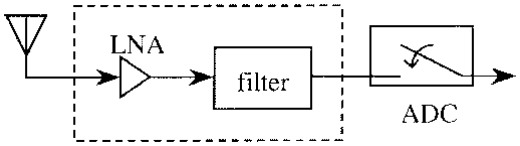

Figure 6.2.: Direct digitization front-end, (picture from [96])

For instance the upper bound of the UMTS Band I is 2170MHz, and would require a sampling frequency of at least 4340MHz. Then assuming a 9-bit resolution[1] —provided that such an ADC exists— the resulting bit stream would be 39.06Gbit/s. Hence the digitizing at the RF carrier frequency using Shannon's theorem, as in Fig. 6.2, is not practical.

Remaining Techniques

Currently two digitizing techniques of the complex base-band envelope[2] exist. They differ by the frequency shifting requirements prior to digitizing:

1. frequency shifting the signal to a lower intermediate frequency (as close as possible to 0Hz frequency as shown in Fig. 6.3), and then use legacy digitizing techniques (Shannon)

2. digitizing the radio signal at its carrier frequency using the Band Pass Sampling (BPS) technique

Of course the latter can also handle signals that are frequency-shifted lower than their initial carrier frequency, yet it is not its main interest.

[1] for a target SNR of 50dB since for an *ideal* ADC: $SNR_{dB} = 6.02 \cdot N + 1.72$, where N is the resolution
[2] in the sense that the I and Q components are mixed and indiscernible

6.2.2. Digitizing using Shannon on frequency-shifted signals

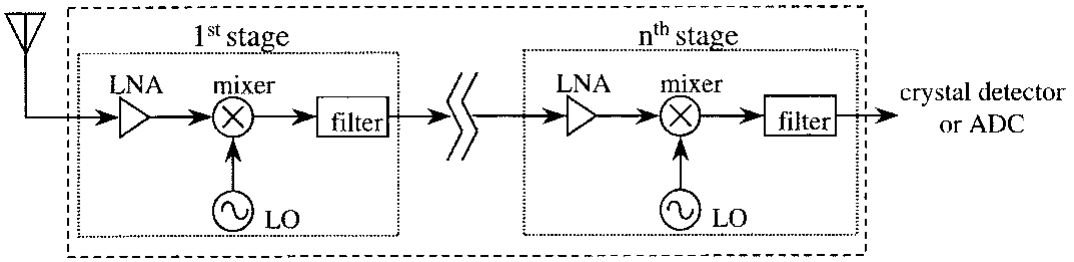

Figure 6.3.: Traditional digitization front-end, (picture from [96])

As far as 1993, [97] suggests to build digital radio over fiber networks by digitizing down-mixed radio signals in order to fit the sampling capabilities of the ADCs.

Example of a commercial product

The *ADC* company proposes such a system that digitizes portions of spectrum, and uses legacy digital transceivers for meeting optical budgets of 25dB.

The maximum bit stream resulting of the digitizing, and that can be handled by the system, values 3.072Gbit/s and allows to carry approximately 60MHz of spectrum, when using UMTS signals. Thus we can assume each 5MHz portion of spectrum *i.e.* each UMTS carrier to represent $1/12^{\text{th}}$ of the bit stream (256Mbit/s). Assuming a 9-bit precision for the Analog to Digital Converter (ADC), the sampling frequency values 28.4MHz. Given the spectral occupancy of an UMTS carrier to be 4.68MHz, the oversampling factor values roughly 6.

Despite the fact that carrying a UMTS carrier only requires one twelfth of the link's capacity, the used protocol's bit rate does not adapt to the payload, and therefore requires a 3.072Gbit/s data flow to transport a single UMTS carrier. Hence this solution limits its integration into current PON's digital flows (2.5Gbit/s in the downlink). As a result, a separated and dedicated wavelength is required.

The main drawback of this technique is the required Local Oscillator (LO) for down- and up converting the radio signal in order to fit the sampling bandwidth of the ADC.

6.2.3. The Band Pass Sampling concept

A digitizing technique that allows to get rid of the carrier frequency issue when digitizing is the BPS theorem [98]. It consists undersampling a modulated signal to achieve frequency translation by intentionally aliasing of the information bandwidth of the signal [97].

Thus the sampling frequency requirement is no longer based on the frequency of the RF carrier, but on the occupied information bandwidth of the signal. As we will see the resulting sampling rate can be significantly reduced.

Sub-sampling and spectral folding

The signal is required to be *bandpass* type, which is the case of radio carriers.

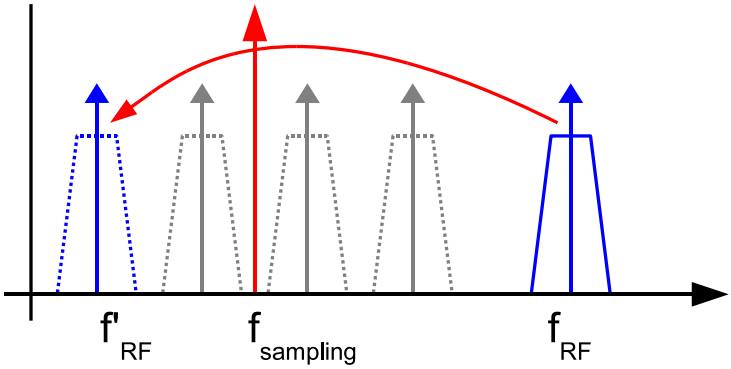

Figure 6.4.: Frequency shift induced by the BPS technique

In this case a signal of bandwidth B, within the frequency range f_{low} to f_{high} can be rebuilt from the samples under the condition that the sample rate f_s abides with the condition:

$$f_s \geq 2 \cdot \frac{f_{high}}{n} \tag{6.1}$$

where n is the greatest integer of the ratio $\frac{f_{high}}{B}$:

$$n = \left\lfloor \frac{f_{high}}{B} \right\rfloor \tag{6.2}$$

Due to the sub-sampling procedure, multiple copies of the sampled frequency band of interest can be found in the spectrum as shown in Fig.6.4. Whether n is odd or even, the first occurrence of the side band of interest is respectively located below or beyond the sampling frequency.

The main advantage of BPS is that the information band is acquired without any LO mixing and image filtering. Only a narrow bandpass filter (Fig. 6.2) centered above the carrier frequency attenuating the frequencies outside the information band is required. However at the re-built stage, a LO is still required.

In a radio environment where several standards exist, the first step is to keep the frequency band of interest isolated (by using standard diplexers), limited, and as narrow as possible in order to lower the specifications of the sampling frequency.

Performances by Nirmalathas [99, 100]

When using the BPS method, according to experiments and formal expressions, the SNR at the output is directly proportional (valid up to 8 bits) to the resolution of the ADC (Fig. 6.5a). Beyond a resolution of 8 bits, the SNR is dominated by the jitter of the ADC.

The digital flow being function of the flow generated by the ADC, it is possible to link the output SNR to the required bit rate of the link (Fig. 6.5b).

However the SNR performance show in Fig. 6.5a is limited to 40dB which is not sufficient for downlink distribution of radio carriers given the ACLR requirements.

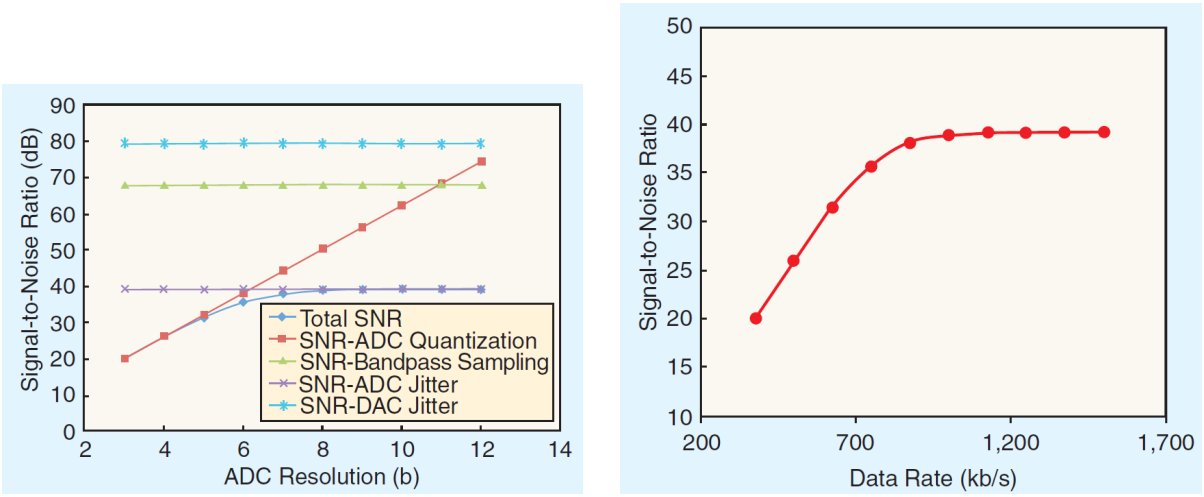

(a) (b)

Figure 6.5.: Performances of the BPS-RF technique (a) SNR as a function of the ADC resolution, contribution from the different components; (b) SNR as a function of the link bit rates. (both pictures from [99]).

Performances by Kim [101]

From [101]'s experimental results, we can derive a quick application for UMTS downlink signals. According to the Fig. 6.6, when targeting an output SNR of 50dB, the ADC resolution is to be at least of 9bits, for the different possible rms jitters, the maximum input frequencies are 850, 1080, and 1450MHz.

Thus directly BPS UMTS carriers in the 2100MHz range is not possible. However, let's assume the RF band of interest can frequency-shifted[3] close to the frequency range for which output SNRs of 50dB are achievable.

The goal is to BPS 25MHz of efficient spectrum —3 UMTS carriers spaced by 10MHz for instance. Also as recommended by [98] *some* guard-band at each side of the band of interest is required. For instance [99] used a 2.5 ratio between the total bandwidth and the effective band of interest, thus let's target a digitization of a 62.5MHz portion of spectrum.

Applying the formulas of §6.2.3, the minimal sampling rates can be found. Assuming a sampling resolution of 9 bits, then the minimum raw bit streams can be found: 1.15 to 1.17Gbit/s. These bit stream are **minimum** and are expected to increase due to overhead information and eventual Forward Error Correction (FEC) code.

Given the ACLR and SNR requirements of downlink UMTS signals, band-pass sampling them at their initial central frequencies of 2.1GHz appears to be limited and even impossible. Yet for central frequencies in the 800MHz range this seems to be possible.

Recently the 832-862MHz band were authorized to be used LTE signals (which has downlink ACLR/SNR requirements of 45dB). Also different operators aim at using the 900MHz band, initially allocated to GSM, for UMTS. Finally this BPS technique could be used for the latter mentioned radio bands on radio signals that do not require to

[3] of course this introduces complexity

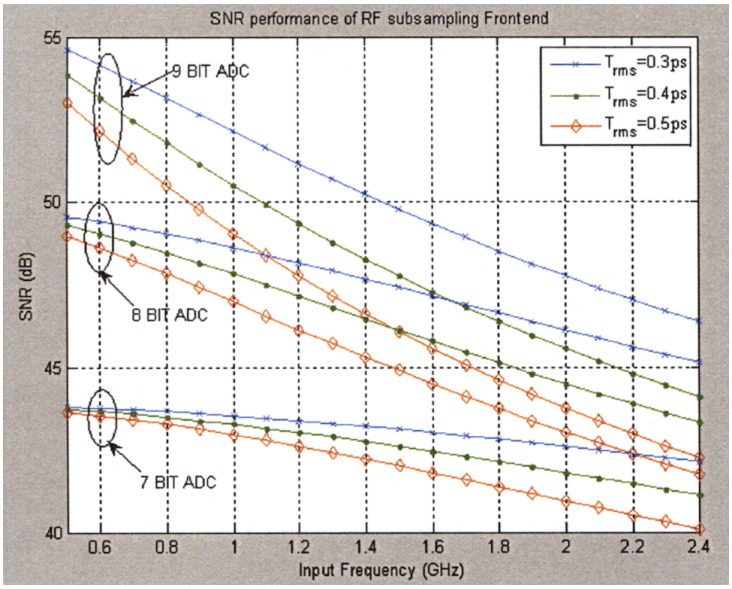

Figure 6.6.: Effect of jitter, ADC resolution and input frequency on the SNR (Fig. from [101])

Table 6.1.: Minimum raw bit streams using [101]'s BPS results (9-bit resolution)

BW [Mhz]	BW w/ guard [Mhz]	fc [Mhz]	fmax [Mhz]	n	fs min [Mhz]	Minimum Raw Bistream [Mbit/s]
25	62.5	800	831.25	13	127.9	1151
25	62.5	1000	1031.25	16	128.9	1160
25	62.5	1400	1431.25	22	130.1	1171
25	62.5	2140	2171.25	34	127.7	1149

be frequency-shifted. Then however the main advantage of the BPS technique (vs. the Shannon theorem technique using a LO for down-mixing) is lost.

6.3. IQ-digitizing with radio-standard adapted sampling frequency

Additionally to the afore exposed digitizing techniques, another method exists for realizing digitized RoF transmissions: it consists in digitizing the In-phase (I) and Quadrature phase (Q) components of the signal. Several samples of each I and Q symbols are then aggregated in a packet[4].

This technique differs from the previous digitizing technique by the fact that only a very specific portion of the spectrum is digitized. Thus this digitizing procedure offers a finer granularity since each flow of IQ-samples reflects the data to/from one antenna for one carrier. However —in no case— the signal is demodulated, which would require synchronization, frame reconstruction... Finally, the sampling rate can be adapted to the symbol rate, to the occupied bandwidth, and to the standard of the transported radio signal.

As the technique exposed in the previous section, this IQ-digitizing process cannot be labelled as a pure *RoF* technique, since once the I and Q channels are sampled and packed into packets, the transport of the latter no longer depends on the transported radio signal.

Currently two specifications, Common Public Radio Interface (CPRI) and the Open Base Station Architecture Initiative (OBSAI), using this technique exist. Both specifications aim at making compatible —by proposing standardized and almost open[5] interfaces— the different radio equipments of different vendors.

Finally both propose a dedicated communication protocol for transfers of digital radio and control data between wireless infrastructure base-station modules.

6.3.1. CPRI

The Common Public Radio Interfance (CPRI) specifications [102] foresee to up-sample each I and Q symbol by a factor of one, two, or four, in order to aggregate them in packets called *IQ Data*.

The up-sampling factor depends on the chip/symbol rate and on the bandwidth of the signal to be digitized. Fig. 6.7 shows the *mapping* of the samples into packets. The purpose of the samples mapping is to provide —at the output of the link— the samples of the I and Q channels as close as possible in time.

CPRI protocol

As shown in Fig. 6.8, additionally to the user plane (containing the IQ data block of Fig. 6.7), a control and management as well as a synchronization (SYNC) signals exist.

Therefore an overhead containing the Operation, Administration, and Management (OAM) signals is added to the raw IQ data block payload. Additionally to the samples, an overhead containing data for OAM, synchronization, and control is added. Finally this allows the information flows to be exchanged (Fig. 6.8a) between the Radio Equipment Control (REC) and the Radio Equipment (RE) over a Time Division Multiplexing (TDM) multiplexed digital serial communication link, either optical of electrical.

[4] the whole radio signal information is contained within the packets. The data packets *can* be aggregated with the PON signal (NRZ for instance) at the bit level.

[5] CPRI foresees the possibility of vendor specific data field, (Fig. 6.8b)

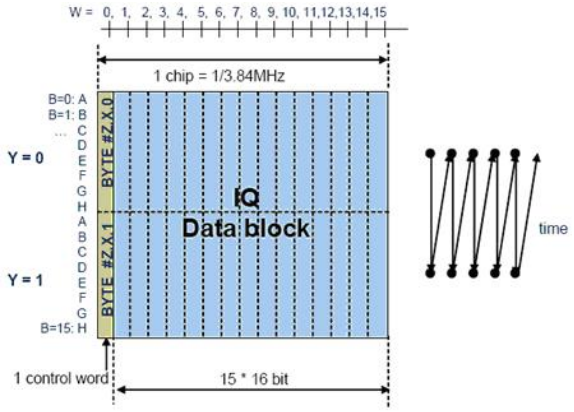

Figure 6.7.: CPRI IQ mapping

The REC unit contains the network interface, and is typically located at the CO, while the RE elements correspond the *distributed* part of the system, and are therefore located closely to the antennas.

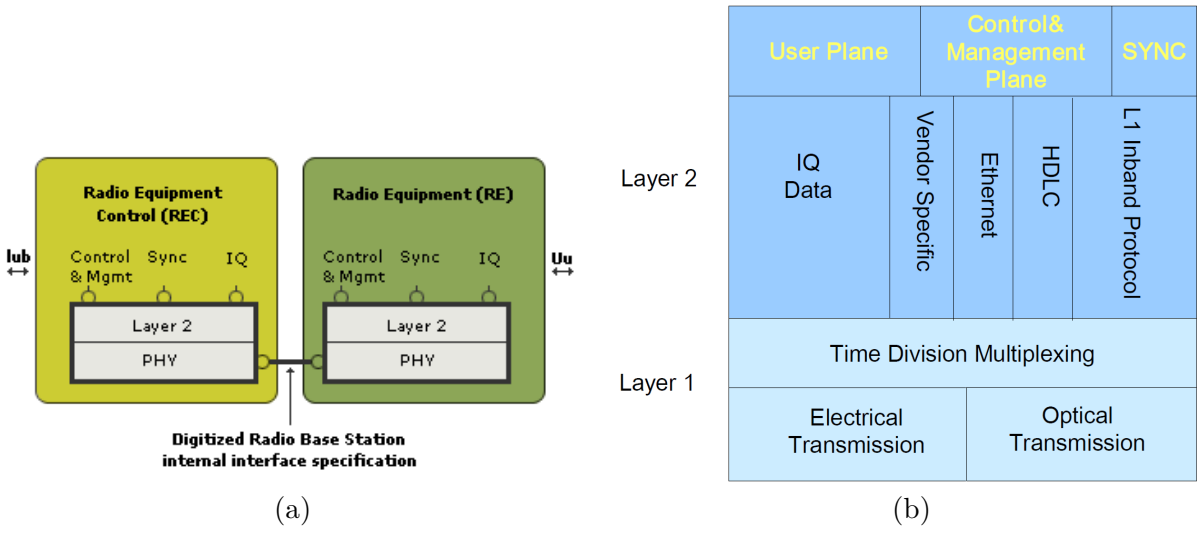

Figure 6.8.: CPRI: (a) interface, (b) protocol layers

The resulting packets generate digital flows with bit rates ranging from 614.4 to 6144.0Mbit/s (other possible values are 1228.8, 2457.8, 3072.0, and 4915.2Mbit/s). For instance the minimal bit rate of 614.4Mbit/s corresponds to 4 UMTS FDD carriers up-sampled by a factor 2, with an 8-bit ADC resolution (minimum), and the whole stream 8B/10B encoded.

The re-use of standard optical transceivers such as *FibreChannel* and *Gigabit Ethernet, IEEE802.3* is encouraged by the CPRI standard.

CPRI topologies

The bit rates of the CPRI flows are function of the standard(s) and the bandwidth(es) of the carried signal(s). However the bit rates also depends on the chosen topology.

Indeed, in a daisy-chained or protected topology, the link being the closest to the central will have to bear the traffic from/towards the other cascaded remote radio sites (Fig. 6.9).

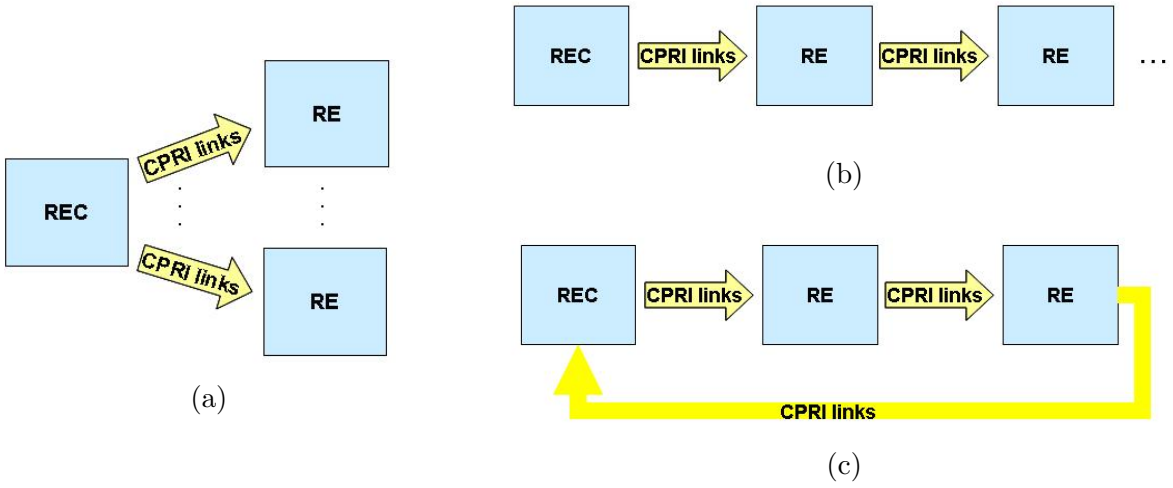

Figure 6.9.: Chaining possibilities of CPRI remote sites: (a) star; (b) daisy chain; (c) unidirectional ring;

CPRI bandwidth requirements

According to [102], the I **and** Q components, of an UMTS FDD downlink signal, should be **each** oversampled by a factor 1 or 2. The ADC resolution for UMTS FDD downlink signals is specified between 8 and 20 bits. Furthermore the raw payload is encoded by 8B/10B scheme. Hence the resulting minimum and maximum bit stream for one and three UMTS FDD downlink carriers are given in Tab. 6.2.

Table 6.2.: CPRI bit streams for one and three UMTS DL carriers

ADC **resolution** * **oversampling** factor	**Bit stream** after 8B/10B coding (Mbit/s)	
	1 carrier	3 carriers
8-bit * 1 sample/chip	76.8	230.4
8-bit * 2 sample/chip	153.6	460.8
20-bit * 1 sample/chip	192	576
20-bit * 2 sample/chip	384	1152

The CPRI specifications are published by the equipment manufacturers Ericsson, Huawei, NEC, Nokia Siemens Networks and Alcatel-Lucent.

Example of a CPRI product

A remote radio head (RRH) built by the company *GPCS* [103] can handle up to 20MHz of radio spectrum. These 20MHz can be composed of, either:

1. three W-CDMA carriers and one LTE carrier of 5MHz
2. two W-CDMA carriers and one LTE carrier of 10MHz
3. a single LTE carrier of whether 5, 10, or 20MHz

According to previous computations the resulting bit stream is 614Mbit/s.

6.3.2. OBSAI

Contrary to the CPRI specifications, the Open Base Station Architecture Initiative (OBSAI) specifications [104], are supported as well by telecommunication equipment manufacturers as by semi-conductor companies.

Yet OBSAI sampling specifications are similar of those in CPRI. For instance a digital link of 3.072Gbit/s is necessary for transporting four UMTS FDD carriers. The performances of an OBSAI compliant product is given in [105], and summarized in Tab. 6.3.2.

Table 6.3.: Capacity in number of transported radio carriers, for 3072 and 6144Mbit/s OBSAI links

			Number of radio carriers	
Air-Interface	Sample Rate	Channel BW	3.072 Gbit/s link	6.144 Gbit/s link
802.16e	11.2 Msps	10 MHz	5	10
802.16e	22.4 Msps	20 MHz	2	5
LTE	15.36 Msps	10 MHz	4	8
LTE	30.72 Msps	20 MHz	2	4

6.3.3. CPRI vs. OBSAI

Despite the similarities between CPRI and OBSAI specifications for transporting samples of the I & Q signals, the implementations differ, and result in different payload efficiencies (Tab. 6.4). Indeed CPRI has less overhead data compared to OBSAI.

Another advantage of using CPRI is that the required Bit Error Rate (BER) of 10^{-12} for the dataplane, is less strict than the OBSAI requirement of 10^{-15}.

6.3.4. Digitized radio symbols with centralized carrier distribution

[107] proposes a variation of the afore mentioned D-RoF architecture using the sampled-symbol technique, by putting the LO sources, required for frequency-shifting the radio signals, at the CO instead of the remote antenna site.

Table 6.4.: OBSAI and CPRI protocol efficiencies for a 3072Mbit/s link, [106]

	OBSAI RP3-01	CPRI
User Data (IQ)	**80.0%**	**93.75%**
Control Data (O&M)	4%	6.225%
Synchronization (K-char)	0.25%	0.025%
Fixed Overheads	15.75%	0%

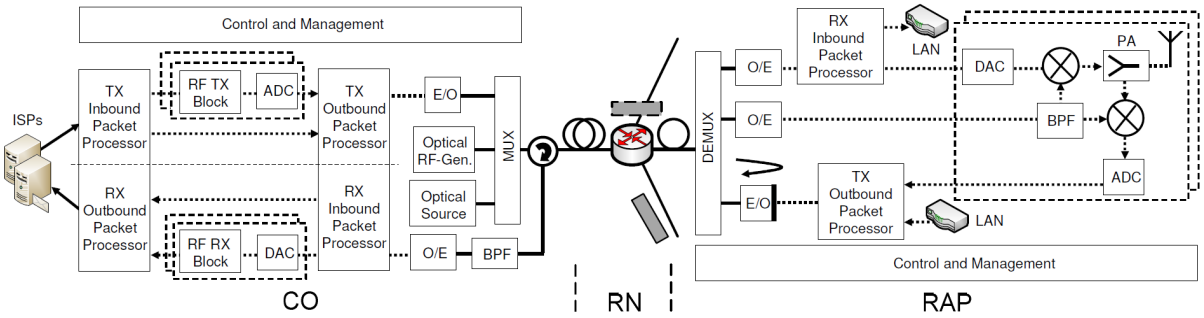

Figure 6.10.: D-RoF with centralized carrier distribution (picture from [107])

In order to realize this, [107] suggests to dedicate wavelengths to the transport of the sampled symbols of the radio signal, and to dedicate one wavelength to the transport of the unmodulated LOs.

At the remote antenna station a Band Pass Filter (BPF) separates the downlink and uplink intended LOs.

The downlink intended sampled-symbols are recovered by an DAC prior to up-mixing with the proper LO, prior to broadcasting. The uplink radio carriers ingressing the Radio Access Point (RAP) are down-mixed by the proper LO before being digitized using the symbol-sampling technique, and sent to the CO.

Compared to the proposal of the previous section, this allows to simplify the Remote Antenna Site (RAS).

Conclusion

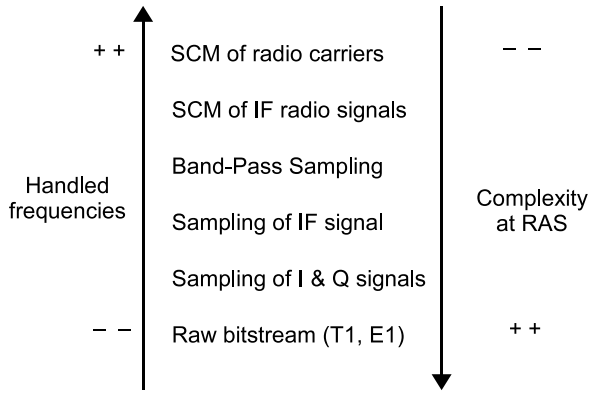

Figure 6.11.: Complexity at RAS and frequency handling capability of different RoF techniques

Fig. 6.11 summarizes the panel and compromises of the various analog and digital radio over fiber techniques exposed in this part: the higher the handled frequencies by the optical transport system increase are, the lower can be the complexity at the remote antenna system (RAS).

The legacy digital bit stream solution, despite its simplicity, requires complex base stations located closely to the antennas thus not taking advantage of distributed antenna systems.

When using the digital sampling technique at IF frequencies, than commercial solutions exists, yet the produced bit stream is larger then the current downlink PON capacity itself.

The Band Pass Sampling technique is interesting thanks to its reduced complexity but even at low optical budget currently reported performances in bibliography do not allow to meet the electrical SNR/ACLR figure of merits for downlink UMTS FDD carriers.

The sampling of the individual IQ components offers the required signal performances but at the expense of huge digital data streams —larger than the PON downlink stream itself.

Of course the current PON downlink stream capacity is expected to increase towards 10Gbit/s, and may be a new opportunity for these digitized RoF concepts.

Finally the analog sub carrier multiplexing techniques are not compatible with the optical budget requirements of typical PON networks. Yet it offers, especially the RF version, compliance with the SEM issues. The challenge consists in making it compatible with typical PON budgets.

Thus the next two following parts will address this technique within a PON framework, and study its limits and possibilities in such a context.

Part III.

Computing & Simulations

Purpose

The goal of this part is to provide, in a first time, some basic analytical expressions when employing analog Radio over Fiber (RoF) techniques. Therefore the output Signal to Noise Ratio (SNR) figures are expressed for pure lossy, and for optically amplified links.

In a second step, we introduce the *VPItransmissionMaker* simulation tool. Using a two tone signal, we evaluate the impact of the Inter-Modulation Distortion (IMD) of order three due to the interaction of the laser's frequency chirp and the fiber's chromatic dispersion.

Finally, we will use the simulation tool to emulate an UMTS carrier transmission over a typical Passive Optical Network (PON) infrastructure. Therefore realistic UMTS signals are used and their influence on the system performance discussed.

7. Analytical expressions for analog RoF

7.1. General signal expressions

In this chapter, we only assume an *internal* Intensity Modulation and Direct Detection (IM-DD) scheme since we target the transport of radio carriers which have their frequencies below 5GHz, and thus do not require to *external* modulation schemes.

7.1.1. Sine signal

Assuming the LD's light intensity to be modulated by the input current, and the modulating signal to be a simple sine tone of peak amplitude a, then the instantaneous optical power is:

$$P_{opt}(t) = P_0 + \eta_{EO} \cdot a \sin(\omega_m t) \tag{7.1}$$

where η_{OE} is the laser diode's static conversion efficiency, and P_0 is the average CW optical output power:

$$P_0 = \eta_{EO} \cdot (I_{BIAS} - I_{THRESH.}) = \eta_{EO} \cdot I_{DYN} \tag{7.2}$$

Transmitted optical signal

The instantaneous emitted optical power $P_{optTX}(t)$ can be written as:

$$P_{opt\ TX}(t) = \eta_{EO} \cdot I_{DYN} \left(1 + \frac{a}{I_{DYN}} \cdot \sin(\omega_m t)\right) \tag{7.3}$$

By setting the Optical Modulation Index (OMI) as:

$$OMI = \frac{a}{I_{DYN}} \tag{7.4}$$

The instantaneous transmitted optical power is :

$$P_{opt\ TX}(t) = P_0 \cdot (1 + OMI \cdot \sin(\omega_m t)) \tag{7.5}$$

Received optical signal

The received optical instantaneous power, after a fiber free link with transmission losses $1/L$, is:

$$P_{opt\ RX}(t) = \frac{1}{L} \cdot P_{opt\ TX}(t) \tag{7.6}$$

Assuming a PIN photodetector, the instantaneous photo-detected current is :

$$i_{photo}(t) = \eta_{OE} \cdot P_{opt\ RX}(t) \tag{7.7}$$

where η_{OE} is the overall conversion efficiency of the photo-diode.

The average detected photo-current is:

$$I_0 = I_{photo} = \eta_{OE} \cdot P_0/L \tag{7.8}$$

At the receiving side, the power of the signal of interest is the RMS power component at ω_m:

$$P_{RF\ out} = \left\langle i_{sig}^2 \right\rangle_{RMS} \cdot Z_{out} \tag{7.9}$$

$$\left\langle i_{sig}^2 \right\rangle_{RMS} = \left\langle \left[\eta_{OE} \frac{P_0}{L} \cdot OMI \cdot \sin(\omega_m) \right]^2 \right\rangle_{RMS} = (I_{photo} \cdot OMI)^2 \cdot 1/2 \tag{7.10}$$

Finally,

$$P_{RF\ out} = 1/2 \cdot I_{photo}^2 \cdot OMI^2 \cdot Z_{out} \tag{7.11}$$

Eq. 7.11 shows the interest of setting the OMI to unity in order to maximize the detected average RF power.

7.1.2. Generalization to any signals

The OMI as it is defined in Eq. 7.4 only highlights the peak amplitude for a sine signal. Thus the resulting expression of the carrier power in Eq. 7.11 is only valid for pure sine signals, which is very limited.

Taking into account the crest factor

The goal of this section is to link the RF output power to the OMI for any type of signals. Therefore in a first step —for any given signal— we link the RMS power to peak power by taking advantage of the crest factor (see §3.3.3, p. 67).

$$P_{peak\ dBm} = P_{RMS\ dBm} + CF_{dB} \tag{7.12}$$

The latter relation ship is usually used for powers. However it can be derived for equivalent currents:

$$I_{peak} = \sqrt{CF} \cdot I_{RMS} \tag{7.13}$$

Transmitted signal

Then Eq. 7.3, for any modulating signal carrying information, can be rewritten as:

$$P_{opt\ TX}(t) = \eta_{EO} \cdot I_{DYN} \left(1 + \frac{1}{I_{DYN}} \cdot i_{info}(t) \right) \tag{7.14}$$

Generalized OMI expression

By identifying with the expression the sine signal version, we can define respectively a *RMS* and a *peak* OMI:

$$OMI_{RMS} = \frac{I_{peak}}{\sqrt{CF} \cdot I_{DYN}} \qquad OMI_{peak} = \sqrt{CF} \cdot OMI_{RMS} \tag{7.15}$$

By substituting the crest factor value of a single tone sine signal ($CF = 2$) into the latter expression, the peak OMI equals the one used in the afore section for a sine signal.

Received signal

The received current, after DC filtering, can be expressed as:

$$\left\langle i_{sig}^2 \right\rangle_{RMS} = \left\langle \left[\eta_{OE} \frac{P_0}{L} \cdot \frac{i_{info}(t)}{I_{DYN}} \right]^2 \right\rangle_{RMS} \tag{7.16}$$

$$= \left(I_{photo} \cdot \frac{I_{info\ RMS}}{I_{DYN}} \right)^2 \tag{7.17}$$

$$= \left(I_{photo} \cdot \frac{I_{peak}}{\sqrt{CF} \cdot I_{DYN}} \right)^2 \tag{7.18}$$

Finally,

$$P_{RF\ out} = I_{photo}^2 \cdot OMI_{RMS}^2 \cdot Z_{out} \tag{7.19}$$

$$= I_{photo}^2 \cdot \frac{OMI_{peak}^2}{CF} \cdot Z_{out} \tag{7.20}$$

Expanding Eq. 7.19 leads to:

$$P_{RF\ out} = \left(\eta_{EO} I_{DYN} \frac{1}{L} \eta_{OE} \right)^2 \cdot \left(\frac{I_{RMS}}{I_{DYN}} \right)^2 \cdot Z_{out} \tag{7.21}$$

$$= \left(\eta_{EO} \frac{1}{L} \eta_{OE} \right)^2 \cdot \left(\frac{P_{RF\ in}}{Z_{in}} \cdot Z_{out} \right) \tag{7.22}$$

which finally allows to retrieve the well known RF gain formula for the link:

$$Gain_{RF} = \frac{P_{RF\ out}}{P_{RF\ in}} = \left(\eta_{EO} \frac{1}{L} \eta_{OE} \right)^2 \cdot \frac{Z_{out}}{Z_{in}} \tag{7.23}$$

Whereas the expansion of Eq. 7.20 demonstrates the interest to dispose of modulating signals with low crest factors for increasing the detected RMS RF power.

For a peak OMI of 100%, the maximum RF power is reached, and values:

$$P_{RF\ out\ max} = P_{RF\ out\ SINUS} - CF_{dB} \tag{7.24}$$

Examples

By computing the afore mentioned equations, the RMS OMI and its sine equivalent for different crest factors and for different current dynamics against the RF power can be appreciated (Fig.7.1).

This brief example shows the importance of the crest factor of a used signal: an increase of 3dB of the crest factor causes —at equivalent OMI, and thus SNR as we will see— to be pass from +11 to +15dBm of required RF input power.

Of course the latter input power requires a higher linear range of the laser diode...

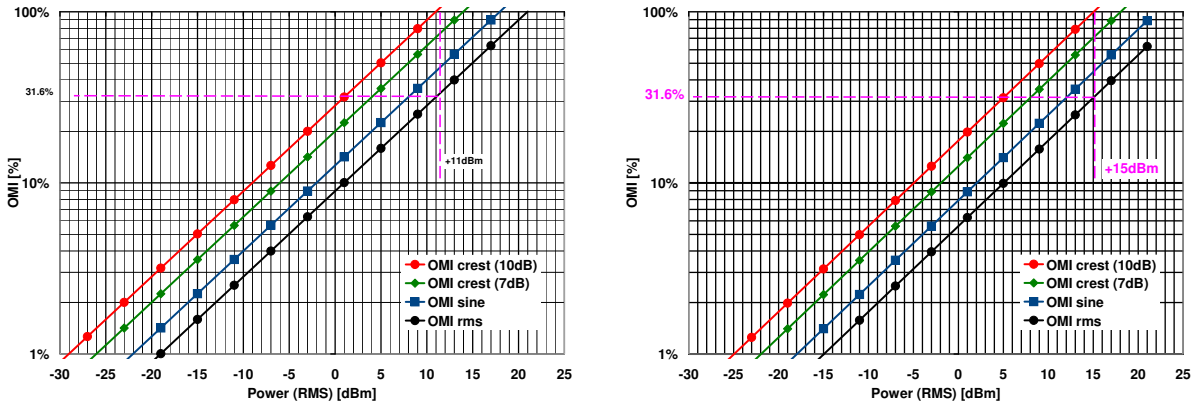

(a) (b)

Figure 7.1.: OMIs for different crest factors and current dynamics (a) 50mA and (b) 80mA versus the RF input power

7.2. Expressions for a passive optical link

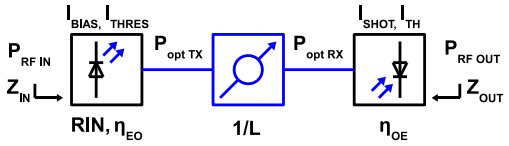

Figure 7.2.: Schematic set-up of a passive optical link

7.2.1. Importance of noise power components versus the optical budget

Taking into account the Relative Intensity Noise (RIN) due to the laser source, the shot noise due to the photo-detection process and the thermal noise of the post photo-detection Trans Impedance Amplifier (TIA), the noise power[1] can be expressed as:

$$P_{noise} = I_{in}^2 \cdot \frac{Z_{TIA}^2}{Z_{Out}} \tag{7.25}$$

$$= \left(\sigma_{RIN}^2 + \sigma_{shot}^2 + \sigma_{therm.}^2\right) \cdot \frac{Z_{TIA}^2}{Z_{Out}} \tag{7.26}$$

$$= \left(RIN \cdot I_0^2 + 2e \cdot I_0 + I_{th}^2\right) \Delta_f \cdot \frac{Z_{TIA}^2}{Z_{Out}} \tag{7.27}$$

where Δ_f is the considered electrical bandwidth, and I_0 the average photo-detected current.

FIg. 7.3a shows the noise power components as a function of the detected photo-current assuming a RIN of -145dB/Hz and a thermal current spectral density I_{th} of 11.54pA/$\sqrt{Hz}$.

Fig. 7.3b shows the noise power components as a function of the optical budget, and assuming —additionally to the previous parameters— an optical launch power of +7dBm, and a PD efficiency of 0.9A/W.

In the latter figure the RIN term dominates the overall noise power for optical budgets ranging from 0 to 8dB. Then the total noise power behaves asymptotically as the shot noise power from 10 to 16dB. For optical budgets greater than 18dB, the total noise power is dominated by the thermal noise.

7.2.2. SNR expressions

Thanks to Eq. 7.22, the resulting SNR is:

$$SNR = \frac{I_0^2 \cdot OMI_{peak}^2/CF}{\left(RIN \cdot I_0^2 + 2e \cdot I_0 + I_{th}^2\right) \Delta_f} \tag{7.28}$$

Henceforth we assume a maximum peak OMI of 100%, hence reducing the SNR expression to:

[1] we neglect here the dark current, and the input noise of the RF source modulating the laser

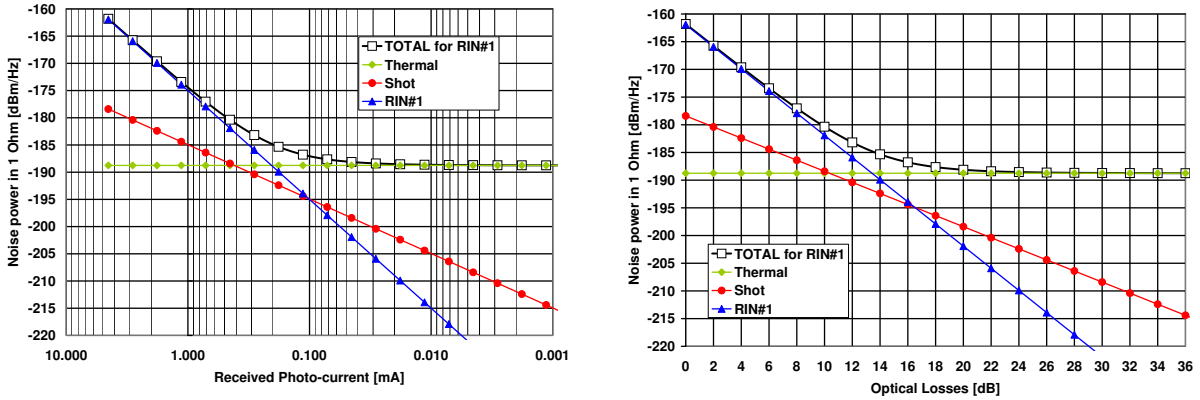

(a) (b)

Figure 7.3.: Noise power components and sum for a lossy optical link as a function of (a) the received photo-current; (b) the optical budget

$$SNR_1 = \frac{I_0^2/CF}{(RIN \cdot I_0^2 + 2e \cdot I_0 + I_{th}^2)\,\Delta_f} \tag{7.29}$$

Since a linear relation exists between the link losses L and the average detected photo-current I_0, the asymptotic behavior of the logarithmic SNR can be expressed as a function of the link losses.

Three different cases are considered whether the SNR is dominated by the RIN, the shot noise or the thermal noise of the receiver:

The RIN term

$$SNR_1 = \frac{1/CF}{RIN \cdot \Delta_f} \qquad SNR_{1\ dB} = +\alpha \tag{7.30}$$

The shot noise

$$SNR_1 = \frac{I_0 \cdot 1/CF}{2e \cdot \Delta_f} \qquad SNR_{1\ dB} = -10\log(L) + \beta \tag{7.31}$$

The thermal noise

$$SNR_1 = \frac{I_0^2 \cdot 1/CF}{I_{th}^2 \cdot \Delta_f} \qquad SNR_{1\ dB} = -20\log(L) + \gamma \tag{7.32}$$

7.2.3. SNR behavior versus the optical budget

As a direct consequence of the noise power components, when reusing the noise power terms exposed in Fig. 7.3b, for plotting the SNR versus the optical budget (Fig. 7.4a, the SNR behavior (let's just consider the 100%-curve) is directly linked: from 0 to 8dB, the SNR is almost constant, while from 10 to 16dB, the SNR drops proportionally to the

optical losses: namely by 1dB per 1dB of optical loss. Finally for 18dB and beyond, the SNR degrades by 2dB for 1dB of optical loss.

Taking into account the remarks of §3.3.1 on page 61, and the chart in Fig. 3.21 we can expect *correct* EVM figures at the transmitter side for optical budgets up to ≈30dB —when assuming a 30dB SNR to be sufficient for a 3.84MHz wide channel using a simple QPSK modulation scheme.

Impact of the CF onto the SNR

In Fig. 7.3b and 7.4 we considered a Crest Factor (CF) of 10dB, which corresponds to an typical W-CDMA downlink carrier.

Yet for a *dummy* QPSK signal with a CF of 7dB, according to Eq. 7.28 the SNR improves by 3dB. While when using two W-CDMA carriers, the SNR will degraded by 3dB. Finally when characterizing the SNR by a sine-signal (CF of 3dB), and keeping the reference bandwidth of 3.84MHz of our case, then the SNR curves will *apparently* improve by 7dB!

Impact of the BW onto the SNR

In Fig. 7.4 the considered bandwidth values 3.84MHz corresponding to the channel width of a W-CDMA carrier. Yet when increasing the bandwidth to 10 or 20MHz (higher channel bandwidths of the recent 4G LTE radio standard), then the SNRs curves in Fig. 7.4a drop by:

$$10 \cdot \log\left(10 \text{ or } 20\text{MHz}/3.84\text{MHz}\right) = 4.2 \text{ or } 7.2\text{dB} \tag{7.33}$$

Impact of the OMI onto the SNR

In Fig. 7.4, the SNR is plotted for several peak OMI since in IM-DD-schemes the individual OMI of a carrier can be reduced in order to operate in the linear part of laser diode... or to avoid over-driving the laser.

This black curve assumed an *ideal* peak OMI of 100%. For instance passing to a peak OMI of 55% causes the SNR to drop by:

$$20 \cdot \log\left(\text{actual peak OMI } \%/100\%\right) = 5.2\text{dB} \tag{7.34}$$

Thus of course the highest possible OMI is targeted...

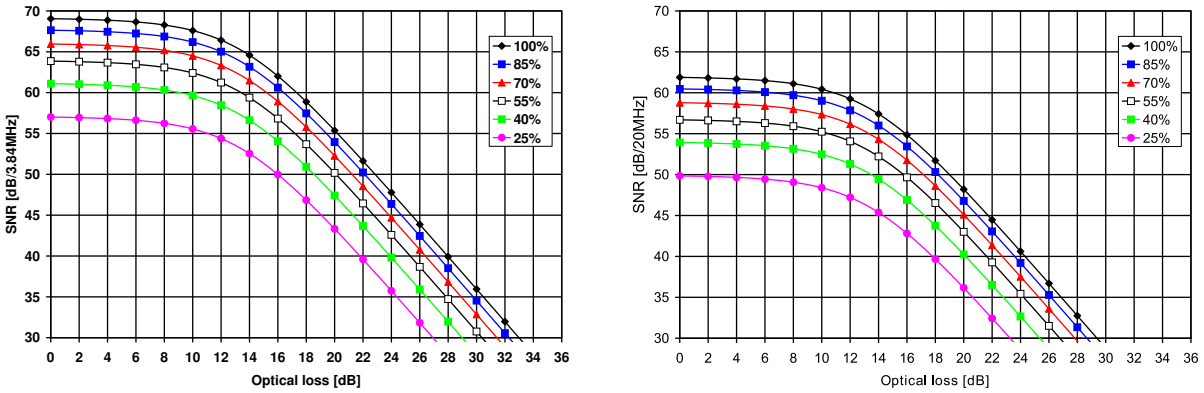

(a) (b)

Figure 7.4.: SNR of a lossy optical link for several peak OMIs and signal bandwidth of (a) 3.84MHz and (b) 20MHz. For both CF=10dB, other parameters as for Fig. 7.3b

Non-Linear Distortion (NLD) noise

...yet the clipping at the transmitter sides causes non-linear distortions and can be considered useless thus as an additional noise component. According to [108, 109] these NLD can be modeled in terms of noise source on the receiver as:

$$P_{NLD} = \sqrt{\frac{2}{\pi}} \cdot I_0^2 \cdot \mu^5 \cdot \exp\left(-\frac{1}{2 \cdot \mu^2}\right) \text{ in } A^2 \tag{7.35}$$

where N is number of multiplexed carriers, and μ is the total Root-Mean-Square (RMS) modulation index (and furthermore assuming identical modulation index for each channel):

$$\mu = \sqrt{N} \cdot \frac{OMI_{peak}}{\sqrt{CF}} = \sqrt{N} \cdot OMI_{RMS} \tag{7.36}$$

Contrary to the contributions of RIN, of the shot and thermal noises, P_{NLD} does not depend upon the considered channel bandwidth. NB: according to [110] this NLD-modeling **is not** included in simulations tools like *VPItransmissionMaker*.

When assuming the NLD to be the dominating noise, then the SNR expression can be simplified to:

$$SNR_1 = \sqrt{\frac{\pi}{2}} \cdot \mu^{-3} \cdot \exp\left(+\frac{1}{2 \cdot \mu^2}\right) \qquad SNR_{1\ dB} = -30 \cdot \log(\mu) + \frac{5}{\ln 10 \cdot \mu^2} + \varepsilon \tag{7.37}$$

Fig. 7.5 illustrates Eq. 7.37 for a single carrier as a function of the RMS OMI, and as a function the peak OMI assuming a signal with a 10dB Crest Factor. The NLDs' contributions to the SNR term are negligible for RMS OMIs up to 20% ($\equiv$ 63% peak OMI for a 10dB-crest-factor signal).

Since in this thesis, we will target —in some cases— applications requiring a SNR of 50dB over *important* optical budgets, the temptation of increasing the OMI in order to

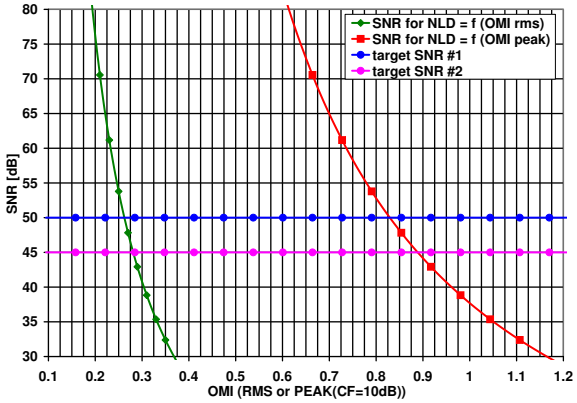

Figure 7.5.: SNR when considering only NLD as function of the OMIs (rms and peak) not taking into account any losses

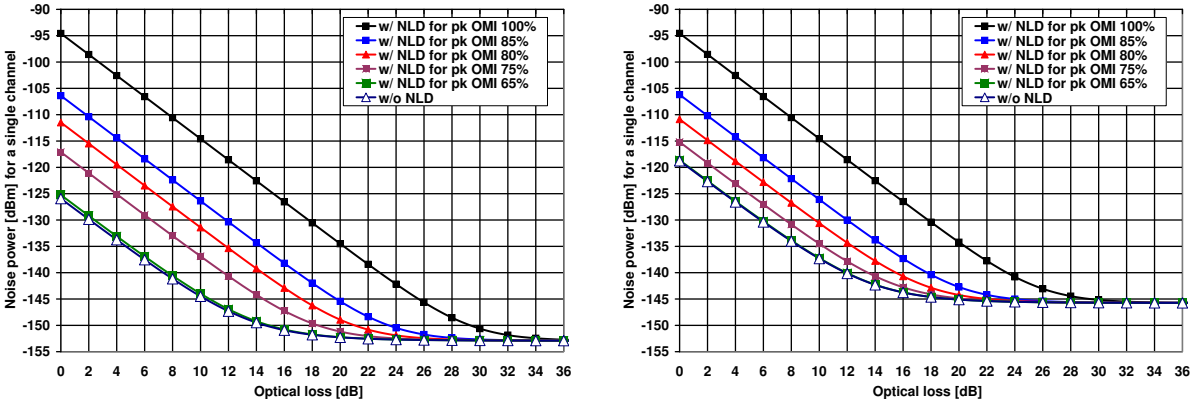

(a) (b)

Figure 7.6.: Noise power with and without the NLD component for several peak OMIs (10dB-crest-factor signal) and for channel bandwidths of (a) 3.84MHz, and (b) 20MHz

maximize the SNR exists. Yet given the NLD, the OMI *should* only be increased to its *tolerable* maximum.

In order to assess the impact of the NLD contribution to the SNR (Eq. 7.38), Fig. 7.6 shows, for several peak OMIs, whether the NLD distortions are prevalent over sum of the RIN, shot, and thermal noises.

$$SNR = \frac{I_0^2 \cdot OMI_{peak}^2/CF}{(\sigma_{RIN}^2 + \sigma_{shot}^2 + \sigma_{therm.}^2) + P_{NLD}} \tag{7.38}$$

Finally

For a 3.84MHz bandwidth, Fig. 7.7a shows that when taking into account the NLD noise term, the highest optical budget is no longer necessarily reached by the highest OMI.

Indeed, for an SNR $\geq$ 50dB, the *optimum* peak OMI (assuming a crest factor of 10dB) ranges from 40 to 65%. For the upper-bound OMI, the SNR is limited by the NLD component while the limit of the lower-bound OMI is mainly set by the thermal noise component. Yet if the targeted SNR is below 40dB, then there is no point in considering the OMI, and over-modulation is no longer an issue.

Similar conclusions can be made when considering a 20MHz channel.

Introducing the NLD issue decreases the maximum SNR.

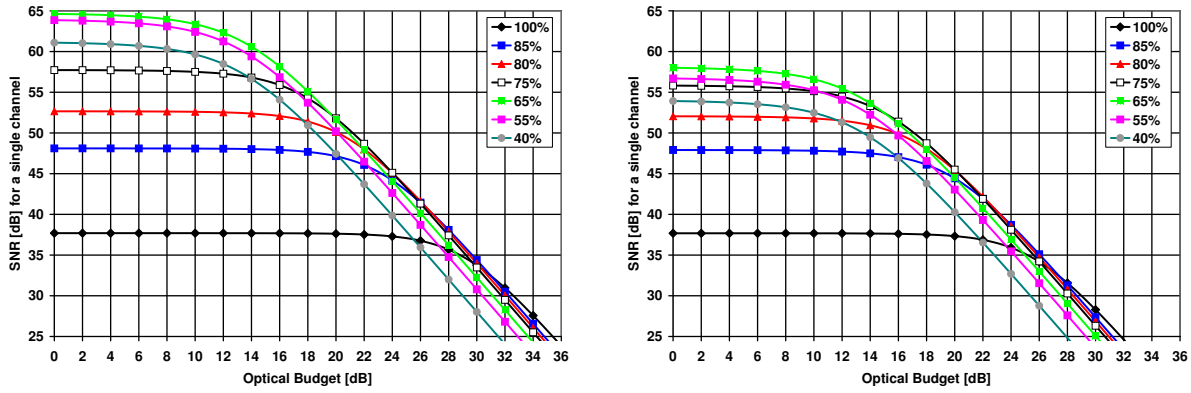

(a) (b)

Figure 7.7.: SNR for several peak OMIs, an optical launch power of +7.02dBm, channel bandwidths of (a) 3.84MHz, and (b) 20MHz

7.2.4. Input power range

Even if it is interesting to compute and observe the SNR as a function of the optical loss budget, it is more convenient to consider the requirements of meeting a given SNR[2] versus the optical loss budget.

Therefore we consider the RF input power into the laser as the key figure since it can be bound to two limits: an upper one (which is the over-driving limit of the Laser Diode (LD) *i.e.* a peak OMI of 100%) and a lower one (which is set by the noise power).

Definition

A maximum admissible RF input power into the LD can be defined by using the equivalent power of the maximum admissible input current (I_{DYN}) for a given bias point. Since we consider the RMS input power, we can link the clipping issue with the crest factor (CF) of the signal, as follows:

$$P_{RF\ in\ max} = I^2_{in\ max} \cdot Z_{in} = \frac{I^2_{DYN} \cdot Z_{in}}{CF} \tag{7.39}$$

since

$$I_{in\ RMS} = \frac{I_{in\ peak}}{\sqrt{CF}} \qquad \text{and} \qquad I_{in\ max} = \frac{I_{DYN}}{\sqrt{CF}} \tag{7.40}$$

Finally, we can define an input power range Δ_{IN}:

$$\Delta_{IN} = 10\log\left(\frac{P_{RF\ in\ max}}{P_{RF\ in\ min}}\right) \tag{7.41}$$

where $P_{RF\ in\ max}$ corresponds to the expression in Eq. 7.39, and where $P_{RF\ in\ min}$ are the expressions extracted from the SNR expressions of the different noise dominating situations.

Expressions

RIN dominated noise power The noise limited SNR has an equivalent input RF power:

$$P_{RF\ in\ min} = RIN \cdot SNR \cdot \Delta_f \cdot \left(I^2_{DYN} \cdot Z_{in}\right) \tag{7.42}$$

which leads to the input power range:

$$\Delta_{IN\ RIN} = -RIN_{dB} - [CF_{dB} + SNR_{dB} + 10\log(\Delta_f)] \tag{7.43}$$

Shot noise dominated noise power In this case the noise limited input power is:

$$P_{RF\ in\ min} = \frac{2e}{I_0} \cdot SNR \cdot \Delta_f \cdot \left(I^2_{DYN} \cdot Z_{in}\right) \tag{7.44}$$

Finally the ratio of the input power range is expressed as:

$$\Delta_{IN\ shot} = P_{0\ dB} - L_{dB} + 10\log(\eta_{OE}) - 10\log(2e) - [CF_{dB} + SNR_{dB} + 10\log(\Delta_f)] \tag{7.45}$$

[2] as it is the case when broadcasting radio signals

Thermal noise dominated noise power

$$P_{RF\ in\ min} = \left(\frac{I_{th}}{I_0}\right)^2 \cdot SNR \cdot \Delta_f \cdot \left(I_{DYN}^2 \cdot Z_{in}\right) \tag{7.46}$$

$$\Delta_{IN\ therm.} = 2P_{0\ dB} - 2L_{dB} + 20\log(\eta_{OE}) - 20\log(I_{th}) - [CF_{dB} + SNR_{dB} + 10\log(\Delta_f)] \tag{7.47}$$

Examples

Fig. 7.8 illustrates the previous expressions assuming optical launch powers of +5 and +7dBm in order to achieve a 50dB SNR.

The maximum input power is derived from the optical launch power assuming a conversion efficiency of 0.0719W/A, and a crest factor of 10dB for the modulating signal. The yielded current dynamics (44 and 70mA respectively) are supposed to be symmetric with respect to the bias point.

A +5dBm optical launch power allows to reach a theoretical maximum optical budget of 21dB for a SNR of 50dB when using a 3.84MHz wide channel. A +7dBm optical launch power allows 25dB.

For a 20MHz-wide channel the theoretical maximum optical budgets fall to 17 and 21.1dB respectively for the optical launch powers of +5 and +7dBm.

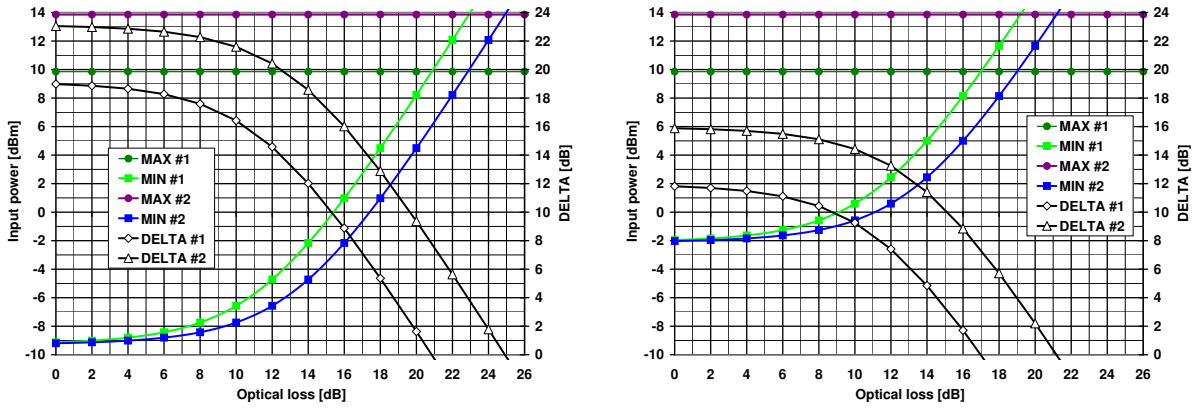

(a) (b)

Figure 7.8.: Input powers (minimum and maximum) and power ranges assuming +5dBm (curves #1) and +7dBm (curves #2) optical launch powers for a channel width of (a) 3.84 and (b) 20MHz, when targeting a 50dB SNR.

In Fig. 7.8, the maximum input powers correspond to 100% peak modulation indexes. However as we have seen in §7.2.3, the Non-Linear Distortions (NLD) can limit the OMI, and thus the RF input power. In order to take the latter aspect into account, we split the overall SNR into two components:

$$SNR_{(lin)} = \frac{P_{signal}}{N_1 + N_2} = \frac{1}{\frac{1}{SNR_{1(lin)}} + \frac{1}{SNR_{2(lin)}}} \tag{7.48}$$

where $SNR_i = P_{signal}/N_i$.

Let's assign a first SNR component to the combined RIN, shot and thermal noises, and a second SNR term to the NLD contributions of Eq. 7.37. Then in order to dispose of a overall SNR of 50dB, we target 53.1dB per SNR_i.

For a target SNR of 53.1dB, by solving Eq. 7.37 (Fig. 7.5) the maximum peak OMI, for a 10dB crest factor signal, is 79.7% (≡ 25.2% RMS). Assuming current dynamics of 44 and 70mA, the corresponding maximum input powers are respectively +7.9 and +11.9dBm instead of +9.9 and +13.9dBm respectively —independently of the channel bandwidth.

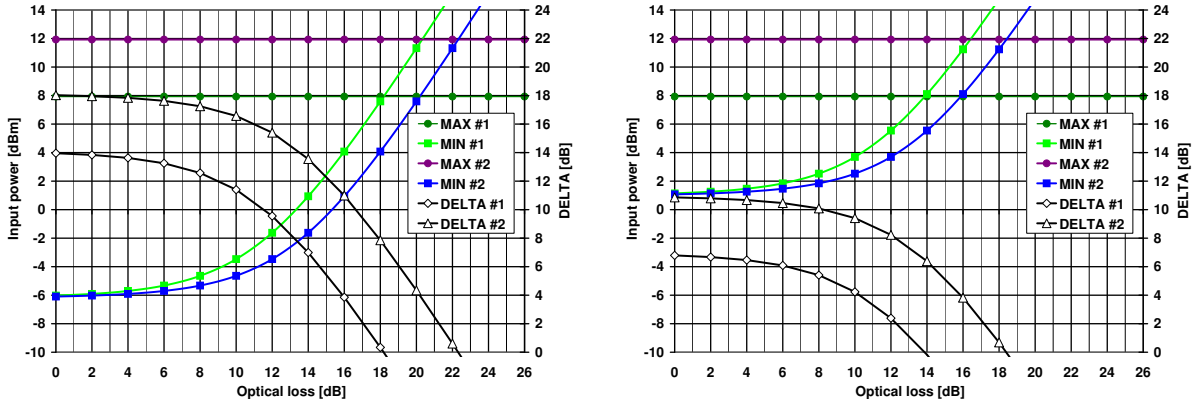

(a) (b)

Figure 7.9.: Input powers (minimum and maximum) and power ranges assuming +5dBm (curves #1) and +7dBm (curves #2) optical launch powers for a channel width of (a) 3.84 and (b) 20MHz, when targeting an overall 50dB SNR.

Finally, these new maximum RF input powers yield maximum optical power budgets, allowing a 50dB SNR, of 18 and 22.2dB (44 and 70mA current dynamic) —for a channel bandwidth of 3.84MHz (Fig. 7.9a). For a channel bandwidth of 20MHz, the maximum optical budgets are respectively 14 and 18.5dB (44 and 70mA current dynamic) (Fig. 7.9b).

7.3. Expressions for an optically amplified link

We now assume an optical amplifier (Erbium Doped Fiber Amplifier (EDFA), or Semiconductor Optical Amplifier (SOA)) with a gain G_{opt} and a noise factor F_{opt} to be placed in front of the PIN.

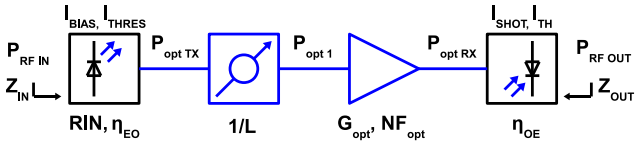

Figure 7.10.: Schematic set-up of an optically amplified link

As a consequence of this the intial average detected photo-current I_0 in Eq. 7.8 becomes:

$$I_0' = G_{opt} \cdot I_0 \tag{7.49}$$

Thus the received RF signal and noise powers are respectively impacted as follows:

$$P_{RX\ signal}' = OMI_{RMS}^2 \cdot (G_{opt} I_0)^2 \cdot \frac{Z_{TIA}^2}{Z_{Out}} \tag{7.50}$$

$$P_{noise}' = \left[RIN \cdot (G_{opt} I_0)^2 + 2e \cdot (G_{opt} I_0) + I_{th}^2\right] \cdot \Delta_f \cdot \frac{Z_{TIA}^2}{Z_{Out}} \tag{7.51}$$

7.3.1. Optical amplified noise

Origin

Eq. 7.50 and 7.51 are *ideal* expressions since they do not take into account the optical noise due to the amplification process taking place inside of the EDFA.

Indeed the EDFA does not only amplifies the input signal but also produces an optical noise known as Amplified Spontaneous Emission (ASE).

The optical amplification and noise production apply to the optical fields. Thus after the square operation at the photo-detection, the optical field of the ASE noise *beats* with the signal's field [25] conceptually as follows:

$$(E_{\text{signal}} + E_{\text{noise}})^2 = (E_{\text{signal}})^2 + \underbrace{2 \cdot (E_{\text{signal}} \cdot E_{\text{noise}})}_{\text{signal-spontaneous}} + \underbrace{(E_{\text{noise}})^2}_{\text{spontaneous-spontaneous}} \tag{7.52}$$

Of course in Eq. 7.52 we retrieve the square-detected signal, but also two terms considered as *noise* —since unwanted.

Expressions

The noise due to optical amplification, modeled by [111,112] as RINs (thus to be multiplied by the average detected photo-current ${I_0'}^2$ for retrieving its spectral power density), can be divided into two components:

1. a signal-spontaneous (sig-sp) beating component:

$$RIN_{sig-sp} = \frac{2h \cdot f_{opt} \cdot F_{opt}}{P_{in}} = 2 \cdot S_{ASE} \cdot \left(\frac{L}{P_{opt\ TX}}\right) = F'_{opt} \cdot \left(\frac{L}{P_{opt\ TX}}\right) \quad (7.53)$$

where

$$S_{ASE} = h \cdot f_{opt} \cdot F_{opt} \qquad \text{and} \qquad F'_{opt} = 2 \cdot S_{ASE} \quad (7.54)$$

and f_{opt} is the optical central carrier frequency.

2. a spontaneous-spontaneous (sp-sp) component corresponding to the amplified optical background noise:

$$RIN_{sp-sp} = \left(\frac{h \cdot f_{opt} \cdot F_{opt}}{P_{in}}\right)^2 \cdot B_{opt} = S_{ASE}^2 \cdot B_0 \cdot \left(\frac{L}{P_{opt\ TX}}\right)^2 = F''_{opt} \cdot \left(\frac{L}{P_{opt\ TX}}\right)^2 \quad (7.55)$$

where

$$F''_{opt} = S_{ASE}^2 \cdot B_0 \quad (7.56)$$

For both, h is Planck's constant, P_{in} is the **optical input power into the EDFA** (*i.e.* $P_{opt\ 1} \equiv P_{opt\ TX}/L$ in Fig. 7.10), F_{opt} the optical noise factor, B_{opt} is the optical bandwidth.

Finally the corrected expression of the noise power is:

$$P'_{noise} = \left[(RIN + RIN_{sig-sp} + RIN_{sp-sp}) \cdot (G_{opt} I_0)^2 + 2e \cdot (G_{opt} I_0) + I_{th}^2\right] \cdot \Delta_f \cdot \frac{Z_{TIA}^2}{Z_{Out}} \quad (7.57)$$

As stated in [111], the EDFA is assumed to operate at high-gain limit. Furthermore it assumed that $B_{opt} \gg f_{RF}$, f_{RF} being the frequency of the information carrying RF signal. Then Eq. 7.53 and 7.55 show that the noise contributions (signal-spontaneaous and spontaneaous-spontaneaous) from the EDFA only depend upon the optical input power prior to amplification, and not upon the optical gain itsself.

Noise power components versus the optical budget

As we have seen the shot and thermal noises, are dominating in unamplified systems, setting fundamental limits on the system's performances.

However for optically amplified links, the signal-spontaneous noise (Eq. 7.53) is expected to dominate [111]. Indeed this is the case as shown in Fig. 7.11 when considering the parameters of Tab. 7.1.

For optical budgets ranging from 0 to 8dB the laser diode's RIN is the dominating noise source. Beyond 18dB, the signal-spontaneous noise is prevailing, while the thermal noise will dominate for budgets greater than 50dB.

7.3.2. SNR expressions

By combining, Eq. 7.50 and 7.57, the SNR can be expressed as:

Table 7.1.: Parameter values

Parameter	**Value**	**Unit**
Optical launch power	+7	dBm
RIN	-145	dB/Hz
Gain of the optical amplifier	20	dB
Noise figure of the optical amplifier	5	dB
Receiver Bandwidth	8	GHz
PD conversion efficiency	0.9	A/W
ASE noise power density	-153.9	dBm/Hz
F'_{opt}	-150.9	dBm/Hz
F''_{opt}	-208.8	dB(mW.mW)/Hz

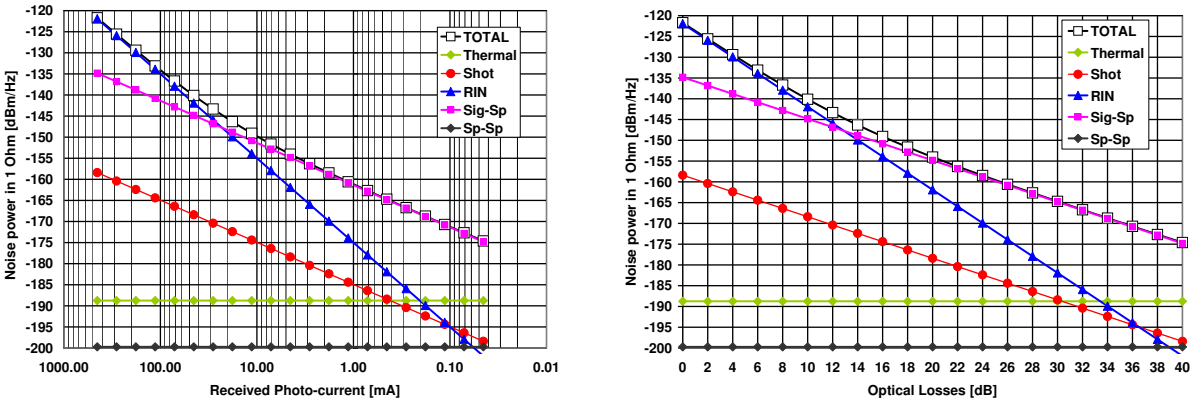

(a) (b)

Figure 7.11.: Received noise power components and sum for an optical amplified link as a function of (a) the received photo-current; (b) the optical budget

$$SNR = \frac{I'_0{}^2 \cdot OMI^2_{RMS}}{[(RIN + RIN_{sig-sp} + RIN_{sp-sp}) \cdot I'_0{}^2 + 2e \cdot I'_0 + I^2_{th}] \cdot \Delta_f} \tag{7.58}$$

As in the previous section, we consider different *domination* cases (in accordance with §7.3.1) for the noise powers and the related SNR:

The amplified RIN term dominates:

As shown in Fig. 7.11b, for optical budgets ranging from 0 to 8dB, we can simplify the SNR as follows:

$$SNR_2 = \frac{OMI^2_{RMS}}{RIN \cdot \Delta_f} = \frac{OMI^2_{PK}}{RIN \cdot CF \cdot \Delta_f} \qquad SNR_{2\ dB} = +\alpha\prime \tag{7.59}$$

The signal-ASE noise term dominates:

For optical budgets ranging from 18 to 50dB (Fig. 7.11b), the signal-ASE noise term dominates. Hence the SNR and its behavior with respect to the optical losses can be appreciated as:

$$SNR_2 = \frac{OMI_{PK}^2}{F'_{opt} \cdot CF \cdot \Delta_f} \cdot \left(\frac{P_{opt\ TX}}{L}\right) \qquad SNR_{2\ dB} = -10\log(L) + \beta\prime \tag{7.60}$$

7.3.3. SNR behavior versus the optical budget

Fig. 7.12 shows the SNRs for several peak OMIs (crest factor of 10dB), and assuming the parameters of Tab. 7.1.

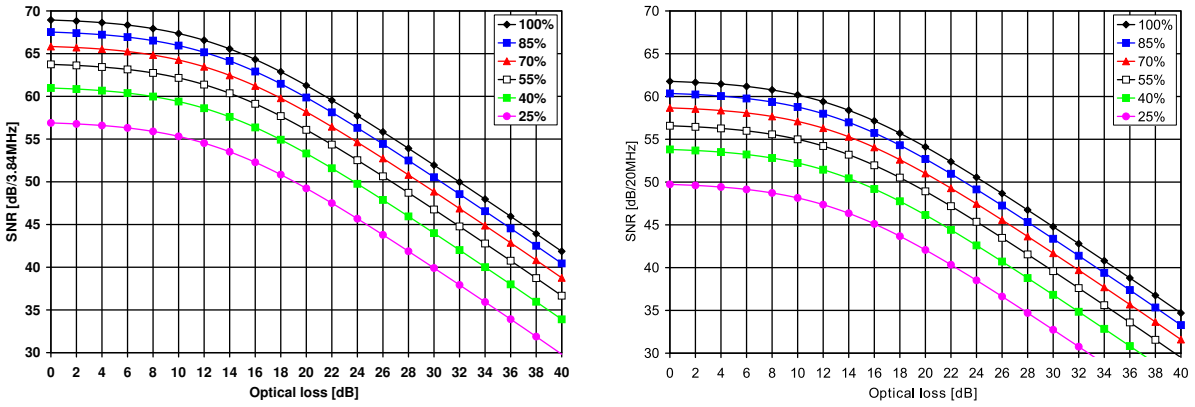

(a) (b)

Figure 7.12.: SNR of an optically amplified link for several peak OMIs and signal bandwidth of (a) 3.84MHz and (b) 20MHz.

Despite the higher noise power densities —the amplified RIN and signal-ASE noise power densities are both higher than the limiting thermal noise for non-amplified optical links— the maximum optical budgets, when targeting a constant SNR of 50dB for instance, are more important than in §7.2 thanks to the increased photo-detected current.

Taking into account the remarks of §3.3.1 on page 61, and the chart in Fig. 3.21 we can expect *correct* EVM figures at the transmitter side for optical budgets exceeding 40dB —when assuming a 30dB SNR to be sufficient for a 3.84MHz wide channel using a simple QPSK modulation scheme.

For a target SNR of 50dB, and an ideal peak OMI of 100%, the theoretical maximum optical budget values 32dB —when using a channel bandwidth of 3.84MHz. Compared to the unamplified case, the maximum optical budget is improved by 9dB. For a 20MHz-wide channel, the theoretical maximum optical budget drops to 25dB, and shows a 6dB improvement versus the case without optical amplification.

Including the NLD noise

Taking into account the NLD noise introduced in §7.2.3, there is a peak OMI below which the resulting NLD noise power is negligible compared to the total noise power.

For instance for the same parameter values as afore, Fig. 7.13 shows a peak OMI of 65% to yield negligible NLD noise contributions for a channel bandwidth of 3.84MHz. A similar conclusion can be made for a 20MHz channel.

As a consequence of this, there is an optimum OMI yielding a given constant SNR over the largest optical budget (Fig.7.14). For instance when targeting an SNR of 50dB, the peak OMIs between 55 and 75% offer the largest $SNR \cdot Optical\ Budget$ product.

Finally for a 3.84MHz-wide channel the highest optical budget at a constant SNR of 50dB values 27 to 29dB for the afore mentioned *optimal* peak OMI range.

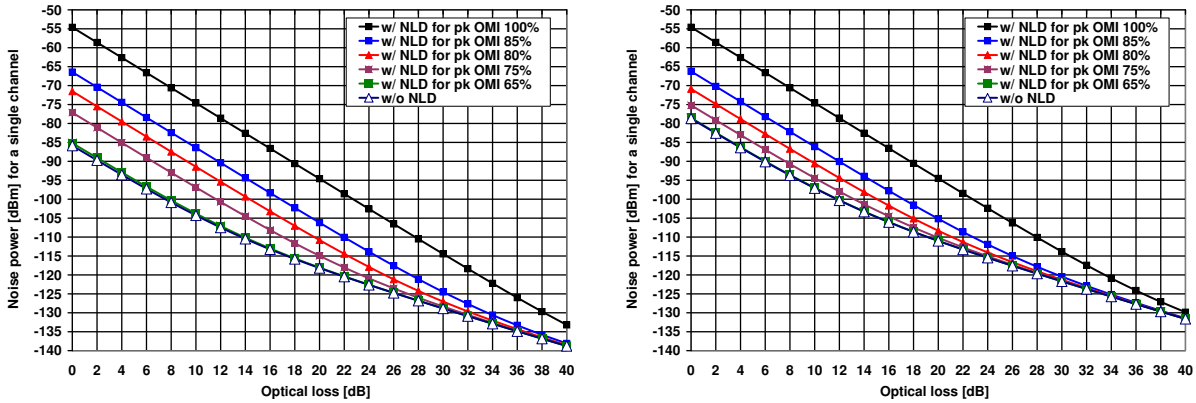

(a) (b)

Figure 7.13.: Received noise power with and without the NLD component for several peak OMIs (10dB-crest-factor signal) for an optically amplified link, and for channel bandwidths of (a) 3.84MHz, and (b) 20MHz

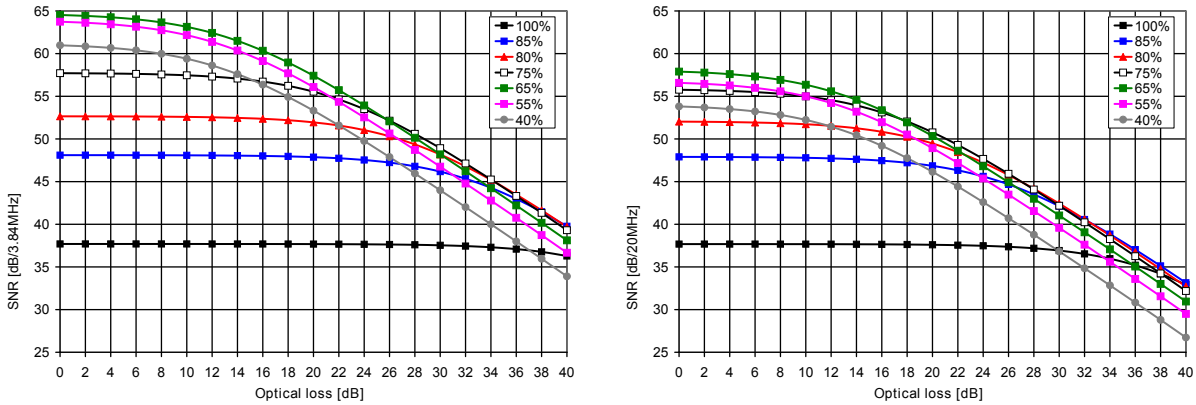

(a) (b)

Figure 7.14.: SNR for several peak OMIs, an optical launch power of +7dBm, channel bandwidths of (a) 3.84MHz, and (b) 20MHz

7.3.4. Input power ranges

For an amplified RIN dominated noise power:

The noise limited SNR has an equivalent input RF power:

$$P'_{RF\ in\ min} = RIN \cdot SNR \cdot \Delta_f \cdot \left(I^2_{DYN} \cdot Z_{in}\right) \tag{7.61}$$

which leads to the input power range:

$$\Delta'_{IN\ RIN} = -RIN_{dB} - [CF_{dB} + SNR_{dB} + 10\log(\Delta_f)] \qquad (\equiv \text{ of Eq.7.43}) \tag{7.62}$$

For a signal-ASE dominated noise power:

In this case the noise limited input power is:

$$P'_{RF\ in\ min} = F'_{opt} \cdot \frac{L}{P_{opt\ TX}} \cdot SNR \cdot \Delta_f \cdot \left(I^2_{DYN} \cdot Z_{in}\right) \tag{7.63}$$

Finally the ratio of the input power range is expressed as:

$$\Delta'_{IN\ sig.-sp.} = P_{opt\ TX\ dB} - \left(F'_{opt} + L_{dB}\right) - [CF_{dB} + SNR_{dB} + 10\log(\Delta_f)] \tag{7.64}$$

7.3.5. Examples

Fig. 7.15 illustrates the previous expressions assuming optical launch powers of +5 and +7dBm in order to achieve a SNR of 50dB.

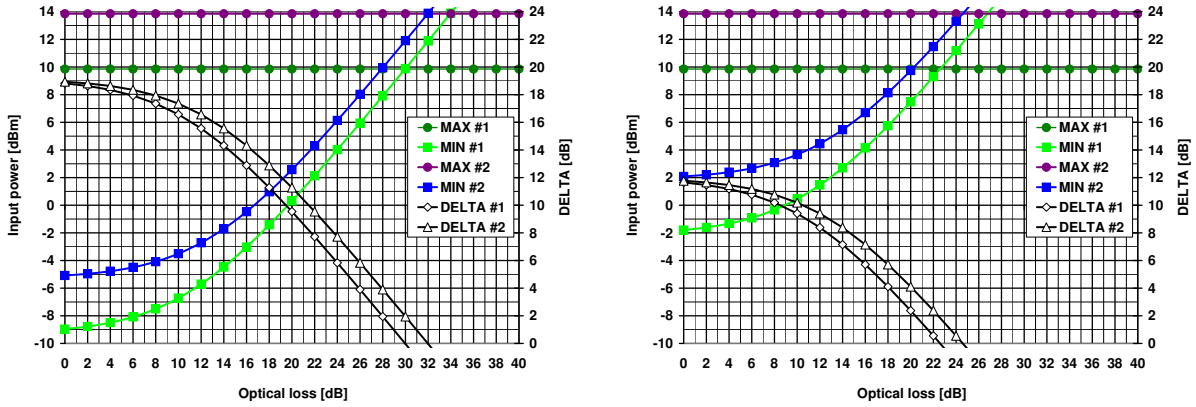

(a) (b)

Figure 7.15.: Input powers (minimum and maximum) and power ranges assuming +5dBm (curves #1) and +7dBm (curves #2) optical launch powers for a channel width of (a) 3.84 and (b) 20MHz, when targeting a 50dB SNR for an optically amplified link

The maximum input powers are derived from the optical launch power assuming a conversion efficiency of 0.0719W/A, and a crest factor of 10dB for the modulating signal. The yielded current dynamics (44 and 70mA respectively) are supposed to be symmetric with respect to the bias point. Furthermore we use the parameters of Tab. 7.1.

A +5dBm optical launch power allows to reach a theoretical maximum optical budget of 30dB for a SNR of 50dB when using a 3.84MHz wide channel. A +7dBm optical launch power allows 32dB. For a 20MHz-wide channel the theoretical maximum optical budgets fall to 22.8 and 24.8dB respectively for the optical launch powers of +5 and +7dBm.

Compared to the results in Fig. 7.8 the maximum optical budgets are increased, for the 3.84MHz bandwidth, by 9 and 7dB to 30 and 32dB respectively for the optical launch powers of +5 and +7dBm.

Hence this demonstrates the benefit of the optical pre-amplification, and furthermore shows that the highest budget increase (9dB), for a 3.84MHz bandwidth, is reached for the lowest of the two transmit powers.

NLD contributions

As in §7.2.4 (page 119), we can target a SNR of 53.1dB for the noise contributions from the RIN, signal-ASE, ASE-ASE, shot and thermal components, and an identical SNR contribution from the NLD. These combined noises than allow to yield an overall SNR of 50dB.

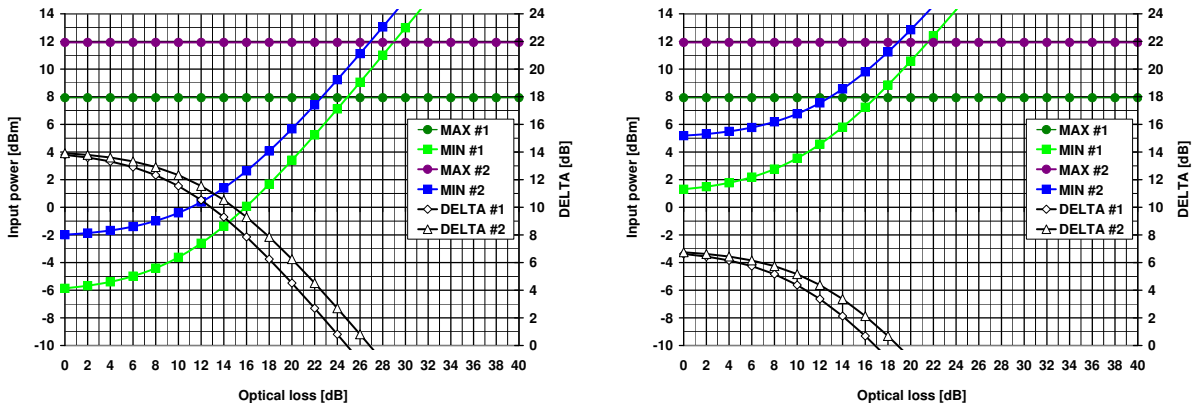

(a) (b)

Figure 7.16.: Input powers (minimum and maximum) and power ranges assuming +5dBm (curves #1) and +7dBm (curves #2) optical launch powers for a channel width of (a) 3.84 and (b) 20MHz, when targeting a 50dB SNR for an optically amplified link

Finally, the *new* maximum RF input powers yield maximum optical power budgets, allowing a overall 50dB SNR, of 25 and 27dB (44 and 70mA current dynamic) —for a channel bandwidth of 3.84MHz (Fig. 7.16a). These corresponds, compared to the amplification-free case, to improvements of 7 and 4dB of the maximum optical budgets respectively for launch powers of +5 and +7dBm. Again the highest budget increase corresponds to the lower optical launch power.

For a channel bandwidth of 20MHz, the maximum optical budgets are respectively 17 and 19dB (44 and 70mA current dynamic) (Fig. 7.16b), and translate improvements of 3 and 0.8dB respectively for the +5 and +7dBm optical launch powers.

8. Two tones simulations using *VPItransmissionMaker*

Interest

The previous section has dealt with signal and noise levels as a function of the optical losses and eventual optical amplification, in order to yield a given minimum SNR at the output of the optical link. Also in the previous section, only the *lossy* aspect of the eventual optical fiber in the link was included in the optical power loss budget —no additional issues caused by the optical fiber were taken into account.

However as shown by Meslener [113] in 1984, for a single sine signal transmitted over an IM-DD link, the interaction of the optical source's chirp with chromatic dispersion of the optical fiber can result in harmonics generation.

By applying [113]'s method (based on a Fourier Series decomposition of the electrical and optical fields) to a two-tone signal, Charles [114] in 1990 analytically showed that IMD of order 3 can be due to the chromatic dispersion of optical fiber interacting with the chirp of the optical source, since the chirp produces nonlinear modulation of the electric (optical) field, which creates many high-order sidebands. If during the transmission there is no dispersion, then all sideband signals maintain their proper relative phases. In presence of dispersion, the sidebands arrive with relative phase delays for different frequencies after transmission and are no longer proportional. Upon square-law detection, the original waveforms are recovered without any distortion...

A summary of the methodology developed in [113, 114] is proposed in Appendix D.

Scope

These IMD-3 topic directly leads us to the ACLR (see §3.3.2, page 64), which specifies maximum noise levels (including any interferences and distortions) at the frequencies of the IMD-3 products, and therefore is a major concern for radio systems broadcasting multiple channels.

In [114] the IMD-3-to-carrier ratios are computed for low modulation indexes. However given that in this thesis we address high optical budgets and high target SNRs (driven by the downlink ACLR specifications of the UMTS signals), we therefore intend to use high modulation indexes in order to maximize the output SNR. Thus the results presented in [114] cannot be reused.

Yet in this thesis we do consider the IMD-3 issue induced by the optical fiber, by taking advantage of a modern simulation tool, *VPItransmissionMaker* , in order to compute the IMD-3 ratios with the respect to the main channel's power.

Finally we will also assess Dispersion Compensating Fiber (DCF) to be a good candidate to yield *good enough* IMD-3 levels.

8.1. Model in *VPItransmissionMaker*

In *VPItransmissionMaker*, we simulate a simple set-up (Fig. 8.1) made of electrical (sine generator) and optical (analog direct modulated laser) sources, optical fibers, and a PIN detector.

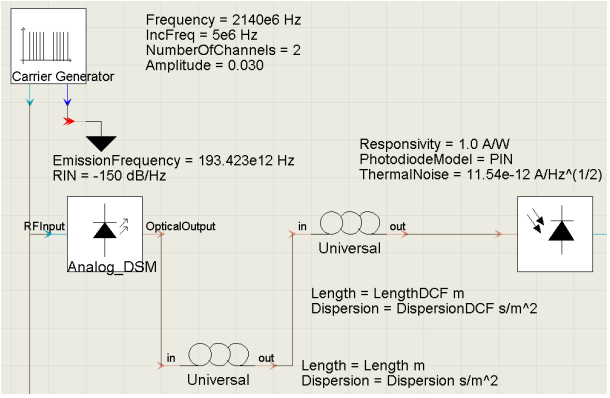

Figure 8.1.: Set-up in VPI

Electrical Source The electrical source is composed of two sine tones of equal power (peak amplitude of 0.030 a.u each) spaced by 5MHz, and centered at 2142.5MHz. The frequency corresponds to the middle of the Universal Mobile Telecommunications System (UMTS) downlink Band I.

Optical Source The optical source is set to have a threshold current of 15mA, a conversion efficiency of 0.07W/A and input impedance of 1Ω. The source is biased at 75mA, thus yielding a mean CW optical power of +6.32dBm. In a first time the peak OMI values 100% and the chirp factor α of the laser is set to 5. These laser parameters correspond to the equipment used in the experiments.

Optical Link The optical link is composed of Standard Single Mode Fiber (S-SMF) with losses of 0.25dB/km, and a chromatic dispersion of 17 $ps/(nm \cdot km)$. Also an optional DCF-fiber spool can be appended to the S-SMF-span.

Optical Receiver In order to focus on the chromatic dispersion issues and to get rid of optical budget dependent noise, the shot noise and dark current at the receiver are deactivated for the simulations. Furthermore the optical receiver is set to have a conversion efficiency of 1A/W, the thermal noise's spectral density is set to $11.54pA/\sqrt{Hz}$.

Simulation parameters The time window values $1\mu s$, and thus the smallest measurable frequency values 1MHz. In the optical domain the frequency windows values 16384GHz and 8192GHz in the electrical domain.

The ratio between the upper IMD-3 and the original upper sine tone is simulated while the optical source's chirp factor α, the optical link's fiber lengths' (S-SMF and DCF) vary.

8.2. Fiber containing links

8.2.1. Back to back

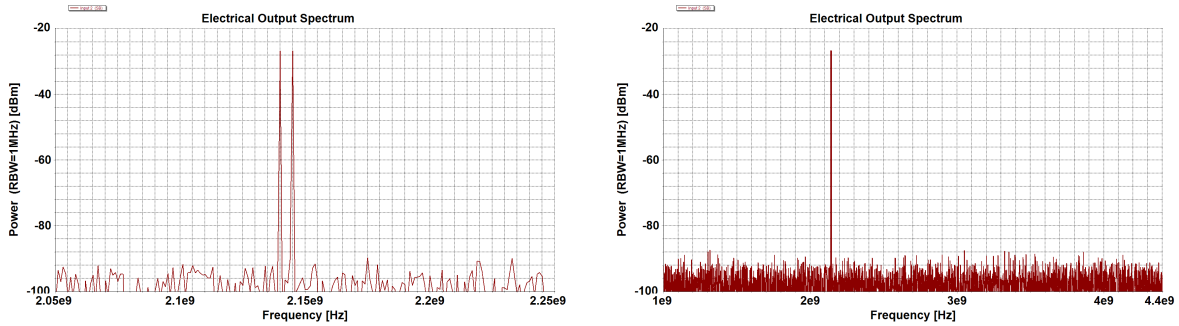

(a) (b)

Figure 8.2.: Spectra for a 2-tone signal for a back-to-back transmission: (a) narrowband; (b) wideband

For a peak OMI of 100% (here the two sine signals are in-phase and thus are fully correlated, hence the individual OMIs (*i.e.* the signal powers) are added linearly instead of following a square-root law), the spectra in Fig. 8.2 are free of spurious signals, thus validating the laser not to be over driven.

8.2.2. 20km S-SMF link

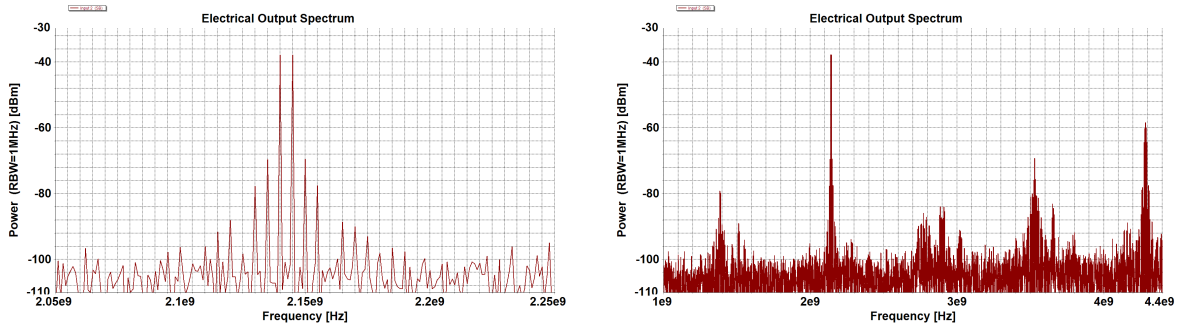

(a) (b)

Figure 8.3.: Spectra for a 2-tone signal transmitted over 20km of S-SMF: (a) narrowband; (b) wideband

For an optical link constituted of 20 km of S-SMF, the spectra in Fig. 8.3 exhibit spurious signals. The C3/C1 ratio values -31.6dBc, and the C5/C1 ratio -39.2dBc.

Influence of the chirp factor

The spectra in Fig. 8.3 are done for a chirp factor of 5.

Fig. 8.4 shows the C3/C1-ratio for several chirp factors (0, 2, 3, 3.5, 4 and 5), and as a function of the S-SMF length.

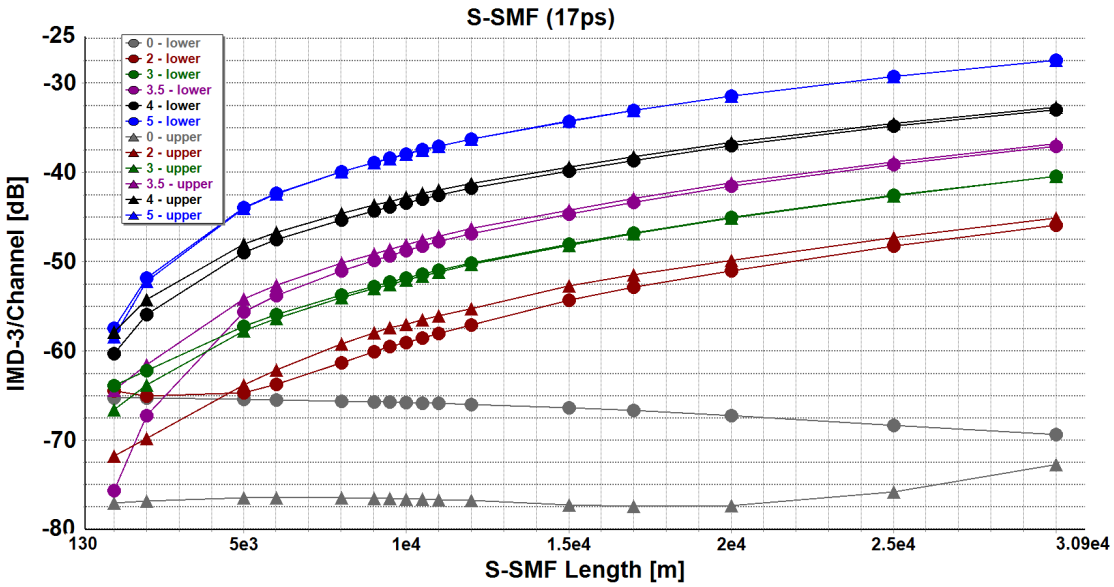

Figure 8.4.: C3/C1 ratio for different chirp factors

It shows that for a given chirp factor, the C3/C1-ratio degrades with an increasing length of S-SMF. Indeed, for a chirp factor of 5, the C3/C1-ratio values -38.5dBc for a 10km link, and -31.6dBc for a 20km link.

For a given fiber length, the higher the chirp factor of the laser source is, the more the C3/C1-ratio is degraded. Indeed, for a 20km S-SMF link, passing from a chirp factor of 5 to 4 causes the C3/C1-ratio to improve by 5.4dB. Passing from 4 to 3 improves the C3/C1 ratio by 8dB.

8.2.3. 20km S-SMF + 10km DCF link

As already mentioned, the IMD-3 result from the interaction of the chirp with the chromatic dispersion of the SMF-span [114]. A common way to contain the effects of the chromatic dispersion is to compensate it by placing a DCF-spool in the link.

The DCF's length is chosen assuming our system to be capable of coping with *some* chromatic dispersion. Given that the PON specifications require up to 20km, we apply here a simple Dichotomy scheme ... and can thus expect lowered IMD-3 levels (*i.e* a reduced C3/C1-ratio) by placing a 10km-spool[1] of DCF cascaded to the 20km of S-SMF.

[1] we anticipate here the order of magnitude of the required length of DCF from the experimental results in Part 4.

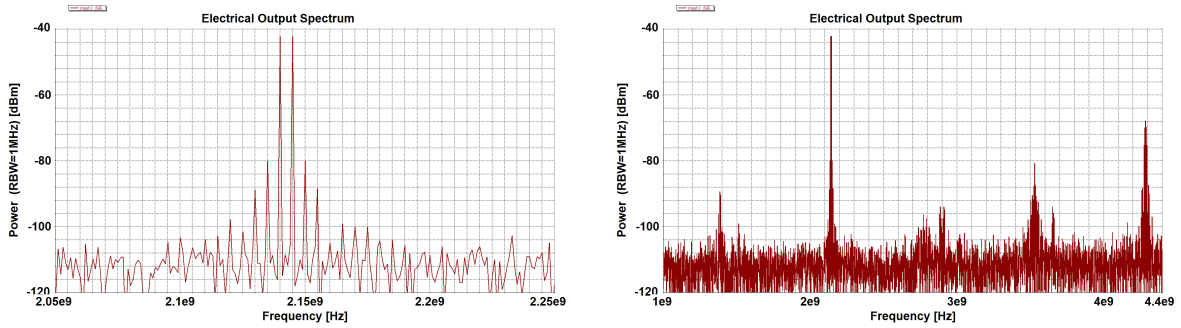

(a) (b)

Figure 8.5.: Spectra for a 2-tone signal transmitted over 20km of S-SMF and 10km of DCF: (a) narrowband; (b) wideband

Indeed, for the optical link constituted of 20km of S-SMF and 10km of DCF, the C3/C1 ratio values -38dBc, and the C5/C1 ratio -45dBc (Fig.8.5). The improvements value respectively 6.4 and 5.8dB for the C3/C1 and the C5/C1 ratios, compared to the case without 10km of DCF.

Thus the interest of DCF for compensating the IMD-3 generated by chromatic dispersion is assessed.

8.3. Influence of the length of the DCF for different chirp factors

The set-up remains the same except that DCF spools of 7.5 and 12.5km are cascaded to the swept S-SMF spool's length. Again several chirp factors (0, 2, 3, 3.5, 4 and 5) are considered.

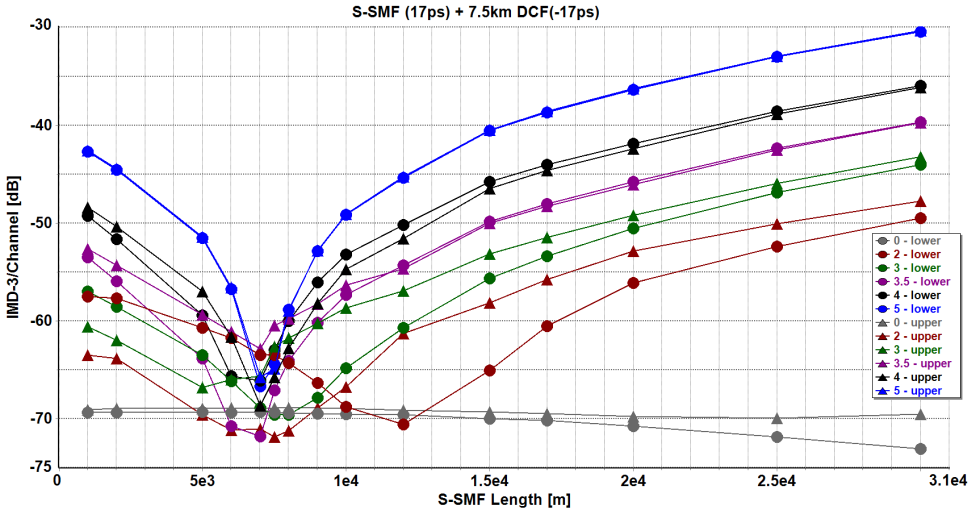

(a)

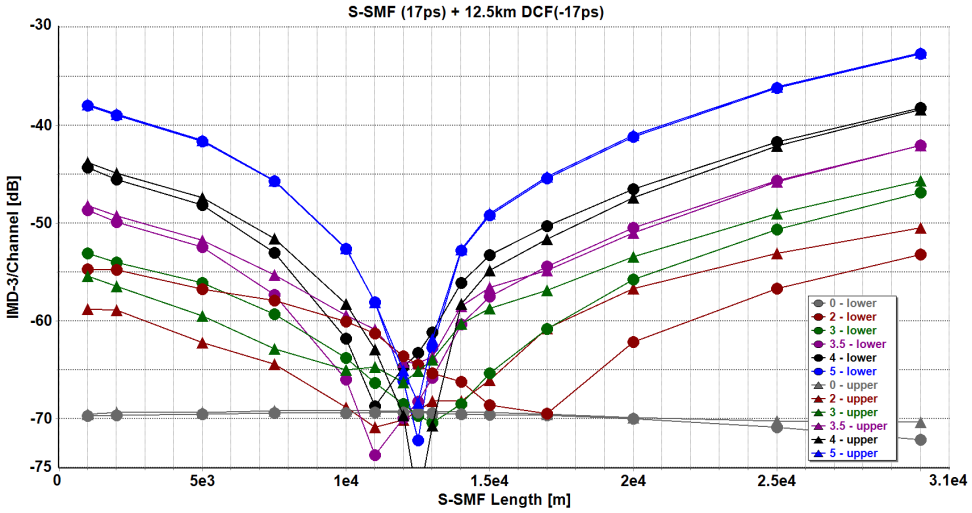

(b)

Figure 8.6.: C3/C1 ratio for different chirp factors when cascading a DCF-spool of (a) 7.5km, and (b) 12.5km. The triangle symbols correspond to the upper frequency C3/C1-ratio, while the filled circles correspond to the lower frequency C3/C1-ratio.

Fig. 8.6 shows that cascading a DCF-spool can enhance the C3/C1 ratio. The C3/C1 ratio tends towards zero when the DCF spool's length matches the length of the S-SMF value, and this independently of the value of the chirp factor.

This *notch* behavior can be used to define the *window width* of the length of S-SMF within which a given target C3/C1-ratio is met. Finally this can be used for designing analog RoF transmissions systems where given target C3/C1 ratios must be met.

8.3.1. Example for a -50dBc ratio threshold

When targeting a C3/C1-ratio of maximum -50dBc for instance, Fig. 8.7a shows the actual minimum (dashed lines) and maximum (solid lines) S-SMF lengths..

Fig. 8.7b summarizes the data in terms of a *margin* length. In most cases the margin length is centered on the used DCF length. Yet since the S-SMF length is swept from 0 to 30km, in some cases the C3/C1-ratio is always below the targeted threshold (for instance in Fig. 8.6b for target C3/C1-ratio of -50 dBc and a chirp factor of 2). Then the margin values 30km (in sense of at least).

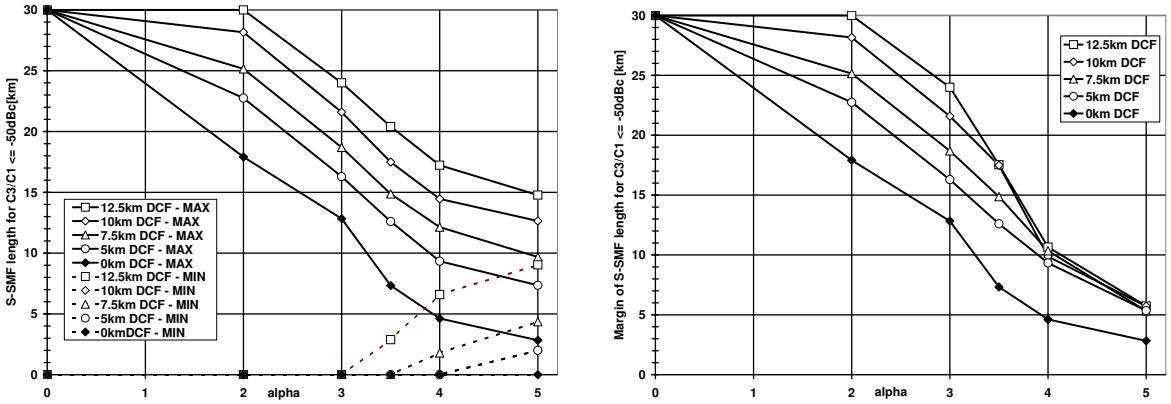

(a) (b)

Figure 8.7.: S-SMF (a) minimum and maximum lengths, and (b) as a function of the source's chirp factor for different DCF lengths when targeting a -50dBc C3/C1 threshold.

For chirp values ranging from 2 to 3.5, the margin increases proportionally with the cascaded DCF's length.

For chirp factors greater than 3.5, the margin tends to be independent of the cascaded DCF's length and to converge: towards 10km for a chirp factor of 4 and towards 5km for a chirp factor of 5. Despite the margin to be constant, the DCF length henceforth matters for the distance at which the system is actually expected to deliver optimal performances.

8.4. Influence of the carrier frequency for different chirp factors

Last but not least, this section shows the frequency dependency of the chirp and chromatic dispersion induced inter-modulations distortions. Therefore we consider successively an optical link made of 20km S-SMF, and then with additional 12.5km of DCF cascaded to the 20km of S-SMF. For both links the modulating carrier frequency is swept from 700 to 3.5GHz, and this for several chirp factor values.

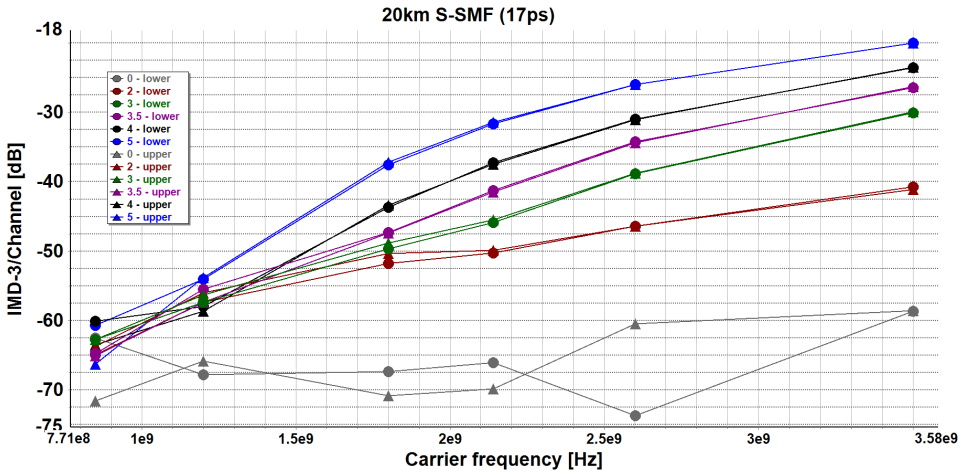

(a)

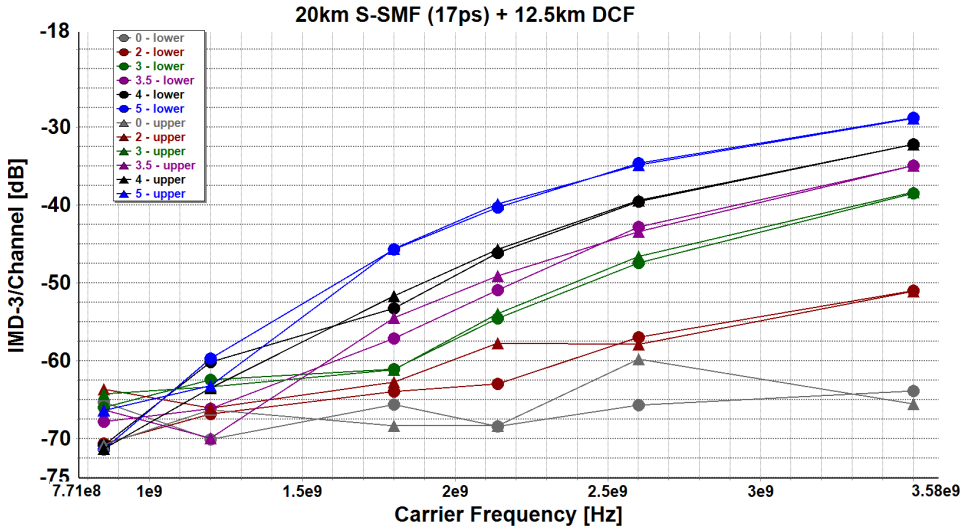

(b)

Figure 8.8.: Influence of the carrier frequency on the IMD-3 for different chirp factors for (top) a 20km S-SMF link (bottom) a 20km S-SMF +12.5km DCF link

Fig. 8.8a shows an increasing carrier frequency to degrade the C3/C1 ratio. For instance, the linear approximation of the C3/C1 ratio for a chirp factor of 3, exhibits a C3/C1 degradation slope coefficient of 11dB per GHz. When the chirp factor values 4, the equivalent slope values 10.3dB/GHz.

Finally this demonstrates the interest of using low carrier frequencies in RoF transmissions, albeit the use of DCF can allow to increase the carrier frequency for a given couple of S-SMF length and chirp factor. Taking into account the native carrier frequencies of the mobile radio standards (§3.1.1, page 42), the most favorable bands are once more the *golden frequencies* around 800-900MHz. For the other frequency bands, DCF can be used, and its length must be tailored to the propagation length.

9. ACLR simulations using *VPItransmissionMaker*

Scope

In the previous section, we showed the IMD-3 issue and the benefit of using DCF for simple two tone signals. Also the latter simulations did not take into account any budget issues. Yet optical power budget issues are primordial in a PON context.

In order to overcome this, we will simulate in this section a more realistic RoF over PON set-up. Therefore UMTS-like signals are generated to emulate *high* crest factors. Then the IMD-3 issues related to the chromatic dispersion, are examined under the scope of the ACLR figures of merit, to show how the transmission of typical UMTS carriers through PONs (typically consisting in optical losses of at least 28dB including up to 20km of S-SMF fiber) can be limited when trying to fulfill the 3GPP requirements —this section anticipates the architecture changes presented in the second half of Part 4, when considering that fulfilling the EVM requirements not to be sufficient.

For the sake of clarity the ACLR is therefore plotted in a density plot as a function of the relative modulating RMS power of the carrier (which can be linked to the total power and hence to the OMI), and as a function of the total optical budget.

9.1. Unamplified optical links

Even if an UMTS signal is sometimes modeled as a *simple* QPSK signal [115], in this simulation study the UMTS signal is modeled in a more complex fashion in order to dispose of a more realistic emulation by increasing its peak-to-average power ratio.

This choice is motivated by the fact that signals with higher peak-to-average power ratios —at equivalent average power— induce distortions due to clipping when modulating the laser diode. Yet one could argue that high crest factor signals can be overcome by increasing the bias of the laser diode. However given that increasing the laser diode bias currents may affect the chirp factor α, the RIN, and last but not least the efficiency and linearity of the electro-optical conversion slope of the laser, the emulation of signals with increased crest factors is mandatory.

9.1.1. Building sources with different crest factors

Therefore similar to the idea of multiple physicals channels added at the base band level —as for the UMTS signal according to the 3GPP specifications (see § 3.2.1, page 52)— we use in this section a superposition of multiple Pseudo Random Bit Sequence (PRBS) sources with different seeds.

VPItransmissionMaker provides a module entitled *Tx_ElQAM*. This module generates an electrical M-QAM signal up-converted at a given carrier frequency, and outputs an up-converted combined in-phase and quadrature electrical symbols.

Table 9.1.: Crest Factors of a QPSK-modulated PRBS-source for different seeds

Random Number Seed	Crest Factor [dB]
1	6.75
5	7.80
2	7.51
3	7.46
5 + 2	8.56
5 + 2 + 3	10.00

By properly choosing the seeds[1] of the different PRBS sources and combining them (electrical RF addition of the module's outputs), the overall crest-factor of the signal can be increased, as shown in Table. 9.1. The source is a ninth order PRBS generator. 64 QPSK symbols at a symbol rate of 3.84Msymbols/s are simulated, resulting in a time window of 16.66μs.

9.1.2. Influence of the crest factor (fiber-free link)

In this section the link is fiber-free thus the chromatic dispersion is not an issue.

Crest factor and input range

The goal of this section is to show the influence of the crest factor on the electrical input dynamic range (see § 7.2.4, page 118 —for an UMTS carrier of equal RMS power. For the Adjacent/Alternate Channel power Leakage Ratio (ACLR) performances at +/-5MHz we fix the threshold for input dynamic range at -45dBc, and at -50dBc for the ACLR performances at +/-10MHz[2].

For the simulation (set-up of Fig. 9.1), the reference power of the UMTS input signal values +12.04dBm, and corresponds to 0dB of the vertical scale (0dB driver Gain in Fig. 9.1). The LD has a conversion efficieny of 0.0719W/A and is biased by a constant current of 65mA, and the RMS power of the carrier and optical budget are swept.

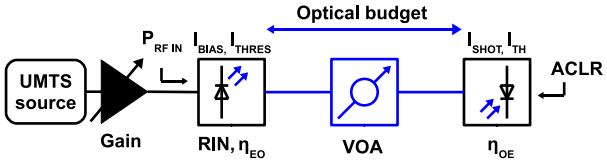

Figure 9.1.: VPI set-up for simulating the UMTS carrier's transport

Without loss of generality, we study the SNR versus input RF power for an optical budget of 6dB set by a Variable Optical Attenuator (VOA), and corresponds to the afore mentioned $1/L$ losses.

[1] A *seed* is set of values for initializing the PRBS-registers
[2] The reasons of these thresholds are exposed in § 3.3.2, p. 64

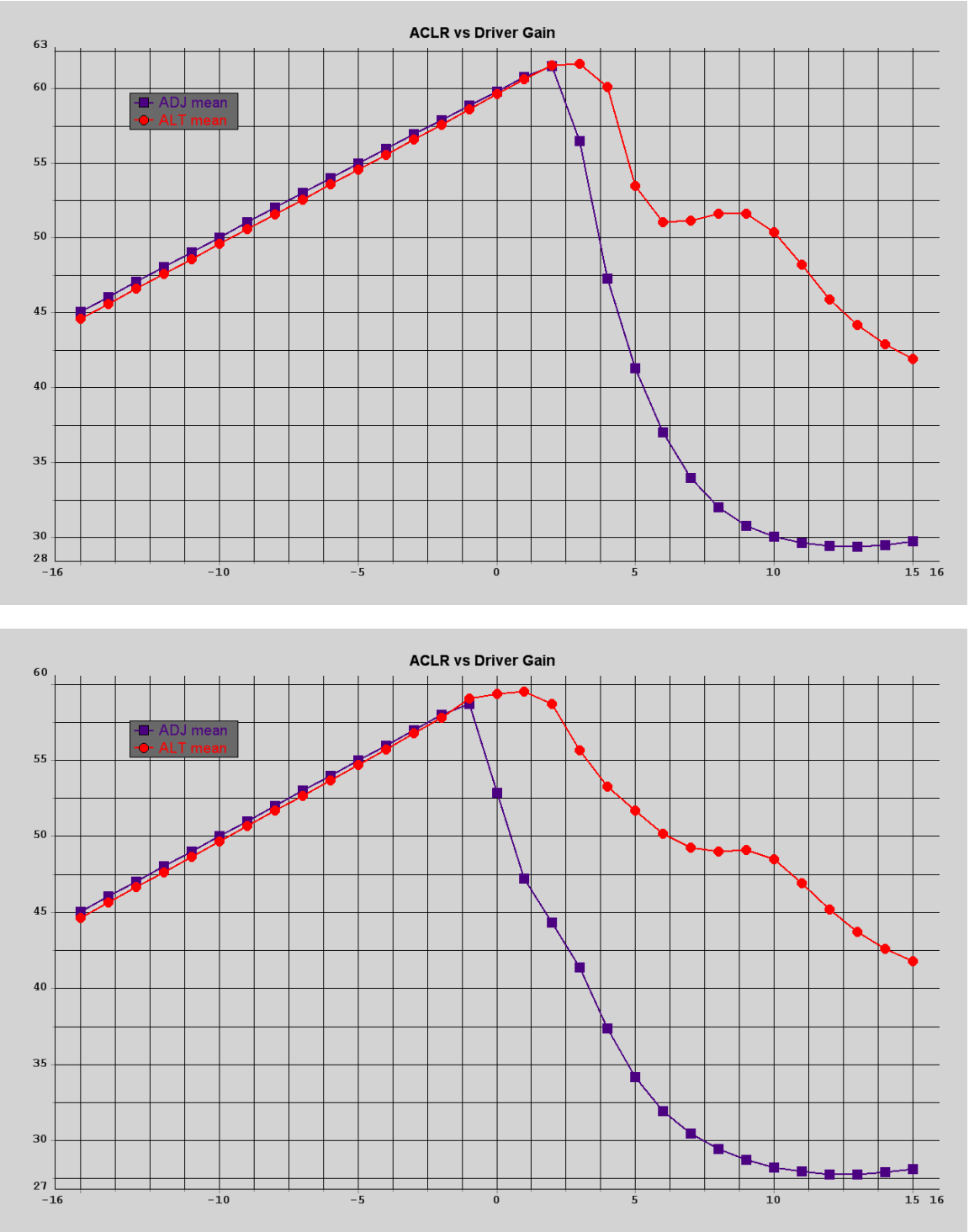

Figure 9.2.: ACLR performances at 6dB optical budget for a fiber free link, 65mA biased laser, and a simple PIN receiver for a signal with a 6.75dB crest factor (top) and a 10.0dB crest factor (bottom).
The horizontal axis corresponds to the relative gain/loss of the input RF power with respect to +12.04dBm. The vertical axis is the ACLR scale expressed in dB.

Results before overdriving: In concordance with Eq. 7.28, in Fig. 9.2 the SNR (*i.e.* here the Adj- and Alt-CLR) increases linearly with the input power (the driver gain). For the 6.75dB crest factor signal, this assertion is valid up to +2dB ($\triangleq$ +14.04dBm of input power). For the 10.0dB crest factor signal, this assertion is valid up to -1dB ($\triangleq$ +11.04dBm of input power).

In both cases, the latter points correspond to the maximum input RF power before *clipping* the laser: indeed, for a bias current of 65mA, and a threshold of 15mA, the peak power at 50Ω values +20.97dBm. Thus the equivalent maximum RMS power for a 6.75dB (10dB) crest factor signal values +14.20dBm (+16.5dBm). thus the OMI is maximum.

Furthermore, we can notice a first benefit of a reduced crest factor: when approaching the maximum OMI before clipping the SNR of the lower crest factor signal is the highest: the *peak* SNR values 62dB for the 6.75dB crest factor, and 59.2dB for the 10dB crest factor. This is in accordance with Eq. 7.28.

Finally, in the linear range when targeting a minimum SNR, the minimum required input power does not depend upon the crest factor as in accordance with § 7.2.4. Indeed, in both cases it is reached for a gain of -15dB ($\triangleq$ -2.96dBm of input power) for a threshold of 45dB, and for a gain of -10dB ($\triangleq$ +2.04dBm of input power).

Results when overdriving: Once the the LD starts to be over-driven, the ACLR components (Adj- and Alt-CLR) are dissociated —and thus no longer correspond to the SNR.

Fig. 9.2 also shows the Adj-CLR component to decrease more rapidly then the Alt-CLR component. Beyond a particular gain we can expect the ACLR components to *fall* below their respective target values. As a consequence of this we can —generally speaking— anticipate that for the higher crest factor signal this will occur for a lower gain.

Indeed, for the 6.75dB crest factor signal the Adj and Alt-CLR respective thresholds are reached for RF driver gains of respectively +4.4dB and +10.1dB, while for the 10dB crest factor signal the Adj and Alt-CLR respective thresholds are reached for RF driver gains of respectively +1.8dB and +6.2dB.

Conclusions:

1. since the ACLR thresholds have to be yielded for a same range of gain, the range of the lower crest factor signal will be obviously the highest: namely $+4.4-(-10) = 14.4dB$, while for the higher crest factor, the gain range values 11.1dB. This range of gain can be used for increasing the number of carriers, for instance.

2. furthermore we recall the benefit of the lower crest factor signal for yielding an optimized SNR, and anticipate that for a same added power of white noise (*i.e.* losses in optical link where shot of thermal noise dominates) the lower crest factor signal *tolerates* more noise (*i.e.* more losses in optical link) for a target SNR or couples of ACLR thresholds.

Crest factors and optical budget

For each couple of swept power and optical power budget, the ACLR[3] performances are simulated and stored, and shown in density plots.

The previous crest factor issue influences the maximum optical budget for specific target Adj- and Alt-CLR values of respectively 45 and 50dB minimum.

Concerning the Adj-CLR performances and the relative threshold, Fig.9.3 shows a maximum optical budget of 15.9dB for the 6.75dB crest factor signal, and a maximum optical budget of 14.1dB for the 10dB crest factor signal.

Concerning the Alt-CLR performances, Fig.9.4 shows a maximum optical budget of 13.7dB for the 6.75dB crest factor signal, and a maximum optical budget of 12.6dB for the 10dB crest factor signal.

These maximum optical budgets for target Adj- and Alt-CLR values are individually optimized with respect to the RF input power: the Adj-CLR's maximum optical budget is reached for a lower input gain than the input gain for which the Alt-CLR's maximum optical budget is reached.

Yet since the Adj- and Alt-CLR performances have to be met for a common range of RF input power, the *corrected* maximum optical budgets are as follows: 13.5dB and 12.3dB respectively for the 6.75dB and 10dB crest factor signals.

Finally this demonstrates the benefit of limiting the crest factor in order to maximize the maximum optical budget for given SNR constraints.

NB: for the simulations a RIN of -140dB/Hz and a thermal noise of 11.54 $10^{-11} A/\sqrt{Hz}$ have been used. The resulting optical budgets and SNRs are thus compliant with the formal expressions developed in §7, p. 108.

For instance let's retrieve the value of the RIN!
Indeed for for the bias current of 95mA and an optical budget of 6dB, we assume the RIN to dominate, and have a SNR of 44.35dB (case of Fig. 9.5a) when the electrical driving gain values -15dB (with respect to the reference RF input power). Then since

$$SNR = OMI_{RMS}^2 / (RIN \cdot \Delta_f) \quad \text{and} \quad OMI_{RMS}^2 = P_{RF}/Z_{in} \cdot 1/I_{DYN}^2 \tag{9.1}$$

$$RIN_{(dB)} = -SNR_{dB} - 10\log\Delta_f - P_{RMS} - 10\log(I_{DYN}^2 \cdot Z_{in} \cdot 10^3) \tag{9.2}$$

$$= -44.35 - 65.8 - 2.96 + 16.99 - 25.05 = -138.2\text{dB} \tag{9.3}$$

9.1.3. Increased bias current (fiber-free link)

When the crest factor of the information carrying signal can not be reduced, then in order to increase maximum optical budget we can increase the bias current to increase the optical launch power.

For demonstrating this, we consider the same signal with a crest factor of 10dB and increase the bias current to 95mA.

[3] average of the left and right hand side of the respective Adj- and Alt-CLR channels

The maximum optical budget, from a pure Adj-CLR specifications' perspective (Fig.9.5a), values now 14.7dB. From a pure Alt-CLR specifications' perspective (Fig.9.5b), the maximum optical budget is 14.6dB.

Finally when meeting all the ACLR specifications at the same time, the maximum optical budgets values 14.4dB —2.1dB more than for the 65mA bias. The latter difference is in accordance with the increase of the optical launch power of 2.05dB.

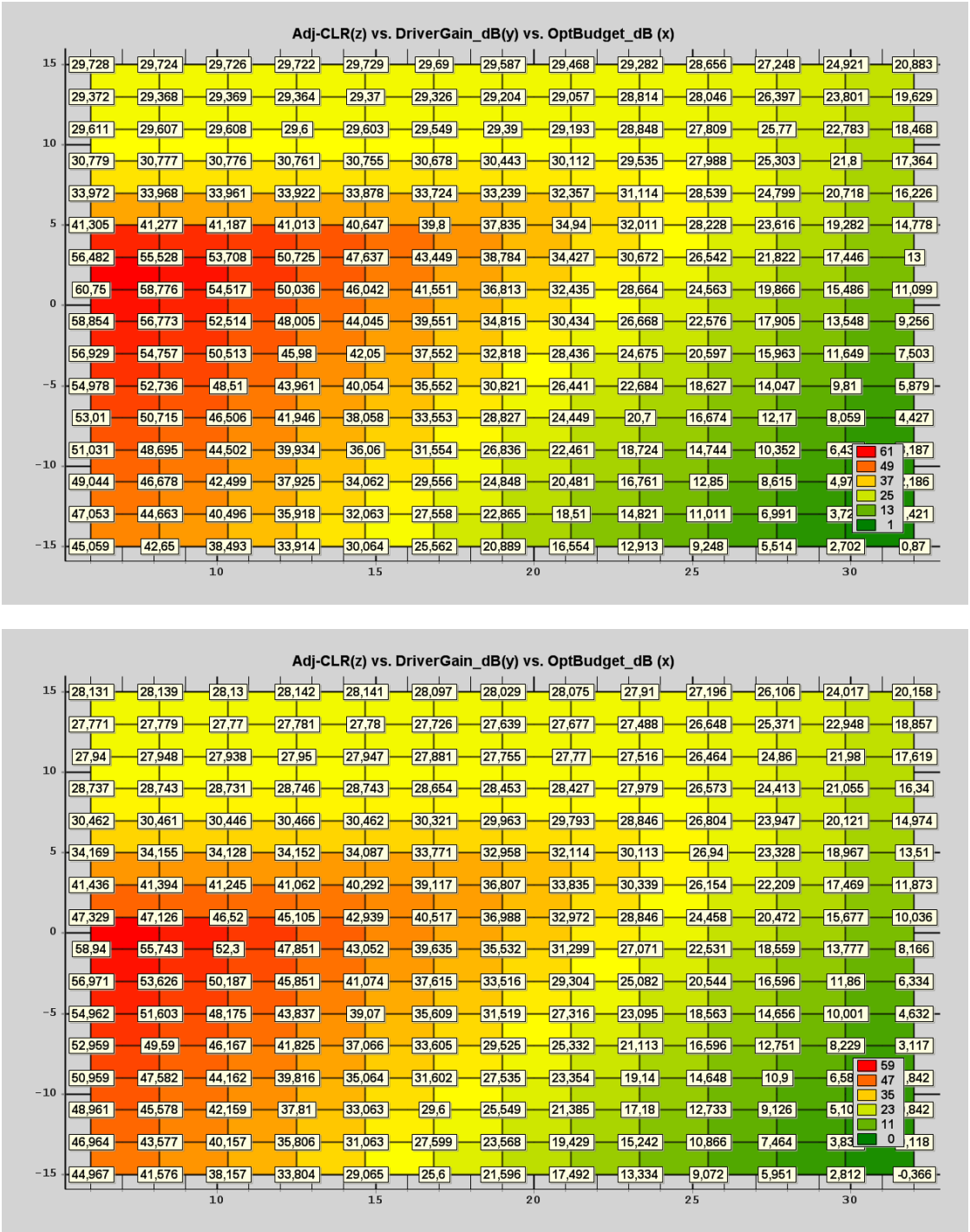

Figure 9.3.: Adjacent-CLR performances over fiber free link, 65mA biased laser, and a simple PIN receiver for a signal with a 6.75dB crest factor (top) and a 10.0dB crest factor (bottom)

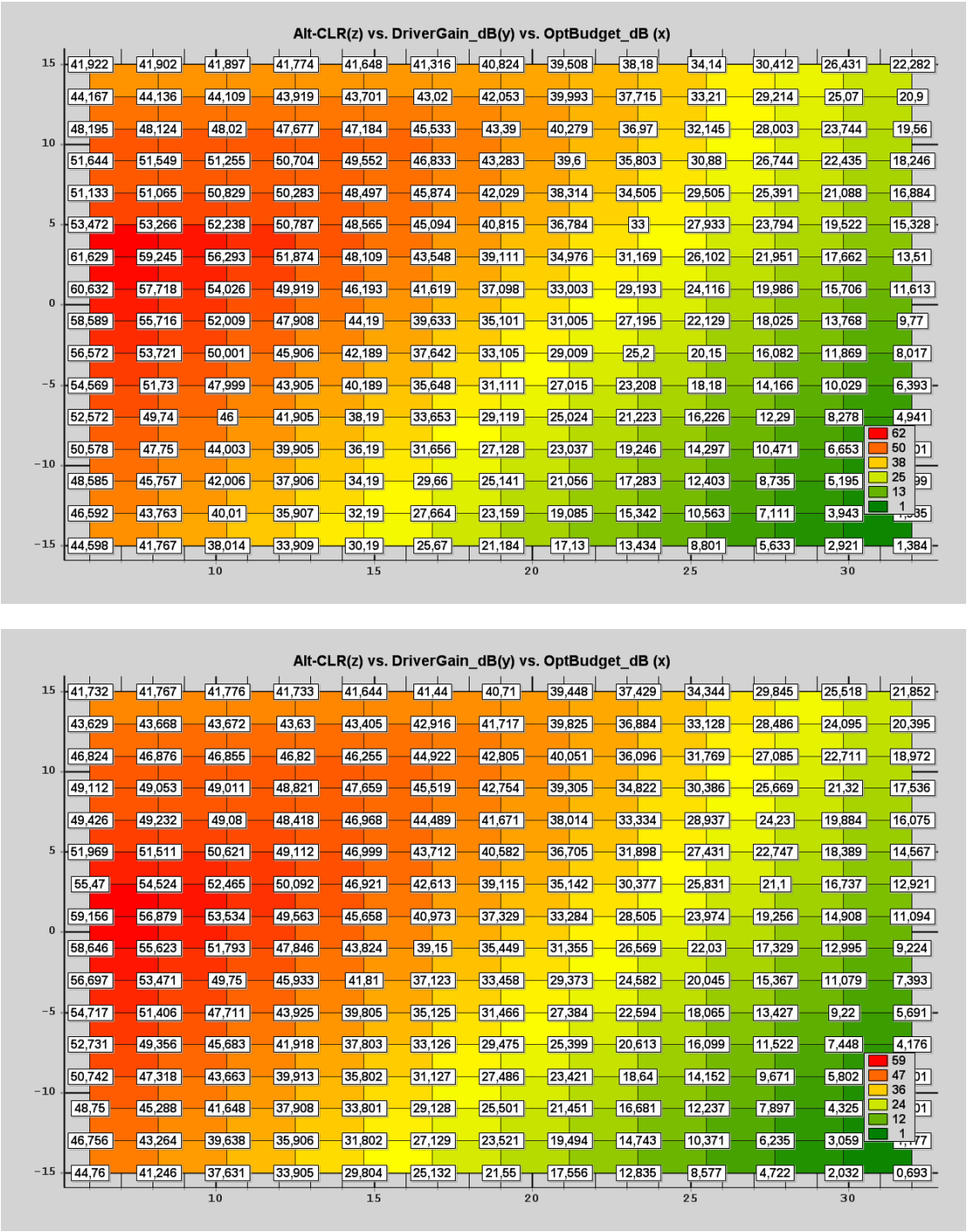

Figure 9.4.: Alternate-CLR performances over fiber free link, 65mA biased laser, and a simple PIN receiver for a signal with a (top) 6.75dB and (bottom) 10.0dB crest factor

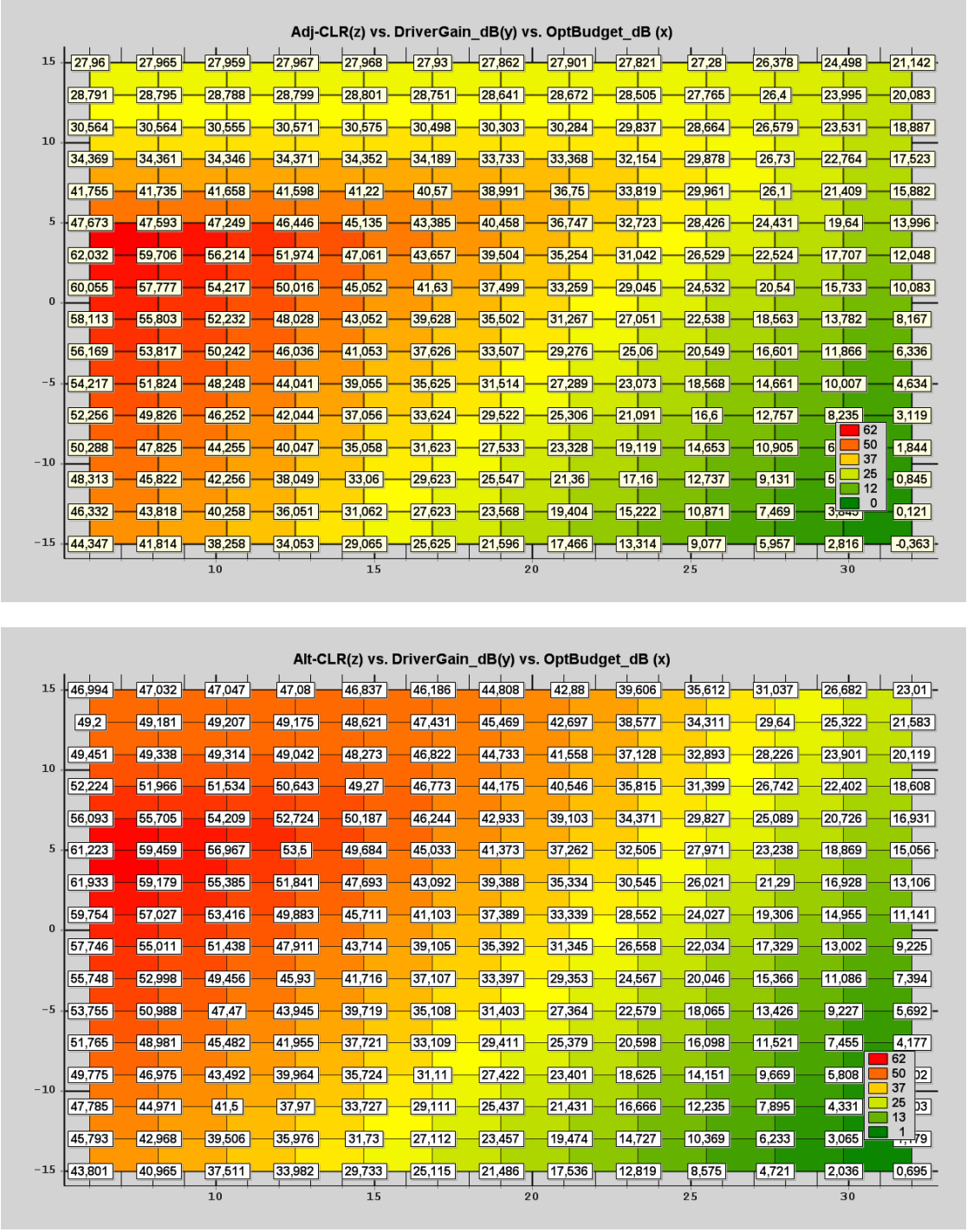

Figure 9.5.: ACLR performances over fiber free link, 95mA biased laser, and a simple PIN, (top) ADJ-CLR, (bottom) ALT-CLR, both for a 10dB crest factor

9.2. Optically amplified links

In order to demonstrate the benefit of optical pre-amplification we place an optical amplifier in front of the PIN (Fig. 9.6). The optical amplifier's parameters are set to correspond to an EDFA: noise figure of 4.5dB, automatic power control (APC) mode with a target optical output power of +1.5mW (+1.76dBm) with a maximum (saturating) optical gain of 45dB.

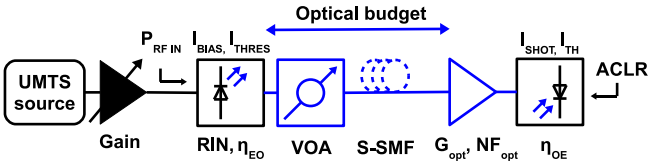

Figure 9.6.: VPI set-up for simulating the UMTS carrier's transport with a booster.

9.2.1. Fiber-free link

In a first time a fiber-free link is simulated, keeping the 10dB crest factor signal still single carrier, and the 95mA bias current.

From a pure Adj-CLR performances point of view, the specifications of 45dB minimum can be hold up to an maximum optical budget of at least 36dB[4]. For the Alt-CLR performances, the specifications of at least 50dB, can be met for a maximum optical budget of 35.3dB.

When combining both set of constraints, the maximum optical budget falls to 34.8dB.

Compared to the set-up using no optical pre-amplification, this represents a maximum optical budget increase of 20dB.

Thus for this single carrier and fiber-free case the benefit of optical pre-amplification is demonstrated.

[4]the simulation was carried out up to 36dB which is 6dB more than the maximum of the typical PON budget classes, and also because each additional point is computing intensive...

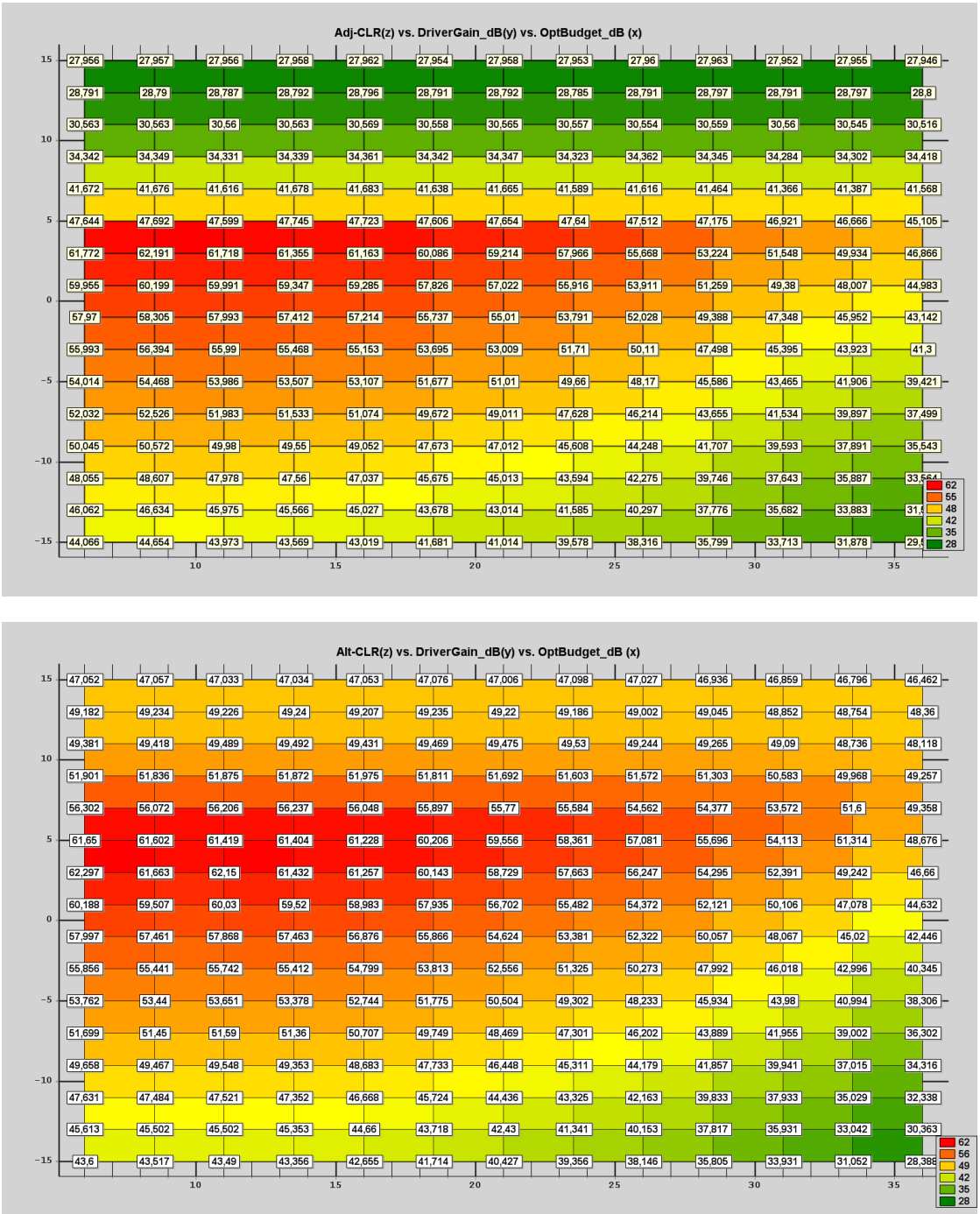

Figure 9.7.: ACLR performances over fiber free link, optically amplified, 95mA biased laser, and a simple PIN, (top) ADJ-CLR, (bottom) ALT-CLR, both for a 10dB crest factor

9.2.2. Fiber-containing links

Since in a PON context up to 20km of S-SMF can be contained in the link, we simulate the previous section's set-up for 10 and 20km of S-SMF. For both lengths the S-SMF spans' parameters are set as follows: linear insertion losses of 0.25dB/km, and chromatic dispersion of 16ps/(nm.km). Furthermore the laser source's chirp factor (α) is set to 5.

10km of S-SMF included in the link

From a pure Adj-CLR performances point of view, the specifications of 45dB minimum can be hold up to a maximum optical budget of at least 36dB. Thus the degradation due to the 10km of S-SMF, compared to the fiber-free case, cannot be compared in terms of an optical budget.

Yet its effect can be compared in terms of an input dynamic range (difference between the maximum and minimum RF input power for meeting a target SNR): for the previous fiber-free case (Fig. 9.7), the input range for Adj-CLR specifications at an optical budget of 36dB values 3.5dB —offering the possibility of an additional UMTS carrier.

When the link contains 10km of S-SMF (Fig. 9.8), then for the same optical budget, the input range value falls to 1.5dB —excluding the possibility of an additional carrier.

The Alt-CLR specifications of 50dB minimum can be met for a maximum optical budget of 33dB —representing a 1.8dB budget loss compared to the fiber-free case.

When both sets of constraints are combined, the maximum optical budget falls to 31.8dB —representing a 2dB loss compared to the fiber-free case.

20km of S-SMF included in the link

From a pure Adj-CLR performances point of view (Fig. 9.9a), the specifications of 45dB minimum can be hold up to a maximum optical budget of 34.2dB.

When only considering the Alt-CLR constraints in Fig. 9.9b and the related minimum specifications of 50dB, the maximum optical budget values 30.7dB.

Finally, all ACLR specifications can be at the same time up to an optical budget of maximum 28.9dB. The latter value hardly exceeds —by 0.9dB— the maximum optical budget of the legacy PON B+ Class.

Yet integration aspects in terms of multiplexing the optical infrastructures (lasers at the Central Office (CO), Photo-Detectors (PDs) and optical pre-amplifier prior to the Optical Network Unit (ONU) and remote antenna sites) require more than 0.9dB of total optical link margin —typically 2dB— to compensate the total insertion losses of the multiplexers and/or circulators located at the *head* and *tail* of the PON.

Summary for the 31dB optical budget point

For example at a 31dB optical budget [5] , a constant OMI (peak of 99.8%, RMS of 31.6%, $\triangleq$ gain of +3dB in Fig. 9.5, 9.7, 9.8, 9.9) and a bias current of 95mA, Tab. 9.2 summarizes

[5] the available (without the need of interpolating them) data are available for optical budgets of 28.75 and 31dB but since we target optical budgets of at least 28dB (PON B+ class) with additional insertion losses of ≈1.6dB for adapting to legacy networks, 31 dB is more realistic

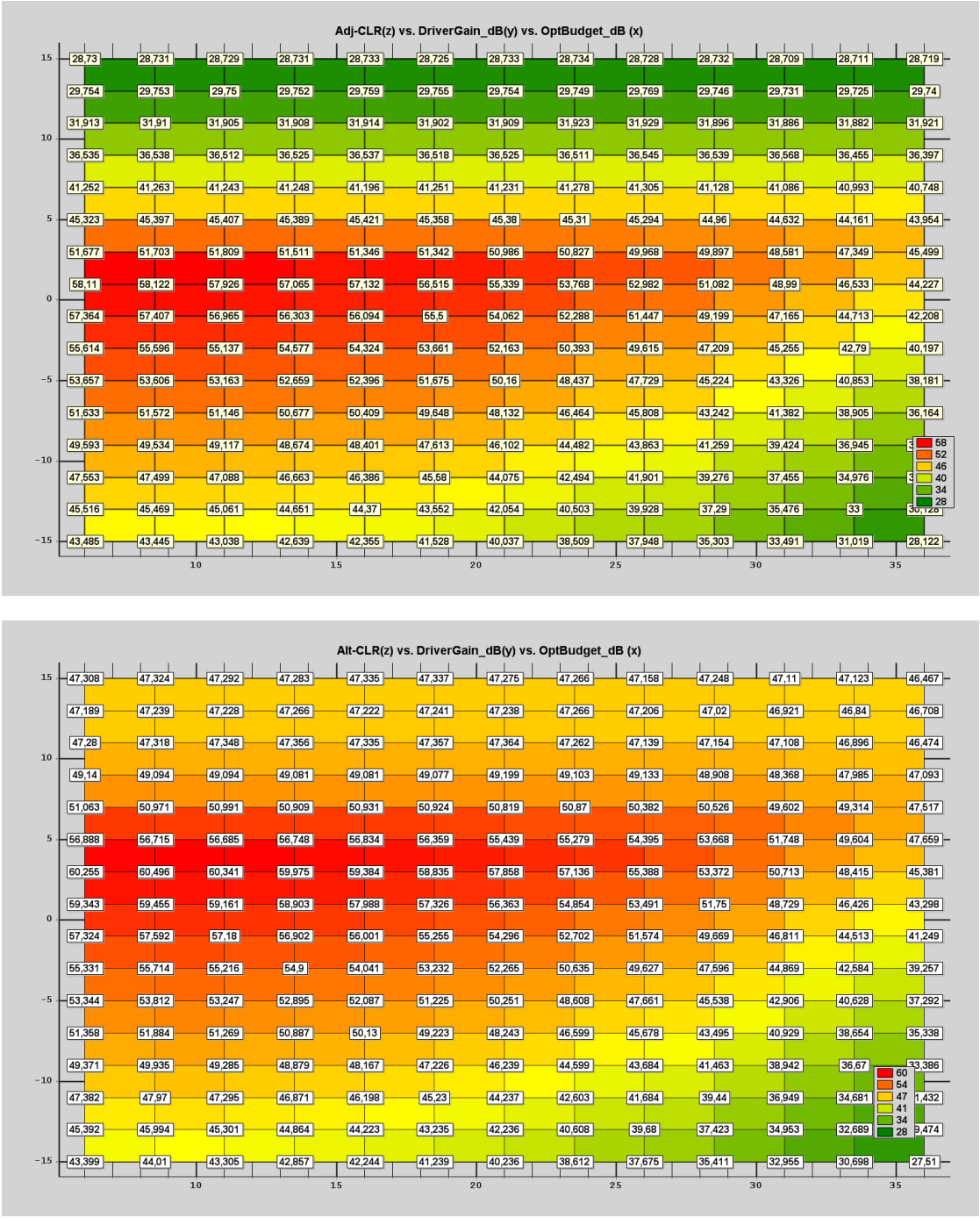

Figure 9.8.: ACLR performances over link containing 10km of fiber, optically pre-amplified, 95mA biased laser, and a simple PIN, (top) ADJ-CLR, (bottom) ALT-CLR, crest factor of 10dB

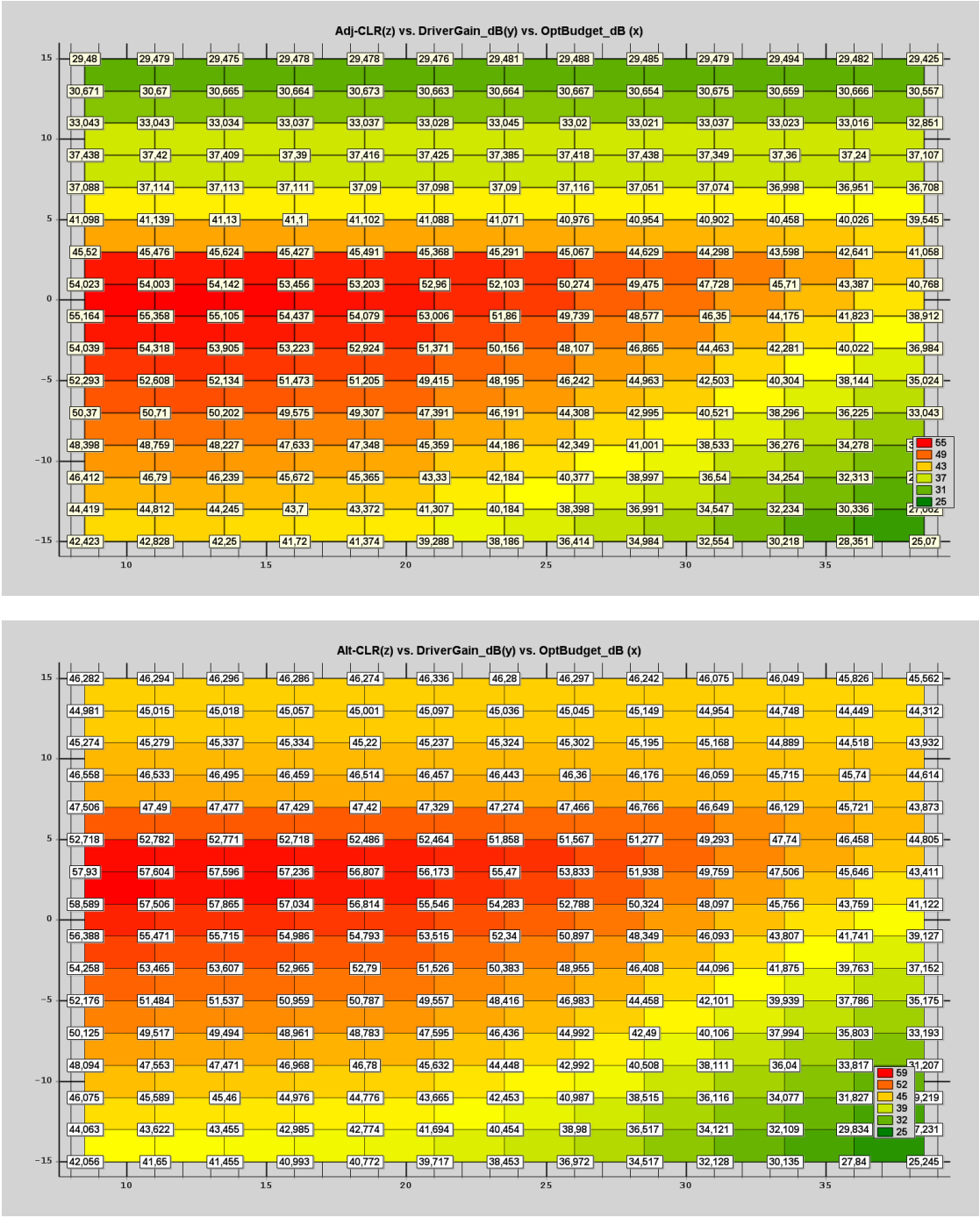

Figure 9.9.: ACLR performances over link containing 20km of fiber, optically pre-amplified, 95mA biased laser, and a simple PIN, (top) ADJ-CLR, (bottom) ALT-CLR, crest factor of 10dB

the different ACLR performances and their compliance with the 3GPP specifications —for a 31dB optical budget.

Table 9.2.: ACLR summary #1 for a 31dB optical budget and a 95mA bias current

S-SMF [km]	**Optical pre-Amplifier**	**Adj-CLR [dB]**	**Alt-CLR [dB]**	**3GPP compliant?**
none	none	12.7	15.9	No
none	Yes	51.5	52.4	Yes
10	Yes	48.6	50.7	Yes
20	Yes	44.3	49.8	No

If we lower the OMI for this optical budget to a peak of 79.3% (RMS of 25.1%, $\triangleq$ gain of +1dB in Fig. 9.7, 9.8, 9.9), then the power of the carrier as well as the chromatic dispersion related third order distortions —since growing/declining three times faster— will be lower... but the overall ACLR results will not necessarily be compliant with the 3GPP specifications!

Indeed for this new OMI the Adj-CLR specifications can be met whether no, 10 or 20km of S-SMF is contained in the link. However for the Alt-CLR specifications only (among the three simulated cases) the fiber-free case allows to meet the specifications. Tab. 9.3 summarizes the results for this lower OMI.

Table 9.3.: ACLR summary #2 for a 31dB optical budget and a 95mA bias current

S-SMF [km]	**Optical pre-Amplifier**	**Adj-CLR [dB]**	**Alt-CLR [dB]**	**3GPP compliant?**
none	Yes	49.4	50.1	Yes
10	Yes	49.0	48.7	No
20	Yes	47.7	48.1	No

Conclusion

Finally these simulations have shown the benefit of the pre-amplifier when targeting the ACLR specifications for optical budgets with a order's magnitude of 30dB. Also the impairments of the S-SMF to the ACLR performances in terms of the maximum optical budget have been demonstrated.

9.2.3. Carrier frequency discussion

Keeping the parameter set of the previous paragraph[6], we briefly discuss the effect of the carrier frequency onto the maximum optical budget. Therefore we simulate the transport

[6]bias of 95mA, 10dB crest factor, identical RF sweeps

over a RoF/PON-architecture of an UMTS carrier centered at 850MHz and 2.6GHz.

A UMTS carrier whether is centered at 850MHz (Fig. 9.10) or 2.6GHz (Fig. 9.11) will yield 3GPP compliant ACLR performances for maximum optical budgets of respectively 35.2dB and 28.6dB —corresponding respectively to an increase of 6.3dB and to a decrease of 0.3dB, when comparing to the case of a 2.14GHz centered carrier (Fig. 9.9).

As in §8.4 for a two-tone signal, the interest of a lower carrier frequency is demonstrated.

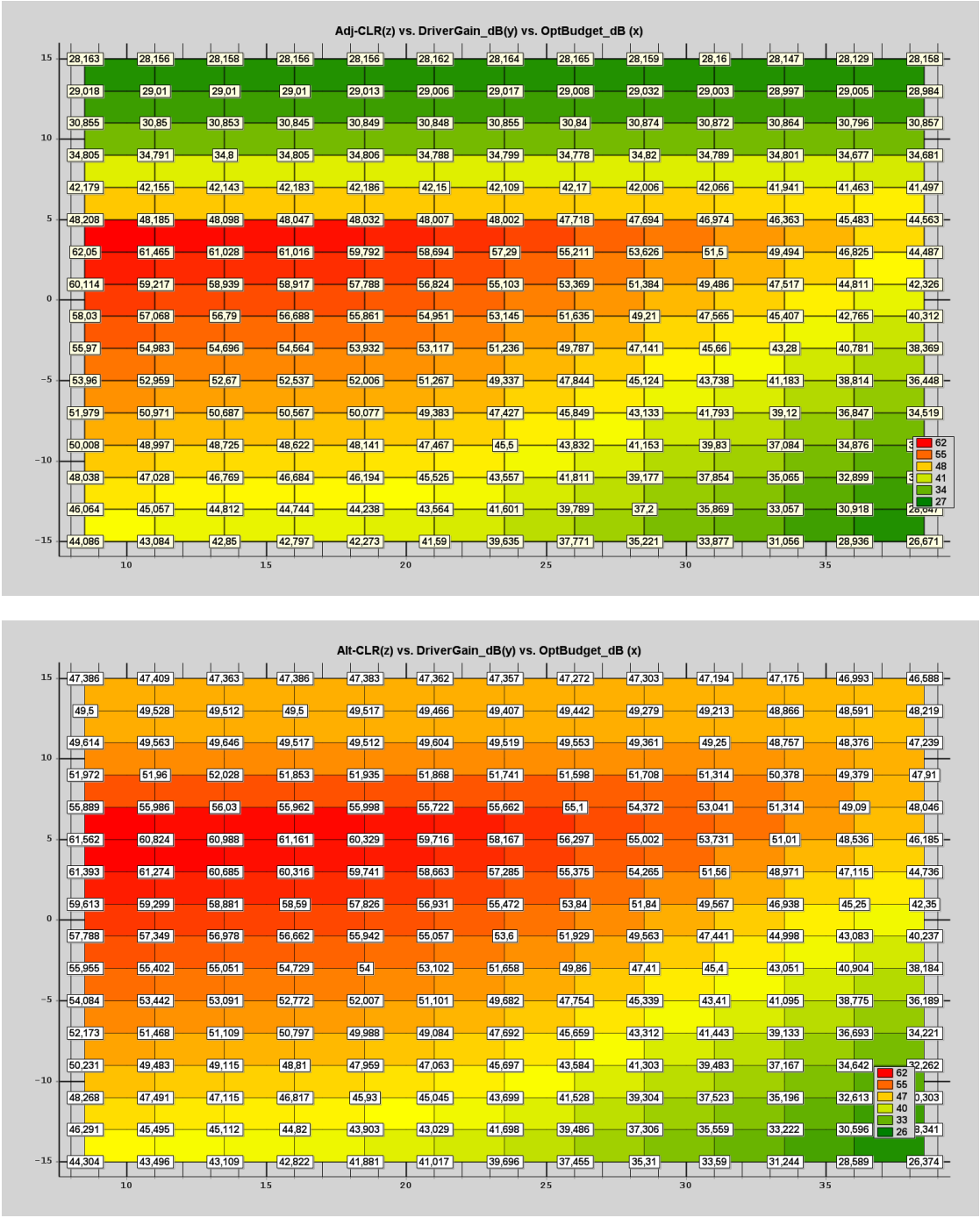

Figure 9.10.: ACLR performances over link containing 20km of fiber, optically pre-amplified, 95mA biased laser, and a simple PIN at 850MHz, (top) ADJ-CLR, (bottom) ALT-CLR, crest factor of 10dB

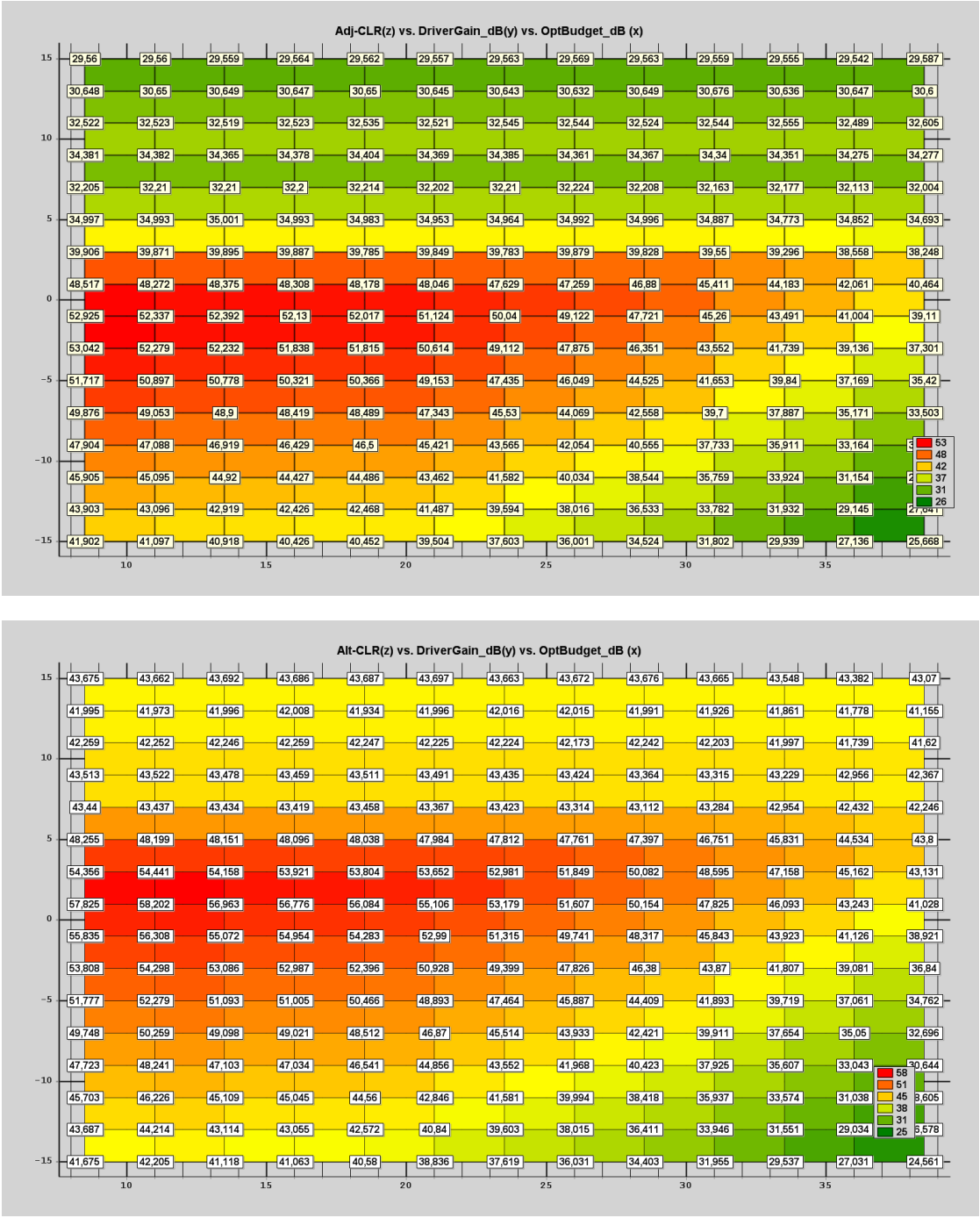

Figure 9.11.: ACLR performances over link containing 20km of fiber, optically pre-amplified, 95mA biased laser, and a simple PIN at 2.6GHz, (top) ADJ-CLR, (bottom) ALT-CLR, crest factor of 10dB

9.2.4. Dispersion compensating fiber and booster

In order to overcome the ACLR impairments due to the S-SMF, we place a DCF spool of 12.5km directly after the laser diode, and an optical booster set to compensate exactly the losses due to the DCF spool. We come back to an UMTS carrier transmitted at a center frequency of 2140MHz.

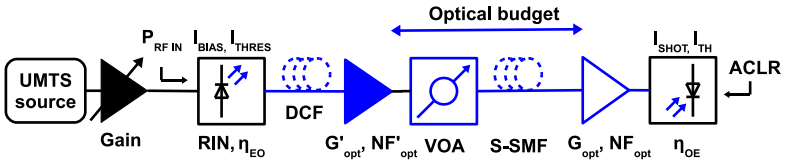

Figure 9.12.: VPI set-up for simulating the UMTS carrier's transport with DCF and a booster

The DCF has linear insertion losses of 0.25dB/km and chromatic dispersion of -16ps/(nm.km). Thus the booster's gain is set to 3.125dB, and its noise figure to 4.5dB.

Again we simulate the set-up for links containing 10 and 20km of S-SMF. In the different figures the term *optical budget* represents the effective useful optical budget —between the booster's output and the pre-amplifier's input (Fig. 9.12).

10km of S-SMF

From a pure Adj-CLR performances point of view, the specifications of 45dB minimum can be hold up to a maximum optical budget of at least 36dB.

Thanks to the DCF the input range for the 36dB optical budget points values 3.5dB —comparable to the fiber-free case.

The Alt-CLR specifications of 50dB minimum can be met for a maximum optical budget of 34.7dB —which is 0.1dB lower than the fiber-free case, and 2.9dB higher than the similar set-up with no DCF.

When both sets of constraints are combined, the maximum optical budget falls to the minimum of both previous budgets, namely 34.7dB —representing again a 2.9dB optical budget improvement compared to the similar set-up with no DCF.

20km of S-SMF

From a pure Adj-CLR performances point of view, the specifications of 45dB minimum can be hold up to a maximum optical budget of at least 37.6dB.

Thanks to the DCF the input range at the 36dB optical budget point values 3.5dB —comparable to the fiber-free case.

The Alt-CLR specifications of 50dB minimum can be met for a maximum optical budget of 34.15dB —which is 0.65dB lower than the fiber-free case, and 2.25dB higher than the similar set-up with no DCF.

When both sets of constraints are combined, the maximum optical budget falls to the minimum of both previous budgets, namely 34.7dB —representing again a 5.25dB optical budget improvement compared to the similar set-up with no DCF.

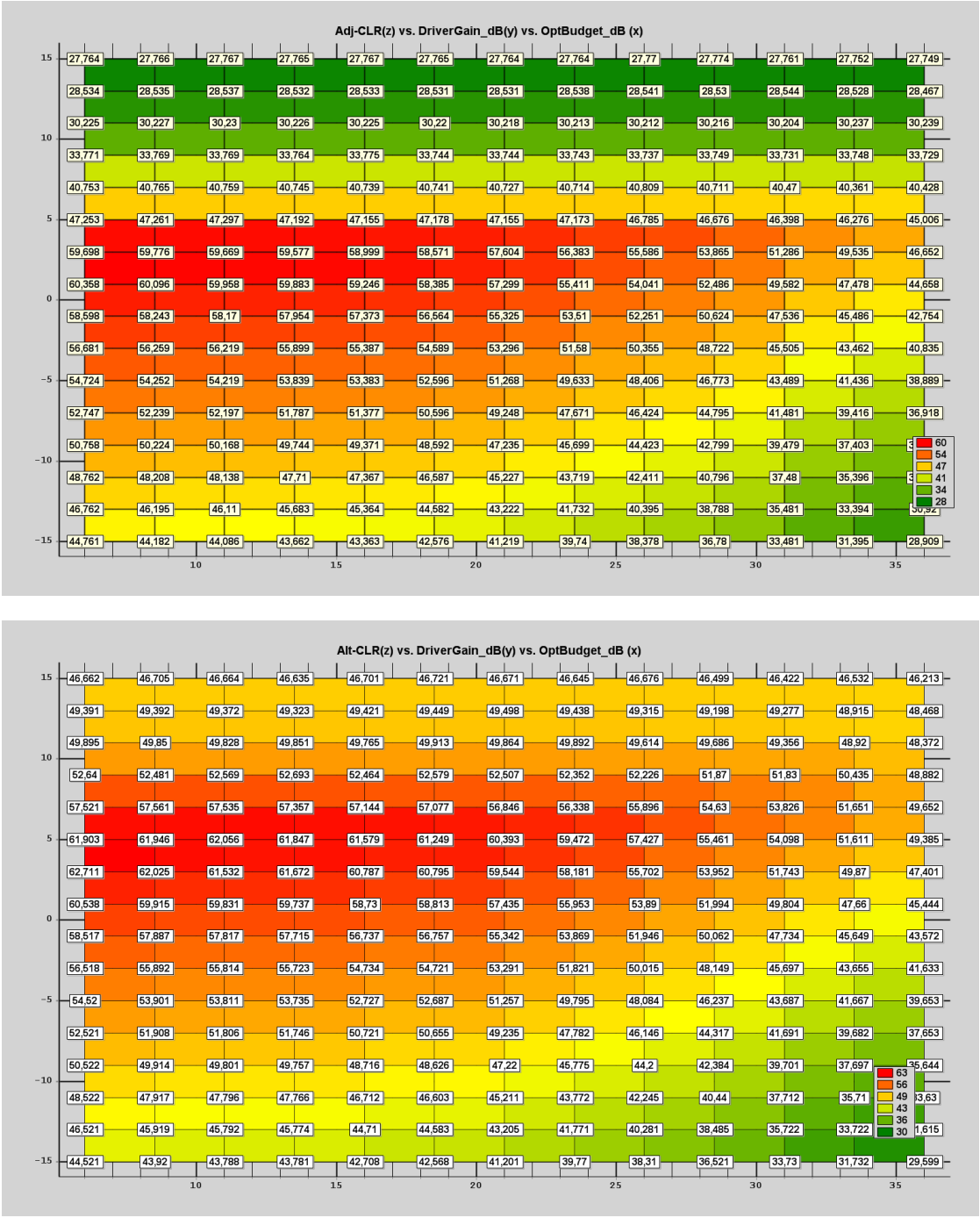

Figure 9.13.: ACLR performances over link containing 12.5km of DCF, a booster, 10km of fiber, optically pre-amplified, 95mA biased laser, and a simple PIN, (top) ADJ-CLR, (bottom) ALT-CLR, crest factor of 10dB

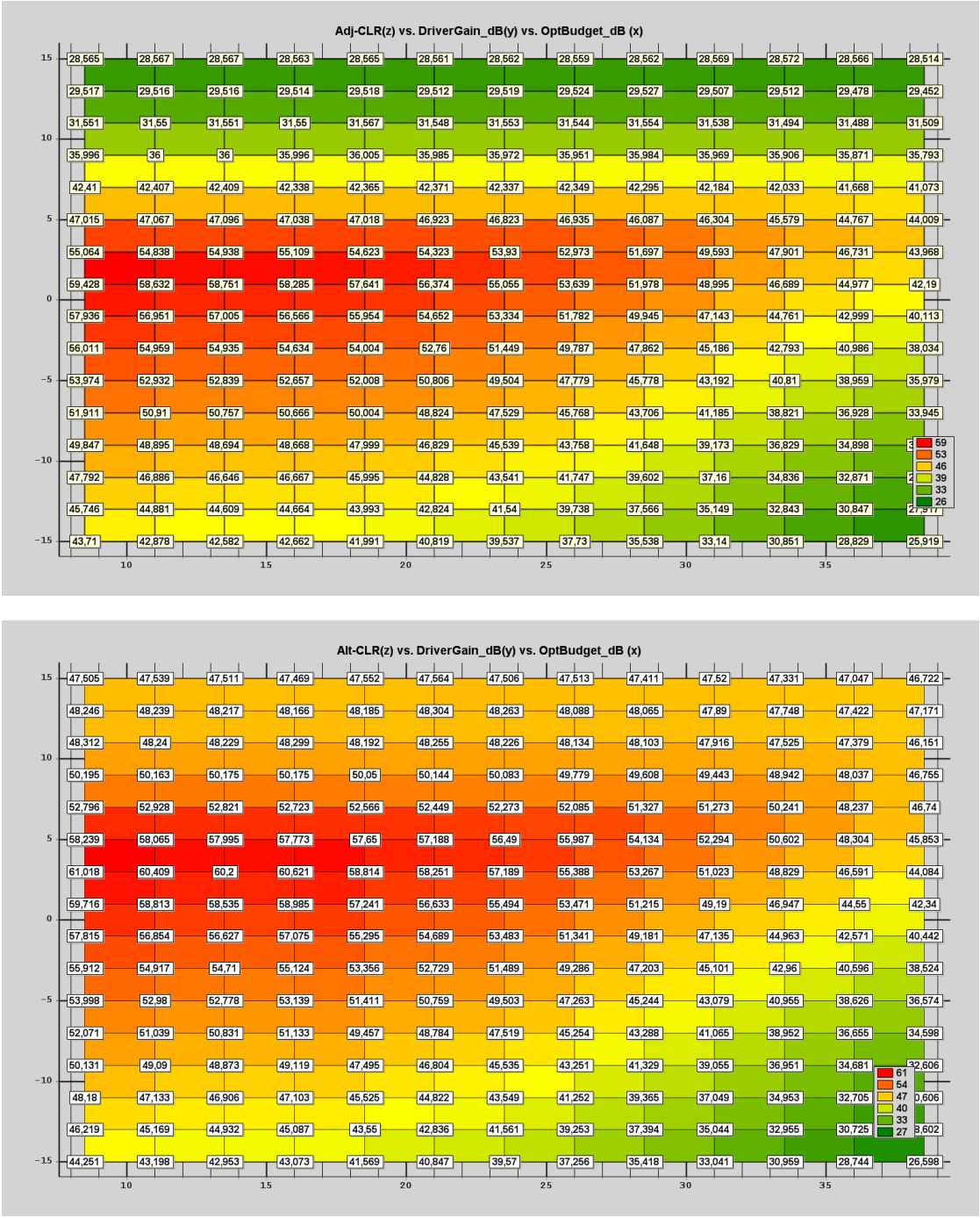

Figure 9.14.: ACLR performances over link containing 12.5km of DCF, a booster, 20km of fiber, optically pre-amplified, 95mA biased laser, and a simple PIN, (top) ADJ-CLR, (bottom) ALT-CLR, crest factor of 10dB

Summary for the 31dB optical budget point

As for the DCF-free case we can summarize the ACLR performances for two OMIs at an optical budget of 31dB in Tab. 9.4 and 9.5 for respective peak OMIs of 99.8% and 78.3%.

Table 9.4.: ACLR summary # 1 for an optical budget of 31dB, optical pre-amplification, booster and DCF

S-SMF [km]	**DCF [km]**	**Pre-Amplifier /Booster**	**Alt-CLR [dB]**	**Alt-CLR [dB]**	**3GPP compliant ?**
10	12.5	Yes/Yes	51.3	51.7	Yes
20	12.5	Yes/Yes	49.6	51.0	Yes

For both OMIs the Adj-CLR specifications can be met whether 10 or 20km of S-SMF are contained in the link. Yet the Alt-CRL specifications can only be met (in these considered examples) by the first OMI.

Table 9.5.: ACLR summary # 2 for an optical budget of 31dB, optical pre-amplification, booster and DCF

S-SMF [km]	**DCF [km]**	**Pre-Amplifier /Booster**	**Alt-CLR [dB]**	**Alt-CLR [dB]**	**3GPP compliant ?**
10	12.5	Yes/Yes	49.2	49.8	No
20	12.5	Yes/Yes	49.0	49.2	No

Conclusion

Thanks to the DCF, and the booster for compensating its insertion loss, the ACLR performances for a single carrier transmission are compliant with the 3GPP specifications up to a maximum optical budget of 34.15dB containing 20km of S-SMF —representing an improvement of 5.25dB compared to the set-up without DCF.

This demonstrates the benefit of the DCF spool for improving the overall ACLR performances.

Finally the interest of DCF in combination with the booster has been demonstrated. We recall this simulations to have been carried out for a **single** UMTS carrier.

9.3. Dual-carrier set-up for optically amplified links

For the simulations carried out in this section we re-use the schematic in Fig. 9.12 and the related parameters. The used UMTS multiplex is made of two UMTS carriers spaced by 10MHz, and centered at 2140MHz.

The here simulated UMTS multiplex has an overall crest factor of 11.6dB. The booster's gain is increased to +7dB of gain, instead of initially +3.125dB, since an increased crest factor reduces the maximum possible OMI per carrier, and hence the SNR is reduced... Thus the total optical power launched into the PON section values +14.6dBm.

When only considering the Adj-CLR performances the maximum optical budget exceeds 35dB [7]. Yet if only the Alt-CLR specifications are taken into account, then the maximum optical budget values 29.9dB. Finally, the latter optical budget sets the value for the effective maximum optical budget for which both ACLR components are compliant with the 3GPP specifications.

9.3.1. Chirp discussion

The previous simulations have been carried out for a chirp factor of 5.

DCF has been inserted between the laser and the optical booster in order to overcome the combined effect of the chirp and of the chromatic dispersion (§8.2.2, p. 131). Also we can consider the used DCF length of 12.5km to be *sufficient* in terms of a maximum optical budget for the single and double UMTS carrier transmissions.

Yet we will briefly review the effect of the chirp by varying it for this final PON architecture containing 20km of S-SMF through which two UMTS carriers are transmitted. Therefore we simulate the previous set-up for a chirp factor valuing successively 4.5, 4, and 3.5.

For illustration's sake, Fig. 9.15a corresponds to the initial case chirp factor of 5, and Fig. 9.16a corresponds to the other simulated extrema, namely 3.5.

Conclusion

Tab.9.6 summarizes the maximum optical budgets corresponding to the simulation of the different chirp factors.

Table 9.6.: Chirp discussion

	Maximum optical budget [dB]		
Chirp	Adj-CLR only	Alt-CLR only	**ACLR**
5	>35	29.9	**29.9**
4.5	>35	30.6	**30.6**
4	>35	32.6	**32.6**
3.5	>35	32.8	**32.8**

Finally these simulations confirm the benefit of a reduced chirp factor. Indeed passing from a chirp factor of 5 to 3.5 allows to improve the maximum optical budget by 2.9dB to 32.8dB.

[7] *i.e.* the largest simulated optical budget. The simulation was carried out up to 36dB which is 6dB more than the maximum of the typical PON budget classes, and also because each additional point is computing intensive...

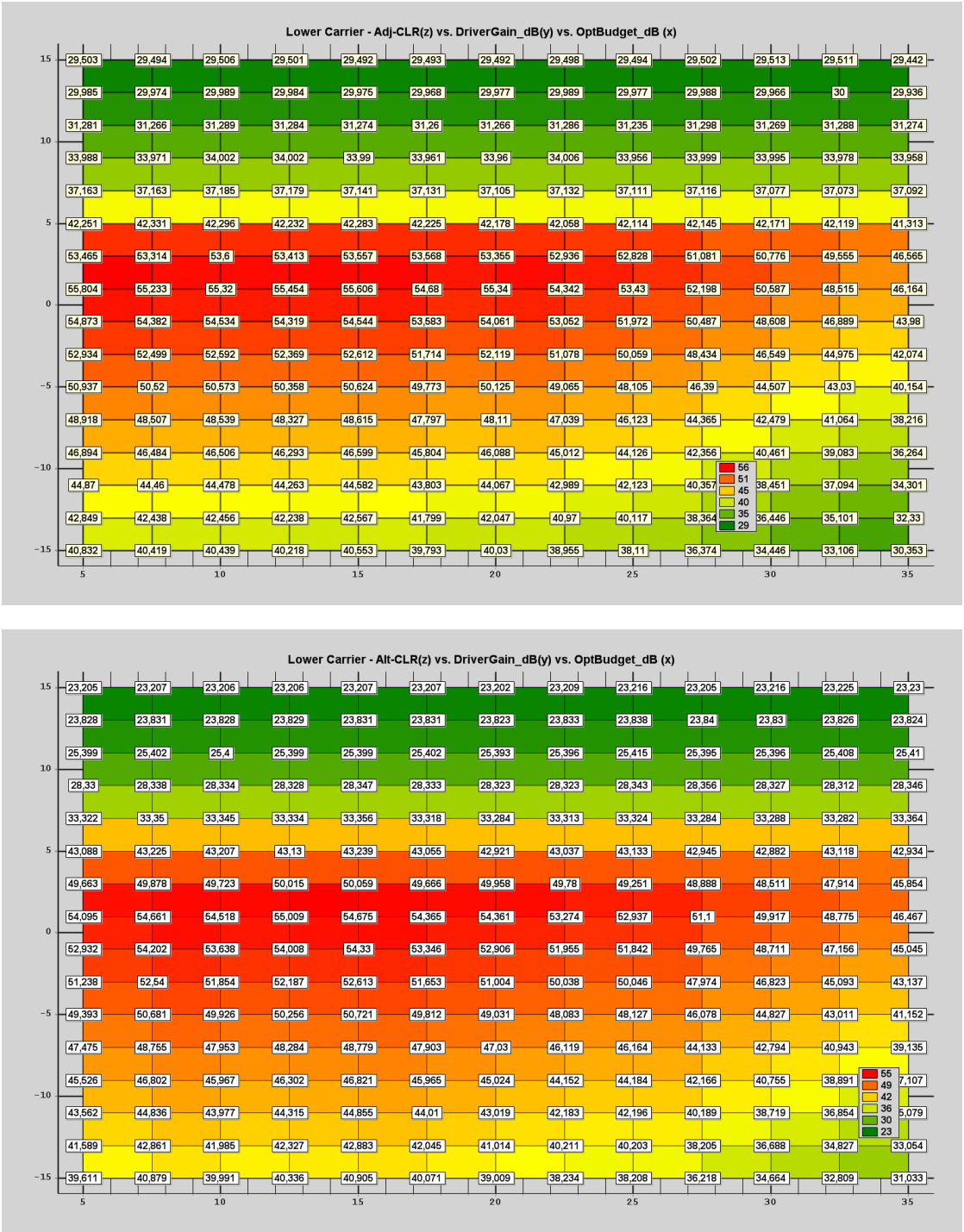

Figure 9.15.: Dual carrier (lower frequency) ACLR performances over link containing 12.5km of DCF, a booster, 20km of fiber, optically pre-amplified, 95mA biased laser (chirp factor of 5), and a simple PIN, (top) ADJ-CLR, (bottom) ALT-CLR, 11.6dB crest factor

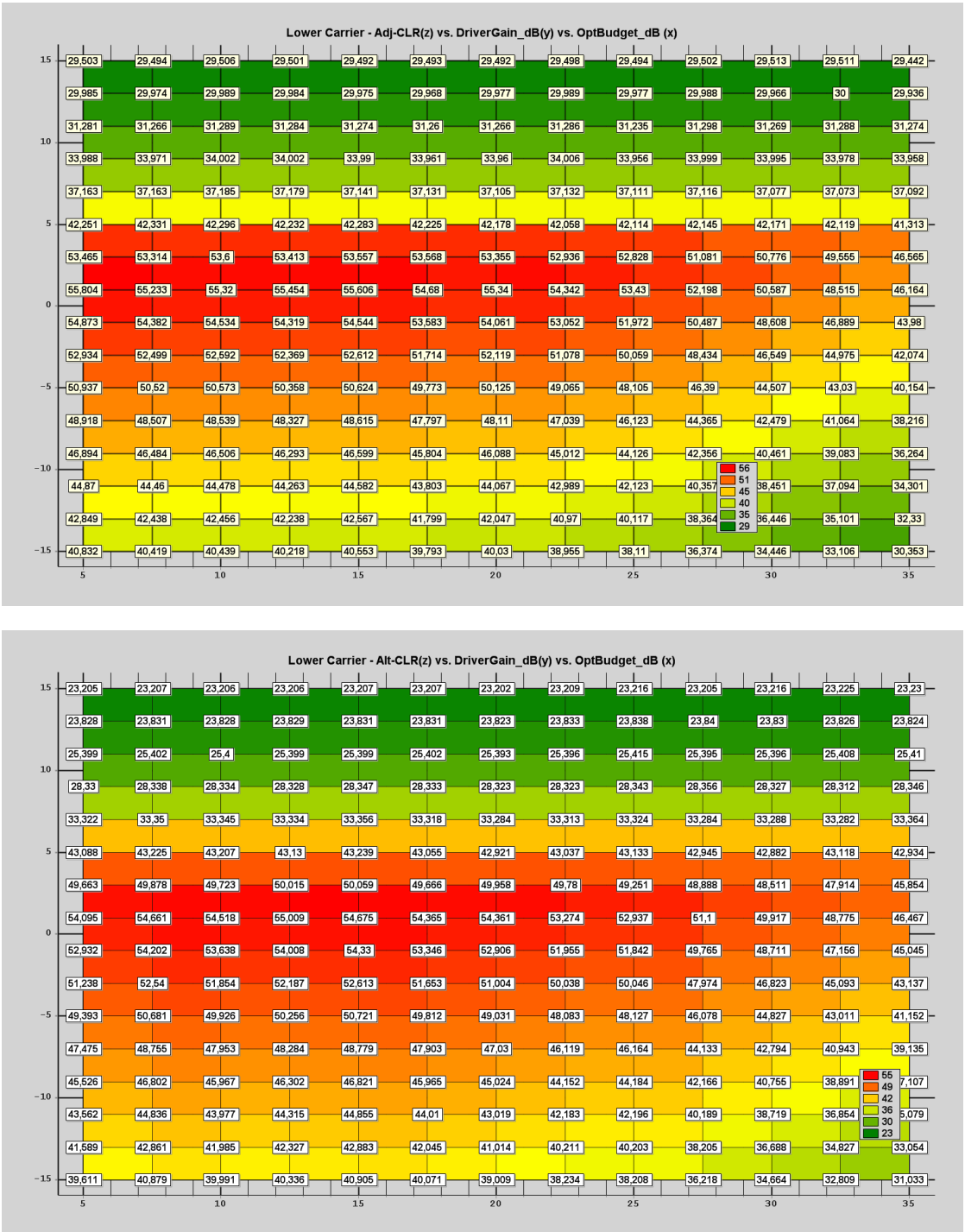

Figure 9.16.: Dual carrier ACLR performances over link containing 12.5km of DCF, a booster, 20km of fiber, optically pre-amplified, 95mA biased laser (chirp factor of 3.5), and a simple PIN, (top) ADJ-CLR, (bottom) ALT-CLR, 11.6dB crest factor

Conclusion

This part has shown successively the issues —from a theoretical perspective— when dealing with analog radio carrier transmissions (at their native carrier frequencies) over typical PON budgets.

Therefore in a first time the RIN, shot and thermal noises were introduced; also the benefit of the optical pre-amplification and its related noise impairments were shown in a formal way. Each time a particular stress has been put on the maximum achievable optical budget for a given SNR —compatible with typical radio specifications.

In a second step we introduced the impairments (third order like inter-modulations) due to the combination of the chirp factor of the laser diode and the chromatic dispersion of the optical fiber; and demonstrated this on a simple two tone signal. Also the benefit of DCF was introduced in order to overcome or at least limit the afore mentioned third order like inter-modulations.

In a last simulation step, we have simulated more realistic UMTS signals for which we could demonstrate the impairments due the combined chirp and chromatic dispersion, and the interest of optical amplification and of DCF. These simulations re-use the results of the two-tone-simulations in order to make a PON architecture containing 20km of fiber capable of supporting the transmissions of two UMTS carriers —while being compliant with the radio standards.

Finally, this leads us to the practical results of Part 4 —where in a first time the focus is set on the EVM figure, and in a second time the SNR issue is stressed.

Part IV.

Experimental results

Introduction

The motivation for re-using the optical infrastructure of the access networks (typically being Passive Optical Networks (PONs)) in order to distribute radio signals has been exposed in §4 of Part 2; while the techniques for distributing radio carriers through optical networks have been developed in §5 and 6 of Part 3.

This fourth part finally deals with the experimental results obtained during the thesis when transmitting analog Universal Mobile Telecommunications System (UMTS) carriers —at their native broadcast frequencies— through typical PON infrastructures. Therefore we briefly recall the used optical access network architectures.

The first reference optical architecture is the one corresponding to the *B+ Class* of the Gigabit-capable PON (G-PON) specifications: between the Optical Line Termination (OLT) and the Optical Network Unit (ONU) the maximum optical power budget values 28dB. These 28dB can include the losses of up to 20km of optical fiber.

In order to operate Radio over Fiber (RoF) in the 1550nm window, in parallel to the existing PON systems, a Wave Division Multiplexing (WDM) scheme is adopted. Of course the WDM functionalities will require our proposed RoF system to be able to cope with optical budgets larger than the initial 28dB in order to account for the additional insertion losses of the multiplexers or circulators.

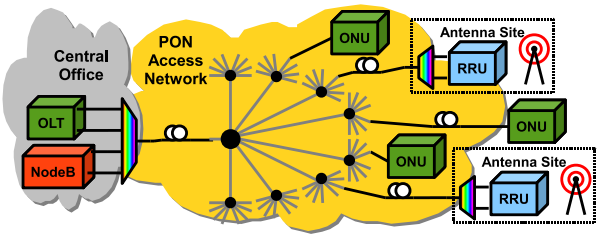

(a) First reference architecture

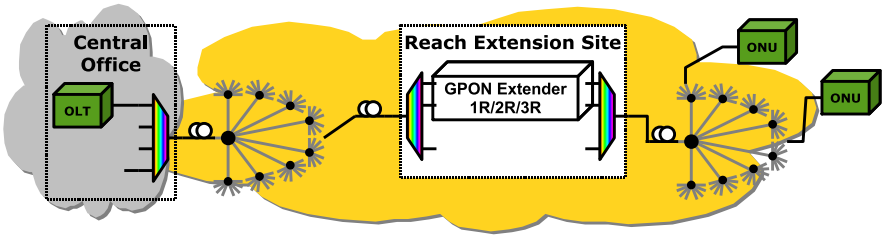

(b) Second reference architecture

The second reference architecture corresponds to an Extended-Reach PON (ER-PON) where between the previous PON and the Central Office (CO) a *reach extension* site an additional optical link is inserted. Given that often the *GPON extenders* (intended at the digital signals) are made of optical-electronic-optical repeaters, the digital and analog carrying wavelengths have to be processed independently one another. The (de)multiplexers located at the in- and outputs of the reach extension site serve this purpose.

10. Architectures using an APD receiver

Choice of an APD

In a first time, we envisage to use an Avalanche Photo-Detector (APD) receiver (§2.3.6, p. 31) in order to benefit from their *high* sensitiveness, which is the reason their are appreciated for in high-speed digital applications.

Indeed the APD receiver used in the following experiments, according to the manufacturer, requires *only* -28dBm of received optical power in order to yield a Bit Error Rate (BER) of 10^{-9} for digital 10Gbit/s Non Return to Zero (NRZ) applications. Hence this receiver seems to be *attractive* for RoF applications.

We evaluate and assess this APD receiver for radio carrier applications mainly under the scope of the Error Vector Magnitude (EVM) figure of merit (§3.3.1, p. 59), more specifically according to the *Composite EVM* of the UMTS standards.

10.1. Simple architectures

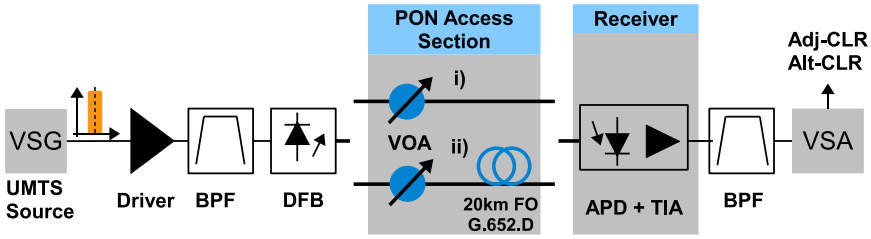

Figure 10.1.: Experimental set-up using an APD receiver

The optical source is a Distributed Feed Back (DFB) laser having a current threshold of 15mA, and is designed for digital applications at 10Gbit/s (NRZ). For the following experiments it is biased at 95mA, and given the efficiency of 0.0719W/A, the optical launch power values ≈+7.6dBm —corresponding to the Laser Diode (LD) parameters used in the previous chapter for the *VPItransmissionMaker* simulations. Furthermore the DFB laser is directly modulated by the UMTS carrier(s).

10.1.1. Single UMTS carrier with pure losses

In a first time, in order to assess the interest of the APD receiver, a single UMTS carrier centered at 2140MHz is transmitted over a fiber-free link (inset i) in Fig. 10.1). The optical insertion losses are emulated thanks to a Variable Optical Attenuator (VOA) and set to yield successively attenuations of 28, 30, and 32dB. We recall these values to correspond to

the typical maximum optical budgets of the different PON Classes (§2.2, p.27). Additional measurements for an optical attenuation of 42dB are also performed[1].

NB: For an electrical back-to-back transmission the minimum reached Composite EVM values 7.8% and is due to an IQ imbalance of the DAC-board of the Vector Signal Analyzer (VSA).

Measured results

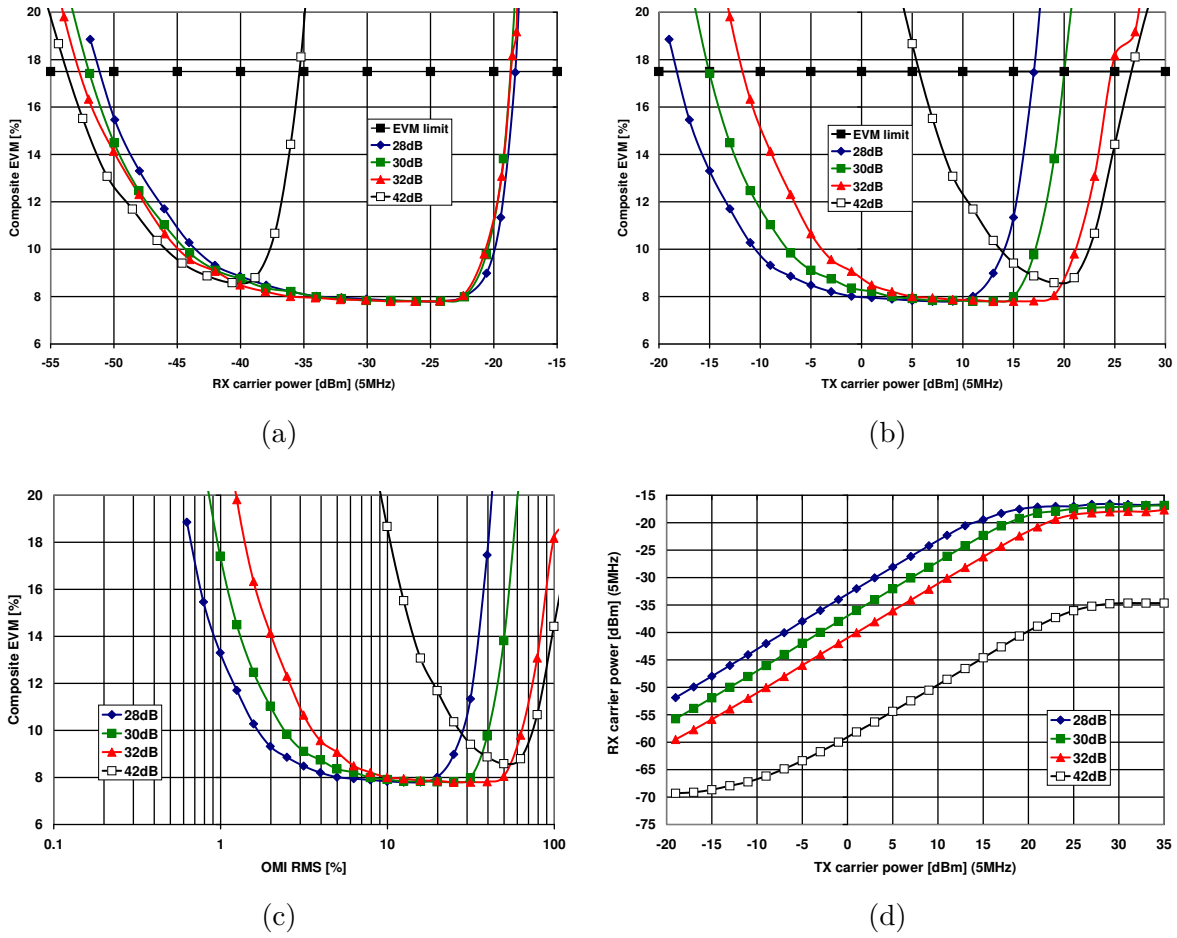

Figure 10.2.: Measurements for an APD receiver and a fiber-free link

When fixing a threshold for the maximum Composite EVM of 17.5% (3GPP specified value), then from a RF input power perspective —for the optical budgets of 28, 30, and 32dB— the Composite EVM is lower than the set threshold for an input dynamic range as wide as 35dB. Except for the 42dB optical budget this RF input power range falls to 21dB.

From a received RF power perspective (Fig. 10.2a), the Composite EVM appears to be limited by noise for the lower values of the received RF powers between -55 and -40dBm.

[1] just for curiosity's sake!

The RF power upper value for which the Composite EVM crosses the threshold values -18dBm, and furthermore common for the 28, 30, and 32dB optical budgets.

This common value of -18dBm (Fig. 10.2d) can be explained by either a saturating avalanche process of the APD, or a limited output power swing of the Trans Impedance Amplifier (TIA), or an overdriven LD.

Conclusion

For fiber-free links with optical budgets of 28, 30, and 32dB the APD allows to recover the UMTS carrier with EVM figures compliant with the 3GPP standard, and this for a input RF power range of 35dB.

10.1.2. Single UMTS carrier with 20km of S-SMF

Given the *acceptable* EVM performances for a fiber-free link, 20km of S-SMF are inserted in the link (inset ii) in Fig. 10.1), and its loss is included in the optical budgets.

Measured results

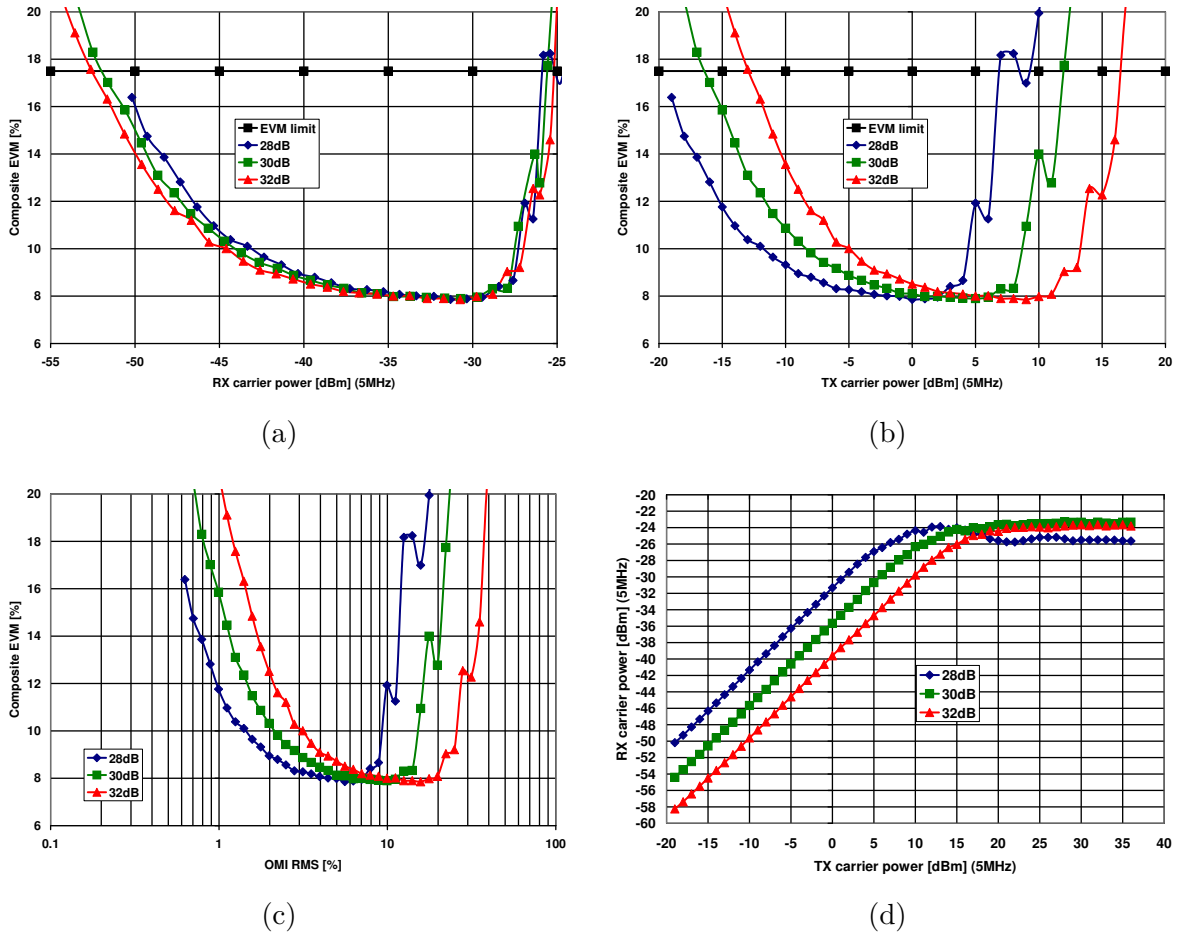

Figure 10.3.: Measurements for an APD receiver after 20km S-SMF containing link

For a maximum Composite EVM of 17.5% (3GPP specified value), then from a RF input power perspective (Fig. 10.3d) —for the optical budgets of 28, 30, and 32dB— the Composite EVM is lower than the set threshold for an input dynamic range of at least 25dB —10dB less than for the fiber-free case.

From a received RF power perspective (Fig. 10.3a), the Composite EVM appears to be limited by noise for the lower values of the received RF powers between -55 and -40dBm. The RF power upper value for which the Composite EVM crosses the threshold values now -26dBm (8dB less than the previous fiber free case), and is again common for the 28, 30, and 32dB optical budgets.

Comparing Fig. 10.2 and 10.3, it is clear that the reduced input dynamic range is strictly

due to the reduction of the maximum input power, corresponding to the inserted non-linear distortions of the optical fiber.

Conclusion

Again the APD allows to recover the UMTS carrier for optical budgets of 28, 30, and 32dB yielding EVM figures compliant with the 3GPP standard, albeit the RF input range values 25dB (transmitted as well as received) and is 10dB lower than the fiber free case, because of the added non-linear distortion of the optical fiber.

10.2. In-line SOA amplification

The two previous sections have assessed the interest of using an APD for transmitting a UMTS carrier over typical PON architectures.

In order to cope with the ER-PON architectures presented in §2.2, we propose to use a Semiconductor Optical Amplifier (SOA) to serve as a Reach-Extender (R-E) for the RoF signals (Fig.10.4), introduced prior to the optical fiber in Fig. 10.1.

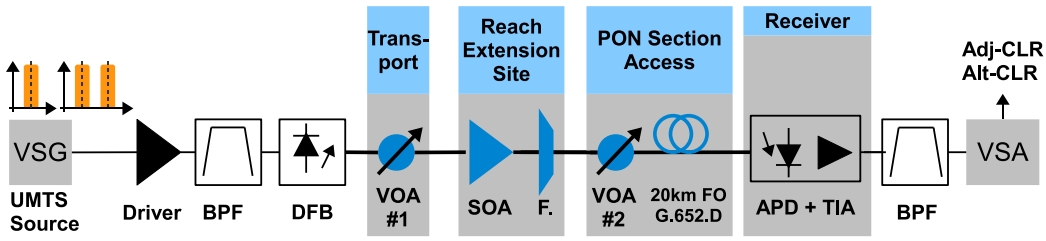

Figure 10.4.: Experimental set-up using an in-line SOA and an APD receiver

Therefore the ER-PON architecture is emulated (Fig. 10.4) by a *Transport Section* composed of pure losses (ranging from 17 to 21dB), a R-E-site composed of the SOA and a Coarse Wave Division Multiplexing (CWDM) filter (F. in Fig. 10.4) , and finally by an *Access Section* composed of losses and 20km of S-SMF, and ranging from 28 to 30dB.

10.2.1. Single UMTS carrier with 20km of S-SMF

Measured results

Fig. 10.5a shows the minimum received RF carrier power for which the EVM threshold of 17.5% is crossed, to value -53dBm, and not to depend upon the optical budgets of the *Transport* and *Access* sections, and is the same as for the later configurations.

Yet Fig. 10.5a also shows the maximum received RF carrier power for which the EVM threshold of 17.5% is crossed to depend upon the combined optical budgets of the *Transport* and *Access* sections.

Indeed for the highest *Transport* and *Access* budgets (21 and 30dB respectively) the maximum RF power values -29dBm, while for the lowest optical budget couples (19 and 28dB respectively) the maximum RF power values -24dBm. Yet these values are still close to the previous cases.

For equivalent over optical losses of 49dB, it is the combination with the lowest *Transport section* budget which yields the highest maximum RF power (-25.5dBm) for the given EVM threshold. These differentiations are confirmed in Fig. 10.5d.

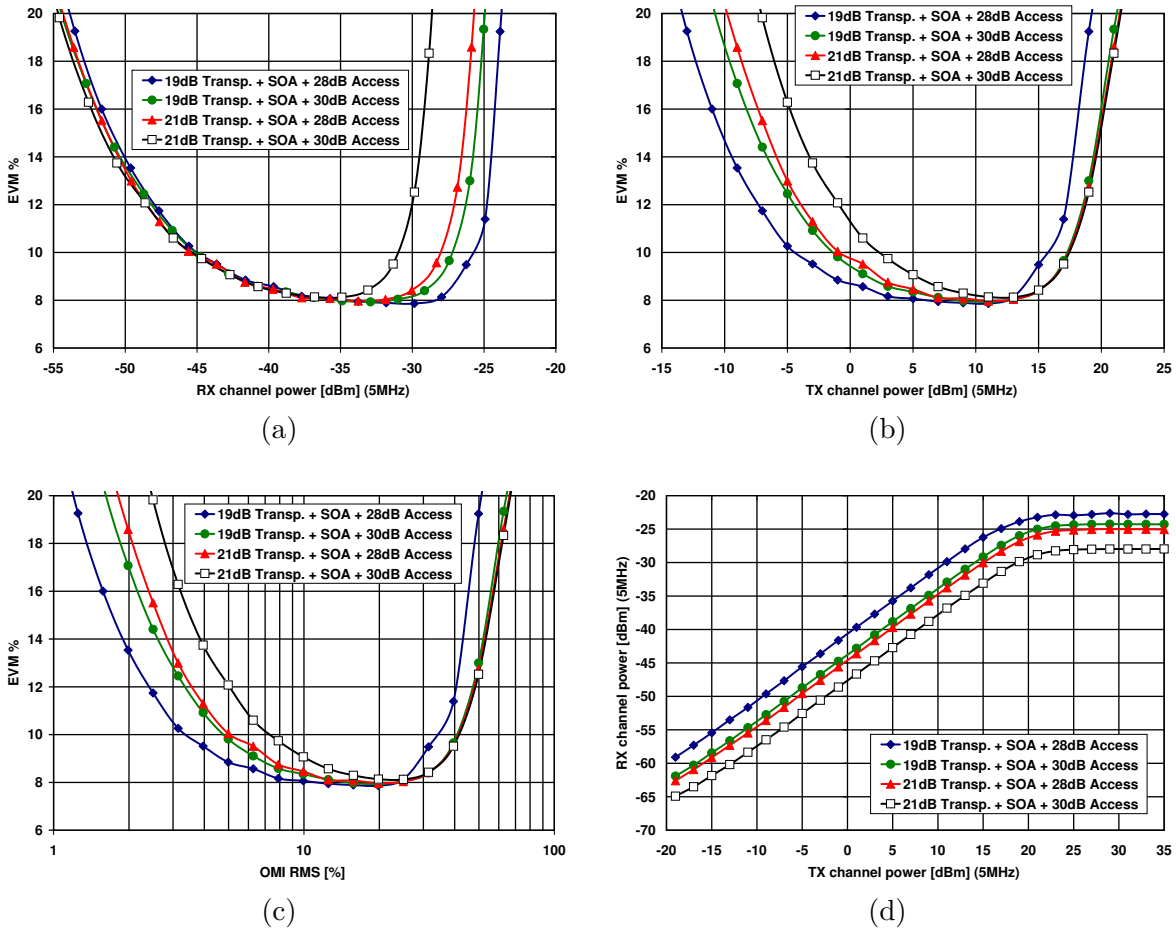

Figure 10.5.: Measurements for an APD receiver after 20km S-SMF containing link and an in-line SOA

Fig. 10.5b (and 10.5c) show that from an RF input power perspective (and OMI point of view), the combination of the highest *Transport* and *Access* budgets (21 and 30dB respectively) requires the highest minimum RF input power (-5.5dBm) for yielding 3GPP compliant EVM performances, while the combinations of the lowest *Transport* and *Access* budgets requires a minimum RF input power of only -11dBm. The other combinations of *Transport* and *Access* budgets require minimum RF input powers ranging in between the previous ones. The RF input power is nearly 5dB higher than in the case of Fig. 10.2.

Fig. 10.5b shows the maximum RF input power, for yielding 3GPP compliant EVM results, to be *almost* common: for RF input powers beyond +15.5dBm the EVM curves leave the *plateau*[2] and increase sharply.

This inflexion points corresponds to an over-modulation of the LD: since the sine peak

[2]which we recall to correspond to the electrical back-to-back measurement

RF over-driving power values +25dBm ($10\log((95mA - 15mA)^2 \cdot 50\Omega \cdot 10^3) = +25dBm$), by subtracting the crest factor of the UMTS carrier of 9 to 10dB, than a correspondence ranging between +15 and +16dBm can be found. The input power range value corresponds to the one measured in the case Fig. 10.2.

Conclusion

These measurements have demonstrated the possibility of using a SOA for realizing the reach extension of UMTS carrier distribution through PON architectures with an additional *Transport Section*. The overall optical budgets range from 47 to 51dB.

Here the benefit of the in-line SOA acting as an optical repeater is to make RoF to become able to take advantage of the reach-extension concept initially developed for cascading several PONs. Indeed if RoF is to be used in RE-PONs, it is suitable that it can be adapted to the latter.

10.2.2. Dual UMTS carrier with 20km of S-SMF

Given the previous sections' results, the transmission of two UMTS carriers is envisaged.

Therefore a second UMTS carrier equal power is emulated by a second Vector Signal Generator (VSG) which outputs a 3.84Mchips/s signal which is pulse-shaped by a Root-Raised Cosine (RRC) filter with a roll-off factor of 0.22, at frequency offsets of 5, 10, or 15MHz. This signal is not a UMTS signal compliant to *TestModel 4* of [59], yet it plays the role of a *dummy* carrier. Thus only the Composite EVM of the compliant signal is measured.

For different couples of optical budgets of the *Transport Section* (19 and 21dB) and of the *Access Section* (28 and 30dB) the EVM of the carrier of interest, in presence of the *dummy* carrier, is measured. The place-holding carrier is successively spaced by 5, 10, and 15MHz.

Measured results

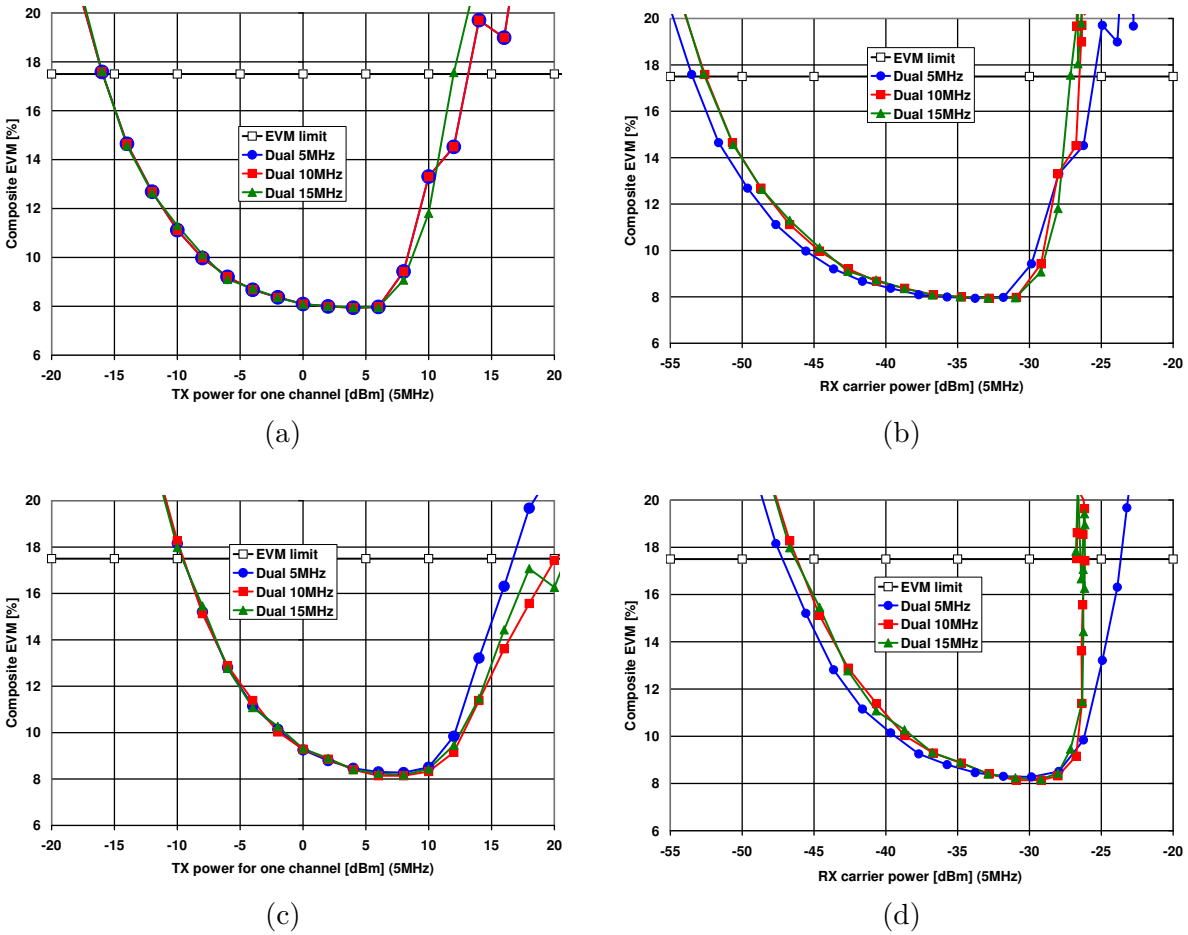

Figure 10.6.: EVM performances for a dual carrier transmission over an ER-PON architecture:
(a)-(b): 19dB Transport budget + 28dB Access budget (best case);
(c)-(d): 21dB Transport budget + 30dB Access budget (worst case)

The reported measurements concern the overall optical budgets of 47 and 51dB. Fig. 10.6 shows the corresponding EVM curves against the transmitted and received carrier power.

From the minimum required RF input power for yielding compliant EVM figures, the 47dB overall optical budget variant requires -16dBm per carrier while the 51dB variant requires 6dB more: -10dBm per carrier.

As a consequence of this the minimum required received RF power for yielding compliant EVM figures is 6dB lower for the 47dB overall optical budget variant than for the 51dB variant. Thus the RF dynamic for which the EVM is compliant with the specifications is 6dB wider for the 47dB overall optical budget variant than for the 51dB variant, since Fig. 10.6b and 10.6d show that maximum received RF power yielding compliant EVM results is common to both optical budgets variants (except for the 5MHz spacing).

Conclusion

These performances were obtained for a single propagating wavelength carrying two UMTS carriers centered at 2140MHz, and demonstrate their possible distribution over ER-PON architectures. Furthermore whether the place-holding carrier was spaced by 5, 10, or 15MHz, the results remain unchanged.

Finally similar performances are obtained when transmitting two UMTS carriers centered at 1940MHz in the uplink direction and when the positions of the *Transport* and *Access Sections* are swapped.

10.3. In-line direction shared SOA amplification

The goal is to achieve the architecture shown in Fig. 10.7 and which is intended at distributing and collecting simultaneously three UMTS Band I RF carrier over an ER-PON architecture by exploiting bi-directional amplification property of the SOA.

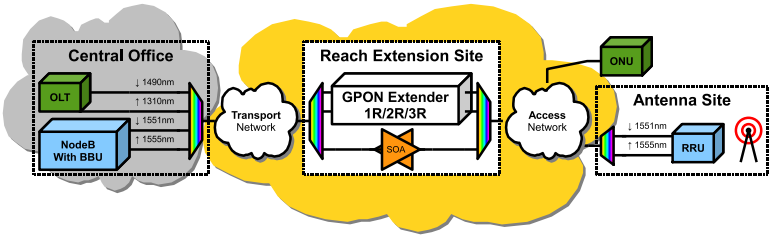

Figure 10.7.: Extended-Reach PON using a direction-shared SOA for bidirectional amplification

Thus this could allow to share the SOA between the counter-propagating up- and downlink wavelengths, as shown in Fig. 10.8, where each wavelength carries a multiplex of three UMTS carriers.

10.3.1. Set-up

To achieve this architecture the set-up in Fig. 10.8 is proposed.

The reach extension is realized by an in-line SOA which is shared between the counter-propagating wavelengths, each wavelength carrying a radio multiplex of three UMTS carriers.

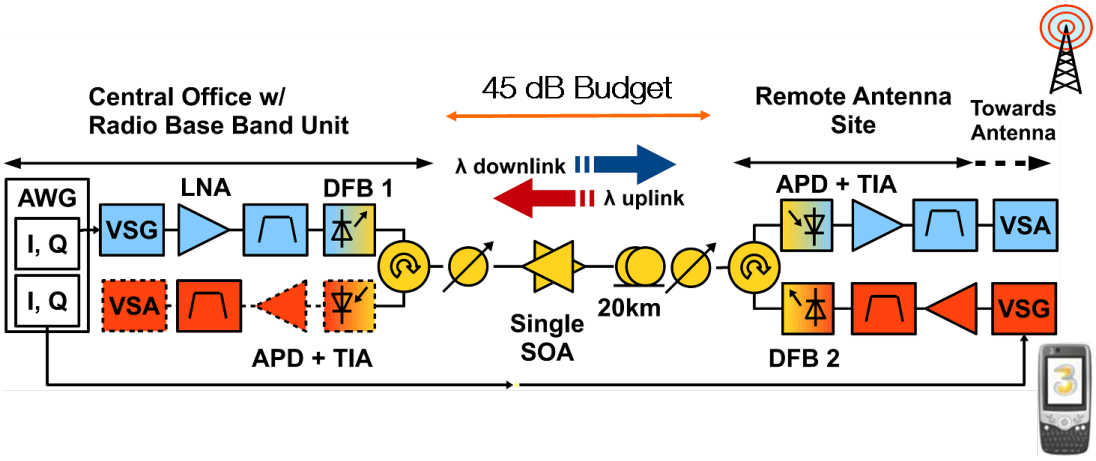

Figure 10.8.: Set-up using a a direction shared SOA and an APD receiver

Radio set-up

The radio set-up is made-of UMTS carriers compliant to the *Test Model 4* of [59] which is a Wide-Band Code Division Multiple Access (W-CDMA) signal with a chip rate of 3.84Mchip/s, and specified by 3GPP for EVM measurement purposes.

The above mentioned UMTS baseband signal is off-line processed on a computer using Matlab in order to be generated on a dual output Arbitrary Waveform Generator (AWG). Each output of the AWG represent the I and Q components of the signal composed of a multiplex of three 10 MHz spaced UMTS carriers. After frequency up-conversion using a VSG (#1 and #2) the three carriers are centered around 1940 MHz for the uplink (UL) and 2140 MHz for the downlink (DL).

The generation of a three UMTS carrier multiplex, required for realizing the set-up of Fig. 10.8, with the help of an AWG is described in Appendix A, p.211.

Finally a Low Noise Amplifier (LNA) is used as a Laser Driver and is followed by a UMTS Band I Diplexer (DL and UL BPF on Fig. 10.8) to filter out residual mixing products.

All three generated carriers are always maintained with the same RF power. For the experiment, each UMTS RF signal power can be swept from -40 to +15dBm per carrier. Performance evaluation is done by a VSA through measurement of the EVM.

Optical set-up

As seen in §10.2, the optical path of an ER-PON can be divided into a *Transport Section* (starting at the CO) and an *Access Section* (finishing at the Remote Antenna Site), the *Reach Extension Site* —made of a single SOA— lying in between.

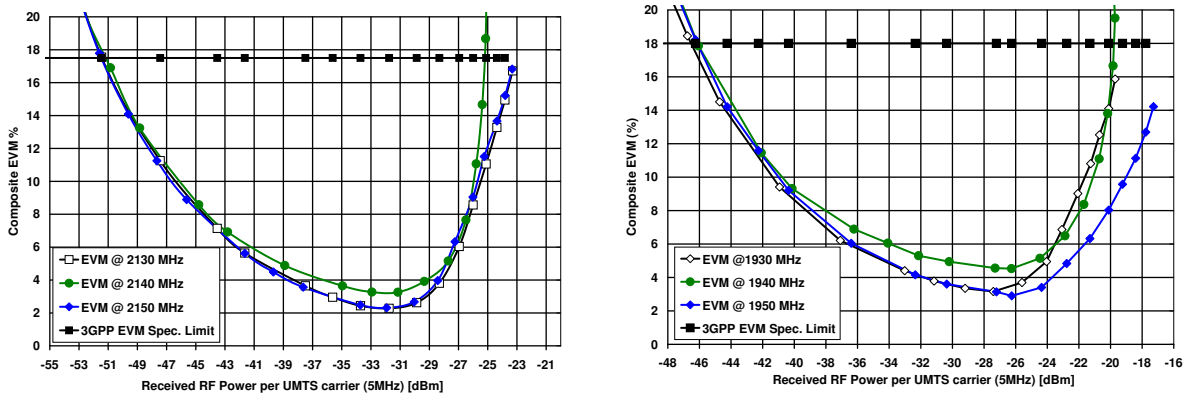

(a) (b)

Figure 10.9.: EVM performances, (a) downlink, (b) uplink, for the architecture with a bidirectional SOA and APD

The *Transport Section* is here represented by pure optical attenuation corresponding to a 17dB budget, whereas the *Access Section* is composed by 20km of optical fiber and optical attenuation representing a typical PON *Class B+* budget of 28dB.

At both transmission sites cooled DFB lasers emit each +9dBm of optical power at 1551nm (downlink) and 1546nm (uplink). The different wavelengths are separated by optical circulators each having an insertion loss of 0.8dB and which are not included when calculting the *useful* PON budgets. The SOA has a gain of 14dB.

For practical purposes the APD and the VSA (shown dotted on Fig. 10.8) are permuted for realizing the up- and downlink measurements, however the optical signals remain unchanged, thus simultaneity and co-existence of the counter propagating wavelengths are guaranteed.

10.3.2. EVM performances

In the downlink

Fig. 10.9a shows that an EVM power margin (calculated as the difference between the maximum and minimum RF power to achieve the UMTS EVM limit value of 17.5%) of 25dB can be achieved. However this limit of 17.5% is specified to be the maximum EVM to be received at the end of the air link, in other words at the mobile device (see Fig. 3.18, p. 59). Thus in our case considering an EVM target of 8% at the output of the RoF-system is more realistic since the RF signals still have to propagate through the air link. In this case we still have a power margin of 18dB.

In the uplink

An EVM power margin —for a limit at 17.5%— of 26dB can be observed on Fig. 10.9b. In this case we do not consider the 8% threshold as we measure the signal after is would have propagated in the air.

Conclusion

From an EVM point of view, it has been shown that a multiplex of three UMTS RF FDD carriers per wavelength direction can be transported transparently and simultaneously over an Extended Reach PON architecture with an optical budget of 47 dB relying on the use of an SOA for reach-extension and an APD for photo-detection.

10.3.3. ACLR performances

Scope

In a first time, in this work [116] only the EVM, as in many publications [86,115,117–119], has been considered.

Despite the *very good* performances in terms of EVM, and this even for three UMTS carriers, yielded by the architecture composed of a bidirectional SOA and an APD receiver, a supplementary Figure Of Merit (FOM) needs to be considered: the Adjacent/Alternate Channel power Leakage Ratio (ACLR). The importance of ACLR, especially in the downlink path, is recalled in § 3.3.2, p.64.

Yet only few author such as [120–122] also consider the ACLR issue. Thus the measurements for this architecture using a direction shared bidirectional SOA and APD have been performed.

Measurements

Fig. 10.10 shows the downlink ACLR performances of the proposed architecture.

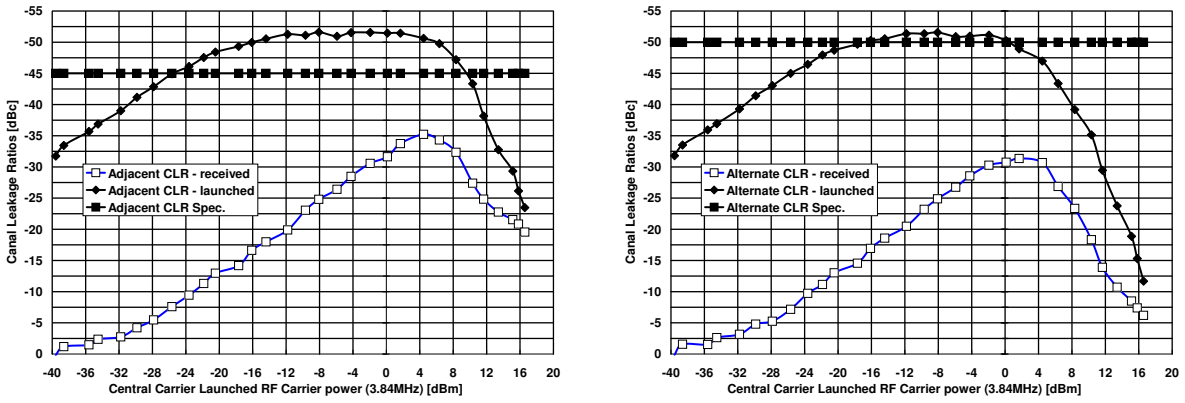

(a) (b)

Figure 10.10.: ACLR performances, (a) Adjacent, (b) Alternate, for the architecture with a bidirectional SOA and an APD

When considering the downlink[3] Adj-CLR performances, Fig. 10.10a shows this set-up to yield values 10dB below the recommendations. Furthermore the Alt-CLR performances,

[3]uplink is not considered since then the ACLR specifications are not mandatory

Fig. 10.10b shows this architecture to have its best performances being by 13dB beyond the downlink specifications.

Fig. 10.10b also shows the ACLR performances of the input source itself to be limited. Indeed the Adj-CLR performances of the source hardly values less than -50dBc. Thus this is an additional factor that has to be taken into account before charging the APD to have *poor* ACLR performances.

Conclusions

Despite a sufficient Signal to Noise Ratio (SNR) for allowing acceptable EVM performances (which is in accordance with §3.3.1, p.61), the SNR measurements are not compliant with the ACLR downlink specifications regulating the radio broadcast of UMTS FDD RF carriers. Thus this set-up cannot be used as it is for transporting downlink UMTS FDD RF carriers.

Albeit these *poor* ACLR results, the proposed architecture has demonstrated the benefit of an APD receiver for detecting radio carriers over typical PON budgets, and has also shown an in-line SOA to be of interest for applications in an ER-PON. Finally this architecture can serve uplink purposes (from the antenna site towards the CO)... where fulfilling the ACLR specifications is not mandatory.

Acknowledging this architecture to be too complex to pin point the element(s) making not possible to meet the ACLR specifications, the next section addresses it.

11. Receiver selection

Scope

The goal of this selection step is to test several receiver architectures about their capability of yielding 3GPP UMTS Frequency Division Duplexing (FDD) downlink compliant ACLR performances. Therefore a simple set-up with a fiber-free link is used (Fig. 11.1).

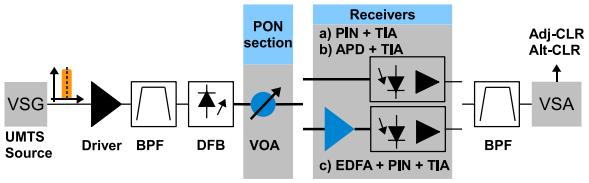

Figure 11.1.: Set-up used for receiver selection

Even if the APD has proven to have yielded limited ACLR performances in the previous section, it is still interesting to test it for comparison. Therefore its ACLR performances will be assessed in a simpler configuration.

Also a *simple* PIN receiver with a 8GHz bandwidth and designed for digital NRZ 10Gbit/s applications will be tested. The last receiver is a combination of an optical amplifier (Erbium Doped Fiber Amplifier (EDFA)) used as a pre-amplifier put in front of the afore mentioned PIN receiver.

11.1. Measurements

For these three receiver architectures (Fig. 11.1) the ACLR performances are measured while the input power of the modulating UMTS carrier is swept (from -40 to +15dBm).

The operation is repeated for optical budgets (the difference of the optical powers at the output of the DFB and at the entrance of the receiver) ranging from 6 to 36dB. Here we no longer focus on Extended-Reach architectures but come back to typical PON budgets of 28 to 32dB maximum.

In Fig. 11.2 the measured Adj- and Alt-CLR figures are plotted against the optical budget. The reported Adj- and Alt-CLR figures are optimized individually with respect to the OMI. The bias current is set to 95mA which is situated in the upper linear part of the current to light conversion curve of the laser.

11.1.1. Receiver type comparisons

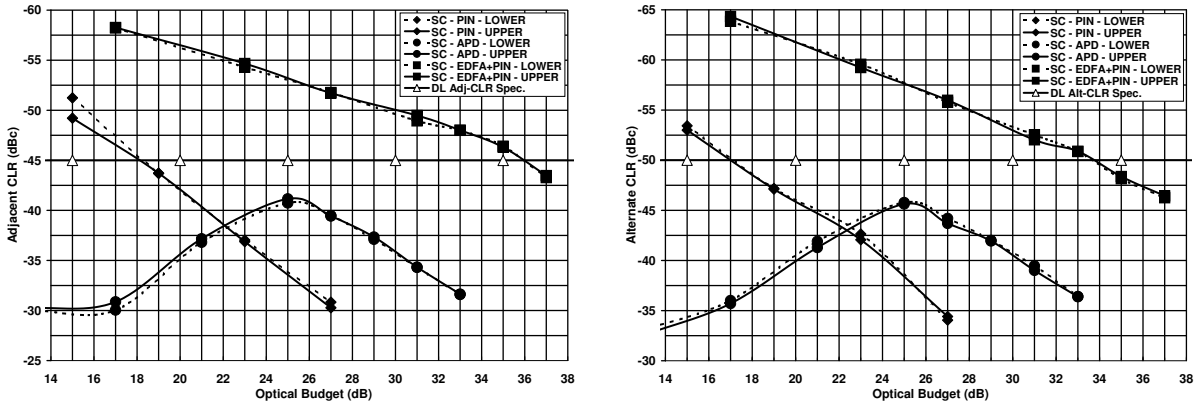

(a) (b)

Figure 11.2.: ACLR performances of different optical receiver architectures

The measurements results are sorted *progressively* per receiver type, and are as follows:

a) The ACLR results for the simple PIN receiver yield 3GPP-compliant figures for optical budgets up to 17dB. Yet the latter is not sufficient compared to the maximum optical budgets of PONs. For different bias currents of the DFB, the maximum optical budget could not be improved for this receiver. Therefore this receiver is discarded.

b) The ACLR performances exhibited by the used APD receiver, which is a standard component designed for digital 10Gbit/s applications, are not compliant with the specifications at any optical budget. The used APD —when yielding its best possible ACLR values— has a noise floor of –65dBm/3.84MHz while the PIN-based receiver has a noise floor of –84dBm/3.84MHz. The best possible overall ACLR figures are obtained at an optical budget of 25dB. However, at this budget, Adj-CLR and Alt-CLR values are respectively 3dB and 5dB below the specifications. Therefore the APD receiver is **definitively** discarded.

c) The used EDFA has a 4dB optical noise figure, and is set to yield 35dB of constant optical gain. In order not to saturate the PIN receiver, 10dB of pure losses (not shown in the set-up of Fig. 11.1) were introduced between the EDFA and the photo-detector in order to to saturate the latter. Finally the receiver made of an EDFA pre-amplifier followed by a simple PIN clearly shows ACLR performances compliant with the specifications and this for optical budgets a priori up to 34dB. Thus this receiver is compatible with the maximum optical budgets of PONs.

In the following, we use this last receiver.

11.1.2. Reverse bias voltage dependency of the APD's ACLR performances

These results were achieved using the same InGaAs APD, from Northlight, designed for 10Gbit/s applications and having an in-built TIA. The range of the reverse bias voltage specified by the data-sheet is within 20 to 40V.

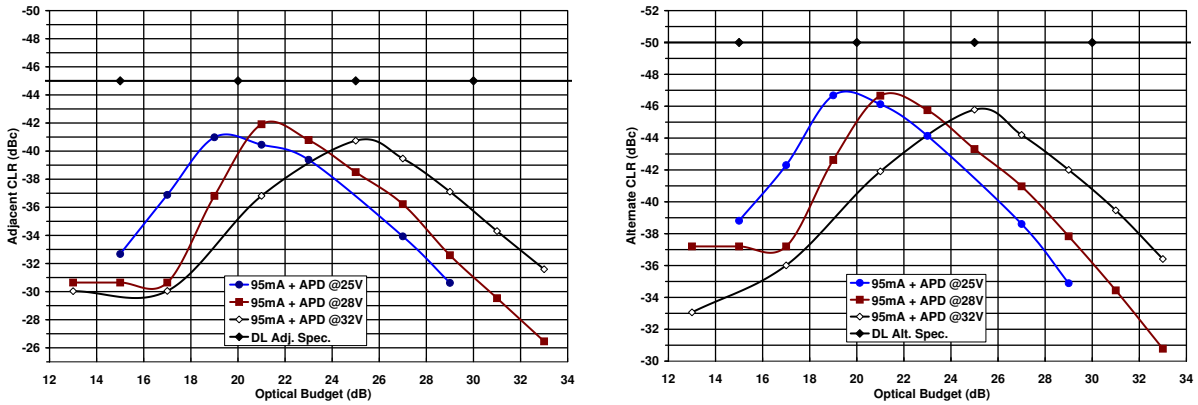

(a) (b)

Figure 11.3.: ACLR performances, (a) Adjacent, (b) Alternate, for different bias voltages of an APD

Fig. 11.3 show a best possible ACLR valuing -42dBc for the Adj-CLR and -47dBc for the Alt-CLR. A local maximum exists for any of the three used reverse bias voltages, and as stated in the Fig. 2.14 the increase of the reverse bias voltage causes an increase of the multiplication factor. Thus, in the here shown example, the optical budget for a constant SNR of 40dB for instance, in other words the sensitivity is improved.

Yet besides these local SNR maximums, there is an additional phenomenon: the SNRs yielded by the APD do not necessarily improve with a diminishing optical budget *i.e.* an increased illumination power. Indeed for the shown measurements, when the APD is reverse biased at 28V, than below an optical budget of 21dB, the SNR decreases and finally reaches a *plateau* at 30dB for optical budgets below 17dB.

The *optimum APD gain* effect and thus the local maximum SNR is exposed in §2.3.6, p. 32 and is due to the trade-off between the avalanche gain and excess noise.

Furthermore the degradation slope when the optical budget decreases can be also explained by this *optimum gain* effect detailed in Eq. 2.15, p. 32. This latter equation shows the APD's optimum gain factor to decrease with in an increasing optical input power —explaining the SNR behavior between 17 and 21dB of optical budget for the considered reverse bias voltage example. For optical budgets below 17dB, we can attribute the *plateau* to the saturation of the optical receiver.

11.2. Conclusion

This brief chapter aimed at justifying the choice of the new reference optical receiver (EDFA+PIN), while adding a focus on the APD receiver showing the latter not to be able to fit the targeted ACLR requirements.

12. Architectures relying on a EDFA+PIN receiver

Scope

The interest of an EDFA used as a pre-amplifier in front of a PIN has already been suggested in the previous section.

In order to further assess this receiver, the Adj- and Alt-CLR specifications will be targeted jointly. Also the realistic conditions are progressively emulated by integrating a second UMTS carrier at the transmitter, and 10km of S-SMF in the optical link.

Measurement methodology

For a given optical budget, the UMTS carrier's power direct-modulating the LD is swept. For each swept RF power, the ACLR figures at the output of RoF link are measured and 4 measurements values are stored: 2 data points for the Adjacent-CLR at + and - 5MHz, and 2 data points at + and - 10MHz offsets from the carrier.

As shown in Fig. 12.1 the constraints are twofold:

- for the 5MHz spaced measurements, the Adjacent-CLR has to yield less than -45dBc
- for the 10MHz spaced measurements, the Alternate-CLR has to yield less than -50dBc

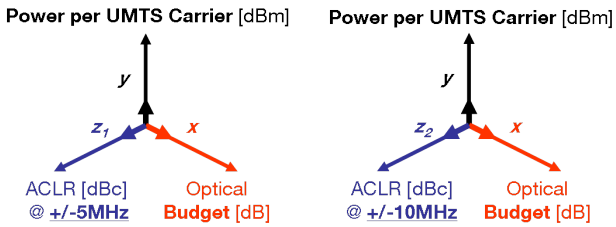

Figure 12.1.: Representation of the measurements constraints axes

Results presentation

The following plots show typical curves of the minimal (dashed lines in Fig. 12.2) and the maximal (continuous lines in Fig. 12.2) RF powers of the UMTS carrier (in dBm per 3.84MHz *i.e.* per UMTS channel width) that allow to meet the 3GPP ACLR requirements: Adjacent-CLR in Fig. 12.2a, and Alternate-CLR in Fig. 12.2b.

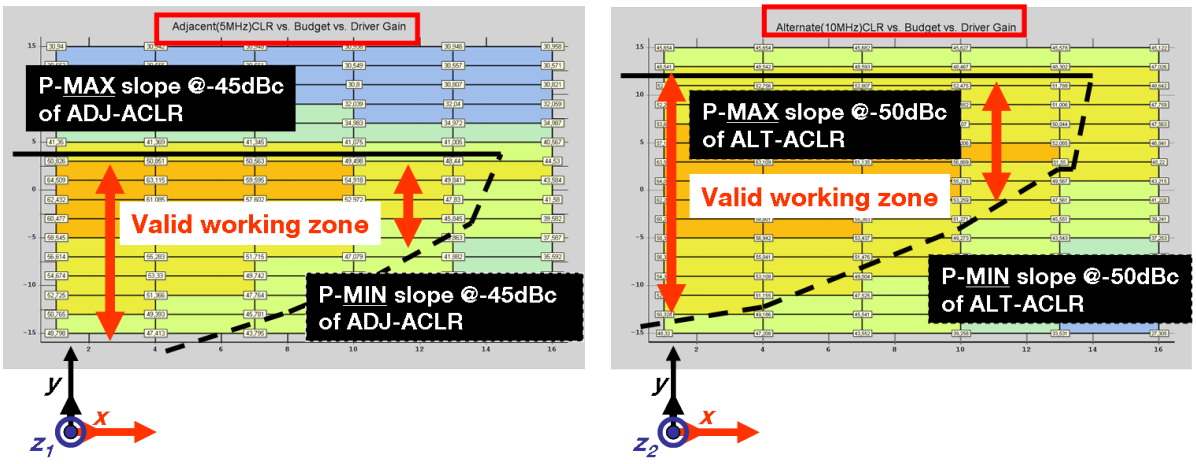

(a) (b)

Figure 12.2.: Cartography of the ACLR figures vs. the optical budget and vs. the RF carrier input power: (a) Adjacent-CLR, (b) Alternate-CLR

However handling two such plots *i.e.* two sets of curves is not handy. Thus for the sake of simplicity, for each measured optical budget point, the ranges of the UMTS carrier powers allowing to yield 3GPP compliant ACLR figures as well at 5 and 10 MHz offsets, are intersected.

Consequently, for each optical budget point, are plotted only the minimal and the maximal powers of the carrier, which are respectively the actual lower and upper bounds within which the 3GPP ACLR requirements are fulfilled.

Henceforth for the sake of ease of reading, the UMTS power[1] is expressed per carrier even if multiple carriers are used. Also the terms *maximum* and *minimum*, when used in a context describing the UMTS carrier input power at laser diode, and unless otherwise stated, refer to the maximum and minimum UMTS carrier input powers for which the 3GPP ACLR (Adjacent as well as Alternate) specifications are met jointly.

12.1. Single UMTS carrier

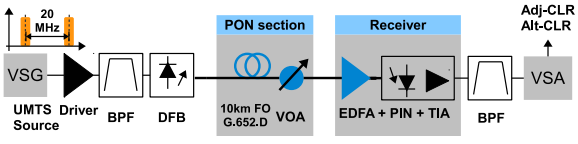

Figure 12.3.: Set-up using an EDFA pre-amplifier in front of the PIN

[1] **NB:** to obtain the effective RF power of the modulating radio signal, 21.5dB have to be added to the displayed RF power, simply because the measurements were done by controlling the RF input power from the VSG into the driver prior to the LD... Yet the presented results keep their general meaning.

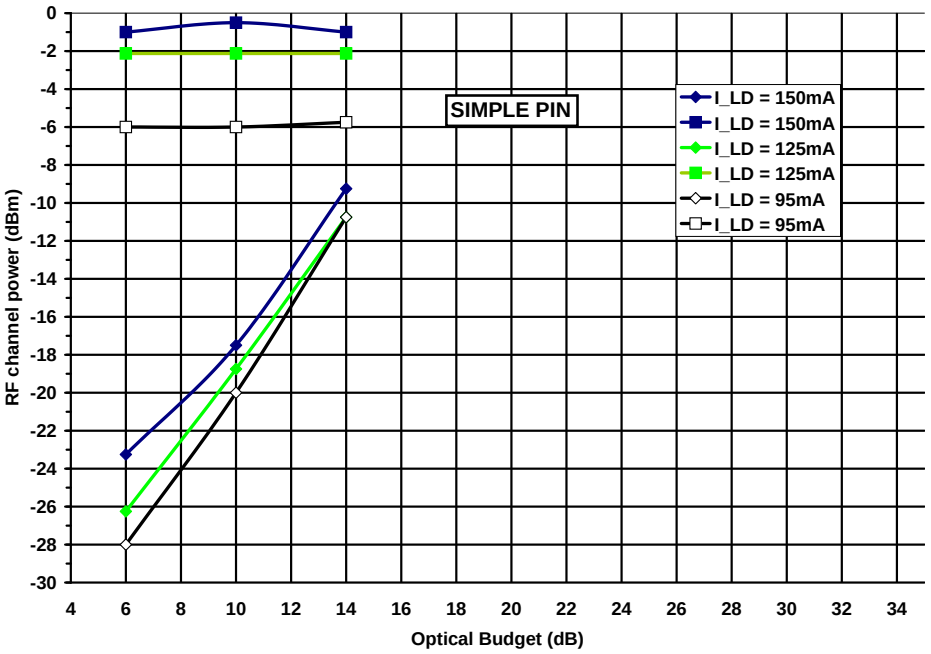

Figure 12.4.: Minimal and maximal RF powers for the ACLR requirements when transmitting a single UMTS carrier over a fiber-free link and using a simple PIN receiver

12.1.1. Fiber-free link

Fig. 12.4 recalls, for different bias currents of the LD, the slopes of the minimal and maximal RF powers of the single UMTS carrier transmitted over a fiber-free link and using a simple PIN receiver, in order to appreciate the improvements brought by the EDFA pre-amplifier.

Curves of the UMTS carrier's maximal power

For a given bias current of the laser, the maximal power of the UMTS carrier is limited by two effects:

- the clipping effect: when the UMTS signals operates in its negative alternate, its swing is limited by the current dynamic of the laser. in this case the signal is hard-clipped, which results in third order like distortions, thus lowering the figure of ACLR measured at +/-5MHz.
- the current-light dynamic of the laser: when the UMTS signals operates in its positive alternate, its swing is limited by the saturation of the optical output power vs. the current relationship.

Thus raising the bias current of the LD allows to decrease the hard-clipping, and to increase the maximal admissible RF power of the modulating UMTS carrier but at the expense of lower modulation efficiency and third order distortions.

These behavior can be explained by the expressions developed in Part 3. Indeed the maximal admissible RF power for avoiding clipping is constant.

Curves of the UMTS carrier's minimal power

The curves of the minimal RF powers show that an increasing of the bias current increases the minimal required RF power. Given the *small* optical budgets of this set-up, the RIN noises dominates, especially at the 6dB optical budget point, and the curves show a difference of 5dB between the minimal RF powers for the bias currents of 95mA and 150mA.

However at 14dB of optical budget, this difference is reduced to less than 1dB.

When approximating the minimum RF power curves with a linear function, then the slope for the 95mA and 125mA currents value respectively 1.9 and $2.2 dB_{el}/dB_{opt}$. These behaviors can be explained by the expressions developed in Part 3. Indeed for a thermal noise dominated link the required minimum RF power for a target SNR behaves as $-2 \cdot L_{dB}$ where L are the insertion losses.

Globally the minimal power curves have a steepness of 2.5dB (electrical) per 1dB (optical).

System point of view

Finally, from a system point of view, for an optical budget of 14dB, the bias currents of 125mA and 150mA yield the highest electrical system margin of 7dB.

12.1.2. Fiber-free link using an EDFA pre-amplifier

Given that the target optical budget of 28dB could not be met by the previous set-up, we propose to use pre-amplification in the optical domain to increase the optical power ingressing the PIN detector. The optical link remains fiber-free.

The added EDFA has a saturating output optical power of +18dBm and noise figure of 4dB (datasheet values). In this section the pre-amp EDFA is operated at constant optical output power of +18dBm, resulting in approx. 35dB of optical gain (equipment read value). Prior to detection a VOA is inserted between the pre-amp and the PIN detector, in order not to saturate the latter, and also to make the PIN work in its maximal efficiency regime.

Curves of the UMTS carrier's maximal power

The curves in Fig. 12.5 still show that an increased bias current allows to increase the maximal RF carrier input power.

Within the optical budget range from 12 to 28dB the maximal RF input power yielded by each bias current is constant. However when passing from 28 to 32dB of optical budget, the maximal RF input powers for the bias currents of 125 and 150mA decrease both by 1dB, whereas the one for the 95mA bias current remains constant.

Curves of the UMTS carrier's minimal power

Compared to the case of using a simple PIN receiver, using an EDFA pre-amplifier affects the steepness of the minimal input RF power. Indeed, the steepness is independent from the bias current, since for the different currents, the minimal RF input power curves have

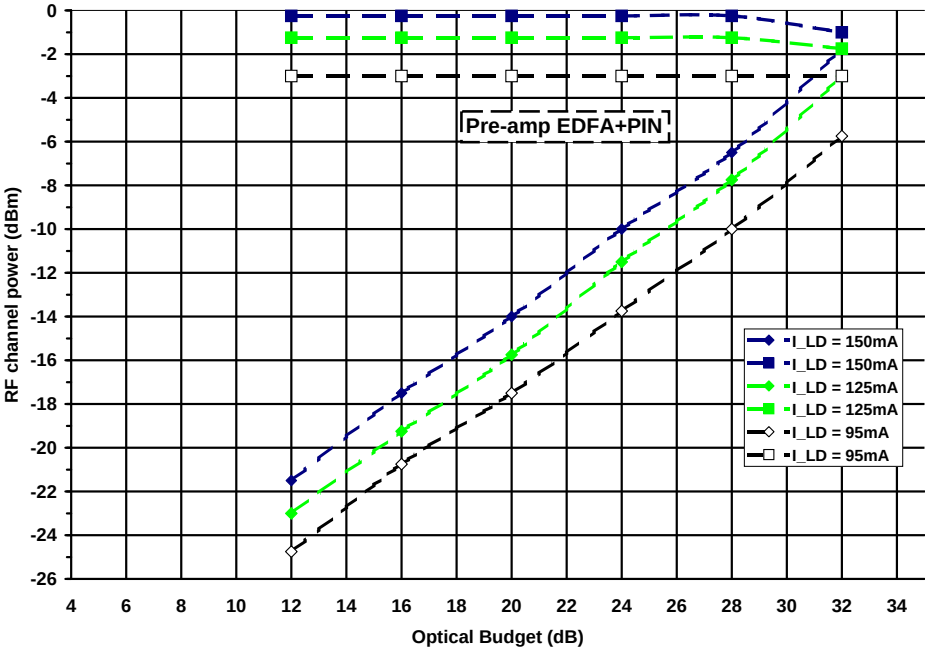

Figure 12.5.: Minimal and maximal RF powers for the ACLR requirements (-45dBc at +/-5MHz and -50dBc at +/-10MHz) when transmitting a single UMTS carrier over a fiber-free link and using an EDFA pre-amplifier

a steepness of 1dB (electrical) per 1dB (optical), and this for the optical budget ranging from 12 to 32dB.

The Fig. 12.5 shows, the lower the bias current of the LD is, and the lower is the minimal required UMTS carrier power at the input.

When approximating the minimum required RF input power by linear functions, then the slopes for 95, 125, and 150mA bias currents value respectively 0.97, 0.99, and 0.93 electrical dBm per optical dB. These behavior can be explained by the expressions developed in Part 3, and more precisely shown in §7.3.1, p. 122, where the signal-spontaneous noise dominates the other noise terms and exhibits a $-1 \cdot L_{dB}$ behavior where L are the insertion losses. The latter in turn makes the minimum required RF power to have the same slope for meeting a given SNR.

System point of view

From an electrical system margin point of view, the EDFA increases the maximal optical budget for which the ACLR requirements are met. The maximum measured optical budget is 32dB, and exceeds the required *B+ Class* budget by 4dB.

Extrapolating the maximal and minimal power curves, show that for the bias currents of 95, 125, and 150mA maximal optical budgets of respectively 34, 33 and 32.5dB could be reached. At 32dB of optical budget, the bias current of 95mA yields the highest system margin: 2.1dB.

Thus the conclusion is twofold, and is opposed to the ones made for the simple PIN

receiver:

- at 0dB electrical system margin, the highest achievable optical budget is yielded by the lowest bias current
- at constant optical budget, within the range of 30 to 32dB, the highest system margin is yielded by the lowest bias current (95mA) among the three tested.

12.1.3. 10km of S-SMF in link using an EDFA pre-amplifier

In order to emulate a more realistic PON architecture, 10km of G.652.D S-SMF is inserted in the link. The optical budget in Fig. 12.6 includes the losses due to the fiber.

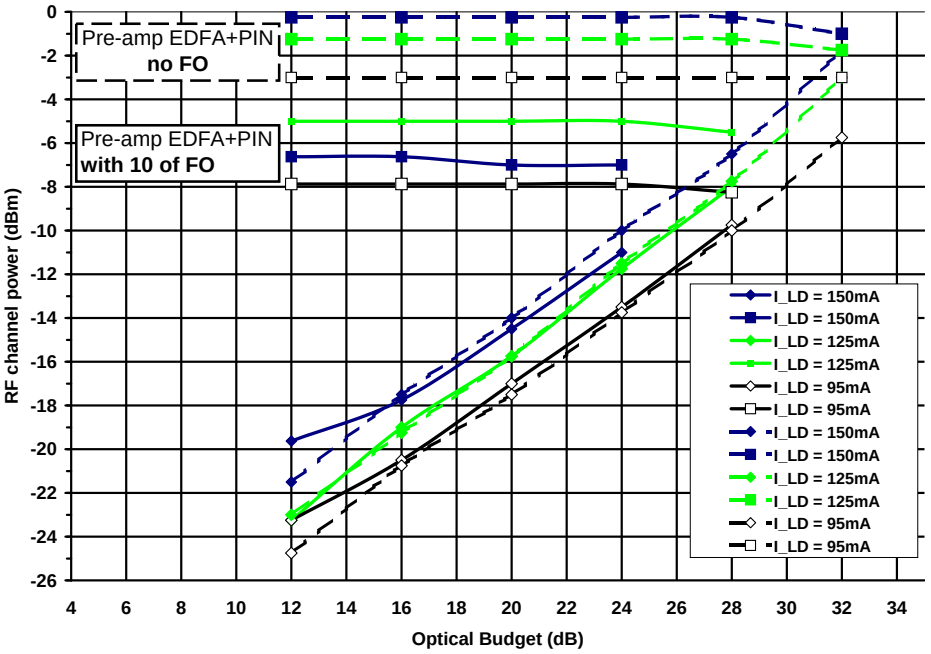

Figure 12.6.: Single UMTS carrier with 10km of S-SMF in link

Curves of the UMTS carrier's maximal power

Inserting 10km of S-SMF in the link lowers the maximum admissible RF carrier power. Compared to the previous section, the maximal admissible RF carrier power does not increases with the bias current. Indeed, Fig. 12.6 shows that among the three used bias current, the highest maximal RF carrier power can be reached for the bias current of 125mA, instead of 150mA.

At an optical budget of 24dB, the maximal admissible RF carrier input power is reduced —when inserting 10km of S-SMF— as follows: by 5.25dB for 95mA, by 3.75dB for 125mA, and by 6.75dB for 150mA.

Curves of the UMTS carrier's minimal power

Up to a budget of 24dB, the minimal admissible RF carrier power, for which the 3GPP ACLR requirements are met, remains unchanged when inserting 10km of S-SMF: the dashed curves (without fiber) and the continuous (with fiber) corresponding to the minimum (*diamond* symbols) RF carrier power —for the three bias currents respectively— superimpose one another.

For an optical budget of 28dB this conclusion is only valid for the bias currents of 95mA and 125mA.

System point of view

At 32dB of optical budget, none of the three bias currents lead to compliant ACLR measurements.

At 28dB of optical budget, only two of the measured bias current configurations allow the system to yield 3GPP compliant ACLR figures: 95 and 125mA. In this case the system margin is 2.2 and 1.9dB for bias currents of respectively 125 and 95mA.

Finally the insertion of 10km of S-SMF lowers the maximal optical budget to 28dB compared to 32dB for the case without fiber. This diminution of the maximum optical budget is *almost* compliant with the numerical results obtained in §9.2.2, p.148 where adding 10km of S-SMF reduced the maximum optical by 2dB. The difference can be attributed to the fact that the practical measurements include any non-linearities which are not modeled in the numerical results.

12.2. Dual UMTS carrier

12.2.1. 10km of S-SMF in the link

In order to emulate a more realistic Node B, a second UMTS carrier spaced by 20MHz is electrically added. The measurements will be done for a link containing 10km of S-SMF.

The reported carrier power in Fig. 12.7 is expressed **per carrier**.

In Fig. 12.7, the dashed curves represent the single carrier measurements whereas the continuous lines are the measurement realized for the dual carrier configuration.

Curves of the UMTS carrier's maximal power

The transmission of a second UMTS carrier onto the same wavelength, reduces the maximum input RF carrier power by 3dB —and this for any of the three bias currents.

The maximum RF carrier input power in the graphic is expressed per carrier. Thus since the two carriers are of equal power, the actual maximal admissible RF power, for yielding 3GPP compliant ACLR figures, remains the same. And this for the three measurements.

Curves of the UMTS carrier's minimal power

The curves of the minimum required UMTS carrier input power is decreased by 1dB approximately.

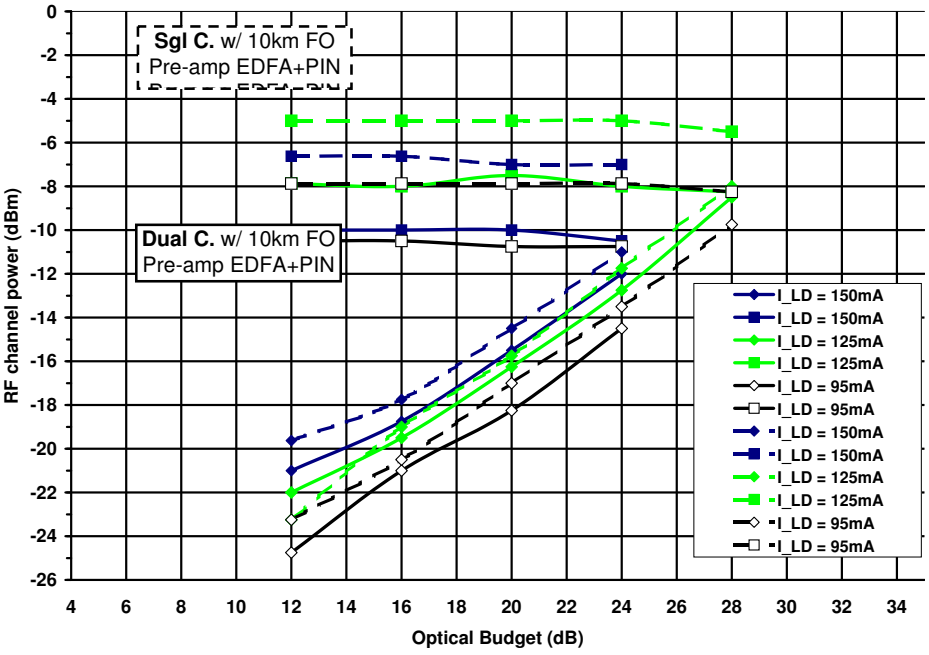

Figure 12.7.: Dual UMTS carriers with 10km of S-SMF in link

System point of view

The maximum measured optical budget, for which the 3GPP ACLR requirements are met, values 28dB for a bias current set to 125mA.

At 28dB of optical budget, the conclusions for a single carrier in the previous section, showed the system to have a 3dB of electrical system margin. When transmitting two carriers, this margin is reduced to 0.1dB. This 3dB loss of system margin is compliant with the theoretical formulations of §7.3.4, p. 127 where an increased crest factor due to the additional carrier increases the required minimum RF power for a given SNR.

Given that the system margin was lower than 3dB for the 95mA bias current measurement of the single carrier configuration at 28dB of optical budget, this bias current cannot lead compliant ACLR results when transmitting two UMTS carriers.

13. Architectures relying on a EDFA+PIN receiver, DCF and a booster

Scope

The previous section showed that the maximum optical budget —for which two transmitted UMTS carriers have ACLR figures compliant with downlink 3GPP specifications— to value *only* 28dB. However in order to transmit three UMTS carriers the presented system lacks electrical system margin. Furthermore this case was realized for *only* 10km of S-SMF, when the PON specifications foresee the possibility of 20km.

The next section shows the issue when 20km of S-SMF are present in the link.

13.1. Interest of using DCF

This section show how the ACLR figures can be improved by placing Dispersion Compensating Fiber (DCF) in the link.

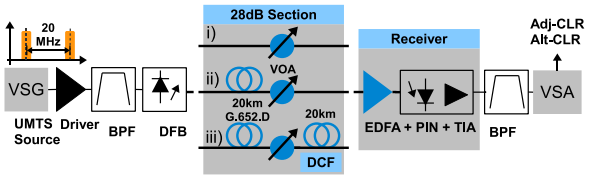

Figure 13.1.: Set-up used to show how simply cascaded DCF improves the ACLR.

[120] and [122] already showed the S-SMF's length to be responsible for the ACLR degradation of the transported UMTS carrier. The additional set-up of Fig. 13.1 and its related electric spectra in Fig. 13.2a–13.2b, and the measurements of Table 13.1 confirm this issue. As predicted by [114], the S-SMF is shown to induce 3rd-order like distortions given the spurious signals occurring at 2110 and 2170MHz, the carriers frequencies being 2130 and 2150MHz.

Table 13.1.: Improved ACLR by cascaded 20km DCF spool

ACLR for 28dB overall optical budget	3GPP specs. (maximum)	No fiber (Fig. 13.2a)	with 20km S-SMF	
			no DCF (Fig. 13.2b)	with 20km DCF (Fig. 13.2c)
Adj-CLR [dBc]	-45.0	-47.6	-37.9	-45.4
Alt-CLR [dBc]	-50.0	-50.2	-47.5	-49.9

Furthermore the S-SMF's chromatic dispersion's effect on the ACLR, is assessed. The spectrum in Fig. 13.2c shows attenuated spurious signals when simply adding (inset iii) in Fig. 13.1) a DCF spool of 20km to the initial 20km of S-SMF (the overall budget of 28dB being conserved). The added DCF allows to improve the Adj-CLR and the Alt-CLR by respectively 7.5 and 2.4dB (Table 13.1).

Thus interest of the DCF for the ACLR performances enhancement is experimentally demonstrated, yet its length and its placement have to be discussed.

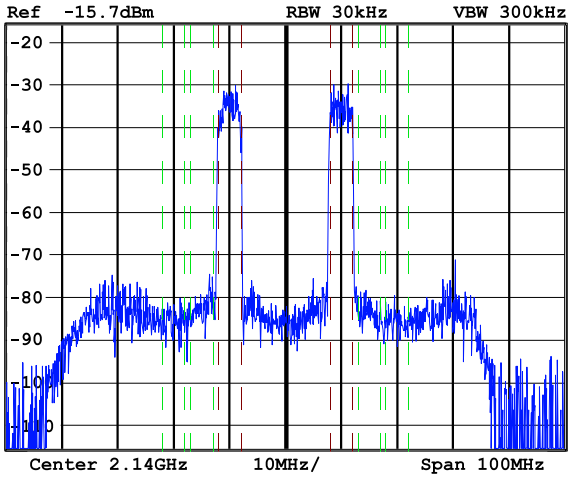

(a)

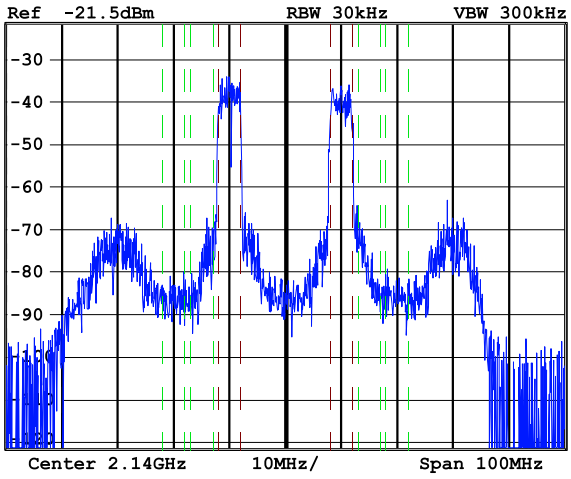

(b)

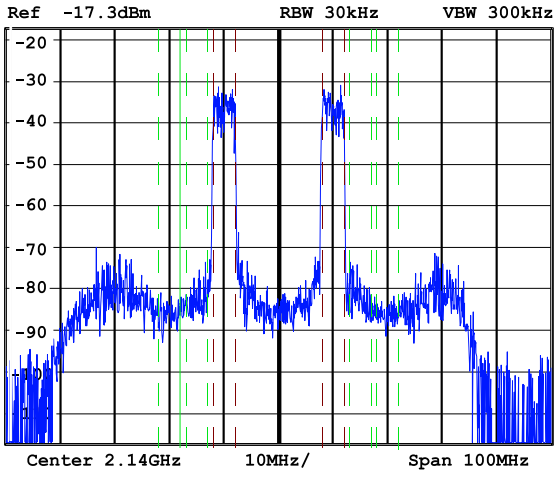

(c)

Figure 13.2.: Spectra of two UMTS carriers transported over a 28dB link using successively the set-ups of Fig. 13.1: (a) no fiber vs. (b) 20km of S-SMF, show the ACLR degradation due to the S-SMF ; whereas (c) 20km of S-SMF **and** 20km of DCF, shows the ACLR improvement. The resolution bandwidth (RBW) of the spectra is 30kHz. TABLE 13.1 summarizes the measurements.

13.2. Interest of using a booster

Given the maximum measured optical budget to be limited to 28dB (with an electrical system margin of 0.2dB) when transmitting two UMTS carrier over a link containing 10km of Standard Single Mode Fiber (S-SMF) when biasing the LD at 125mA, and to 24dB (with an electrical system margin of 3.5dB) when biasing at 95mA as in Fig 12.7 —the optical *boosting* thanks to an EDFA is proposed in this section.

13.2.1. Dual UMTS carriers and 10km of S-SMF

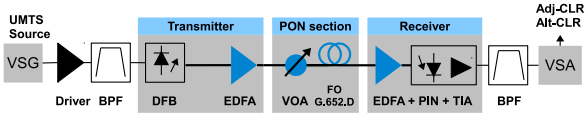

Figure 13.3.: Set-up used to demonstrate the boosting-EDFA's interest for the ACLR.

The set-up is similar to the one of Fig. 12.3 except that a boosting intended EDFA is located between the DFB laser and the *PON section* (Fig. 13.3). The EDFA is set to operate at constant output power (+15dBm set on the equipment).

The boosting EDFA allows to take advantage of the provided gain by lowering the bias current of the LD (*i.e.* the average optical launch power), and finally to operate in the most linear part of the electro-optical conversion curve: the bias current of the DFB is successively set to 50, 65, 80, and 95mA. The latter is for comparison's sake.

Again for a dual carrier configuration, and a 10km S-SMF containing link, the ACLR performances are measured.

Curves of the UMTS carrier's maximal power

When only considering the maximal RF input power per carrier (Fig. 13.4), then the maximum measured optical budget for which the ACLR specifications are met (for both carriers!) values 34dB for the 50, 65, and 80mA bias currents. While for the 95mA current, the maximum optical budget values *only* 32dB.

Globally speaking all the highest input RF powers range within 3dB. Yet it can be noticed that it is not the highest bias current (95mA) that yields the highest RF acceptable RF input power, namely 80mA. For the remaining bias currents the *hierarchy* is however conserved: the 80mA current has a corresponding maximum RF input power higher (by 3dB) than the 65mA current.

Finally this shows that the 80mA current is a local optimum.

Curves of the UMTS carrier's minimum power

When only considering the minimum RF input power per carrier, then the maximum measured optical budget for which the ACLR specifications are met values 34dB for the 50, 65, and 80mA bias currents, and 32dB for the 95mA bias current —thus similar to the maximum RF input powers.

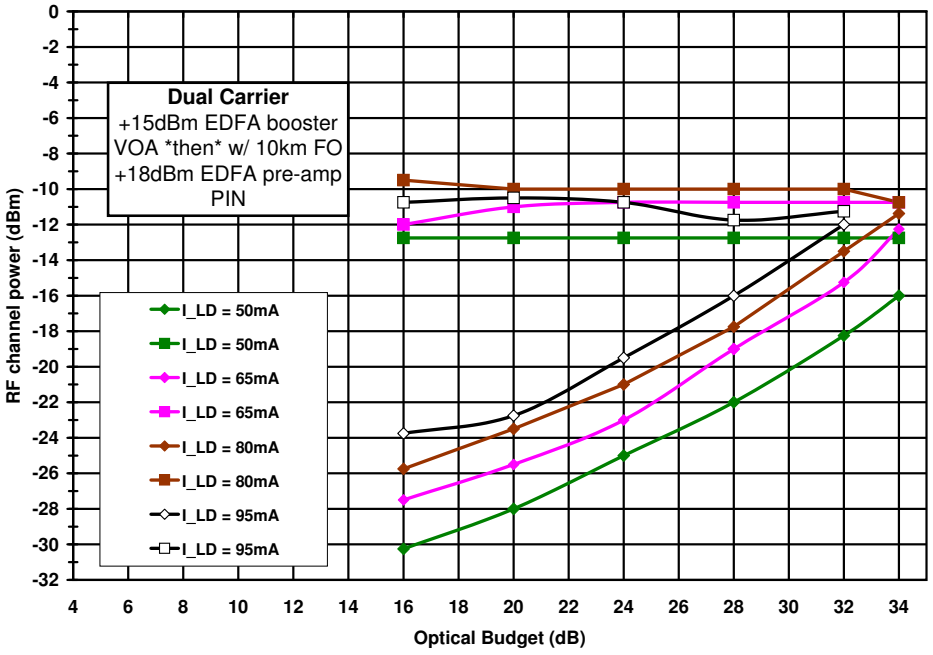

Figure 13.4.: Dual UMTS carriers EDFA-booster with 10km of S-SMF for different bias currents

System point of view

Finally only the 50, 65, and 80mA bias currents allow to meet the ACLR performances for a maximum measured optical budget of 34dB. Yet among the these three currents, it is the lowest one (50mA) that makes the system to yield —for the maximum optical budget of 34dB— the highest electrical input margin: 3dB. The 65 and 80mA currents allow electrical input margins of respectively 1.5 and 0.7dB. Finally this shows the electrical input margin to be inversely proportional to the bias current.

The 95mA bias current for which a maximum optical budget of 32dB could be measured, exhibits then an electrical input margin of 0.7dB.

Finally this section has demonstrated the benefit of the boosting EDFA for increasing the maximum optical budget for which the ACLR specifications are met: passing from 28dB with almost no electrical margin to 34dB with an electrical margin of 3dB. Furthermore the interest of decreasing the LD's bias current has been demonstrated.

13.2.2. Effect of swapping the VOA's and the S-SMF's positions

Since we have increased the optical launch power into the *PON section*, we can wonder about its influence onto the ACLR results. This question originates from the fact that so

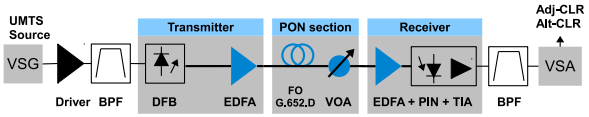

Figure 13.5.: Set-up used to demonstrate the boosting-EDFA's interest for the ACLR.

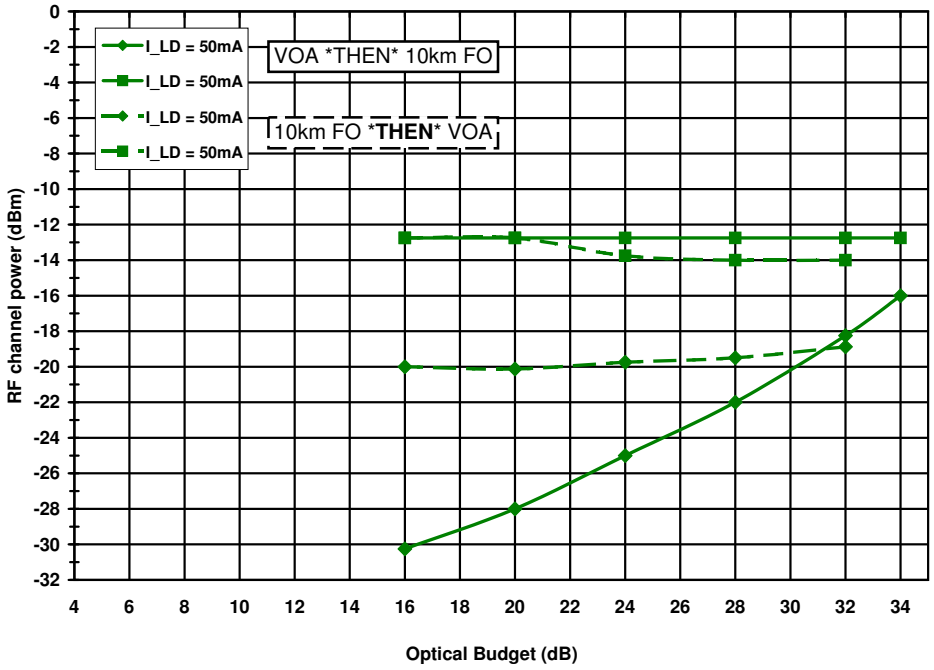

Figure 13.6.: Dual UMTS carriers with 10km of S-SMF in link

far the *PON section* has been emulated by a VOA followed by eventual fiber. Yet in a real PON the fiber is distributed over the PON (Fig. 2.3, p. 19). Thus we think it to be worth to swap the VOA and the S-SMF blocks (Fig. 13.5). Its effect can be appreciated for the 50mA bias current in Fig. 13.6.

Curves of the UMTS carrier's maximal power

Up to optical budgets of 20dB, the maximum acceptable RF input power per carrier for yielding 3GPP compliant ACLR values is not affected by the swapping. Yet for optical budgets superior to 24dB, the swapping causes the maximum admissible RF input power to decrease by 1.5dB, and the maximum measured optical budget to decrease by 2dB to 32dB.

Curves of the UMTS carrier's minimum power

Placing the S-SMF in front of the boosting EDFA's output causes the minimum required RF input power, for yielding 3GPP compliant ACLR values, to increase and furthermore to pass from a linear slope to a *plateau*. It is also to be noticed that maximum measured optical budget falls from 34 to 32dB.

System point of view

Globally speaking the swapping the VOA's and the S-SMF's positions limits the maximum measured optical budget to 32dB yielding then a system margin of 5dB. Finally the proposed swapping is a very conservative approach, as the performances are.

13.2.3. Placement strategy of the DCF spool (with the booster)

The interest of DCF has been demonstrated, yet it has to be used in a way not disturbing the rolled-out legacy PON architecture.

Given that the PON specifications [17] do not foresee to use DCF, the DCF spool is to be placed *outside* of the PON tree through which the UMTS carriers are to be transported. Thus the DCF spool is to be located upstream or downstream from the PON section.

Finally the first way is more elegant since it allows to share the DCF spool between the different remote antenna sites addressed by the CO, provided the chosen DCF spool's length enhances the ACLR for the shortest as well as for the longest S-SMF links.

Yet if the DCF spool is placed at the transmitter side, its additional losses (0.2dB/km) furthermore reduce the maximum optical budget. To compensate these losses, and given the target optical budget of at least 28dB of the PON section, we propose to boost the optical signal, by placing an EDFA between the DCF spool and the PON section (Fig. 13.7). The optical budget is still defined as the optical power losses in the PON section.

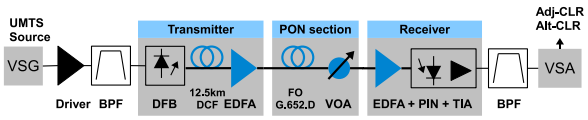

Figure 13.7.: Optimized set-up

We briefly show the ACLR performances (Fig. 13.8) for a dual carrier set-up using the booster of the afore section, with 10km of DCF located between the DFB and the booster. A conservative approach is maintained by locating the 10km of S-SMF directly at the booster's output.

Curves of the UMTS carrier's maximal power

The DCF causes the maximum tolerable RF input power to be *restored* to its initial value prior to swapping.

Curves of the UMTS carrier's minimum power

The *plateau* effect caused by the previous swapping is not recovered by the insertion of the DCF, however the maximum measured optical budget is restored to 34dB. For this optical budget the minimum required RF input power is increased by 2dB compared to the case prior to swapping.

System point of view

Finally the DCF allows to recover the maximum optical budget of 34dB prior to swapping, and this for an electrical system margin of 5dB which is 2dB more than the case prior to swapping using no DCF.

The main framework being set (DCF, EDFA booster and pre-amplifier) a detailed discussion of the DCF length is proposed in the next section.

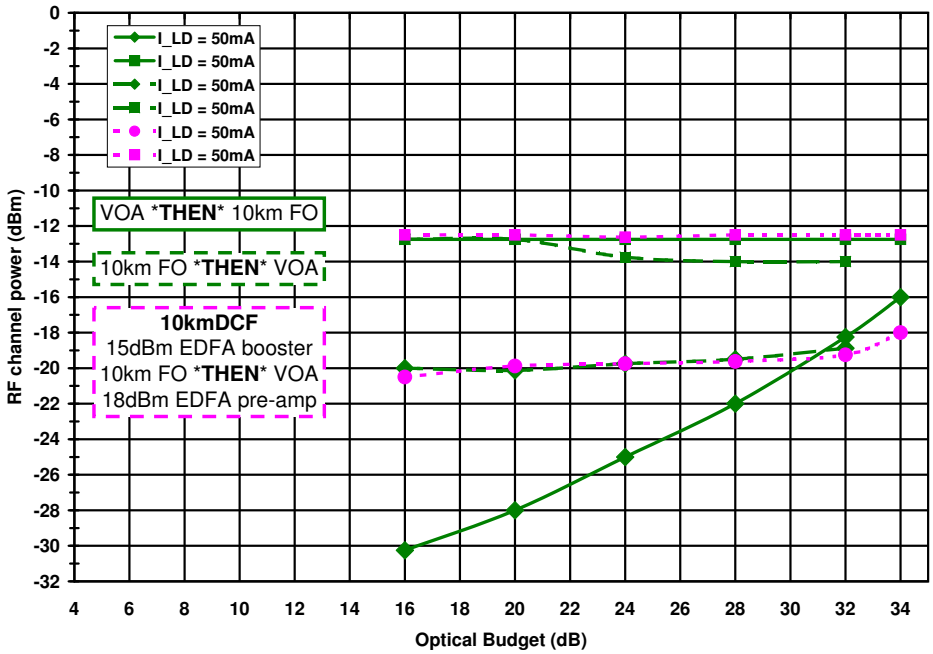

Figure 13.8.: Dual UMTS carriers with 10km of S-SMF in link

13.3. DCF Length discussion

The placement of the DCF spool being set, we aim at finding a length of DCF suitable for transmissions regardless of the distance in PONs (0 to 20km of S-SMF).

To answer this question the Adj- and Alt-CLR performances of a single carrier were measured for DCF spools of different lengths (0 to 12.5km), in a set-up (Fig. 13.7) having an overall optical budget of 30.90dB containing a PON-like trunk with 20km of S-SMF.

For these measurements the total RF modulating power is set to +7.5dBm, and the biasing current of the DFB is reduced to 77mA in order to not to saturate the boosting EDFA. Thus the transmitter has a Root-Mean-Square (RMS) Optical Modulation Index (OMI) of 17.1%.

The boosting EDFA (noise figure of 4dB, output saturating power of +18dBm) outputs +13.15dBm of optical power. The pre-amplifying EDFA outputs +11dBm of optical power, the latter being attenuated by 10dB (not shown in the set-up) in order not to saturate the PIN photo-detector.

The results are summarized in Tab. 13.2. The left and the middle columns show an increasing length of DCF to improve the Adj-CLR. The right column shows the ratio between the Adj-CLR and the noise floor [1] [2] and thus allows to appreciate the improvements with respect to the actually best possible value, which would be to have 0dB *i.e.* the Adj-CLR distortions and the thermal noise of the receiver being of equal power.

Finally a 12.5km long DCF spool yields an acceptable compromise between length and ACLR improvement.

Table 13.2.: Adj-CLR improvement of a single carrier for different DCF lengths and a fix S-SMF length of 20km

DCF [km]	Adj-CLR [dBc]	Adj-CLR to Noise Floor [dB]
0	-51.20	4.75
3.0	-52.74	3.44
7.5	-54.72	1.82
10.0	-55.51	1.03
12.5	**-56.00**	**0.66**

[1] which is calculated using the average power at channels located at even multiples of 5MHz from the carrier of interest, and thus not being affected by the 3rd or eventual 5th-order distortions occurring in the channels centered at odd multiples of 5Mhz from the carrier of interest

[2] the here presented noise floor is not the noise floor of the equipment which of course is lower

13.3.1. Spectra for different DCF lengths when using a single UMTS carrier

The spectra in Fig. 13.9 illustrate the improvement (Tab. 13.2) of the ACLR figure when the length of DCF increases.

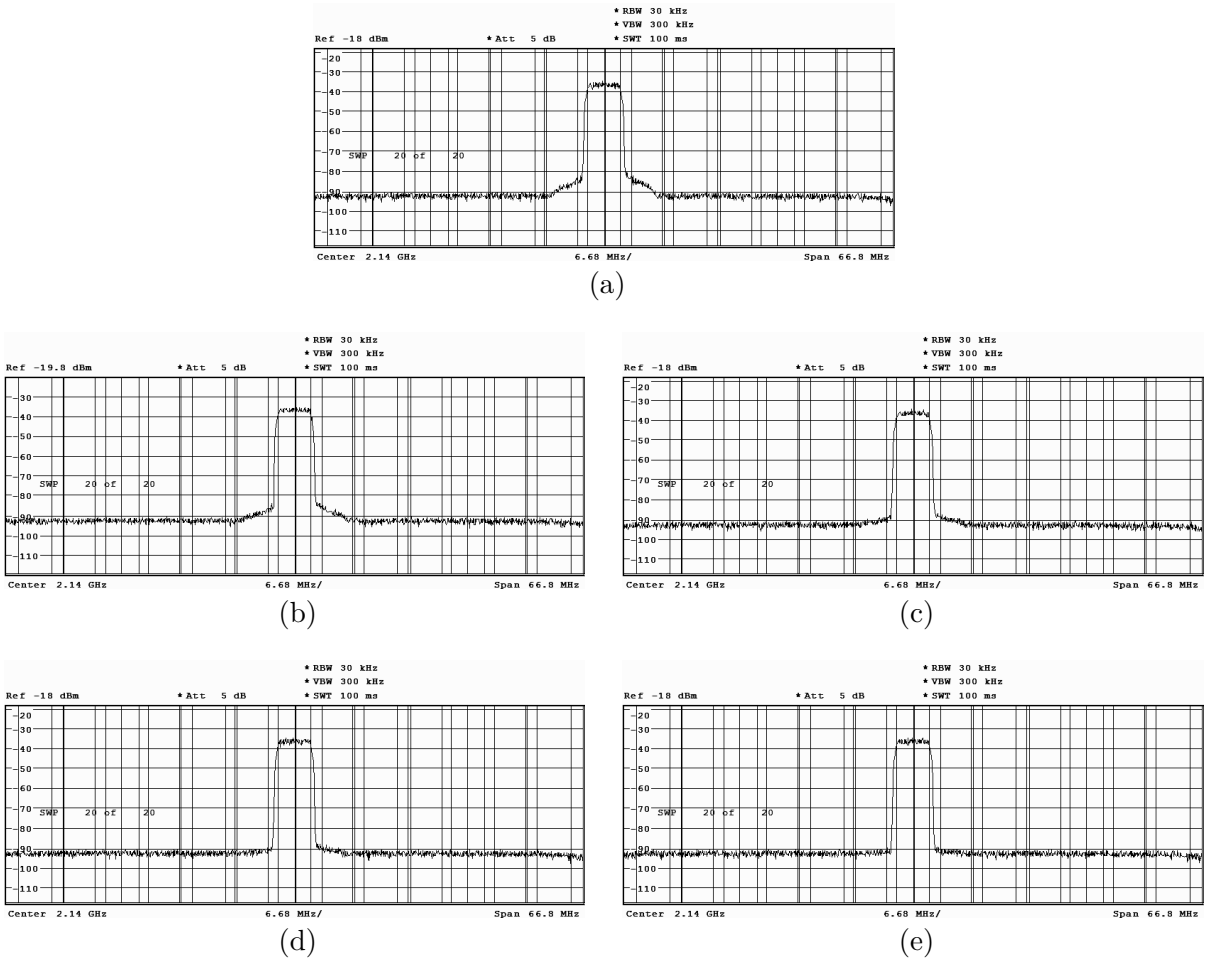

Figure 13.9.: ACLR improvement vs. DCF lengths between the DFB and the EDFA for a 30.90dB budget: (a) no DCF, (b) 3.5km, (c) 7.5km, (d) 10.0km, and (e) 12.5km of DCF.

13.3.2. Spectra for different DCF lengths when using two UMTS carrier

According to the corresponding ACLR measurements of the spectra shown in Fig. 13.10 at least 12.5km of DCF are required for meeting the 3GPP specifications.

It is worth to mention that in none of the presented cases the Adj-CLR is the limiting factor but instead it is the Alt-CLR. Indeed the Alt-CLR requirement is higher by 5dB, yet when considering the average Adj- and Alt-CLR, that for a same value of DCF the Adj-CLR performance is lower better (*i.e.* lower values) than the Alt-CLR measurement.

The latter aspect is simply explained by the fact the resulting/residual inter-modulations effect of the fiber chromatic dispersion acting on the dual carrier and creating the third-order distortions signals falling strait into Alt-CLR measurements bands... Compared to the single carrier case where the same distortions are not really an issue (the ACLR

performances despite the small distortions are generally speaking *acceptable*), yet passing to a dual carrier case makes the unwanted side-effects to cause now no longer acceptable distortions!

Table 13.3.: Dual carrier ACLR improvement

DCF [km]	ADJ-CLR	ALT-CLR
null	-46.4	-41.2
7.5	-50.8	-47.5
10	-51.9	-49.8
12.5	-52.8	-51.7

Finally only 12.5km of DCF allows the set-up to yield ACLR performances compliant with the 3GPP specifications for the dual carrier case (Tab. 13.3).

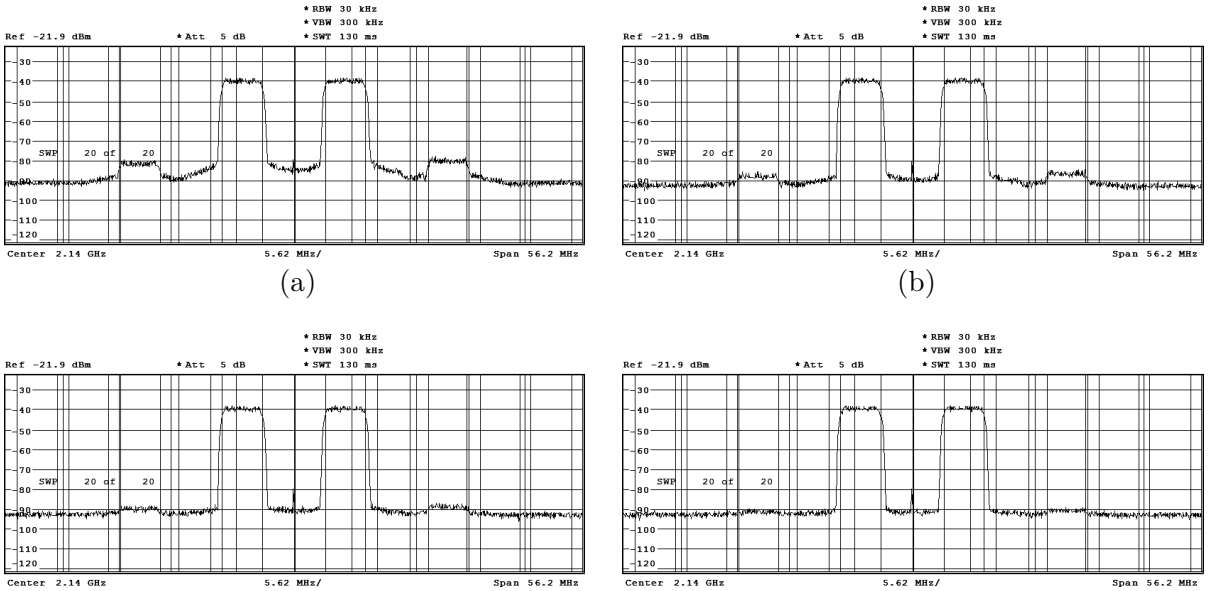

Figure 13.10.: Dual carrier ACLR improvement vs. DCF lengths between the DFB and the EDFA for a 30.90dB budget: (a) no DCF, (b) 7.5km, (c) 10km, and (d) 12.5km of DCF

13.3.3. Spectra for different DCF lengths when using three UMTS carriers

For the three carrier case (Fig. 13.11 and Tab. 13.4) almost similar comments to the dual carrier case can be made: up to DCF lengths of 7.5km the Alt-CLR performances are the limiting factor. Furthermore again, in terms of absolute performances, the Alt-CLR measurements are worser than the ones for the Adj-CLR. For DCF lengths greater than

Table 13.4.: Triple carrier ACLR improvement

DCF [km]	ADJ-CLR	ALT-CLR
null	-47.6	-44.6
3.5	-48.9	-46.4
7.5	-50.1	-48.9
10	-49.6	-49.1
12.5	-51.6	-51.4
16	-51.8	-51.8

10km the Adj- and Alt-CLR performances are equivalent. However only DCF lengths of at least 12.5km yield compliant ACLR performances for the 3 carrier case.

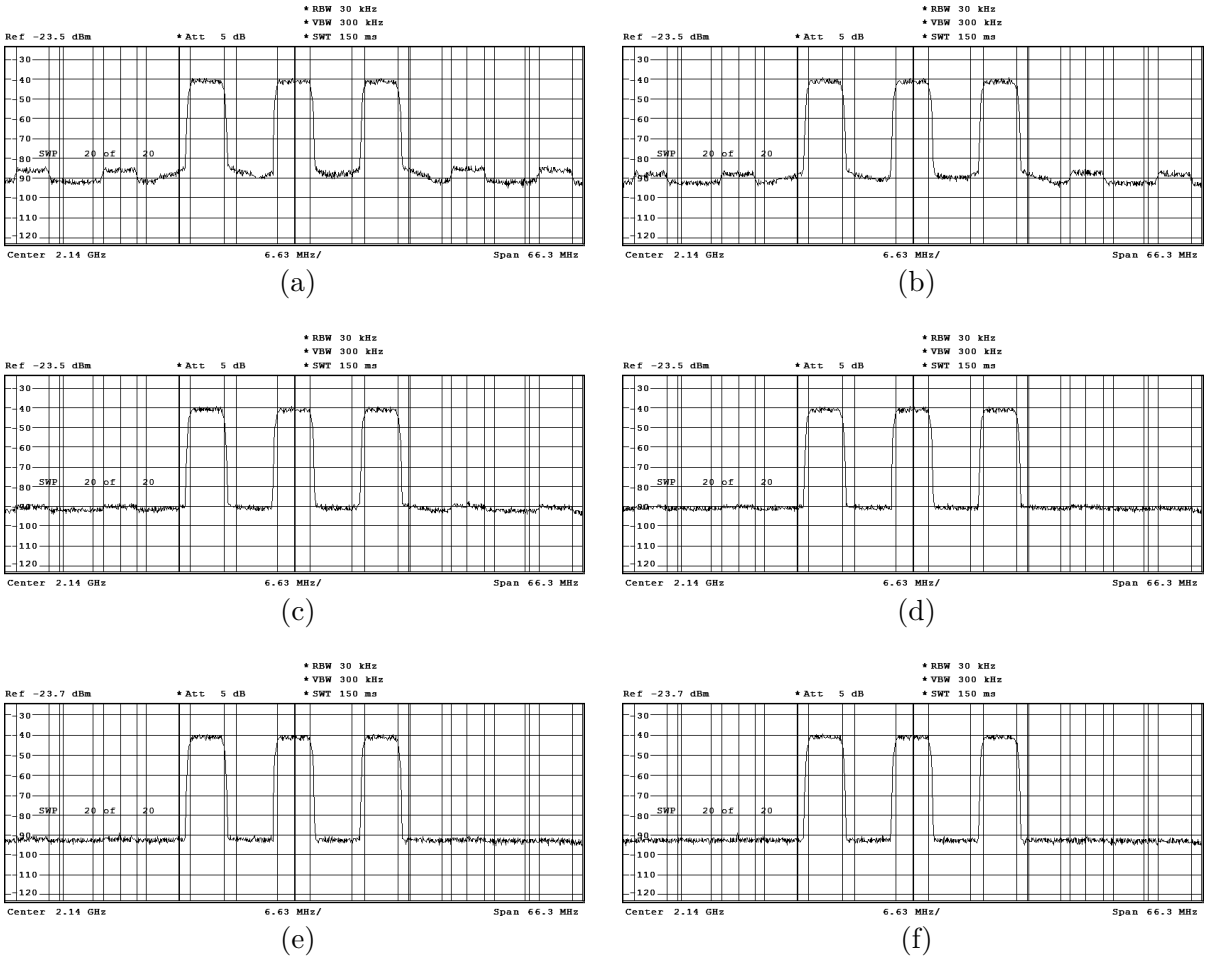

Figure 13.11.: Triple carrier ACLR improvement vs. DCF lengths between the DFB and the EDFA for a 30.90dB budget: (a) no DCF, (b) 3.5km, (c) 7.5km, (d) 10km, (e) 12.5km, and (f) 16km of DCF

13.4. Optimized architecture

13.4.1. Single DCF length fitting variable budgets and S-SMF lengths

We will finally show a single DCF length to fit variable optical budgets and, last but not least, to fit variable and S-SMF lengths contained in the link.

Therefore we use the set-up of Fig. 13.7. The laser's modulating conditions (biasing at 77mA, and constant overall OMI of 17.1%) as well as the EDFAs' configurations remain the same. However in order to further assess our proposed set-up, we increase the number of the transmitted UMTS carriers to three, which are of equal power, equally spaced by 5 or 10MHz, and centered at 2140MHz.

ACLR performances as a function of the optical budget

The displayed curves (Adj-CLR FIT#1 and Alt-CLR FIT#1) in Fig. 13.12 and 13.13 asymptotically fit the ACLR behavior versus the optical budget. Since theses approximations are constant versus the optical budget, we can attribute the dominating noise for these curves to be the amplified Relative Intensity Noise (RIN).

The displayed curves (Adj-CLR FIT#2 and Alt-CLR FIT#2) in Fig. 13.12 and 13.13 asymptotically fit the ACLR behavior versus the optical budget exhibiting slopes of -1 dB (electrical) per 1dB of optical budget. Thus we can attribute the dominating noise, and ACLR limiting factor, to be the signal-spontaneous noise.

Finally the proposed set-up containing 12.5km of DCF allows meeting the ACLR specifications for 3 UMTS carriers over optical budgets up to 32dB (Fig. 13.12), and this whether 10km or 20km of S-SMF are contained within the PON section. The same conclusions can me made when spacing the three carriers by 10MHz (Fig. 13.13).

Thus *comfortable* 4dB optical margin remain for multiplexers or circulators which are to be placed upstream and downstream of the 28dB PON section in order to aggregate the RoF emitter and receivers blocks with the PON equipments and infrastructure.

EVM performances

In fact, complying to the ACLR specification implies that the SNR of the channel is better than 50dB and that the non-linearity of the system is negligibly small. This, in turn, implies that the EVM values obtained when the system complies with the ACLR specifications are very small (typically less than 2%).

Indeed, the measured Composite EVMs value less than 1.8% and 1.1% respectively for 13 and 32dB budgets, while the specified maximum is 17.5% [59].

Thus the EVM of the *emitted* signals at the antenna-level are expected to be able to cope with the typical distortions due to the propagation in air, and to thus to finally yield **at the receiving mobile phone/equipment** EVM performances below the specified maximum.

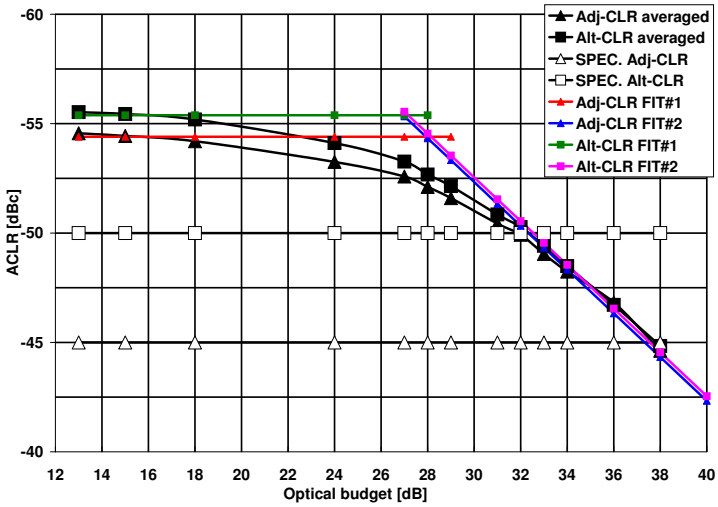

(a)

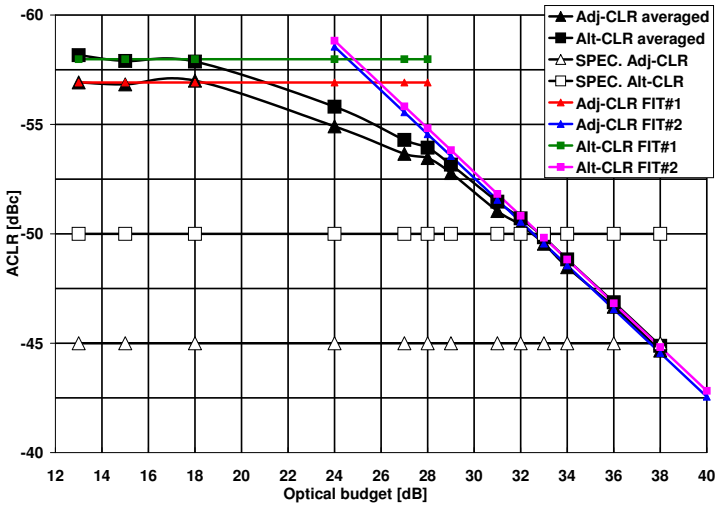

(b)

Figure 13.12.: ACLR performances of 3 UMTS carriers (5MHz spaced) transported over the set-up of Fig. 13.7 for (a) 20km, (b) 10km of S-SMF

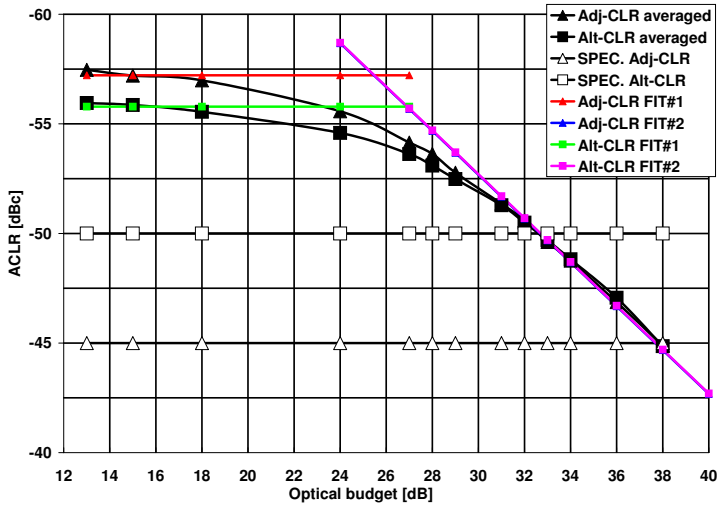

(a)

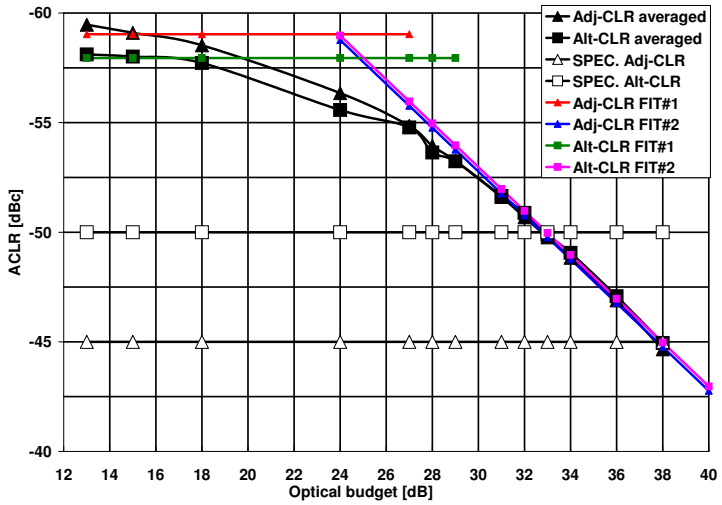

(b)

Figure 13.13.: ACLR performances of 3 UMTS carriers (10MHz spaced) transported over the set-up of Fig. 13.7 for (a) 20km, (b) 10km of S-SMF

Electrical spectra at the PON extrema budgets

For the 13dB budget spectrum in Fig. 13.14a and 13.14c, small ripples (below -95dBm/30kHz, for a noise floor of -100dBm/30kHz) remain at the 3rd order distortions inter-modulation products' frequencies , and are induced by the chromatic dispersion of the S-SMF, its dispersion being not completely recovered by the 12.5km of DCF. Whereas for the 32dB budget spectrum in Fig. 13.14b and 13.14d, the afore mentioned ripples are below the noise floor yielding -90dBm/30kHz.

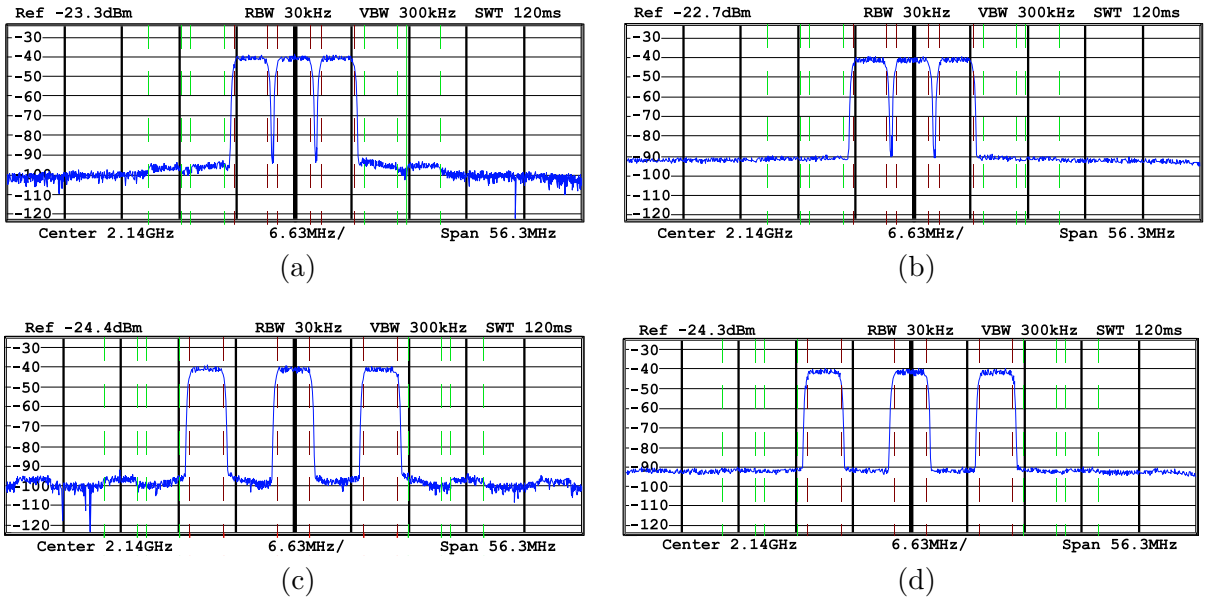

Figure 13.14.: Measured spectra of 3 UMTS carriers (spaced by 5 and 10MHz) transported over the optimized architecture of Fig. 13.7 with 20km of S-SMF. The measured spectra correspond, to the ACLR performances of Fig. 13.12-13.13, and are taken at 13dB budgets for (a)&(c), and at 32dB budgets for (b)&(d).

13.4.2. Deducted design rules

We used a DCF-span of 12.5km with a chromatic dispersion of –17ps/nm/km.

For a transmission including a length L_{SMF} of 10.0km, according to

$$\Delta_{acc} = D_{SMF} \cdot L_{SMF} + D_{DCF} \cdot L_{DCF} \tag{13.1}$$

the accumulated chromatic dispersion Δ_{acc} values –42.5ps/nm.

Assuming the chromatic dispersion's induced Inter-Modulation Distortion (IMD)-3 to be symmetric with respect to the sign of the accumulated chromatic dispersion, we can suppose the required ACLR specifications to be guaranteed for +42.5ps/nm of accumulated chromatic dispersion. Solving the Eq. 13.1 for the latter value, the maximal S-SMF length is 12.5km, leading to fiber length's dynamic of 5km.

Given that the measurements showed also 3GPP compliant ACLR values for a S-SMF length of 20km, the same scheme can be applied to this case. Then the accumulated

chromatic dispersion is +127.5ps/nm. Solving the Eq. 13.1 for -127.5ps/nm results in a minimal S-SMF length of 5km, resulting in a fiber length's dynamic of 15km.

These two cases show a trade-off to exist between the length of DCF, and the dynamic range of the S-SMF that can be included in the link.

Assuming the maximal acceptable accumulated chromatic dispersion to value $\pm 127.5 ps/nm$, and

$$D_{DCF} = -D_{SMF} = 17\text{ps/nm/km} \tag{13.2}$$

then Eq. 13.1 can be reduced to:

$$|L_{SMF} - L_{DCF}| \leq 7.5 \tag{13.3}$$

where L_{SMF} and L_{DCF} are expressed in km.

For instance this shows that —in the presented configuration— for up to 7.5km of S-SMF no DCF is required.

These results are summarized in the following *dispersion map*:

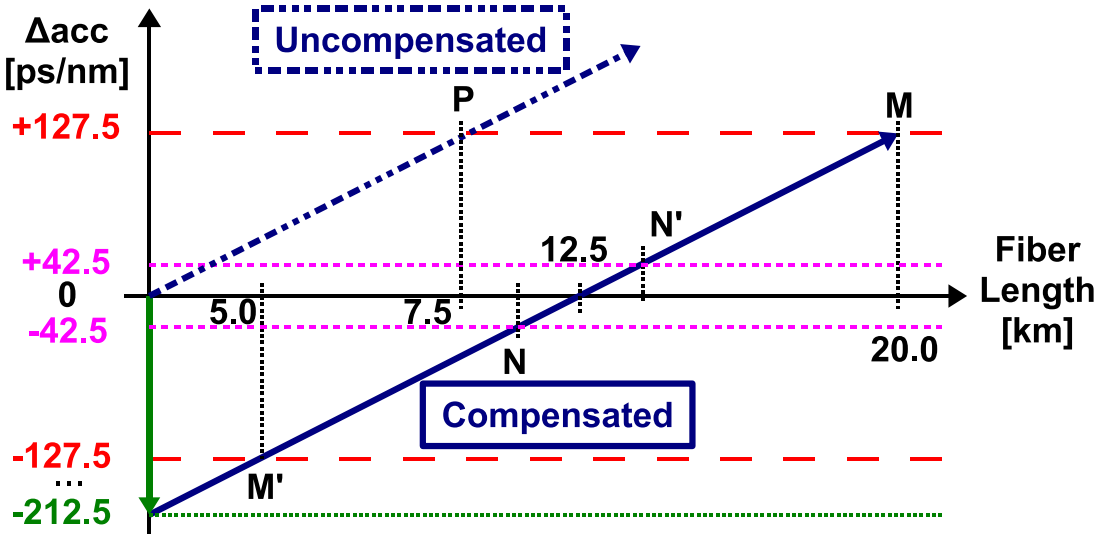

Figure 13.15.: Dispersion map

DCF with higher compensating values

Supposing DCF with chromatic dispersion of –80ps/nm/km to exist, and assuming the 20km S-SMF case, then the DCF-span's length can be reduced to 2.65km. The interest of using such a DCF is the reduced overall propagation time.

Conclusion

This fourth and last part of this thesis has dealt with the practical results and measurements.

We have successively seen that the APD receiver can recover transmitted UMTS carriers, fits our purpose in terms of EVM and this for optical architectures ranging from the simple PON with optical budgets of 28 to 32dB, eventually including up yo 20km of S-SMF, to ER-PON architectures with a single SOA shared between the counter-propagating wavelengths. The latter architectures allow to cover overall optical budgets up to 45dB.

Despite these promising experimental results, the APD receiver, under the scope of an additional figure of merit used in mobile radio access networks, namely the ACLR, showed to yield limited and non compliant performances, especially in the downlink, with respect to the current UMTS and up-coming mobile radio Spurious Emissions Mask (SEM) regulation aspects. Nevertheless the APD receiver can serve uplink transmission of UMTS carriers where SEM do not matter since no air broadcasting beyond the CO is expected.

This drawback has lead to finding a more suitable optical receiver for replacing the APD one. Therefore a simple PIN and its EDFA pre-amplified variant have been assessed. Despite the facts that higher optical budgets and the ACLR specifications could be met with the latter receiver, it has turned out that when multiple UMTS carriers are transmitted over links containing up to 20km of fiber, combating the chromatic dispersion through DCF fiber is mandatory.

Therefore it was decided to place the DCF spool at the CO in order not to interfere with the already rolled-out PON infrastructure. An additional optical booster was cascaded to the DCF for overcoming its insertion loss. This finally constitutes our final architecture which has shown to be able to transport three UMTS carriers up to optical budgets of 32dB and including 20km of fiber, **and to yield compliant ACLR performances**.

Finally a transparent path for the distribution of downlink UMTS carriers through PON architectures guaranteeing the ACLR specifications is realized. Compared to the initial architectures (simple PON and ER-PON) using an APD receiver, the last architecture has gained in complexity.

However the efforts and complexity spent on meeting the ACLR specifications of downlink UMTS FDD carriers can be re-used for other recent radio standards such as WiMAX and LTE, which we recall require very similar ACLR and SEM related specifications and the latter can neither be neglected nor put aside —at the expense of making a RoF architecture/system to become not viable!

General Conclusion

The objective of the research conducted during this thesis was to study the possibilities of hybrid analog and digital access networks in order to realize a convergence of the different optical infrastructures. Therefore three key points have been addressed:

- the assessment of legacy and *affordable* 10Gbit/s digital applications aimed components, such as Distributed Feed Back (DFB) lasers and Avalanche Photo-Detectors (APDs) for Radio over Fiber (RoF) applications in Passive Optical Networks (PONs),
- their in-aptitude for recovering downlink radio carriers which have very stringent Adjacent/Alternate Channel power Leakage Ratio (ACLR) requirements —and this not depending upon the radio standards.
- the assessment of a more suitable receiver made of PIN and an Erbium Doped Fiber Amplifier (EDFA) pre-amplifier; around this composite receiver an adapted framework using Dispersion Compensating Fiber (DCF) and an EDFA-booster, was proposed, tested and validated by measurements as well as by simulations.

In a first time the characteristics in terms of capabilities, used components, of current, near-future and long-term PON architectures have been exposed. Also the main physical properties of radio access networks and the used figure of merits were introduced.

Then the reasons for re-using the optical access network infrastructures for the distribution of radio carriers through them have been exposed, by introducing the Distributed Antenna System (DAS) concept.

Also we have taken a review of the different radio over fiber techniques analog as well as digital ones. These techniques were evaluated under the criteria of given target Signal to Noise Ratio (SNR) with respect to the maximum optical budget, since the distribution of radio carriers through PON architectures constituted the main goal of this thesis. Unfortunately none of the reviewed techniques *satisfied* the criteria.

In a third step we have exposed the theoretical maximum optical budgets for passive and for optically amplified links by focusing on the Optical Modulation Index (OMI), by defining an OMI that can be used for any type of signals (no longer limited to sinusoidal ones).

Numerical results using the VPI transmission maker demonstrated the combination of chromatic dispersion and of the laser source's chirp to cause non-negligible third order inter-modulation effects for simple sinusoidal signals. Taking into account this distortions, the benefit of DCF for lowering them is demonstrated.

For realistic UMTS signals numerical results targeting compliant ACLR values over the maximum optical budget are carried out. Again the benefit of DCF is demonstrated. Furthermore the interest of using an EDFA pre-amplifier and an EDFA-booster is successively exposed.

From a practical point of view, the experimental results could not *fully* assess the interest of using a legacy and *affordable* 10Gbit/s APD in RoF/PON applications. When recovering downlink radio carriers, the Error Vector Magnitude (EVM) requirements

could be fulfilled. Unfortunately the latter aspect, as earlier mentioned in this thesis, is not sufficient in the downlink, where furthermore fulfilling the very stringent ACLR requirements is mandatory. Because of this the APD cannot be used in the downlink.

However the APD remains a component of choice when considering transmissions of RF carriers from the distributed antenna towards the Central Office (CO). Indeed in this latter situation fulfilling the EVM requirements is sufficient.

Yet the digital applications oriented DFB lasers could be used when changing the optical receiver to a PIN and an EDFA pre-amplifier. Then around this composite receiver an adapted framework using DCF and an EDFA-booster, was proposed, tested and validated.

Finally a transparent path for the distribution of downlink UMTS carriers through PON architectures guaranteeing the ACLR specifications is realized at the expense of gained complexity compared to the initial architectures (simple PON and ER-PON) using an APD receiver. Yet the reasons leading to the final architectures are mandatory.

An interesting perspective of the experimental work carried-out in the framework of this thesis, would be to make a *best of* of the APD and EDFA+PIN results (Fig. 13.16). Indeed, the EDFA+PIN architecture (including the DCF) could be used in the downlink path where the ACLR figure is the main concern, while in the uplink path an APD receiver is fully sufficient since the EVM figure is the main requirement.

Given the achievable optical budgets of the two individually studied solutions, realizing such a working combo seems, from my perspective, within reach. Yet as shown in [93] who studied the impact of an Cable Access Television (CATV) signal onto A and B-PON signals and vice versa, some impairments due to optical crosstalk are to be expected.

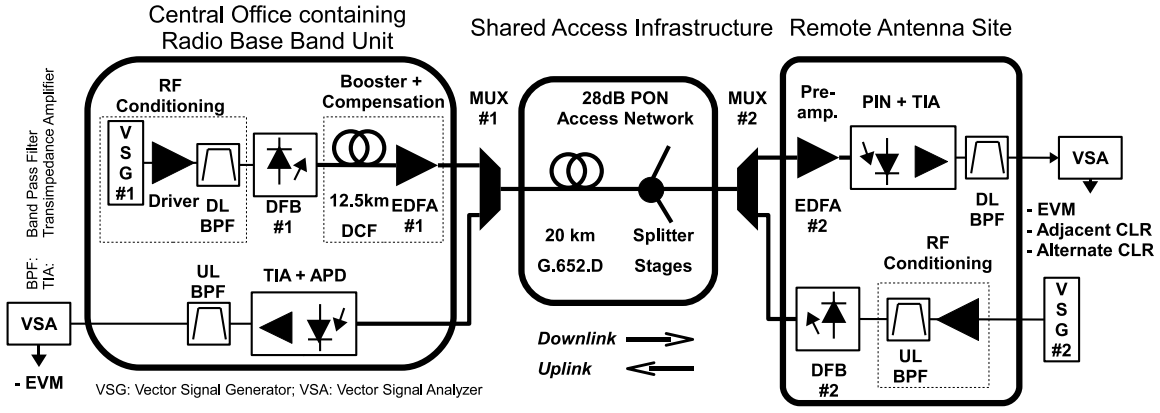

Figure 13.16.: Perspective set-up

Part V.

Appendix

A. Multiple UMTS carrier generation with Matlab and an dual port AWG

A.1. Principle

In [123] a method describing how to generate an Wide-Band Code Division Multiple Access (W-CDMA) signal with the help of an Arbitrary Waveform Generator (AWG) is proposed. The technique relies on a signal generated at Intermediate-Frequency (IF) (approx. 170MHz), which is then up-mixed by an Local Oscillator (LO) towards RF frequencies.

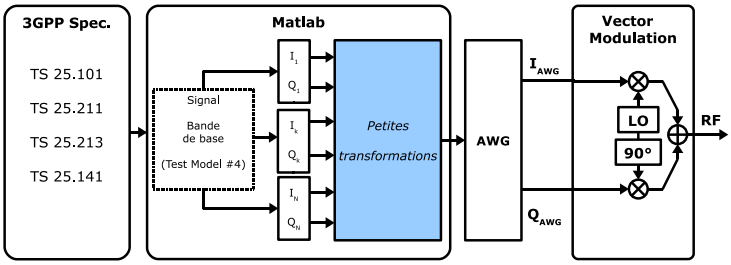

Figure A.1.: Principe of multiple RF carrier generation using a dual output port AWG

In order to get rid of the up-mixing procedure and the required filtering to remove the LO component of the previous technique, we decided to take advantage of a dual output port AWG combined to a VSG which performs the vector modulation of the provided I and Q parts of the UMTS signals, as shown in Fig. A.1.

A.2. Analytical expressions

A.2.1. Particular case of 2 carriers

The goal is to generate two carriers of frequencies ω_{RF_1} et ω_{RF_2}, and centered on ω_{RF}, as:

$$\omega_{RF} = \frac{\omega_{RF_1} + \omega_{RF_2}}{2} \qquad \text{et} \qquad \Delta\omega_{RF_{2,1}} = \frac{\omega_{RF_2} - \omega_{RF_1}}{2} \tag{A.1}$$

In the real time domain, the targeted signals looks like:

$$\Re(s) = r_1 \cdot \cos(\omega_{RF_1} + \theta_1) + r_2 \cdot \cos(\omega_{RF_2} + \theta_2)$$

Signal synthesis

In the complex domain the signal s can be written as:

$$s = r_1 \cdot e^{j\left(\omega_{RF_1}+\theta_1\right)} + r_2 \cdot e^{j\left(\omega_{RF_2}+\theta_2\right)} \tag{A.2}$$

$$= e^{j\left(\frac{\omega_{RF_1}+\omega_{RF_2}}{2}\right)} \cdot \left[r_1 \cdot e^{j\left(\frac{\omega_{RF_1}-\omega_{RF_2}}{2}+\theta_1\right)} + r_2 \cdot e^{j\left(\frac{\omega_{RF_2}-\omega_{RF_1}}{2}+\theta_2\right)}\right] \tag{A.3}$$

$$= e^{j(\omega_{RF})} \cdot \left[r_1 \cdot e^{j\left(-\Delta\omega_{RF_{2,1}}+\theta_1\right)} + r_2 \cdot e^{j\left(\Delta\omega_{RF_{2,1}}+\theta_2\right)}\right] \tag{A.4}$$

By defining the base band signals BB_1 and BB_2:

$$BB_1 = I_1 + jQ_1 = r_1 \cdot e^{j\theta_1} \qquad \text{et} \qquad BB_2 = I_2 + jQ_2 = r_2 \cdot e^{j\theta_2} \tag{A.5}$$

the signa s can be expressed as follows:

$$s = e^{j(\omega_{RF})} \cdot \left[BB_1 \cdot e^{-j\Delta\omega_{RF_{2,1}}} + BB_2 \cdot e^{+j\Delta\omega_{RF_{2,1}}}\right] \tag{A.6}$$

NOTE: For a carrier spacing of 10 MHz[1], the terms containing $e^{\pm j\Delta\omega_{RF_{2,1}}}$ are *complex carriers* with a frequency of 5MHz – which should not be an issue in a Matlab multiplication, and neither increase the number of points in the AWG.

I and Q separation in order to generate the signal s by the AWG

The signal s can be expressed as:

$$s = e^{j(\omega_{RF})} \cdot BB_{AWG} \qquad \text{with} \qquad BB_{AWG} = I_{AWG} + jQ_{AWG} \tag{A.7}$$

By separating the real and imaginary parts of BB_{AWG} –which will be the signals egressing the I and Q ports of the AWG– as a function of the complex components (I_1, Q_1, I_2 et Q_2) of the initial baseband signals BB_1 et BB_2:

$$BB_{AWG} = (I_1 + jQ_1) \cdot e^{-j\Delta\omega_{RF_{2,1}}} + (I_2 + jQ_2) \cdot e^{+j\Delta\omega_{RF_{2,1}}} \tag{A.8}$$

$$= (I_1 + jQ_1) \cdot \left(\cos(\Delta\omega_{RF_{2,1}}) - j\sin(\Delta\omega_{RF_{2,1}})\right) \tag{A.9}$$

$$+ (I_2 + jQ_2) \cdot \left(\cos(\Delta\omega_{RF_{2,1}}) + j\sin(\Delta\omega_{RF_{2,1}})\right) \tag{A.10}$$

Finally:

$$I_{AWG} = (I_1 + I_2)\cos(\Delta\omega_{RF_{2,1}}) + (Q_1 - Q_2)\sin(\Delta\omega_{RF_{2,1}}) \tag{A.11}$$

$$Q_{AWG} = (Q_1 + Q_2)\cos(\Delta\omega_{RF_{2,1}}) + (-I_1 + I_2)\sin(\Delta\omega_{RF_{2,1}}) \tag{A.12}$$

[1]The only consequence of this spacing is that the sampling frequency of the base band signals has, at least, to be twice the frequency spacing of the 2 carriers

A.2.2. Generalizing to N carriers

Now we wish to generate N channles of carrier frequencies $\omega_{RF_k}, \quad \forall k \in N$, centered on ω_{RF}, and equally spaced as:

$$\omega_{RF} = \frac{1}{N}\sum_{k=1}^{N}\omega_{RF_k} \qquad \text{and} \qquad \forall k \in \ N, \quad \omega_{RF_{k+1}} - \omega_{RF_k} = \Delta\omega_{RF} \geqslant 0 \tag{A.13}$$

The aimed real signal s looks like:

$$\Re(s) = \sum_{k=1}^{N} r_k \cdot \cos(\omega_{RF_k} + \theta_k)$$

Signal synthesis

As for the 2 carrier case, we re-use the complex base-band signals:

$$\forall k, \quad BB_k = r_k \cdot e^{j\theta_k}$$

The signal s in the complex domain can be expressed as a function of the BB_k signals:

$$s = \sum_{k=1}^{N} BB_k \cdot e^{j\omega_{RF_k}} \tag{A.14}$$

By factoring with respect to central RFcarrier frequency: (A.15)

$$s = \left(e^{j\frac{1}{N}\sum_{i=1}^{N}\omega_{RF_i}}\right) \cdot \sum_{m=1} BB_m \cdot e^{j\left(\frac{N-1}{N}\cdot\omega_{RF_i} - \frac{1}{N}\cdot\sum_{\substack{k=1\\k\neq i}}^{N}\omega_{RF_k}\right)} \tag{A.16}$$

$$s = e^{j\omega_{RF}} \cdot \sum_{m=1}^{N} BB_m \cdot e^{j\left(\frac{N-1}{N}\cdot\omega_{RF_i} - \frac{1}{N}\cdot\sum_{\substack{k=1\\k\neq i}}^{N}\omega_{RF_k}\right)} \tag{A.17}$$

Expressing the sequence S_N as a function of $\Delta\omega_{RF}$ Let S_N be the sequence defined as follows:

$$\forall i \quad / \quad 1 \leqslant i \leqslant N, \quad S_N(i) = \frac{N-1}{N}\cdot\omega_{RF_i} - \frac{1}{N}\cdot\sum_{\substack{k=1\\k\neq i}}^{N}\omega_{RF_k}$$

This sequence can be expressed as follows:

$$S_N(i) = -\frac{1}{N}\left(\sum_{\substack{j=1\\j\neq i}}^{N}\omega_{RF_j} - (N-1)\cdot\omega_{RF_i}\right) \tag{A.18}$$

$$= -\frac{1}{N}\left(\sum_{\substack{j=1\\j\neq i}}^{N}\omega_{RF_j} - \omega_{RF_i}\cdot\sum_{\substack{j=1\\j\neq i}}^{N}1\right) \tag{A.19}$$

$$= -\frac{1}{N}\sum_{\substack{j=1\\j\neq i}}^{N}\left(\omega_{RF_j} - \omega_{RF_i}\right) \tag{A.20}$$

(A.21)

Let re-use the definition of the beginning:

$$\forall i \quad / \quad 1 \leqslant i \leqslant N-1, \quad \omega_{RF_{i+1}} - \omega_{RF_i} = \Delta\omega_{RF}$$

by *summing* this expression from 1 to $m-1$ where $1 \leqslant m \leqslant N$, we obtain:

$$\forall m \quad / \quad 1 \leqslant m \leqslant N, \quad \sum_{i=1}^{m-1} \left(\omega_{RF_{i+1}} - \omega_{RF_i}\right) = \sum_{i=1}^{m-1} \Delta\omega_{RF} \tag{A.22}$$

$$\forall m \quad / \quad 1 \leqslant m \leqslant N, \quad \omega_{RF_m} - \omega_{RF_1} = (m-1) \cdot \Delta\omega_{RF} \tag{A.23}$$

This last expression can be rewritten for two indexes m and l as:

$$\omega_{RF_l} - \omega_{RF_1} = (l-1) \cdot \Delta\omega_{RF} \qquad \text{and} \qquad \omega_{RF_m} - \omega_{RF_1} = (m-1) \cdot \Delta\omega_{RF} \tag{A.24}$$

By subtracting the latter expressions, we get:

$$\omega_{RF_l} - \omega_{RF_m} = (l-m) \cdot \Delta\omega_{RF} \tag{A.25}$$

By re-injecting the latter expression into the expression S_N, we obtain:

$$S_N(k) = -\frac{1}{N} \cdot \sum_{\substack{j=1 \\ j \neq k}}^{N} (j-k)\, \Delta\omega_{RF} \tag{A.26}$$

$$S_N(k) = -\frac{1}{N} \cdot \Delta\omega_{RF} \left(\sum_{\substack{j=1 \\ j \neq k}}^{N} j - \sum_{\substack{j=1 \\ j \neq k}}^{N} k \right) \tag{A.27}$$

$$S_N(k) = -\frac{1}{N} \cdot \Delta\omega_{RF} \left(\frac{N \cdot (N+1)}{2} - k - k \cdot (N-1) \right) \tag{A.28}$$

$$S_N(k) = -\Delta\omega_{RF} \cdot \left(\frac{N+1}{2} - k \right) \tag{A.29}$$

Expressing the signal s as a function of $\Delta\omega_{RF}$

We can now express s as a function of S_N:

$$s = e^{j\omega_{RF}} \cdot \sum_{m=1}^{N} BB_m \cdot e^{j \cdot S_N(m)} \tag{A.30}$$

$$s = e^{j\omega_{RF}} \cdot \sum_{m=1}^{N} BB_m \cdot e^{-j \cdot \Delta\omega_{RF} \cdot \left(\frac{N+1}{2} - m\right)} \tag{A.31}$$

I and Q parts of s for the generation by the AWG

A part of the signal s can be expressed in a so called base band term, and noted BB_{AWG}:

$$s = e^{j(\omega_{RF})} \cdot BB_{AWG} \qquad \text{where } BB_{AWG} = I_{AWG} + jQ_{AWG} \tag{A.32}$$

Now we try to isolate the real and imaginary parts of BB_{AWG} – which will be the I and Q output signals of the AWG — as a function of the complex components of the starting baseband signals :

$$\forall k, \quad BB_k = I_k + jQ_k$$

Thus:

$$BB_{AWG} = \sum_{k=1}^{N} BB_k \cdot e^{j \cdot S_n(k)} \tag{A.33}$$

$$BB_{AWG} = \sum_{k=1}^{N} (I_k + jQ_k) \cdot (\cos(S_N(k)) + j \sin(S_N(k))) \tag{A.34}$$

The latter expressions lead to:

$$I_{AWG} = \sum_{k=1}^{N} I_k \cdot \cos(S_N(k)) - Q_k \cdot \sin(S_N(k)) \tag{A.35}$$

$$Q_{AWG} = \sum_{k=1}^{N} I_k \cdot \sin(S_N(k)) + Q_k \cdot \cos(S_N(k)) \tag{A.36}$$

By finally replacing with the expression of the sequence S_N, we get:

$$I_{AWG} = \sum_{k=1}^{N} I_k \cdot \cos\left(\Delta\omega_{RF} \cdot \left(\frac{N+1}{2} - k\right)\right) + Q_k \cdot \sin\left(\Delta\omega_{RF} \cdot \left(\frac{N+1}{2} - k\right)\right) \tag{A.37}$$

$$Q_{AWG} = \sum_{k=1}^{N} Q_k \cdot \cos\left(\Delta\omega_{RF} \cdot \left(\frac{N+1}{2} - k\right)\right) - I_k \cdot \sin\left(\Delta\omega_{RF} \cdot \left(\frac{N+1}{2} - k\right)\right) \tag{A.38}$$

3 carrier case

$$\begin{aligned} I_{AWG} &= I_1 \cdot \cos(\Delta\omega_{RF}) + Q_1 \cdot \cos(\Delta\omega_{RF}) && \text{(A.39)} \\ &\quad + I_2 && \text{(A.40)} \\ &\quad + I_3 \cdot \cos(\Delta\omega_{RF}) - Q_3 \cdot \cos(\Delta\omega_{RF}) && \text{(A.41)} \\ Q_{AWG} &= Q_1 \cdot \cos(\Delta\omega_{RF}) - I_1 \cdot \cos(\Delta\omega_{RF}) && \text{(A.42)} \\ &\quad + Q_2 && \text{(A.43)} \\ &\quad + Q_3 \cdot \cos(\Delta\omega_{RF}) + I_3 \cdot \cos(\Delta\omega_{RF}) && \text{(A.44)} \\ & && \text{(A.45)} \end{aligned}$$

A.3. Additional frequency shifting of the multiplex and the LO

A.3.1. Measurements and practical feedback

By generating[2] 3 UMTS carriers equally spaced by 10MHz and centered on $f_{LO} = 2140MHz$, the following Composite EVM values were measured:

[2] with a Rohde & Schwarz SMIQ03 VSG

- EVM @ $f_{LO} = 1.75\%$
- EVM @ $f_{LO-\Delta\omega} = 0.95\%$
- EVM @ $f_{LO+\Delta\omega} = 0.81\%$

This difference can be explained by a residual LO component remaining at the end of the mixing, and leaking into the central carrier since the LO's frequency corresponds to the frequency of the central UMTS carrrier.

The LO leakage, for an even number of generated carriers is located between the 2 central carriers of the multiplex. While for a odd number of generated carriers, the residual LO component is superimposed on the central generated carrier.

As a consequence of this we propose to generate a multiplex with a frequency offset from the LO which does the mixing.

Principle, interest and restrictions

The idea of this section is to generate a UMTS carrier multiplex which is no longer centered on the frequency of the LO which is used for the mixing. Instead the multiplex is set to have such a frequency offset[3] that its residual component does not fall into the band of interest. Furthermore, Band Pass Sampling (BPS) filters can attenuate the out-of-band residual LO component.

The association of Matlab and the AWG, actually allowed a over-sampling factor of 40 of the base-band signal. Hence the maximal frequency offset is:

$$1/2 \cdot 40 \cdot 3.84MHz = 76.8MHz$$

In case of a 3 carrier multiplex equally spaced by 10MHz, the LO and the *last* carrier can be spaced by 70MHz.

Concerning the Band I for UMTS FDD, the paired spectrum is 1920 to 1980MHz, and from 2110 to 2170MHz. If the LO is located in the frequency gap, 2090MHz for isntance, then 3 UMTS carriers can be located in the first half of the downlink band: 2120, 2130, and 2140MHz.

Synthesis of the offset multiplex

This time the LO carrier is offset by $\Delta\omega_{offset}$ from the central frequency – ω_1 – of the first channel . The n generated carriers are still equally spaced by $\Delta\omega$:

$$\omega_1 = \omega_{LO} + \Delta\omega_{offset} \qquad \forall n \geq 1, \quad \omega_n = (n-1) \cdot \Delta\omega + \omega_1 \tag{A.46}$$

[3]Again this frequency offset depends on the over-sampling factor – with respect to 3.84MHz – of the baseband channels, and of the IF bandwidth of the equipment which does the mixing

The synthesis of the final complex signal is as follows:

$$s = \sum_{k=1}^{N} r_k \cdot e^{j\cdot(\omega_k+\theta_k)} \tag{A.47}$$

$$= \sum_{k=1}^{N} BB_k \cdot e^{j\cdot\left(\omega_{LO}+\Delta\omega_{offset}+(k-1)\cdot\Delta\omega\right)} \tag{A.48}$$

$$= \underbrace{e^{j\omega_{LO}}}_{\text{RF-domain}} \cdot \underbrace{e^{j\Delta\omega_{offset}}}_{\text{IF}} \cdot \sum_{k=1}^{N} \underbrace{BB_k \cdot e^{j\cdot(k-1)\Delta\omega}}_{\text{Channel specific IF-domain multiplication}} \tag{A.49}$$

$$= \underbrace{e^{j(\omega_{LO}+\Delta\omega_{offset})}}_{\text{New LO in RF-domain}} \cdot \underbrace{\sum_{k=1}^{N} BB_k \cdot e^{j\cdot(k-1)\Delta\omega}}_{BB_{AWG}} \tag{A.50}$$

Let be

$$BB_{AWG} = I_{AWG} + jQ_{AWG} \qquad \text{and} \qquad \forall k, \quad BB_k = I_k + jQ_k$$

Finally we obtain:

$$I_{AWG} = \sum_{k=1}^{N} I_k \cdot \cos\left((k-1)\cdot\Delta\omega\right) - Q_k \cdot \sin\left((k-1)\cdot\Delta\omega\right) \tag{A.51}$$

$$Q_{AWG} = \sum_{k=1}^{N} I_k \cdot \sin\left((k-1)\cdot\Delta\omega\right) + Q_k \cdot \cos\left((k-1)\cdot\Delta\omega\right) \tag{A.52}$$

A.4. Matlab Code for 3GPP UMTS FDD Test Model 4 generation

The Test Model 4 is generated for a whole radio frame (10ms), however only one radio slot (1/15th of a radio frame) is over-sampled and sent to the AWG.

One radio slot is the frame length over which the Composite EVM according to 3GPP must be measured. Besides this requirement, the AWG has a limited memory depth when running in a looped generation mode, thus the whole radio frame cannot be generated. Furthermore by using a single radio slot, the over sampling factors can be maximized in order to exploit the memory depth of the AWG.

The 3GPP Test Model 4 is generated by Matlab using the following source code :

A.4.1. Main file

Listing A.1: ./code/3gpp_downlink/TestModel4.m

```
1 % ------------------------------------------------------------------
2 % Desciption     : 3GPP Base Station Test Model 4
3 % Author         : Florian FRANK
4 % Date of beginning : 08 jan. 2009
5 % To-Do List : x
6 % ------------------------------------------------------------------
7
8 clear all
```

```
close all
%% OPTIONS
% SIGNAL GENERATION
    do_SCRAMBLING = 1;
% DISPLAY
    do_FFT  = 1;
    dessins = 1;
% SAVING & AWG
    sauvegarde = 0 ;
    do_SAVETIME = 0 ;
    AWG_RF      = 0;
    AWG_IQ      = 0;
%% CHANNEL generation for a whole Frame at BIT or CHIP level
%CPICH
    PCPICH_frame = gen_PCPICH_frame();
%P-CCPCH : bit_level
    PCCPCH_frame = gen_PCCPCH_frame();
    %PCCPCH_frame = gen_PCCPCH_frame_LUT();
    %PCCPCH_frame = gen_PCCPCH_frame_PATTERN([ 0  1  0  ]);
    PCCPCH_frame = [2*ones(15,2) PCCPCH_frame]; %encoding DTX symbols
%P-SCH : chip level
    PSCH_frame = gen_PSCH_frame();
    %Since PCCPCH is ***NOT*** STTD () encoded :
    a = -1;
    PSCH_frame = a * PSCH_frame;
    %'0' padding after the 256 first chips
    PSCH_frame = [PSCH_frame  zeros(15, 2560-256)];
%S-SCH : chip_level
    scrambling_code_group = 0;
    SSCH_frame = gen_SSCH_frame(scrambling_code_group);
    % Since PCCPCH is ***NOT*** STTD encoded :
    a = -1;
    SSCH_frame = a * SSCH_frame;
    %'0' padding after the 256 first chips
    SSCH_frame = [SSCH_frame  zeros(15, 2560-256)];
%% SERRIAL to PARALLEL
%P-CPICH
    [PCPICH_frame_impair , PCPICH_frame_pair]= ser2par_frame(PCPICH_frame);
%P-CCPCH
    [PCCPCH_frame_impair , PCCPCH_frame_pair]= ser2par_frame(PCCPCH_frame);
%P-SCH
    % nothing to do
%S-SCH
    % nothing to do
%% MODULATION MAPPER
%P-CPICH
    PCPICH_frame_i = modulation_mapper('qpsk', PCPICH_frame_pair);
    PCPICH_frame_q = modulation_mapper('qpsk', PCPICH_frame_impair);
%P-CCPCH
    PCCPCH_frame_i = modulation_mapper('qpsk', PCCPCH_frame_pair);
    PCCPCH_frame_q = modulation_mapper('qpsk', PCCPCH_frame_impair);
%P-SCH
    % nothing to do
%S-SCH
```

```
63      % nothing to do
64  %% CHANELLISATION
65  %CPICH
66      SF_PCPICH = 256;
67      pcpich_ch_code = 0 ;
68      PCPICH_channel_code = OVSF(SF_PCPICH, pcpich_ch_code);
69      %frame channelisation : slot wise w/ the sme code
70      PCPICH_frame_channeled_i = channelisation(PCPICH_frame_i,
            PCPICH_channel_code);
71      PCPICH_frame_channeled_q = channelisation(PCPICH_frame_q,
            PCPICH_channel_code);
72  %P-CCPCH :15 x 18 = 270 P-CCPCH bits per frame
73      SF_PCCPCH = 256;
74      pccpch_ch_code = 1 ;
75      PCCPCH_channel_code = OVSF(SF_PCCPCH, pccpch_ch_code);
76      %frame channelisation : slot wise w/ the same code
77      PCCPCH_frame_channeled_i = channelisation(PCCPCH_frame_i,
            PCCPCH_channel_code);
78      PCCPCH_frame_channeled_q = channelisation(PCCPCH_frame_q,
            PCCPCH_channel_code);
79  %P-SCH
80      % nothing to do
81  %S-SCH
82      % nothing to do
83  %% COMPLEX SUMMING #1
84  %P-CPICH
85      PCPICH_frame_channeled_cpx = PCPICH_frame_channeled_i + j *
            PCPICH_frame_channeled_q;
86  %P-CCPCH
87      PCCPCH_frame_channeled_cpx = PCCPCH_frame_channeled_i + j *
            PCCPCH_frame_channeled_i;
88  %P-SCH
89      % nothing to do
90  %S-SCH
91      % nothing to do
92  %% SCRAMBLING
93  if do_SCRAMBLING == 1
94  %Primary Scrambling Code for whole Cell is: 0
95      n_S_dl = 0;
96      S_dl = scrambling_code_gen(n_S_dl);
97  %CPICH
98      PCPICH_frame_channeled_cpx_scr = scrambling(PCPICH_frame_channeled_cpx,
            S_dl);
99  %P-CCPCH
100     PCCPCH_frame_channeled_cpx_scr = scrambling(PCCPCH_frame_channeled_cpx,
            S_dl);
101 %P-SCH
102     % nothing to do
103 %S-SCH
104     % nothing to do
105 elseif do_SCRAMBLING == 0
106     PCPICH_frame_channeled_cpx_scr = PCPICH_frame_channeled_cpx;
107     PCCPCH_frame_channeled_cpx_scr = PCCPCH_frame_channeled_cpx;
108 end
```

```
109 %% COMPLEX SUMMING & WEIGHTING #2
110     factor1 = 1;
111     factor2 = 1;
112     factor3 = 1/2;
113     factor4 = 1/2;
114     T = factor1*PCPICH_frame_channeled_cpx_scr + factor2*
            PCCPCH_frame_channeled_cpx_scr + factor3*PSCH_frame + factor4*
            SSCH_frame;
115     % Weigthing
116     for k=1:15
117         power1_PCPICH(k,1:2560)      =  abs(factor1*
                PCPICH_frame_channeled_cpx_scr(k,:)) .^2;
118         power1_PCCPCH(k,1:2560)      = abs(factor2*
                PCCPCH_frame_channeled_cpx_scr(k,:)) .^2;
119         power1_PSCH(k,1:2560)        = abs(factor3*PSCH_frame(k,:)) .^2;
120         power1_SSCH(k,1:2560)        = abs(factor4*SSCH_frame(k,:)) .^2;
121         power1_BCH(k,1:2560)         = abs(factor3*PSCH_frame(k,:) + factor4
                *SSCH_frame(k,:)) .^2;
122         power1_T(k,1:2560)           = abs(T(k,:)) .^2;
123     end
124     pwr_slot1_0_PCPICH = sum(power1_PCPICH(1,:)) ;
125     pwr_slot1_1_PCPICH = sum(power1_PCPICH(1,1:256));
126     pwr_slot1_2_PCPICH = sum(power1_PCPICH(1,257:2560)) ;
127     pwr_slot1_PCCPCH = sum(power1_PCCPCH(1, 257:2560)) ;
128     pwr_slot1_PSCH = sum(power1_PSCH(1, 1:256)) ;
129     pwr_slot1_SSCH = sum(power1_SSCH(1, 1:256)) ;
130     pwr_slot1_BCH = sum(power1_BCH(1, 1:256)) ;
131 %% WHOLE FRAME RE-ASSEMBLY (slots alignement)
132     T2 = reshape(T.', 1, numel(T));
133     %T2 = T2( 1: 1*2560);
134 %% SPLITTING + SHAPING (still IF)
135     % Splitting
136     T2_real = real(T2);
137     T2_imag = imag(T2);
138     % RRC filter
139     f_chip = 3.84e6 ;
140     sequence_length = 32; %10
141     oversampling_factor = 10; %40
142     fs = f_chip * oversampling_factor ;
143     order = sequence_length * oversampling_factor;
144     f_cut = f_chip/2;%*1.22;
145     % Oversampling the 'T' files
146     T2_real_os = zeros(1, numel(T2_real)*oversampling_factor);
147     T2_imag_os = zeros(1, numel(T2_imag)*oversampling_factor);
148     % Filling & Reshaping
149     T2_real_os(1 : oversampling_factor : end) = T2_real(1:end);
150     T2_imag_os(1 : oversampling_factor : end) = T2_imag(1:end);
151     % Padding
152     padding_length = 1;%order - sequence_length;
153     T2_real_padded = [T2_real_os zeros(1,order*oversampling_factor)];
154     T2_imag_padded = [T2_imag_os zeros(1,order*oversampling_factor)];
155     % Chip Filter20
156     RRC = firrcos( order, f_cut, 0.22, fs, 'rolloff','sqrt');
157     %RRC = gen_rc0( order, 0.22, fs, f_chip);
```

```
158     filter_size = numel(RRC) ;
159     T2_real_padded_rrc = filter( RRC, 1, T2_real_padded);
160     T2_imag_padded_rrc = filter( RRC, 1, T2_imag_padded);
161     % Removing Padding at Beggining
162     T2_real_rrc = T2_real_padded_rrc(padding_length: end);%padding_length:
            end
163     T2_imag_rrc = T2_imag_padded_rrc(padding_length: end);%padding_length:
            end
164     T2 = T2_real_rrc + j*T2_imag_rrc;
165     %Final RC filtering
166     T3_real_rrc = filter( RRC, 1, T2_real_rrc);
167     T3_imag_rrc = filter( RRC, 1, T2_imag_rrc);
168 %% FFT
169     sig = T2_real_rrc + j*T2_imag_rrc;
170     n_fft = 2^nextpow2(numel(sig));
171 if do_FFT == 1
172     y = fft(sig, n_fft)/n_fft;
173     y = fftshift(y);
174     y_dB = 10*log10(abs(y).^2);
175     y_mean = mean(y_dB);
176     f_axis= (-n_fft/2:1: n_fft/2-1)*fs/n_fft *1/1e6;
177 end
178
179 %% AWG loading programs
180 if AWG_RF == 1
181     Load_into_AWG7102
182 elseif AWG_IQ == 1
183     FS_AWG = 400.0e6;
184     sig_I = T2_real_rrc(:)';
185     sig_Q = T2_imag_rrc(:)';
186     Load_into_AWG7102_IQ
187 end
188 %% APPENDIX
189
190 %% DATA SAVING
191 if sauvegarde == 1
192 points = 0 : (numel(T2_imag_rrc)-1);
193 time = points/(fs);
194 data1 = T2_real_rrc';
195 data2 = T2_imag_rrc';
196 if do_SAVETIME ==1
197     data1 = [time' data1];
198     data2 = [time' data2];
199 end
200 save('i_rrc.dat', 'data1', '-ASCII');
201 save('q_rrc.dat', 'data2', '-ASCII');
202 end
203 %% PLOTS SECTION
204 if dessins == 1
205     TestModel4_PLOTS
206 end
```

A.4.2. Individual Physical Channel

P-CPICH relative files

Listing A.2: ./code/3gpp_downlink/gen_PCPICH_frame.m

```
1  function frame = gen_PCPICH_frame(void)
2  % generates P-CPICH frame
3  N_bits = 20;
4  frame = zeros(15, N_bits);
```

P-CCCPCH relative files

Listing A.3: ./code/3gpp_downlink/gen_PCCPCH_frame.m

```
1  function res  = gen_PCCPCH_frame()
2  % returns the aggregate 15x18=270 P-CCPCH bits per frame
3  % which is filled with a PN9 sequence using the primitive
4  % trinomial x9+x4+1 ... seeded with the channel code Cch,256,1
5  % -- according to 3GPP 25.123 6.1.1.6.1 --
6  %% seed of register
7  chan_code = OVSF(256, 1);
8  seed = chan_code(1:8);
9  seed = [seed 1] ;
10 %% register
11 reg = zeros(1,9);
12 %#1 is LSB, #9 is MSB
13 reg = [1 ones(1,8)] ;
14 %% register shifting
15 out= zeros(1, 270);
16 for i = 1 : 18*15
17     %buf = xor(reg(4+1), reg(0+1));
18     buf = mod(sum([reg(4+1),reg(0+1)]),2);
19     out(i) = reg(1);
20     reg(1:8)=reg(2:9);
21     reg(8+1)= buf ;
22 end
23 %% only 270 bits per frame are needed !
24 res = out(1:end);
25 res = reshape(res, 18, 15);
26 res = res';
```

P-SCH relative files

Listing A.4: ./code/3gpp_downlink/gen_PSCH_frame.m

```
1  function frame = gen_PSCH_frame()
2  %generates the Primary SCH : 256 chips
3      buf = ones(15, 1);
4      frame = buf * psc_code_gen();
```

Listing A.5: ./code/3gpp_downlink/psc_code_gen.m

```
function code = psc_code_gen()
% generates a Primary Synchronisation Code for P-SCH

% a is common to PSC and SSC
a = [1 1 1 1 1 1 -1 -1 1 -1 1 -1 1 -1 -1 1];
% PSC:: C_psc(1) is the fist chip to be transmitted in time
code = (1+j)*horzcat(a, a, a, -a, -a, a, -a, -a, a, a, a, -a, a, -a, a, a);
```

S-SCH relative files

Listing A.6: ./code/3gpp_downlink/gen_SSCH_frame.m

```
function frame_out = gen_SSCH_frame(scrambling_code_group)
% Returns Secondary SCH (S-SCH) in frame format
% frame format is a 15 rows (slots) x 256 column (Chips) matrix
    frame_out = zeros(15, 256);
    for slot_number = 0:14
        ssc_code_number = ssc_allocation(scrambling_code_group, slot_number
            );
        frame_out(slot_number+1, :) = ssc_code_gen(ssc_code_number);
    end
```

Listing A.7: ./code/3gpp_downlink/ssc_allocation.m

```
function ssc_code_number = ssc_allocation(scrambling_code_group,
    slot_number)
% gives the 'SSC Code' for 'Secondary SCH' to be used according to the
    provided
% 'Scrambling Code Group' and actual 'Slot Number'.
% 'Slot Numbers' goes from 0 to 14
% 'Scrambling Code Group' goes from 0 to 63
allocation_table = zeros(1,15) ;
% following LUT should be placed in a file
% only first 2 lines are defined for the moment :
allocation_table(1, :) = [1 1 2  8 9 10 15  8 10 16 2  7 15  7 16];
allocation_table(2, :) = [1 1 5 16 7  3 14 16  3 10 5 12 14 12 10];

% output

ssc_code_number = allocation_table(scrambling_code_group+1, slot_number+1);
```

Listing A.8: ./code/3gpp_downlink/ssc_code_gen.m

```
function code = ssc_code_gen(code_number)
% 'Code Number' goes from 1 to 16

%% SSC
    k = code_number ;
    % a is common to PSC and SSC
    a = [1 1 1 1 1 1 -1 -1 1 -1 1 -1 1 -1 -1 1];
    % b is build from a
    b(1:8) = a(1:8);
```

```
10      b(9:16)= - a(9:16);
11      z = horzcat( b, b, b, -b, b, b, -b, -b, b, -b, b, -b, -b, -b, -b, -b);
12      H8 = hadamard(2^8);
13      %line #k represents k:th code of C_ssc
14      m = 16*(k-1);
15      code = (1+j) * H8(m +1 , :).*z ;
```

A.4.3. Common processes

Modulation mapper

Listing A.9: ./code/3gpp_downlink/modulation_mapper.m

```
1  function frame_out = modulation_mapper(type, frame_in)
2  % Applies ModulationMapper to a Frame
3  % Works line-wise (ie. slot-wise) on frame_in using modulation_mapper_core
4  % Associates '0' binary  to 1.0 real value
5  % Associates '1' binary  to -1.0 real value
6  % Associates 'DTX' binary  to 0.0 real value
7  % -- According to 3GPP TS.25213 paragraph 5.1.1 --
8
9  taille = size(frame_in);
10 lignes = taille(1);
11 frame_out = zeros( taille(1), taille(2));
12 % line-wise modulation_mapper
13 for i = 1 : lignes
14         frame_out(i,:) = modulation_mapper_core(type, frame_in(i,:) );
15 end
```

Listing A.10: ./code/3gpp_downlink/modulation_mapper_core.m

```
1  function res = modulation_mapper_core(type, input)
2  % Associates '0' binary  to 1.0 real value
3  % Associates '1' binary  to -1.0 real value
4  % Associates 'DTX' binary  to 0.0 real value
5  % -- According to 3GPP TS.25213 paragraph 5.1.1 --
6  if type ='qpsk'
7      res = zeros(1, length(input));
8      for i=1:length(input)
9          buf =input(i);
10         if buf == 0
11             res(i) = 1.0;
12         elseif buf == 1
13             res(i) = -1.0;
14         elseif input == 2 % DTX is coded '2' within the bit sequence
15             res(i) = 0.0;
16         end
17     end
18 end
```

Channelization

Listing A.11: ./code/3gpp_downlink/OVSF.m

```
function res = OVSF(N, m)
% Returns m^th Orthogonal Variable Spreading Factor (OVSF) of length N
% Ex : OVSF(256, 0) returns SF Code #0 of SpreadingLength =256
% For 3GPP
k=round(log(N)/log(2)) ;
temp = 1;
for i=1:k
    if k==0
        temp = OVSF_core(2^i, 1);
    else
        temp = OVSF_core(2^i, temp);
    end
end
res = temp(m+1, :) ;
```

Listing A.12: ./code/3gpp_downlink/channelisation.m

```
function res = channelisation(frame, channel_code)
% channelizes each LINE of the provided frame (Matrix) with the
    channel_code
% frame : data MATRIX to be channelized
% code  : channelizarion code to be used
taille = size(frame);
lignes = taille(1);
frame_channeled = zeros( lignes, taille(2)*length(channel_code));

for i = 1 : lignes
        frame_channeled(i,:) = channelisation_core(frame(i,:), channel_code
            );
end

res = frame_channeled;
```

Listing A.13: ./code/3gpp_downlink/channelisation_core.m

```
function res = channelisation_core(input, code)
% input : data VECTOR to be channelized
% code  : channelizarion code to be used
len_input=length(input);
len_code=length(code);
res = zeros(1, len_input*len_code);
for i=1:len_input
    res(1+len_code*(i-1):len_code*i)= input(i)*code;
end
```

Scrambling

Listing A.14: ./code/3gpp_downlink/scrambling_code_gen.m

```
function code = scrambling_code_gen2(n)
% generates the n:th Scrambling Code 'normally' compliant with 3GPP TS
% 25.213 V8.3.0, where n = 0 .. 262 142(=2^18-1);
```

```
4
5  %% INIT
6  N = 2^18 -20 +1 ;
7  % creating registers
8  x_reg = zeros(1, 18);
9  y_reg = zeros(1, 18);
10 % creating init vectors
11 x_init = [1 zeros(1,17)];
12 y_init = ones(1, 18);
13 % loading init vectors
14 x_reg = x_init;
15 y_reg = y_init;
16 % allocating output vectors
17 x_out = zeros(1, N);
18 y_out = zeros(1, N);
19 %% MAIN LOOP
20 for k = 1 : (N+18)  % +18 for emptying the registers
21     % operations on x vector
22         %XOR #0 : LFSR
23         buf_0 = xor(x_reg(1), x_reg(8));
24         %XOR #2 : GOLD
25         buf_2 = xor(xor( x_reg(5), x_reg(7)), x_reg(16));
26         %XOR #4
27         buf_4 = xor(x_reg(1), y_reg(1));
28     % operations on y vector
29         %XOR #1 : LFSR
30         buf_1 = mod(sum([y_reg(1) y_reg(6) y_reg(8)  y_reg(11)]), 2);
31         %XOR #3 : GOLD
32         %buf_3 = xor( xor(xor( xor( xor( xor( xor( xor( y_reg(16),
               y_reg(15)), y_reg(14)), y_reg(13)), y_reg(12)), y_reg(11)),
               y_reg(10)), y_reg(9)), y_reg(7)), y_reg(6));
33         buf_3 = mod(sum([y_reg(16) y_reg(15) y_reg(14) y_reg(13) y_reg(12)
               y_reg(11) y_reg(10) y_reg(9) y_reg(7) y_reg(6)]), 2);
34         %XOR #5
35         buf_5 = xor(buf_2, buf_3);
36     % shifting registers
37         x_out(k) = buf_4;
38         y_out(k) = buf_5;
39         x_reg(1:17) = x_reg(2:18);
40         x_reg(18) = buf_0;
41         y_reg(1:17) = y_reg(2:18);
42         y_reg(18) = buf_1;
43 end
44 %% Final Complex Scrambling Code
45 code = x_out(1, 1:38399+1)+j*y_out(1, 1:38399+1);
46 %Zero Centering since x_out and y_out are 'bits' : passing from bits to
47 %polar
48 code = code - 0.5*(1+j);
```

Listing A.15: ./code/3gpp_downlink/scrambling.m

```
1  function frame_out = scrambling(frame_in, code)
2  % Applies the provided Scrambling Code to the whole frame
3  % works slot-wise on 'frame_in'
4  taille = size(frame_in);
```

```
5 lignes = taille(1);
6 frame_out = zeros(taille(1), taille(2));
7 for k=1:lignes
8     frame_out(k, :) = scrambling_core(frame_in(k, :), code(1 + 2560*(k-1):
          2560*k) ) ;
9 end
```

Listing A.16: ./code/3gpp_downlink/scrambling_core.m

```
1 function vector_out = scrambling_core(vector_in, code)
2 % Applies the provided Scrambling Code to the input vector
3 % Scrambling is a Complex scalar multiplication
4 vector_out = zeros(1, length(vector_in));
5 if length(vector_in) == length(code)
6     vector_out = vector_in.*code;
7 end
```

A.4.4. Multi-carrier generation (with loading into the AWG)

Listing A.17: ./code/3gpp_downlink/Load_into_AWG7102_IQ.m

```
1  directory_Local = 'C:\matlab_temp\';
2  filename_param = '3GPP_TestMod_4_PARAM_IN.mat';
3  filename_IN_I = '3GPPP_TestMod_4_SIGNAL_IN_I.mat';
4  filename_IN_Q = '3GPPP_TestMod_4_SIGNAL_IN_Q.mat';
5  filename_i = [directory_Local,'\',filename_IN_I];
6  filename_q = [directory_Local,'\',filename_IN_Q];
7
8  resample = 'freq';
9
10 multi_channel = 0;
11 ch_idx = [1 1 1 ];
12 method = 1;
13 %% MULTI-CHANNEL GENERATION
14
15 if multi_channel == 1
16     sig_I1 = sig_I;      sig_Q1 = sig_Q;
17     sig_I2 = sig_I;      sig_Q2 = sig_Q;
18     sig_I3 = sig_I;      sig_Q3 = sig_Q;
19     delta_freq = 5.0e6;              %freq. spacing
20     points = 0: numel(sig_I)-1;      %
21     time = points / fs;              %time vector
22     if method == 1 % LO is centered among the channels, even may overlay
23         cos_1 = cos(-2*pi*time* delta_freq* ((3+1)/2 - 1));
24         sin_1 = sin(-2*pi*time* delta_freq* ((3+1)/2 - 1));
25         cos_2 = cos(-2*pi*time* delta_freq* ((3+1)/2 - 2));
26         sin_2 = sin(-2*pi*time* delta_freq* ((3+1)/2 - 2));
27         cos_3 = cos(-2*pi*time* delta_freq* ((3+1)/2 - 3));
28         sin_3 = sin(-2*pi*time* delta_freq* ((3+1)/2 - 3));
29     elseif method == 2 % LO is spaced delta_offset from the channels, the
           latter being delta_freq spaced.
30         delta_offset = 20.0e6;
31         cos_1 = cos(2*pi*time* (delta_freq* 1 + delta_offset));
```

```
32          sin_1 = sin(2*pi*time* (delta_freq* 1 + delta_offset));
33          cos_2 = cos(2*pi*time* (delta_freq* 2 + delta_offset));
34          sin_2 = sin(2*pi*time* (delta_freq* 2 + delta_offset));
35          cos_3 = cos(2*pi*time* (delta_freq* 3 + delta_offset));
36          sin_3 = sin(2*pi*time* (delta_freq* 3 + delta_offset));
37      end
38       % I_AWG, Q_AWG definition.
39      I_AWG = (sig_I1.*cos_1   -  sig_Q1.*sin_1)*ch_idx(1) + (sig_I2.*cos_2
              -  sig_Q2.*sin_2)*ch_idx(2) + (sig_I3.*cos_3   -  sig_Q3.*sin_3)*
            ch_idx(3);
40      Q_AWG = (sig_I1.*sin_1   +  sig_Q1.*cos_1)*ch_idx(1) + (sig_I2.*sin_2
              +  sig_Q2.*cos_2)*ch_idx(2) + (sig_I3.*sin_3   +  sig_Q3.*cos_3)*
            ch_idx(3);
41      % Assignement
42      sig_I = I_AWG;
43      sig_Q = Q_AWG;
44  end
45  %% INPTERPOLATION section
46  if resample == 'freq'
47  %% Resampling in the  freq domain from intial 'fs' to 'FS_AWG'
48          n_fft = (numel(sig_I));
49          FS = fs;
50          NZ0 = 2^nextpow2(n_fft*FS_AWG/FS);
51          FS_AWG = FS * NZ0/n_fft;
52          sig_I = interpft(sig_I,NZ0);
53          sig_Q = interpft(sig_Q,NZ0);
54          n_fft = NZ0;
55          dt = 1/FS_AWG;
56          t = (0:(NZ0-1)) *dt;
57          fmax = 1/dt;
58          df = 1/(n_fft*dt);
59          f = (-fmax/2):df:(fmax/2-df);
60      % Compensate for Sinc response
61          sig_I = fftshift(fft(sig_I));
62          sig_I = sig_I./ sinc(f/FS_AWG);
63          sig_I = ifft(ifftshift(sig_I));
64
65          sig_Q = fftshift(fft(sig_Q));
66          sig_Q = sig_Q./ sinc(f/FS_AWG);
67          sig_Q = ifft(ifftshift(sig_Q));
68      % Set the max excursion
69          max_sig_I    = max(abs(sig_I)) ;
70          sig_I        = sig_I / max_sig_I/2   ;
71          max_sig_Q    = max(abs(sig_Q)) ;
72          sig_Q        = sig_Q / max_sig_Q/2   ;
73
74      disp(['IF I Power = ',num2str(10*log10(std(sig_I).^2 / 50)),' dBm'])
75      disp(['IF Q Power = ',num2str(10*log10(std(sig_Q).^2 / 50)),' dBm'])
76      % Time offset on I or Q
77      %sig_Q = circshift(sig_Q,[0 20]);
78  %% Resampling in the TIME domain
79  elseif resample == 'time'
80          FS = fs;
81      % new time defintion
```

```
82          points_old = 0: numel(sig_I)-1;
83          time_old = points_old /fs ;
84          points_new = 0: (ceil(FS_AWG/fs)*numel(sig_I)-1);
85          time_new = points_new / FS_AWG;
86          sig_I = interp1(time_old, sig_I, time_new, 'spline');
87          sig_Q = interp1(time_old, sig_Q, time_new, 'spline');
88      % Compensate for Sinc response
89          n_fft = 2^nextpow2(numel(sig_I));
90          fmax = FS_AWG;
91          dt = 1/FS_AWG;
92          df = 1/(n_fft*dt);
93          f = linspace(-fmax/2, fmax/2-df , numel(sig_I));
94          sig_I = fftshift(fft(sig_I));
95          sig_I = sig_I./ sinc(f/FS_AWG);
96          sig_I = ifft(ifftshift(sig_I));
97          sig_Q = fftshift(fft(sig_Q));
98          sig_Q = sig_Q./ sinc(f/FS_AWG);
99          sig_Q = ifft(ifftshift(sig_Q));
100         n_fft = numel(sig_I);
101     % Set the max excursion
102         max_sig_I   = max(abs(sig_I)) ;
103         sig_I       = sig_I / max_sig_I/2  ;
104         max_sig_Q   = max(abs(sig_Q)) ;
105         sig_Q       = sig_Q / max_sig_Q/2  ;
106 end
107 %% Save the signal:
108 directory_Local = 'C:\matlab_temp\';
109 %directory = pwd ;
110 filename_param = '3GPP_TestMod_4_PARAM_IN.mat';
111 filename_IN_I = '3GPPP_TestMod_4_SIGNAL_IN_I.mat';
112 filename_IN_Q = '3GPPP_TestMod_4_SIGNAL_IN_Q.mat';
113 filename_i = [directory_Local,'\',filename_IN_I];
114 filename_q = [directory_Local,'\',filename_IN_Q];
115 disp(['Saving to ',filename_i,' and ', filename_q]);
116 Rec_Length = n_fft;
117 Sampl_Rate = FS_AWG;
118 sig_3GPP_i = sig_I;
119 sig_3GPP_q = sig_Q;
120 save(filename_i,'Rec_Length','Sampl_Rate','sig_3GPP_i');
121 save(filename_q,'Rec_Length','Sampl_Rate','sig_3GPP_q');
122
123 % write the parameter file:
124 filename = [directory_Local,'\',filename_param];
125 disp(['Saving to ',filename]);
126 save(filename,'FS','FS_AWG');
127
128 %% Read the files:
129 filename = [directory_Local,'\',filename_param];
130 disp(filename);
131 load(filename);
132 filename = [directory_Local,'\',filename_IN_I];
133 disp(filename);
134 load(filename);
135 n_fft = Rec_Length;
```

```
136 FS_AWG = Sampl_Rate;
137
138 % Delay Q wrt I
139 % OFDM_Signal = real(OFDM_Signal)+ i*circshift(imag(OFDM_Signal),[0 10]);
140
141 % Must have a n_fft multiple of four.
142 n_fft = floor(n_fft/4)*4;
143 NFFT = n_fft;
144 %% Write the WFM files:
145 % For the I component
146 disp('Start conversion to WFM (I)');
147
148 filename_I = [directory_Local,'\',filename_IN_I(1:(max(find(filename_IN_I==
        '.')-1))),'_I.wfm'];
149 fid = fopen(filename_I,'w');
150 tmp = sprintf('%d',5*n_fft);
151 fprintf(fid,'MAGIC 1000\r\n#%d%s',length(tmp),tmp);
152 markerCount = 0;
153 NZPS = 0;
154 markerCountMax = (NFFT+NZPS)*FS_AWG/FS;
155 for i_fft = 1:n_fft
156     fwrite(fid, sig_3GPP_i(i_fft),'float32');
157     % fwrite(fid,0,'uint8');
158     if (markerCount < markerCountMax)
159         fwrite(fid,1,'uint8');
160     else
161         fwrite (fid,0,'uint8');
162     end
163     markerCount = markerCount + 1;
164 end
165 clk_str = sprintf('CLOCK %12.10e\r\n',FS_AWG);
166 clk_str = strrep(clk_str,'e+0','e+');
167 fprintf(fid,'%s',clk_str);
168 err = fclose(fid);
169 % For the Q component
170 disp('Start conversion to WFM (Q)');
171 filename_Q = [directory_Local,'\',filename_IN_Q(1:(max(find(filename_IN_Q==
        '.')-1))),'_Q.wfm'];
172 fid = fopen(filename_Q,'w');
173 tmp = sprintf('%d',5*n_fft);
174 fprintf(fid,'MAGIC 1000\r\n#%d%s',length(tmp),tmp);
175 markerCount = 0;
176 markerCountMax = (NFFT+NZPS)*FS_AWG/FS;
177 for i_fft = 1:n_fft
178     fwrite(fid, sig_3GPP_q(i_fft),'float32');
179     % fwrite(fid,0,'uint8');
180     if (markerCount < markerCountMax)
181         fwrite(fid,1,'uint8');
182     else
183         fwrite (fid,0,'uint8');
184     end
185     markerCount = markerCount + 1;
186 end
187 clk_str = sprintf('CLOCK %12.10e\r\n',FS_AWG);
```

```
188 clk_str = strrep(clk_str,'e+0','e+');
189 fprintf(fid,'%s',clk_str);
190 err = fclose(fid);
191
192 % FTP the file onto the AWG7102:
193 disp('Start FTP')
194 g = ftp('10.193.66.250','anonymous','')
195 mput(g,filename_I)
196 mput(g,filename_Q)
197 close(g)
198
199 % Load the file and set the clock:
200 disp('Start Configuring AWG')
201 g = tcpip('10.193.66.221',4000)
202 fopen(g)
203 % Command = ['MMEM:IMP "CH1WFM","',root_filename,'.wfm",WFM'];
204 % fprintf(g,sprintf(':SOUR:FREQ:CW %.10E\n',FS_AWG))
205 Command = [':SOUR1:FUNC:USER "',filename_IN_I(1:(max(find(filename_IN_I=='
      ')-1))),'_I.wfm"\n'];
206 fprintf(g,Command)
207 Command = [':SOUR2:FUNC:USER "',filename_IN_Q(1:(max(find(filename_IN_Q=='
      ')-1))),'_Q.wfm"\n'];
208 fprintf(g,Command)
209 fclose(g)
210 delete(g);
211 clear g;
```

B. SEM issues for WiMAX

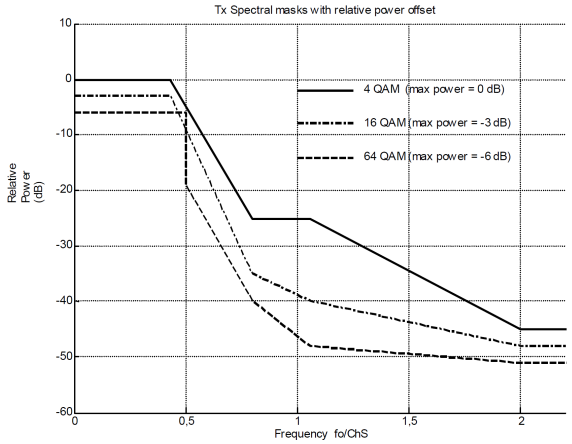

(a)

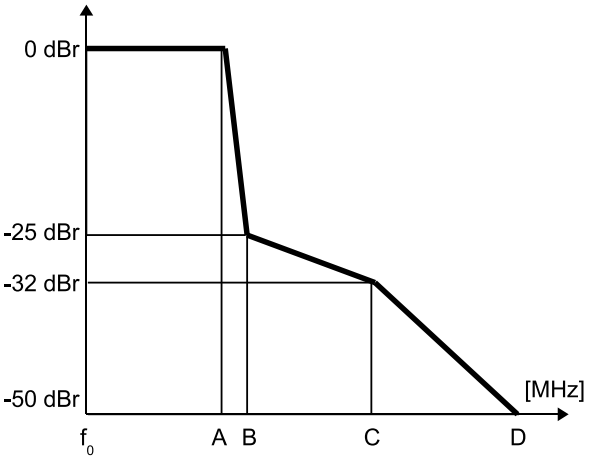

(b)

Figure B.1.: (a) ETSI spectral specifications for emission [124, p. 61/70]; (b) Unlicensed spectrum in the USA: WiMAX spectral mask

Table B.1.: Unlicensed spectrum in the USA: WiMAX spectral limits

Channelization (Mhz)	A	B	C	D
20	9.5	10.9	19.5	29.5
10	4.75	5.45	9.75	14.75

C. Laser conversion slope

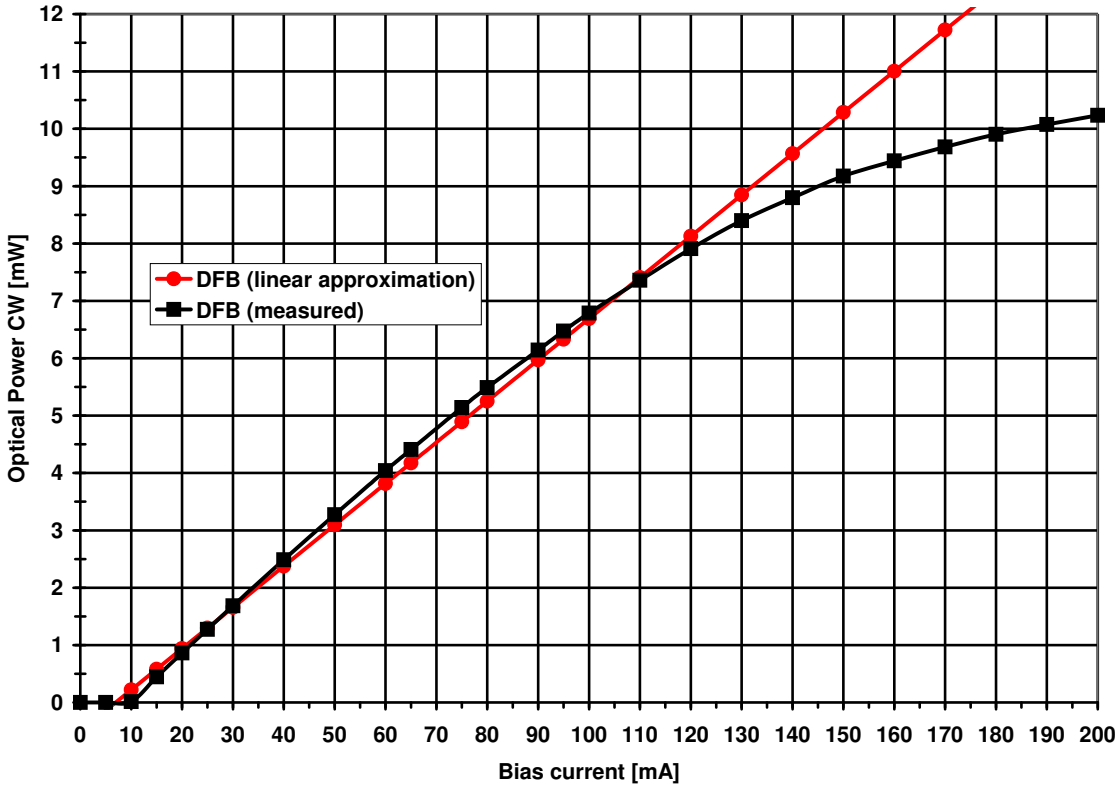

Figure C.1.: Static conversion curve of the NEL laser diode (1551nm)

D. Chromatic dispersion induced distortions

The purpose of this chapter is to provide some analytical elements developed in [113, 114] of how the chromatic dispersion [1] of the optical fiber interacts with the optical source's chirp.

D.1. Single tone case

[113] used Fourier Series decompositions of the optical and electrical fields in order to show, for a single-tone signal, the harmonic distortions resulting of the chromatic dispersion of the optical fiber interacting with the chirp of the optical source.

D.1.1. Analysis of the initial spectrum

Since for Intensity Modulation (IM), the normalized amplitude of the modulated light varying as the square root of the modulating signal, can be written as:

$$e = \underbrace{(1 + m_i \cdot \cos(\omega_m t))^{1/2}}_{\text{IM term}} \underbrace{\exp\left[j\left(\omega_0 t + m_f \sin(\omega_m t)\right)\right]}_{FM\ term} \tag{D.1}$$

where m_i is the intensity modulation index, ω_m the pulsation of the modulating signal, and m_f the frequency modulation index linked to the chirp.

Since we are interested in the spectral behavior of the signal, Fourier Series can be used, to decompose the elements of Eq. D.1 as follows.

Amplitude function

The amplitude term can be expended as:

$$(1 + m_i * \cos(\omega_m t))^{1/2} = K_0 + K_1 \cos(\omega_m t) + K_2 \cos(\omega_m t) + \cdots \tag{D.2}$$

FM Term

Using the Bessel functions of first kind, and the following identity:

$$\exp(x \sin\theta) = J_0(x) + 2\sum_{k=1}^{+\infty} J_k(x)\left[e^{jk\theta} + (-1)^n e^{-jk\theta}\right] \tag{D.3}$$

[1] often the considered impairment only translates the RF power loss which is governed by $P_{RF} \propto \cos^2\left(\pi \cdot c \cdot L \cdot D\left(\frac{f_{mm}}{f_{0\ opt}}\right)^2\right)$ where L is the transmission length, D the dispersion parameter, c the light's velocity, f_{mm} and $f_{0\ opt}$ are respectively the modulating and optical carrier frequencies.

The frequency modulating (*chirp*) term can be decomposed in spectral components by grouping the around the side-bands as:

$$J_0(m_f)\exp(j\omega_0 t) + \sum_{k=1}^{+\infty} J_k(m_f)\left[e^{j(\omega_0+k\omega_m)t} + (-1)^n e^{j(\omega_0-k\omega_m)t}\right] \tag{D.4}$$

Combined spectrum

By multiplying the Fourier series expansions of Eq. D.2 and Eq. D.4, and by collecting the frequency like terms, the optical electrical field can be expressed as:

$$\begin{aligned} e_{in} = {} & L_0 e^{j\omega_0 t} \\ & + L_{1+} e^{j[(\omega_0+\omega_m)t]} + L_{2+} e^{j[(\omega_0+2\omega_m)t]} + \cdots \\ & + L_{1-} e^{j[(\omega_0-\omega_m)t]} + L_{2-} e^{j[(\omega_0-2\omega_m)t]} + \cdots \end{aligned}$$

D.1.2. Phase changes due to the chromatic dispersion

"The relationship between phase and arrival time of each frequency component is used to determine the effects of chromatic dispersion on the modulated signal", [113].

The phase of a **single optical frequency component** propagating through the fiber is:

$$\theta = \beta \cdot z \tag{D.5}$$

where β is the propagation constant and z is the distance traveled. β can be expanded using a the Taylor series, then

$$\theta = z\cdot\beta(\omega_0) + z\cdot\frac{\partial\beta}{\partial\omega}\Big|_{\omega=\omega_0}\cdot(\omega-\omega_0) + \frac{z}{2}\cdot\frac{\partial^2\beta}{\partial\omega^2}\Big|_{\omega=\omega_0}\cdot(\omega-\omega_0)^2 + \cdots \tag{D.6}$$

$$\theta = z\cdot\beta_0 + z\cdot\beta_1\cdot(\omega-\omega_0) + z\cdot\beta_2\cdot(\omega-\omega_0)^2 + \cdots \tag{D.7}$$

where ω is the optical radian frequency, and ω_0 the central component of the optical spectrum of the optical carrier.

The time required (group delay) to travel the distance z by the signal is:

$$T = z\cdot\frac{\partial\beta}{\partial\omega}\Big|_{\omega_0} \tag{D.8}$$

According to the previous equations:

$$T = \underbrace{z\cdot\beta_1}_{\text{constant delay}} + \underbrace{z\cdot\beta_2\cdot(\omega-\omega_0)}_{\text{assumed dominant}} + \underbrace{\frac{z}{2}\cdot\beta_3\cdot(\omega-\omega_0)^2}_{\text{third order}} + \cdots \tag{D.9}$$

if not operating at or close to the zero dispersion wavelength, the second order term dominates the group delay while the first order is constant delay, and the third order term dominates system performance near zero dispersion point is not taken into account.

Finally,

$$T = z\cdot\beta_2\cdot(\omega-\omega_0) \tag{D.10}$$

Chromatic dispersion is the derivate of T with respect to wavelength, since:

$$\omega = 2\pi c/\lambda \tag{D.11}$$

where c is the velocity of light in free space.

Since chromatic dispersion is normalized to kilometer lengths of fiber:

$$D = \frac{1}{z} \cdot \frac{dT}{d\lambda} = (-\omega/\lambda)\beta_2 \tag{D.12}$$

D is expressed in $ps/(nm \cdot km)$, λ in nm, and ω in $radian/s$.

Neglecting the constant phase and the constant delay, and higher order terms, the phase angle θ is:

$$\theta = \left(z\frac{\lambda_0}{2\omega_0}\right) D\left(\omega - \omega_0\right)^2 = \left(-z\frac{\lambda_0^2}{4\pi c}\right) D\left(\omega - \omega_0\right)^2 \tag{D.13}$$

When evaluating θ at the optical carrier, and the sidebands:

$$\theta = \begin{cases} 0, & \\ \left(-z\dfrac{\lambda_0}{2\omega_0}\right) D\omega_m^2, & \text{first sidebands, } \omega_0 \pm \omega_m \\ \left(-z\dfrac{\lambda_0}{2\omega_0}\right) Dn^2\omega_m^2, & \text{other sidebands, } \omega_0 \pm n\omega_m \end{cases} \tag{D.14}$$

According to the last equation, the region where the first order chromatic dispersion dominates, the phase difference between any frequency component and the optical carrier varies as the square of the frequency separation ($\pm n\omega_m$).

If θ_1 is the phase of the first upper sideband (θ evaluated at $\omega = \omega_0 + \omega_m$, then the phase of any sideband, either upper or lower is,

$$\theta_n = n^2\theta_1$$

θ_1 is illustrated in Fig. D.1.

D.1.3. Optical signal leaving the fiber

Due to the phase change (θ_n) in the optical fiber, the optical field evolves from Eq. D.1.1 to:

$$\begin{aligned} e_{out} = {} & L_0 e^{j\omega_0 t} \\ & + L_{1+} e^{j[(\omega_0+\omega_m)t+\theta_1]} + L_{2+} e^{j[(\omega_0+2\omega_m)t+4\theta_1]} + \cdots \\ & + L_{1-} e^{j[(\omega_0-\omega_m)t+\theta_1]} + L_{2-} e^{j[(\omega_0-2\omega_m)t+4\theta_1]} + \cdots \end{aligned} \tag{D.15}$$

At this stage, it can be said that in the absence of FM (chirp) the spectrum exhibits even symmetry around the optical carrier. The FM term introduces odd symmetry about the optical carrier for the odd sidebands, and even symmetry around the even sidebands. Yet the combined spectrum has lost its symmetry, the latter aspect has an effect on the on the dispersion induced harmonic dispersion.

Figure D.1.: Phase angle (θ_1) as a function of frequency for different fiber lengths (dispersion: 17ps/nm/km) at 1551nm

D.1.4. Detected optical signal

Many high-order sidebands are produced by the nonlinear modulation of the electric (optical) field and by the chirp. If during the transmission there is no dispersion, then all **sideband signals maintain** their proper **relative phases**, even in the presence of source FM (chirp).

Yet in presence of dispersion, the sidebands arrive with relative phase delays for different frequencies after transmission and are no longer proportional.

Upon square-law detection, the original waveforms are recovered without any distortion.

The detected current is the square of the optical wave's module:

$$i = \left| e_{out} \right|^2 \tag{D.16}$$

After trigonometric expansions and gathering of Eq. D.16 using Eq. D.15, the recovered modulating signal (*i.e.* fundamental) can be separated into an in-phase and quadrature component as follows:

$$\begin{aligned} &2\left\{\sum_{n=0}^{\infty}\left[L_{n^+}L_{(n+1)^+}+L_{n^-}L_{(n+1)^-}\right]\cdot\cos\left(2n+1\right)\theta_1\right\}\cos\omega_m t \\ &-2\left\{\sum_{n=0}^{\infty}\left[L_{n^+}L_{(n+1)^+}+L_{n^-}L_{(n+1)^-}\right]\cdot\sin\left(2n+1\right)\theta_1\right\}\sin\omega_m t \end{aligned} \tag{D.17}$$

The presence of the quadrature term is a necessary although not sufficient condition for baseband phase distortion. If the modulated optical spectrum is exhibits even symmetry about the optical carrier (no FM (chirp)), or if there is no chromatic dispersion ($\theta_1 = 0$), then the quadrature term is zero and there can be no phase distortion.

Similarly to Eq. D.17, the second and third order harmonics can be recovered and formally expressed:

$$\begin{aligned} &2\left\{L_{1^+}L_{1^-}-\sum_{n=0}^{\infty}\left[L_{n^+}L_{(n+2)^+}+L_{n^-}L_{(n+2)^-}\right]\cdot\cos 4\left(n+1\right)\theta_1\right\}\cos 2\omega_m t \\ &-2\left\{\sum_{n=0}^{\infty}\left[L_{n^+}L_{(n+2)^+}-L_{n^-}L_{(n+2)^-}\right]\cdot\sin 4\left(n+1\right)\theta_1\right\}\sin 2\omega_m t \end{aligned} \tag{D.18}$$

$$\begin{aligned} &2\left\{\sum_{n=0}^{\infty}\left[L_{(n-1)^+}L_{(n+2)^+}+L_{(n-1)^-}L_{(n+2)^-}\right]\cdot\cos 3\left(2n+1\right)\theta_1\right\}\cos 3\omega_m t \\ &-2\left\{\sum_{n=0}^{\infty}\left[L_{(n-1)^+}L_{(n+2)^+}-L_{(n-1)^-}L_{(n+2)^-}\right]\cdot\sin 3\left(2n+1\right)\theta_1\right\}\sin 3\omega_m t \end{aligned} \tag{D.19}$$

Without FM

Again in Eq. D.18 and D.19, even symmetry in the optical spectrum eleminates the quadrature terms, thus reducing harmonic distortion.

According to [113], the amplitude of the second and third harmonics increase as the square of θ_1. The second harmonic increases linearly with m_i but the third harmonic increases as the square of m_i.

At low values of θ_1 the third harmonic is much less than the second harmonic but increases rapidly with m_i and is greater than the second when $m_i > 0.8$.

With FM

Adding a small level of FM causes a large increase (due to the quadrature term in Eq. D.18 caused by FM induced spectral asymmetry) in the second harmonic. The second harmonic linearly increases proportional with m_f and θ_1.

Yet for the third harmonic a small level of FM causes a small increase. However the increase if proportional to the square of both m_f and θ_1. As a result of this, the third harmonic increases rapidly with m_f and θ_1 and soon reaches the level of the second harmonic. Thus for large values of m_f and θ_1, the third harmonic distortion becomes an important issue.

D.2. Dual-tone case

[114] re-used the Fourier Series decomposition method of [113] by applying it to a two-tone signal. The latter aspects opens the possibility of considering third-order inter-modulation distortions.

D.2.1. Harmonic distortions

The electrical field of the modulated optical wave

$$e = \left[1 + m_i \cos\left(\omega_m t\right)\right]^{1/2} \sqrt{2} \cos\left[\omega_0 t + m_f \sin\left(\omega_m t\right)\right] \tag{D.20}$$

can be decomposed in an odd and even part:

$$\begin{aligned} e = &\left[1 + m_i \cos\left(\omega_m t\right)\right]^{1/2} \sqrt{2} \cos\left[m_f \sin\left(\omega_m t\right)\right] \cdot \sqrt{2} \cos\left(\omega_0 t\right) \\ &- \left[1 + m_i \cos\left(\omega_m t\right)\right]^{1/2} \sqrt{2} \sin\left[m_f \sin\left(\omega_m t\right)\right] \cdot \sqrt{2} \sin\left(\omega_0 t\right) \\ = &\, e_1 - e_2 \end{aligned} \tag{D.21}$$

Then e_1 and e_2 can be rewritten (by using the Bessel functions) in Fourier-Coefficient containing expressions:

$$e_1 = \frac{1}{\sqrt{2}} \sum_{i=0}^{\infty} a_i \left[\cos\left(\omega_0 t + i\omega_m t\right) + \cos\left(\omega_0 t - i\omega_m t\right)\right] \tag{D.22}$$

$$e_2 = -\frac{1}{\sqrt{2}} \sum_{j=1}^{\infty} b_j \left[\cos\left(\omega_0 t + j\omega_m t\right) - \cos\left(\omega_0 t - j\omega_m t\right)\right] \tag{D.23}$$

Detected signal

The third and higher dispersion approximation can be neglected when not working at a non-zero dispersion point.

The signal current is then proportional to:

$$\begin{aligned}|e|^2 = &\frac{1}{2}\left(\sum_{i=0}^{\infty} a_i \left[\cos\left(\omega_0 t + i\omega_m t\right) + \cos\left(\omega_0 t - i\omega_m t\right)\right]\right)^2 \\ &+ \frac{1}{2}\left(\sum_{j=1}^{\infty} b_j \left[\cos\left(\omega_0 t + j\omega_m t\right) - \cos\left(\omega_0 t - j\omega_m t\right)\right]\right)^2 \\ &- \left(\sum_{i=0}^{\infty} a_i \left[\cos\left(\omega_0 t + i\omega_m t\right) + \cos\left(\omega_0 t - i\omega_m t\right)\right]\right) \cdot \\ &\cdot \left(\sum_{j=1}^{\infty} b_j \left[\cos\left(\omega_0 t + j\omega_m t\right) - \cos\left(\omega_0 t - j\omega_m t\right)\right]\right)\end{aligned} \tag{D.24}$$

D.2.2. Inter-modulation distortions

The Inter-Modulation Distortion (IMD) modeling which two pure sine tones of frequencies ω_1 and ω_2 with their respective modulating indexes m_{i1} and m_{i2} , is done similarly to Eq. D.20:

$$\begin{aligned}e = &\left[1 + m_{i1}\cos\left(\omega_{m1} t\right) + m_{i2}\cos\left(\omega_{m2} t\right)\right]^{1/2} \\ &\cdot \sqrt{2}\cos\left[\omega_0 t + m_{f1}\sin\left(\omega_{m1} t\right) + m_{f2}\sin\left(\omega_{m2} t\right)\right]\end{aligned} \tag{D.25}$$

By assuming for simplicity's sake:

$$\begin{aligned}m_{i1} &= m_{i2} = m_i \\ m_{f1} &= m_{f2} = m_f\end{aligned} \tag{D.26}$$

Given the Fourier-coefficient envisaged method for solving, the integration period is the one of the *slowest* signal. Thus the frequencies ω_1 and ω_2 are defined to have a common multiple ω_u:

$$\omega_u = \omega_1/m = \omega_2/n \tag{D.27}$$

Eq. D.25 (after simplifications with the afore mentioned assumptions) can itself be decomposed in a odd and even term, as follows:

$$\begin{aligned}e &= \left[1 + m_i\cos\left(m\omega_u t\right) + m_i\cos\left(n\omega_u t\right)\right]^{1/2} \cdot \sqrt{2}\cos\left[\omega_0 t + m_f\sin\left(m\omega_u t\right) + m_f\sin\left(n\omega_u t\right)\right] \\ &= \sqrt{2}\left[1 + m_i\cos\left(m\omega_u t\right) + m_i\cos\left(n\omega_u t\right)\right]^{1/2} \cdot \cos\left[m_f\sin\left(m\omega_u t\right) + m_f\sin\left(n\omega_u t\right)\right]\cos\left(\omega_0 t\right) \\ &\quad - \sqrt{2}\left[1 + m_i\cos\left(m\omega_u t\right) + m_i\cos\left(n\omega_u t\right)\right]^{1/2} \cdot \sin\left[m_f\sin\left(m\omega_u t\right) + m_f\sin\left(n\omega_u t\right)\right]\sin\left(\omega_0 t\right) \\ &= e_1 - e_2\end{aligned} \tag{D.28}$$

Again, squaring of Eq. D.28 prior to gathering the frequency-depending terms and their evaluation is required...

Complexity issue linked to the common integration period

Table D.1 shows the issue of the common integration period when applied to the UMTS-FDD downlink band. Of course, the higher the common frequency the shorter the

Table D.1.: IM-FM interaction producing IMD-3

f_1 MHz	2140	2140	2140	2100
f_2 MHz	2145	2150	2160	2150
f_u MHz= MOD(f_2 / f_1)	5	10	20	50
n	428	214	107	42
m	429	215	108	43
m * n	183 612	46 010	11 556	1 806
lower IMD-3 nth f_u	427	213	106	41
upper IMD-3 nth f_u	430	216	109	44

integration duration[2], and thus the computation time. Unfortunately when considering the Adjacent-CLR, the frequency spacing values 5MHz, and this in turn corresponds in Table D.1 to the most computing intensive case!

[2]at same resolution

Bibliography

[1] M. Borgne and Y. Chen, "Next Generation Broadband Access White Paper - MR185," *Broadband Forum Marketing Report*, p. 8, August 2009. http://www.broadband-forum.org/marketing/download/mktgdocs/NextGenAccessWhitePaper.pdf. 5

[2] DSL Forum, "White Paper: ADSL2/ADSL2PLUS - The new ADSL standards," March 2003. http://www.broadband-forum.org/marketing/download/mktgdocs/ADSL2_wp.pdf. 6

[3] "DSL Technology Evolution," *Broadband Forum*, 2008. http://www.broadband-forum.org/downloads/About_DSL.pdf. 6

[4] R. Glatty, *Introduction of TDM/WDM flexibility in Optical Access Netowrk: Physical Layer Design and Resource Allocation Optimization*. PhD thesis, Université Rennes 1, Science de la matière, November, 21 2008. (in English). 6, 41

[5] C. Pennings and T. Ramahandry, "Next Generation Access (NGA) Regulation," tech. rep., IDATE, October 2010. 7, 9, 10

[6] M. Baudry, V. Chaillou, and S. Villaret, "Très haut débit par satellite en Europe & Afrique du Nord," tech. rep., IDATE, April 2010. (in French). 8, 9, 72

[7] P. W. Shumate, "Fiber-to-the-Home: 1977 –2007," *J. Lightwave Technol.*, vol. 26, no. 9, pp. 1093–1103, 2008. 8, 17, 19

[8] R. Montagne and V. Chaillou, "FTTX Watch Service - Insight 5 - Le plan fibre en France," tech. rep., IDATE, September 2010. (in French). 8, 10

[9] Anritsu, "White Paper - Future Technologies and testing for Fixed Mobile Convergence, SAE and LTE in cellular mobile communications," tech. rep., Oct. 2008. 12

[10] P. Kendall and S. Welsh de Grimaldo, "Mobile Broadband Opportunities - Examining the Mobile Broadband Ecosystem and Market Dynamics," tech. rep., Strategy Analytics, January 2010. 14, 15, 75, 76

[11] T. Tjelta, T. Jensen, and A.-G. Karasen, "An Evaluation of Future Mobile Networks Backhaul Operation," *Fifth International Conference on Wireless and Mobile Communications*, pp. 146 – 151, 2009. 15, 71

[12] A. Daviaud, "3GPP System Architecture Evolution: the Evolved Packet Core," Tech. Rep. F89465 - 3GPP - 14 - SAE v1.0.ppt, France Telecom Group, November, 17 2008. 14

[13] CCS Insight, "Mobile broadband in Europe, 4Q09," 2009. 15

[14] D. Nowak and J. Murphy, "FTTH: The overview of existing technologies," *SPIE, the International Society for Optical Engineering. Proceedings of,*, vol. 5825, pp. 500–509, 2005. 18

[15] ITU, "G.983.1 - Broadband optical access systems based on Passive Optical Networks," *ITU*, October 1998. 18

[16] A. Cauvin, A. Tofanelli, J. Lorentzen, J. Brannan, A. Templin, T. Park, and K. Saito, "Common Technical Specification of the G-PON System among Major Worldwide Access Carriers," *IEEE Communications Magazine*, October 2006. 19

[17] ITU, "G.984.2 - G-PON: Physical Media Dependent layer specification," *ITU*, March 2003. 19, 26, 195

[18] ITU, "G.984.3 - G-PON: Transmission convergence layer specification," *ITU*, March 2003. 19

[19] IEEE, "IEEE 802.3ah - (G)E-PON," *IEEE*, 2004. `http://www.ieee802.org/3/`. 19

[20] F. Effenberger, "Next Generation PON: Lessons Learned from G-PON and GE-PON," *ECOC, Proc.*, no. 4.7.3, 2009. 19

[21] ITU, "G.984.2 - G-PON: Physical Media Dependent layer specification - Amendment 2," *ITU*, March 2008. 20, 26

[22] ITU, "G.984.1 - G-PON: General characteristics," *ITU*, March 2003. 21, 26

[23] B. Capelle, S. Durel, P. Chanclou, and F. Merlaud, "Evolutions for FTTH Deployment in the Access Network," *Global Telecommunications Conference, 2008. IEEE GLOBECOM 2008. IEEE*, pp. 1 –5, nov. 2008. 21, 34

[24] H. J. Dutton, *IBM - Understanding Optical Communications*. Prentice Hall PTR, 1998. `http://www.redbooks.ibm.com/redbooks/pdfs/sg245230.pdf`. 21, 24, 25

[25] E. Säckinger, *Broadband circuits for Optical Fiber Communications*. Wiley InterScience, Wiley & Sons, April 2005. 22, 26, 28, 30, 31, 32, 33, 121

[26] L. Bechou, *Composants pour les télécommunications par fibre optique*. ENSEIRB 3e année, option SRT, 2007. 22

[27] K. Yamane, "S4AM-P02 - New funitonalities for advanced optical interfaces (Dispersion Compensation)," tech. rep., Fujitsu - ITU workshop, July 2002. 23

[28] J.-C. Simon, *Télécommunications Optiques*. ENSSAT, Master PHOT-IN / UETC1, 2008. 23

[29] F. Saliou, *Extension de budget PON*. PhD thesis, Graduate School ParisTech (ex Telecom Paris), June, 14 2010. (in French). 25

[30] Corning, "Single Fiber Fusion Splicing - Application Note 103," 2009. `http://www.corning.com/WorkArea/downloadasset.aspx?id=27299`. 24

[31] ITU, "G.984.2 - G-PON: Physical Media Dependent layer specification - Amendment 1," *ITU*, February 2006. 26

[32] A. Villafranca, J. Lasobras, and I. Garces, "Precise characterization of the frequency chirp in directly modulated DFB lasers," *Electron Devices, 2007 Spanish Conference on*, pp. 173 –176, jan. 2007. 27, 28

[33] G. P. Agrawal, *Fiber-Optic Communication Systems*. John Wiley & Sons, third ed., 2002. 28, 29, 31, 32, 33

[34] G. Ghione, *Semiconductor Devices for High-Speed Optoelectronics*. Cambride University Press, 2009. 33

[35] ITU, "G.984.6 - G-PON: Reach extension," *ITU*, March 2008. 34

[36] P. Chanclou, Z. Belfqih, B. Charbonnier, T. Duong, F. Frank, N. Genay, M. Huchard, P. Guignard, L. Guillo, B. Landousies, A. Pizzinat, H. Ramanitra, F. Saliou, S. Durel, A. Othmani, P. Urvoas, M. Ouzzif, and J. Le Masson, "Optical Access Evolutions and their Impact on the Metropolitan and Home Networks (Invited)," *ECOC, Proc.*, no. We.3.F.1, 2008. 34

[37] R. Davey, P. Healey, I. Hope, P. Watkinson, D. Payne, O. Marmur, J. Ruhmann, and Y. Zuiderveld, "DWDM reach extension of a GPON to 135 km," *Lightwave Technology, Journal of*, vol. 24, pp. 29 – 31, jan. 2006. 34

[38] ITU, "G.984.5 - G-PON: Enhancement band," *ITU*, September 2007. 35

[39] J. Kani, "Standardization Trends of Optical Access Networks in ITU-T," *NTT Technical Review*, vol. 5, Sept. 2007. 35

[40] J. Kani and K.-I. Suzuki, "Standardization Trends of Next-generation 10 Gigabit-class Passive Optical Network Systems," *NTT Technical Review*, vol. 7, no. 11, 2009. 35, 36, 38

[41] ITU, "G.987.1 - 10-Gigabit-capable passive optical network (XG-PON) systems: General requirements," *ITU*, January 2010. 35, 37

[42] ITU, "G.987.2 - 10-Gigabit-capable passive optical network (XG-PON) systems: Physical media dependent (PMD) layer specification," *ITU*, January 2010. 35

[43] T. Duong, N. Genay, B. Charbonnier, P. Urvoas, P. Chanclou, and A. Pizzinat, "Experimental demonstration of 10Gbit/s transmission over 110km SMF by direct modulation of 2 GHz bandwidth DFB laser using Discrete Multi-tone Modulation for Passive Optical Network," *Optical Fiber communication/National Fiber Optic Engineers Conference, 2008. OFC/NFOEC 2008. Conference on*, pp. 1 –3, feb. 2008. 37, 38

[44] F. Saliou, P. Chanclou, B. Charbonnier, T. Duong, N. Genay, A. Gharba, J. Le Masson, C. Milion, and M. Ouzzif, "SOA or EDFA amplifying 10Gbit/s OFDM signals for access networks," *ECOC, Proc.*, pp. 1 –2, 20-24 2009. 38, 39

[45] K. Grobe and J.-P. Elbers, "PON in Adolescence: From TDMA to WDM-PON," *IEEE Communications Magazine*, 2008. 39, 40

[46] S. Dahlfort, "Comparison of 10 Gbit/s PON vs WDM-PON," *ECOC, Proc.*, no. 5.7.3, 2009. 41, 77

[47] H. Friis, "A Note on a Simple Transmission Formula," *Proceedings of the IRE*, vol. 34, pp. 254 – 256, may 1946. 42

[48] FCC, "Tech Topic 17: Propagation Characterization," 2010. `http://www.fcc.gov/pshs/techtopics/techtopics17.html`. 42, 49

[49] F. Pujol, *Radio spectrum - Which conditions for mobile broadband and 4G growth?* IDATE Consulting and Research, Montpellier, France, September 2009. 43, 44, 45, 52

[50] B. H. Walke, S. Mangold, and L. Berlemann, *IEEE 802 Wireless Systems - Protocols, Multi-Hop Mesh/Relaying, Performance and Spectrum Coexistence*. John Wiley & Sons, 2006. 46, 47, 51, 52

[51] J. Parsons, *The Mobile Radio Propagation Channel*. 1992. 46

[52] M. K. Simon and M.-S. Alouini, *Digital Communication over Fading Channels*. John Wiley & Sons, second ed., 2005. 47, 48

[53] A. Goldsmith, *Wireless Communications*. Standford University, 2005. `http://wsl.stanford.edu/andrea/Wireless/Book.pdf`. 47, 50

[54] B. Escrig, *Communications numériques avancées*. ENSEIRB 3^{e} année, option SRT, 2007. 47

[55] V. Erceg, L. J. Greenstein, S. Y. Tjandra, S. R. Parkoff, A. Gupta, B. Kulic, A. A. Julius, and R. Bianchi, "An empirically based path loss model for wireless channels in suburban environments," *IEEE Journal on Selected Areas in Communications*, vol. 17, no. 7, pp. 1205–1211, 1999. 48

[56] S. Kun, W. Ping, and L. Yingze, "Path loss models for suburban scenario at 2.3GHz, 2.6GHz and 3.5GHz," *Antennas, Propagation and EM Theory, 2008. ISAPE 2008. 8th International Symposium on*, pp. 438 –441, nov. 2008. 48, 49

[57] M. Suarez, M. Villegas, and G. Baudoin, *Advanced Microwave and Millimeter Wave Technologies Semiconductor Devices Circuits and Systems*. INTECH, 2010. 52

[58] Agilent, "Designing and Testing 3GPP W-CDMA Base Transceiver Stations (Including Femtocells)," application note 1355, Agilent Technologies, August, 1 2010. `http://cp.literature.agilent.com/litweb/pdf/5980-1239E.pdf`. 52, 64, 65

[59] 3GPP, "TS 25.141 - Base Station Conformance Testing," *3GPP*, 2008. 54, 64, 172, 174, 201

[60] J. Dumont, S. Lasaulce, and J.-M. Chaufray, "Adjacent channel interference in WCDMA networks equipped with multiple antennas mobile stations," *Signal Processing Advances in Wireless Communications, 2004 IEEE 5th Workshop on*, pp. 512 – 516, 11-14 2004. 55

[61] D. V. Figueiredo, P. Matos, and A. Rodrigues, "Impact of Adjacent Channel Interference on the Capacity of WCDMA/FDD Networks," *Wireless Personal Mobile Communications, (WPMC). Proc.*, September 2004. 56

[62] T. Kaiser, A. Bordoux, H. Boche, J. R. Fonollosa, J. B. Andersen, and W. Utschick, eds., *Smart Antennas - State of the Art*, ch. 38: MIMO systems for the HSDPA FDD mode UMTS service, pp. 787 –809. EURASIP Signal Processing and Communications, Hindawi, 2005. `downloads.hindawi.com/books/9789775945099/art38.pdf`. 57, 66

[63] G. Americas, "MIMO Transmissions Schemes for LTE and HSPA Networks," tech. rep., 3G Americas, 2009. `http://www.3gamericas.org/documents/Mimo_Transmission_Schemes_for_LTE_and_HSPA_Networks_June-2009.pdf`. 57, 65

[64] M. Kottkamp, "HSPA+ Technology Introduction - Application Note," Application Note 1MA121_02E, Rohde Schwarz, May 2009. 57, 58

[65] B. Schulz, "Coexistence Digital TV and LTE - Application Note," Tech. Rep. 1MA176_3e, Rohde Schwarz, August 2010. `http://www2.rohde-schwarz.com/file_14100/1MA176_3e.pdf`. 57, 63

[66] E. Seidel, J. Afzal, and G. Liebl, "White Paper - Dual Cell HSDPA and its Future Evolution," tech. rep., Nomor Research GmbH, Munich, Germany, January 2009. `http://www.nomor.de/uploads/1h/pA/1hpAccByjinAOWBDzTNt4w/WhitePaper_DC-HSDPA_2009-01.pdf`. 58

[67] M. D. McKinley, K. A. Remley, M. Myslinski, J. S. Kenney, D. Schreurs, and B. Nauwelaers, "EVM Calculation for Broadband Modulated Signals," *64th ARFTG Conf. Dig.*, pp. 44 – 52, December 2004. `http://www.eeel.nist.gov/kate_papers/R1_ARFTG64_McKinley_com.pdf`. 60

[68] Agilent, "Application Note - 8 Hints for Making and Interpreting EVM Measurements," tech. rep., Agilent, 2005. `http://cp.literature.agilent.com/litweb/pdf/5989-3144EN.pdf`. 60

[69] R. A. Shafik, S. Rahman, and A. R. Islam, "On the Extended Relationships Among EVM, BER and SNR as Performance Metrics," *Proc. Int. Conf. Electrical and Computer Engineering ICECE*, pp. 408–411, 2006. 60, 61

[70] J. Kwak, "EVM Simulations for OFDM, doc: IEEE 802.11-03/773r2," tech. rep., InterDigital Communications Corporation, November 2003. https://mentor.ieee.org/802.11/dcn/03/11-03-0773-02-000k-ofdm-evm-simulations-psni.ppt. 60, 61

[71] ITU, "Unwanted emissions in the spurious domain - Recomendation SM.329-10," *ITU*, January 2003. 63

[72] G. Povey, l. Gatzoulis, L. Stewart, and I. Band, "WCDMA inter-operator interference and 'dead zones'," *IEE Personal Mobile Comm. Conf. Proc, of*, pp. 560–564, April 2003. 65, 66

[73] Agilent, "Digital Modulation in Communications Systems – An introduction, Application Note 1298," vol. 1298, p. 21, March 2001. http://cp.literature.agilent.com/litweb/pdf/5965-7160E.pdf. 67

[74] A. Wegener, "High-performance crest factor reduction processor for W-CDMA and OFDM applications," *Radio Frequency Integrated Circuits (RFIC) Symposium, 2006 IEEE*, p. 4 pp., 11-13 2006. 68, 69

[75] S. Little, "Is Microwave Backhaul Up to the 4G Task?," *IEEE Microwave Magazine*, pp. 67 – 74, August 2009. 71

[76] S. Purge, "UTRAN Interfaces and Protocols - 3GPP," Tech. Rep. F89465 - 3GPP - 5 - UTRAN Interfaces and Protocols PhH - V1.ppt, France Telecom Group, October, 14 2008. 71, 72

[77] A. Brydon and M. Heath, *Will 3G Networks Cope? 3G traffic and capacity forecasts for 2009 -2014*. Unwired Insight Limited, Huntingdon Business Centre, Blackstone Road, Huntingdon, Cambridgeshire, 2009. 72

[78] F. Ivanek, "Mobile Backhaul," *IEEE Microwave Magazine*, pp. 10–20, 2009. 72

[79] M.-G. Kim, G. Shen, J. Choi, B. Jung, H.-S. Park, and M. Kang, "Distributed antenna-based epon-wimax integration and its cost-efficient cell planning," *Selected Areas in Communications, IEEE Journal on*, vol. 28, pp. 808 –817, aug. 2010. 76

[80] D. Wake and K. Beacham, "A novel switched radio over fiber architecture for distributed antenna systems," *Lasers and Electro-Optics Society, 2004. LEOS 2004. The 17th Annual Meeting of the IEEE*, vol. 1, pp. 55 – 56, 7-11 2004. 78

[81] A. Casini and P. Faccin, "Wavelength division multiplation technologies for UMTS radio coverage extension by using the radio over fibre technique," *Microwave Photonics, 2003. MWP 2003 Proceedings. International Topical Meeting on*, pp. 123 – 128, 10-12 2003. 80

[82] C. Lim, A. Nirmalathas, M. Bakaul, P. Gamage, K.-L. Lee, Y. Yang, D. Novak, and R. Waterhouse, "Fiber-Wireless Networks and Subsystem Technologies," *Lightwave Technology, Journal of*, vol. 28, pp. 390 –405, feb.15, 2010. 81, 91, 92

[83] V. Diascorn, "PRINSIP Seminar - VoIP capacity results over HSPA," internal report, Orange Labs, January 2008. 82

[84] B. Badard, "HSUPA packet schedulers' performance for the support of VoIP," Internal Report R&D/RESA/MNA/06.0712/NN, France Telecom Research & Development, May, 29 2007. 83, 84

[85] ITU-T, "One-Way Transmission Time," *ITU-T*, May 2003. 83

[86] H. Le Bras and M. Moignard, "Demonstration of Overlay UMTS signal transmission on a Gigabit Passive Optical Network (PON)," *Photononics Europe*, 2006. 85, 176

[87] P. Gamage, A. Nirmalathas, C. Lim, E. Wong, D. Novak, and R. Waterhouse, "Multi-services distribution using power-efficient low-cost VCSELs," *Microwave Photonics, 2008. International Topicsl Meeting on*, pp. 169 –172, 9 2008-oct. 3 2008. 85

[88] M. Milosavljevic, P. Kourtessis, A. Gliwan, and J. M. Senior, "Advanced PON Topologies with Wireless Connectivity," *ICTON, Proc.*, no. Tu.A5.4, 2009. 85, 86

[89] M. Milosavljevic, P. Kourtessis, and J. M. Senior, "Wireless-PONs with Extended Wavelength Band Overlay," *OSA ANIC, Proc.*, no. AWC6, 2010. 85, 86

[90] M. Milosavljevic, M. P. Thakur, P. Kourtessis, J. E. Mitchell, and J. M. Senior, "A Multi-Wavelength Access Network featuring WiMAX Transmission over GPON Links," *ECOC, Proc.*, no. Th.9.B.7, 2010. 87

[91] D. Qian, J. Hu, P. NanJi, T. Wang, and M. Cvijetic, "10-Gb/s OFDMA-PON for Delivery of Heterogeneous Services," *OFC/NFOEC, Proc.*, no. OWH4, 2008. 88

[92] Y.-M. Lin, P.-L. Tien, M. C. Yuang, S. S. W. Lee, J. J. Chen, S.-Y. Chen, Y.-M. Huang, J.-L. Shih, and C.-H. Hsu, "A Novel Optical Access Network Architecture Supporting Seamless Integration of RoF and OFDMA Signals," *ECOC, Proc.*, September 2009. 88, 89, 90

[93] R. Schoop, F. Fredricx, T. Koonen, and C. Hardalov, "WDM Isolation Requirements for CATV in BPON," *Proc. 28th European Conf. Optical Communication ECOC 2002*, vol. 4, pp. 1–2, 2002. 91, 209

[94] J. Hu, D. Qian, T. Wang, and M. Cvijetic, "Wireless Intermediate Frequency Signal over Passive Optical Networks: Architecture and Experimental Performance Evaluation," *OFC/NFOEC, Proc.*, no. NthD4, 2008. 92

[95] G. Shen, R. Tucker, and C.-J. Chae, "Fixed mobile convergence architectures for broadband access: Integration of epon and wimax [topics in optical communications]," *Communications Magazine, IEEE*, vol. 45, pp. 44 –50, aug. 2007. 93

[96] D. M. Akos, M. Stockmaster, J. B. Y.Tsui, and J. Caschera, "Direct Bandpass Sampling of Multiple Distinct RF Signals," *IEEE Transactions on Communications*, vol. 47, pp. 983 –988, July 1999. 95, 96

[97] P. Wala, "A new microcell architecture using digital optical transport," *Vehicular Technology Conference, 1993 IEEE 43rd*, pp. 585 –588, may. 1993. 96

[98] R. Vaughan, N. Scott, and D. White, "The theory of bandpass sampling," *Signal Processing, IEEE Transactions on*, vol. 39, pp. 1973 –1984, sep 1991. 96, 98

[99] A. Nirmalathas, P. Gamage, C. Lim, D. Novak, R. Waterhouse, and Y. Yang, "Digitized RF Transmission over Fiber," *Microwave Magazine, IEEE*, vol. 10, pp. 75 –81, june 2009. 97, 98

[100] A. Nirmalathas, P. Gamage, C. Lim, D. Novak, and R. Waterhouse, "Digitized Radio-over-Fiber Technologies for Converged Optical Wireless Access Network," *Lightwave Technology, Journal of*, vol. 99, May 2010. 97

[101] J.-H. Kim, H. Wang, J.-U. Kim, S.-H. Lee, J.-H. Yu, and D.-H. Lee, "The analysis and design of RF sub-sampling frontend for SDR," *Communications and Networking in China, 2008. ChinaCom 2008. Third International Conference on*, pp. 1216 –1220, 25-27 2008. 98, 99

[102] Ericsson, Huawei, NEC, Nokia Siemens Networks, and Alcatel-Lucent, "Common Public Radio Interface; Interface Specification," February 2009. `http://www.cpri.info/spec.html`. 100, 102

[103] Global PCS Inc., Taiwan, "G21RRH-48-01B Product Datasheet; 4-Carrier WCDMA/HSDPA+/LTE CPRI Remote Radio Head," 2009. 103

[104] OBSAI, "Reference Point 3 Specification," July 2008. `http://www.obsai.org/`. 103

[105] C. F. Lanzani, "OBSAI RP3-01 6.144 Gbps Interface Implementation," *FPAGworld.com*, 2007. `http://www.obsai.org/obsai/content/download/17606/154920/file/rp301_6144Gbps.pdf`. 103

[106] Radiocomp Aps, "Open Base Station Architecture: Can Standardization enable true innovation ?," p. 12/18, 2008. `http://www.radiocomp.com/Technology/Technical-papers.aspx`. 104

[107] B. Huiszoon, J. Aracil, H. Jung, A. Koonen, E. Tangdiongga, I. Tomkos, and C. Tsekrekos, "Optical-Wireless Network with Multi-Layer Reconfigurability," *Access Networks and In-house Communications*, p. AWC2, 2010. 103, 104

[108] A. A. M. Saleh, "Fundamental Limit on Number of Channels in Subcarrier Multiplexed Lightwave CATV system," *Electronics Letters*, vol. 25, no. 12, pp. 776–777, 1989. 115

[109] O. K. Tonguz and H. Jung, "Personal Communications Access Networks Using Subcarrier Multiplexed Optical Links," *IEEE/OSA Journal of Lightwave Technology*, vol. 14, no. 6, pp. 1400–1409, 1996. 115

[110] J. Zhang, A. N. Hone, and T. E. Darcie, "Clipping-Free Dynamic Range: the Fundamental Limit for Class-B Microwave-Photonic Links," *Photonics Technology Letters, IEEE*, vol. 19, pp. 1033 –1035, oct. 2007. 115

[111] V. Urick, M. Rogge, F. Bucholtz, and K. Williams, "The Performance of Analog Photonic Links Employing Highly Compressed Erbium-Doped Fiber Amplifiers," *Microwave Theory and Techniques, IEEE Transactions on*, vol. 54, pp. 3141 – 3145, July 2006. 121, 122

[112] P. Dua, K. Lu, N. K. Dutta, and J. Jacques, "Analog and digital transmission using high-power fiber amplifiers," *Society of Photo-Optical Instrumentation Engineers (SPIE) Conference Series*, vol. 4653, pp. 111–118, June 2002. `http://lib.semi.ac.cn:8080/tsh/dzzy/wsqk/SPIE/vol4653/4653-111.pdf`. 121

[113] G. Meslener, "Chromatic Dispersion induced Distortion of Modulated Monochromatic Light Employing Direct Detection," *Quantum Electronics, IEEE Journal of*, vol. 20, pp. 1208 – 1216, oct 1984. 129, 234, 235, 239

[114] S. I. Charles and W. Gu, "Fiber Induced Distortions in a Subcarrier Multiplexed Lightwave System," *IEEE J. Sel. Areas Commun.*, vol. 8, pp. 1296–1303, September 1990. 129, 132, 189, 234, 239

[115] C. Almeida, A. Teixeira, and M. Lima, "Performance Analysis of Multi-Format Multi-wavelength Radio over Fiber Systems Based on Low Cost optical Components," *ICTON, Proc. of*, no. Tu.C4.4, pp. 106 –109, 2008. 137, 176

[116] F. Frank, B. Charbonnier, A. Pizzinat, P. Chanclou, and C. Algani, "Bidirectional Multi-UMTS FDD Carrier Distribution over an Extended-Reach PON Architecture using a shared SOA," *ECOC, Proc. of*, 2009. 176

[117] S. Di Bartolo, A. Teixeira, G. M. T. Beleffi, and F. Curti, "Effects of Semiconductor Optical Amplifier Phase Distortion in Radio Over Fiber Signals," *Proc. 9th Int. Conf. Transparent Optical Networks ICTON '07*, vol. 3, pp. 261–264, 2007. 176

[118] A. Brizido, "3G radio distribution based on directly modulated lasers over PONs," *IMOC*, pp. 658–661, Oct. 2007. 176

[119] H. Nasoha and S. M. Idrus, "Modeling and Performance Analysis of WCDMA Radio over Fiber System," *APACE, Proc. of*, pp. 1 –4, December 2007. 176

[120] R. E. Schuh and D. Wake, "Distortion of W-CDMA signals over optical Fibre Links," *Microwave Photonics*, pp. 9 –12, 1999. 176, 189

[121] D. Wake and R. Schuh, "Measurement and simulation of W-CDMA signal transmission over optical fibre," *Electronics Letters*, vol. 36, May, 11 2000. 176

[122] D. Visani, G. Tartarini, L. Tarlazzi, and P. Faccin, "Transmission of UMTS and WIMAX Signals Over Cost-Effective Radio Over Fiber Systems," *IEEE Microw. Wireless Compon. Lett.*, vol. 19, no. 12, 2009. 176, 189

[123] K. Asami, Y. Furukawa, M. Purtell, M. Ueda, K. Watanabe, and T. Watanabe, "WCDMA testing with a baseband/IF range AWG," *Test Conference, 2002. Proceedings. International*, pp. 1140 – 1145, 2002. 211

[124] ETSI, "Fixed Radio Systems; Multipoint Equipment and Antennas; Part 1: Overview and Requirements for Digital Radio Systems," *European Standard*, January 2007. (Final draft). 232

Personal publications

- "Bidirectional Multi-UMTS FDD Carrier Distribution over an Extended-Reach PON Architecture using a shared SOA",
  F. Frank, B. Charbonnier, A. Pizzinat, Ph. Chanclou, C. Algani,
  IEEE ECOC 2009, Vienna, Austria

- "Bidirectional Multi-UMTS FDD Carrier Distribution over an Extended-Reach PON Architecture using a shared SOA",
  F. Frank, B. Charbonnier, A. Pizzinat, Ph. Chanclou, C. Algani,
  IPHOBAC Workshop 2009, Duisburg, Germany

- "3GPP Compliant Downlink ACLR Performances Of PON Distributed Multiple UMTS FDD Carriers",
  Florian FRANK, Benoit CHARBONNIER, Catherine ALGANI,
  OSA ANIC 2010, Karlsruhe, Germany

- "Sharing the infrastructures of Optical Access Networks with Mobile Networks",
  F. Frank, L. Kadri, a. Pizzinat, B. Charbonnier, P. Chanclou,
  Workshop on Wireline and Wireless Access, OFC 2011, Los Angeles, California, USA

- "Optical access evolutions and their impact on the metropolitan and home networks",
  P. Chanclou, Z. Belfqih, B. Charbonnier, T. Duong, F. Frank, N. Genay, M. Huchard, P. Guignard, L. Guillo, B. Landousies, A. Pizzinat, H. Ramanitra, F. Saliou, S. Durel, A. Othmani, P. Urvoas, M. Ouzzif, J. Le Masson,
  IEEE ECOC 2008, Brussels, Belgium

Bidirectional Multi-UMTS FDD Carrier Distribution over an Extended-Reach PON Architecture using a shared SOA

F. Frank[(1)], B. Charbonnier[(1)], A. Pizzinat[(1)], Ph. Chanclou[(1)], C. Algani[(2)]

[(1)] France Telecom – Orange Labs, 2 av. P. Marzin, 22307 Lannion, France, florian.frank@orange-ftgroup.com
[(2)] CNAM, ESYCOM (EA2552), Communications Systems, 292 rue St-Martin, 75003 Paris, France

Abstract *We demonstrate the distribution of a multiplex of UMTS RF carriers over extended reach PON architectures for overall optical budgets up to 47 dB. A SOA and an APD are respectively used for the reach extension and the photodetection.*

.

Introduction

Today, there are more than 1.3 million FTTH/B customers throughout Europe [1] and this figure is expected to rise to 14.5 millions by 2013 [2]. Similarly to what is currently seen is Asia FTTH/B will gradually replace DSL connections. However, FTTH connection costs are estimated to be around 1500€ in most densely populated areas (i.e. Paris) and rising to 2500€ for average density areas [3]. This is the most expensive connectivity solution among all the others (WiFi Hot spots, xDSL, WiMAX, etc…) and 70% of this sum is engineering work for the actual fiber installation. Nevertheless, it is the technology of choice by all operators because of the large bandwidth provided and its ability to meet all potential future bandwidth demands. For instance, IDATE has identified in 2007, 201 optical fibre current deployments in Europe [4]. In parallel, optical infrastructures are also deployed mainly for upgrading the mobile telephony network to 3G (UMTS) and 3.5G as there are now more than 116 million 3G users in Europe [1]. It is then the key for operators to study ways of sharing the optical infrastructure investments between mobile telephony networks and access networks.

The goal of this paper is to demonstrate experimentally the possibility of transporting UMTS FDD (Frequency Division Duplexing) signals over current and more importantly over future GPON architecture (Extended reach) so as to validate this infrastructure sharing concept. Hence, we describe in this paper a system for distributing and collecting simultaneously three UMTS Band I RF signals over an Extended Reach Passive Optical Network (ER-PON) Architecture using radio-over-fiber techniques. Experimental results are reported. The reach extension is realized by an in-line Semiconductor Optical Amplifier (SOA) which is shared between the uplink and downlink radio signals each carried by a dedicated wavelength.

Experimental Radio Set-up

The used UMTS signal is a Wideband–Code Division Multiplex Access (W-CDMA) QPSK signal at 3.84MChip/s composed of the five Physical Channels composing the Test Model 4 of [5] which is specified by 3GPP for EVM (Error Vector Magnitude) measurement purposes.

The above mentioned UMTS baseband signal is processed offline on a computer using Matlab® in order to be generated on a dual output Arbitrary Waveform Generator (AWG). Each output of the AWG represent the I and Q components of a signal composed of a multiplex of three 10 MHz spaced UMTS carriers. After frequency up-conversion using a Vector Signal Generator (VSG#1, 2) the three carriers are centered around 1940 MHz for the uplink (UL) and 2140 MHz for the downlink (DL). Finally a Low Noise Amplifier (LNA) is used as a Laser Driver and is followed by a UMTS Band I Diplexer (DL and UL BPF on Figure 1) to filter out the noise and unwanted mixing products. All three carriers are always maintained with the same RF power.

For the experiment, each UMTS RF signal power can be swept from -40 to +15 dBm/carrier. Performance evaluation is done by a Vector Signal Analyzer (VSA) through measurement of the Error Vector Magnitude (EVM).

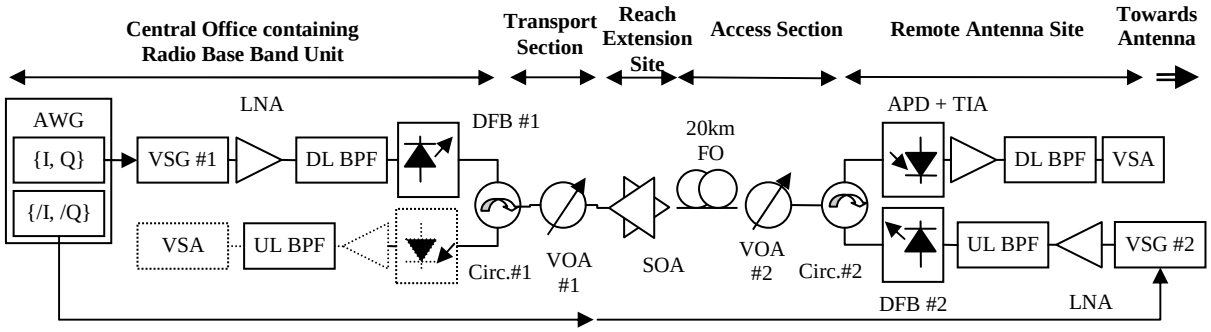

Fig. 1: Experimental Radio & Optical Set-up

Experimental Optical Set-up

The optical path of an ER-PON can be divided into a Transport Section (starting at the Central Office) and an Access Section (finishing at the Remote Antenna Site), the Reach Extension Site – made of a single SOA – lying in between. The Transport Section is represented by pure optical attenuation corresponding to a 17dB budget, whereas the latter is composed by 20km of optical fiber and optical attenuation representing a typical PON Class B+ budget of 28dB.

Here we used cooled DFB lasers emitting each ~ +9dBm of optical power at 1551nm and 1546nm for the downlink and the uplink respectively. The different wavelengths are separated by optical circulators each having an insertion loss of ~0.8dB and which are not included in the PON budget calculations. The SOA has a gain of 14dB.

For practical purposes the APD and the VSA (shown dotted on Figure 1) are permuted for realizing the up- and downlink measurements, however optical signals remain unchanged, thus *simultaneity* is conserved.

Results

For an overall optical budget of 47dB, the EVM is plotted against the received RF power (in a 5 MHz band) for each one of the three multiplexed carriers. The EVM measurements are referenced to electrical back to back evaluations in order to differentiate between the distortions originating from the optoelectrical conversions and the optical amplification from the ones originating from our test equipment.

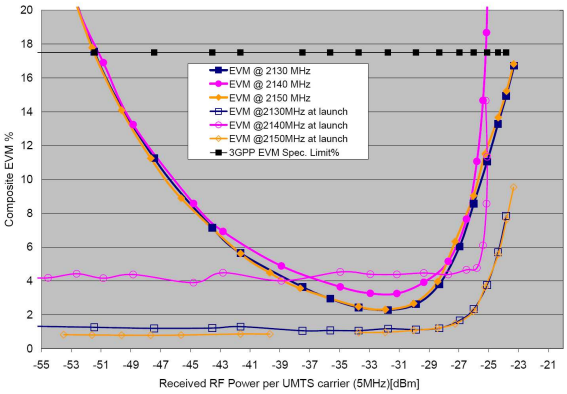

Fig. 2: UMTS RF carrier multiplex on Downlink Wavelength

In the downlink direction, Figure 2 shows that an EVM power margin (calculated as the difference between the maximum and minimum RF power to achieve the UMTS EVM limit value of 17.5%) of 25dB can be achieved. However this limit of 17.5% is specified to be the maximum EVM to be received at the end of the air link. Thus in our case considering an EVM target of 8% at the output of the radio-over-fiber-system is more realistic since the RF signals still have to propagate through the air link. In this case we still have a power margin of 18dB.

In the uplink direction, an EVM power margin - for a limit at 17.5% - of 26dB can be observed on Figure 3. In this case we do not consider the 8% threshold as we measure the signal after is would have propagated in the air.

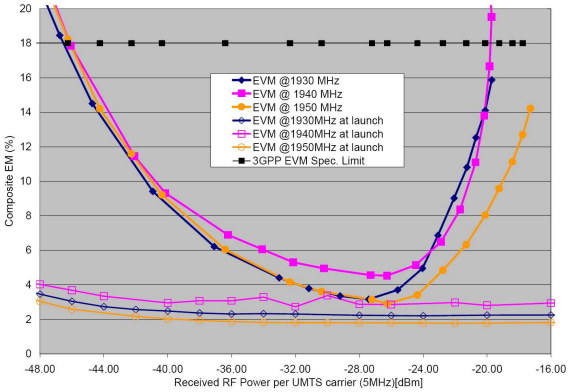

Fig. 3: UMTS RF carrier multiplex on Uplink Wavelength

Conclusions

We prove the capability of transporting transparently and simultaneously a Multiplex of three UMTS RF FDD carriers per direction over an Extended Reach PON architecture with an optical budget of 47 dB relying on the use of an SOA for reach extension and an APD for photodetection.

This work validates that current and next generation PON infrastructures can be shared with the UMTS FDD mobile networks' backhaul infrastructure leading to potentially large investment savings.

Acknowledgement

The research leading to these results has received funding from the European Community's Seventh Framework Programme (FP7) under project 212 352 ALPHA “Architectures for fLexible Photonic Home and Access networks”.

References

1 Didier Pouillot, "World Market for Telecom Services", IDATE, December 2008.
2 FTTX Watch Service, IDATE July 2008.
3 Roland Montagne, "FFTH deployments: what solutions to lower the costs?", IDATE, August 2008.
4 Roland Montagne, "FFTx Market Watch 2008", IDATE, March 2008.
5 TS 25.141 - Base Station (BS) Conformance Testing (FDD)
6 TS 25.104 - BS radio transmission and reception
7 TS 25.101 - UE radio transmission and reception

Bidirectional Multi-UMTS FDD Carrier Distribution over an Extended-Reach PON Architecture using a shared SOA

F. FRANK[1,*], B. CHARBONNIER[1], A. PIZZINAT[1], Ph. CHANCLOU[1], C. ALGANI[2]
[1] Orange Labs, 22307 Lannion, France, * florian.frank@orange-ftgroup.com
[2] CNAM ESYCOM, 75003 Paris, France

Introduction

From Separated Network Infrastructures...

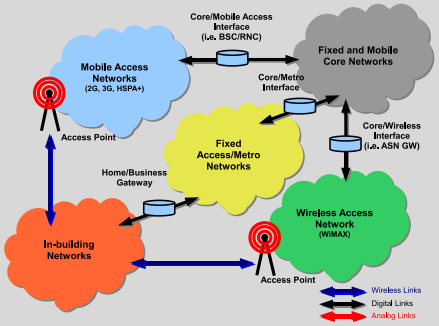

- Duplicated network Infrastructures
- Multiple Operation and Maintainance of networks

...towards Infrastructure Converged Optical Networks

- Simplified Operation and Maintainance of infrastructure
- Shared networks' snfrastructure
- Increased deployment speed of new radio sites

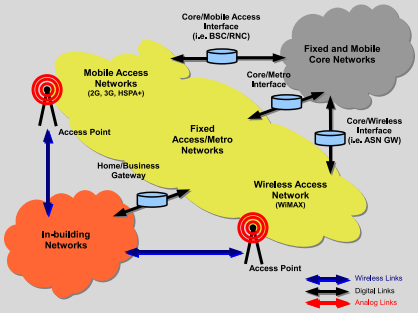

Extended Reach PONs can be reused for Radio

Wavelength Multiplexing

Using the 1550nm grid for radio over PON signals

Shared Bidirectionnal Amplification

The amplification unit can be shared between the radio dedicated wavelengths

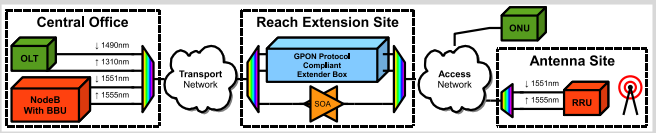

Experimental Set-Up

Radio Part

- Using UMTS Band I : 1920-1990 (UL) and 2110-2170 MHz (DL)
- 3 UMTS 10 MHz spaced carriers are generated at each side (VSG# 1,2)
- Each UMTS RF signal power is swept from -40 to +15dBm
- EVM measurement of the 3 carriers is performed at each side (VSA)

Optical Part

- Optical Budget: Transport Section (17dB), Access Section (28dB), Circulators(1.6dB)
- Two lasers sources emmiting each +9dBm (DFB# 1,2)
- The SOA has a gain of 14dB and is direction shared
- The APD with built-in TIA is place permuted (dotted) for optical simultaneity
- VOAs and 20km of G.652.D Fiber emulate a realistic Extended Reach PON

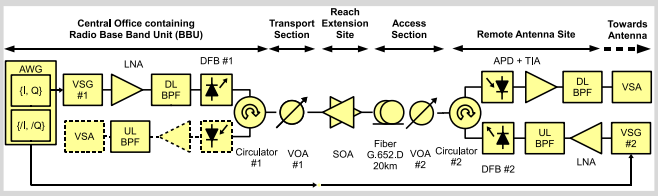

Experimental Results over 45dB:

17dB Transport Budget & 28dB Access Budget

EVM Measurements

- For each carrier, EVM is plotted against its received RF power
- The EVM of the initial launched signal is superposed

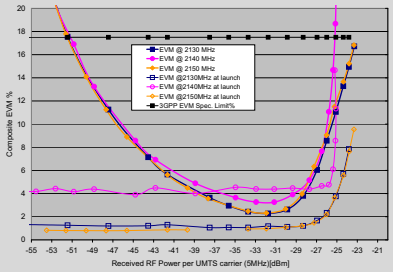

Downlink
From Central Office towards Remote Antenna Site

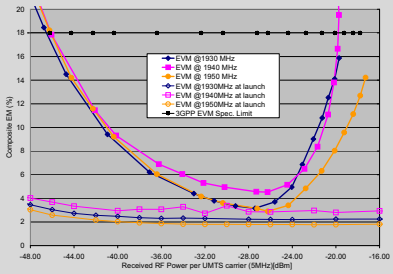

Uplink
From Remote Antenna Site towards Central Office

Adjacent/Alternate Canal Leakage Ratio (ACLR) Measurements

- Adjacent (and Alternate) CLR are measured 5 (and 10) MHz below the lower frequency carrier and beyond upper frequency carrier
- The ACLR of the received signals is plotted against the central carrier's RF launch power
- The ACLR of the initial launched signal is superposed

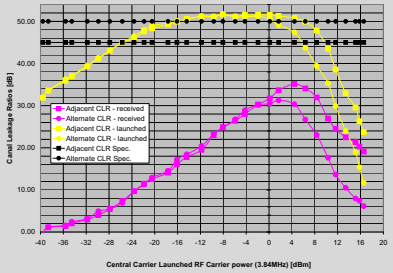

Downlink

- Uplink ACLR is not relevant since no more air link transmission is expected after optical transmission, however similar performances as in the downlink were obtained

Conclusions

EVM Issue

- Downlink : Power margin of 25dB for an EVM limit set at 17.5% (3GPP Spec.)
- Downlink : Power margin of 18dB for an EVM limit set at 8% (margin for air link)
- Uplink : Power margin of 26dB for an EVM limit set at 17.5% (3GPP Spec). – no air link margin needed

ACLR Issue

- The downlink ACLR specifications are not met and need to be improved

Global

- Transparent and simultaneous transmission of an UMTS RF multiplex per direction over an Extended Reach PON is shown
- The next generation PON infrastructures can be shared with UMTS mobile networks' backhaul infrastructure

3GPP Compliant Downlink ACLR Performances Of PON Distributed Multiple UMTS FDD Carriers

Florian FRANK[1], Benoit CHARBONNIER[1], Catherine ALGANI[2]

[1] *Orange Labs, 2 av Pierre Marzin, 22307 Lannion Cedex, France*
[2] *ESYCOM, CNAM, 292 rue St-Martin, 75141 Paris Cedex 03, France*
florian.frank@orange-ftgroup.com

Abstract: To reuse the fixed broadband optical infrastructures for mobile networks, we report experimental results, compliant with 3GPP's Downlink ACLR specifications, of UMTS FDD carriers distributed over PON using RoF, for optical budgets up to 30dB.

© 2010 Optical Society of America
OCIS codes: (060.2330) Fiber optics communications; (060.5625) Radio frequency photonics

1. Introduction

Currently, generalization of 3G and the induced increased data traffic volume in the radio access networks, lead to the need of additional radio sites with smaller cell radius providing higher bit rates for users. In dense urban areas, proximity to FTTH creates opportunities to reuse the installed fixed broadband fiber infrastructure for deploying new radio sites. These radio sites could consist in *simple* remote antennas, being connected to the Central Office (CO) through *transparent* Radio over Fiber (RoF) links, while their NodeBs (3G Base Stations) being grouped at the CO.

Since the ITU foresees [1] the 1360–1480 nm, the 1565–1600 nm, and the 1539–1565 nm windows to be reserved, Radio over Fiber (RoF) could make advantage of these spectra for distributing UMTS FDD (Frequency Division Duplex) carriers over Passive Optical Network (PON) infrastructure. Current rolled-out PON infrastructure uses Class B+ optical budgets of 28dB including up to 20km of S-SMF (Standard Single Mode Fiber).

Transparency of a RoF link versus the transported radio standard is mandatory. Even if successful transmissions of UMTS RF carriers are reported [2–4] in terms of EVM (Error Vector Magnitude) or BER (Bit Error Rate), the Adjacent Channel Leakage power Ratio (Adj-CLR) figures at the output of the RoF-systems are not systematically taken into account despite their importance when broadcasting the signal since they contribute to the Adjacent Channel Interference Ratio (ACIR). The latter, if degraded, leads to so called "dead-zones" and unwanted call drops [5] in the cell, making the concerned part of the network less profitable.

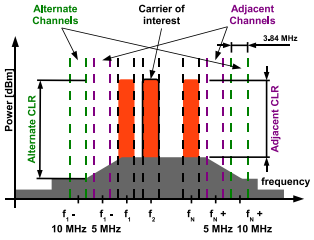

Fig. 1: Multiple Carriers

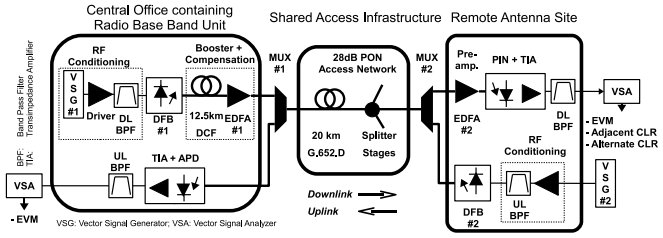

Fig. 2: Electrical and optical Set-up

In [6] the Adj-CLR is defined, as the ratio of the RF mean powers within 3.84 MHz between the carrier of interest and the adjacent bands at 5 MHz offset below the lowest and beyond the highest carrier frequencies of the multiplex (Fig. 1). The Alternate CLR (Alt-CLR) is specified for 10MHz offsets. [6] specifies *downlink* Adj- and Alt-CLRs respectively of -45dB and -50dB. Henceforth, unless stated, ACLR indifferently describes Adj- and Alt-CLR.

The ACLR issue for UMTS carriers transmitted by RoF, has so far been reported by [7, 8], who showed the fiber optic's length to be—at a given modulation index—responsible for the degradation of the ACLR.

In the uplink, the ACLR issue concerns the mobile phone transmitter, and is no issue since no more radio broadcast is expected beyond the RoF link. As discussed in [9], good EVM performances for uplink UMTS carriers over PON Class B+ budgets can be achieved by using an APD photo receiver as shown in Fig. 2.

Therefore this paper focuses on the downlink ACLR figures in order to be compliant with the 3GPP specifications for optical budgets up to 30dB, using the downlink set-up shown in Fig. 2.

2. Experimental Set-up

The radio source consists of three UMTS FDD Wideband–Code Division Multiplex Access (W–CDMA) QPSK *Test Model 4* [10] carrier signals of equal power, equally spaced by 5 or 10MHz, and centered at 2140MHz.

The optical source is a cooled DFB laser emitting +6.8dBm of optical power at 1551nm. The modulated laser source first passes a 12.5km DCF (Dispersion Compensating Fiber) spool, before being boosted by an EDFA (Erbium Doped Fiber Amplifier) set to +12.8dBm of constant output power. After the 28dB PON section containing 20km of S-SMF, and two additional 2dB of attenuation, the optical signal is pre-amplified by an EDFA set to +0.9dBm of constant output power. Finally a PIN photo-detector, and an UMTS Band I Diplexer allow the analysis of the electric signal.

The presented downlink set-up, Fig. 2, intentionally uses *only* 12.5km of DCF located at the CO. Thus indifferently the length of S-SMF (up to 20km for a PON) contained within the branch between the CO and any remote antenna, the set-up remains the same. Furthermore the cost of the DCF can be shared between the different remote antenna sites connected to the PON.

3. Results

Averaged over 20 measurements, the received spectra (Fig. 3 & 4) show the 5 and 10 MHz ACLR figures to be compliant with 3GPP at least in excess of 5.9dB and 1.2dB respectively. Additional ACLR measurements for 15, 20, and 25 MHz offsets (2nd, 3rd, and 4th Alternate) witness of a spurious free spectrum. Furthermore each carrier's Composite EVM yields in both cases less than 1.1%, for a specified maximum of 17.5% [6].

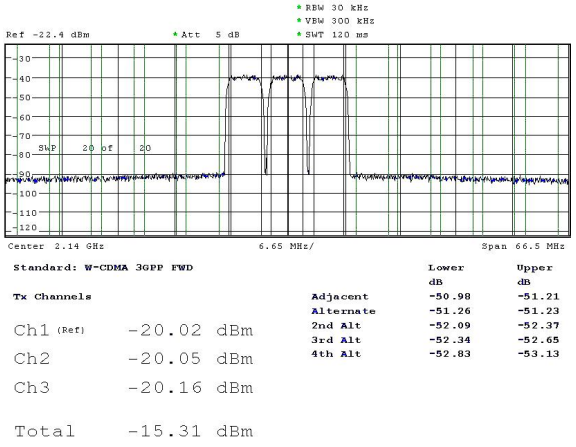

Fig. 3: 5MHz spacing, Optical Modulation Index=29%

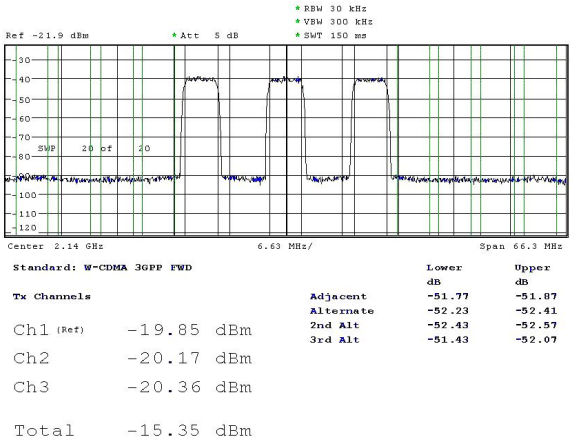

Fig. 4: 10MHz spacing, Optical Modulation Index=29%

The results show 12.5km of DCF to be sufficient for compensating 20km of S-SMF. Thus providing a distortion free spectrum over the whole UMTS Downlink Band I, for PON Class B+ optical budgets of 28dB, with additional 2dB budget margin for circulators or (de)multiplexers as suggested in Figure 2.

4. Conclusion

We strengthened the importance of ACLR in case of broadcasting RoF signal transported over PON budgets; and showed a *simple* and almost *transparent* set-up allowing 3GPP compliant ACLR figures for multiple UMTS downlink carriers transmitted over PONs for optical budgets up to 30dB, while maintaining very low EVM figures.

References

[1] Kani, "Standardization Trends of Optical Access-area Networks in ITU-T," in *NTT Technical Review, vol. 5*, Sept. 2007

[2] Brizido, "3G Radio Distribution based on Directly Modulated Lasers over PON," in *Proc. IMOC, vol 35*, 2007

[3] Nasoha, "Modeling and Performance Analysis of W-CDMA RoF System," in *Proc. APACE*, 2007

[4] Almeida, "Performance Analysis of Multi-format WDM-RoF links Based on Low Cost Laser and SOA," in *Proc. AccessNets, vol. 6*, 2008

[5] Povey, "WCDMA Inter-Operator Interference and 'Dead Zones'," in *Proc. EPMCC*, 2003

[6] 3GPP, "Base Station radio transmission and reception (FDD)," in *3GPP TS 25.104*, 2009

[7] Schuh, "Distortion of WCDMA Signals over Optical Fiber Links,", in *Proc. MWP*, 1999

[8] Visani, "Transmission of UMTS & WiMAX Signals Over [. . .] RoF Systems," in *IEEE Microw. & Wirel. Comp. Lett., vol. 19*, Dec. 2009

[9] Frank, "Bidirectional Multi-UMTS FDD Carrier Distribution over an Extended-Reach PON using a shared SOA," in *Proc. ECOC*, 2009

[10] 3GPP, "UMTS FDD Base Station Conformance Testing," in *3GPP TS 25.141*, 2009

Sharing the infrastructures of Optical Access Networks with Mobile Networks

F. Frank, L. Kadri, A. Pizzinat, B. Charbonnier, P. Chanclou

OFC'2011 Workshop on Wireline and Wireless Access

Outline of the presentation

- Mobile Network context
- Optical Access and PON context
- Why try to re-use PON for Mobile Networks?
- Backhauling
- Remoting:
  - Digital Distributed Antenna System
  - Analog Distributed Antenna System
- Conclusions & perspectives

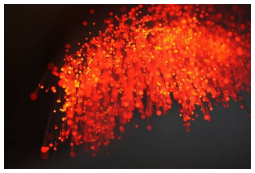

Mobile Network Context

- Capacity per user has to increase
- Carrier Frequencies increase
- Radiated power decreases

Densification of the antenna sites

Reduced cell size
Increased handovers between cells
Traffic optimization per cell needed

PON context

http://www.fiberevolution.com/2011/02/deployment-projections-for-orange.html

Orange announcement:
By 2015, 3600 Towns will be fibered →10M homes

By 2020 → 15M homes (60% of French Homes)

- PON = Passive Optical Network
  - Passive optical couplers
  - ↓1490nm, ↑1310nm
  - B+ class ≡ 28dB of optical budget
    - 64 customers per PON "tree"
    - 20km of FO (max.) & is considered worst case
      - but ~5km average in France (because of. copper…)

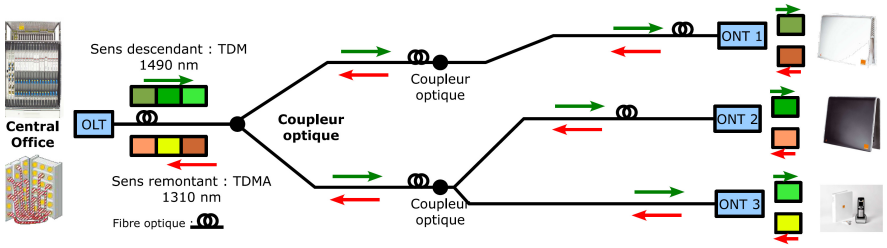

Backhauling using PON

- The mobile network traffic is encapsulated into the PON traffic
- This solution is already commercial for GSM and UMTS
  - All future PON solutions are specified for this.
  - In the future, mobile network traffic will increase (LTE) but also PON capacity.

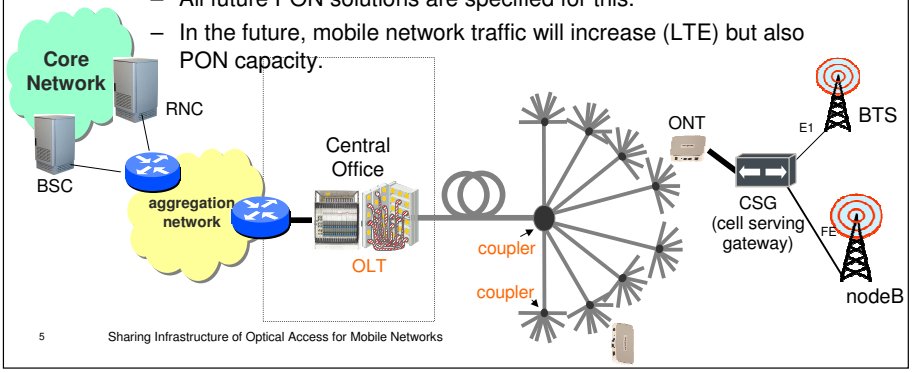

Antenna Remoting Using PON

- Strong advantages for mobile networks
  - Distributed Antennas ➔ processing power adaptable to cell load
  - Co-localized equipments➔ sites of presence are fewer
  - For LTE X2 links are facilitated
  - Future CoMP between cells easier
- Which architecture? Which Technique?

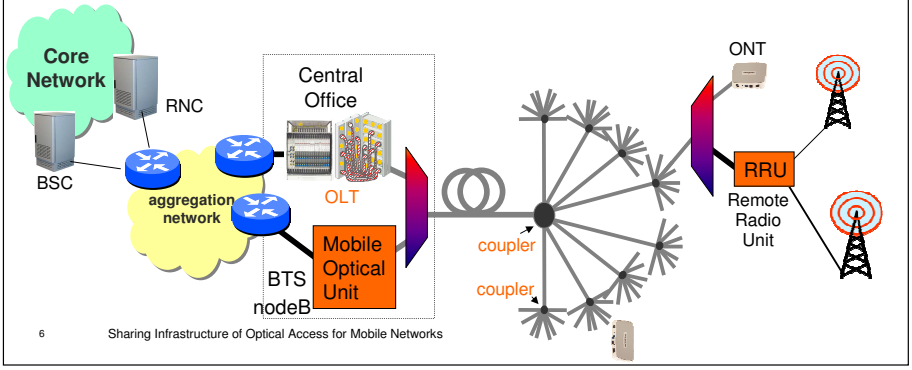

Antenna Remoting using PON
Digital RoF

- the radio signal is digitized
- Link capacity is up to 3Gbps (for LTE) per cell and per RRU
  - Need dedicated wavelength
- All equipment vendors propose base stations with digital RoF interfaces:
  - Integrated equipment to generate/receive the digital signal
  - Standard SFP modules are compliant
  - Transport over Metro Network compatible
- No equipment today capable to transmit over PON type B+
  - Requires pt to pt links → need WDM enabled SFP with adequate budget
  - Requires a dedicated wavelength window in the PON standard
  - But no technical difficulties here.

Antenna Remoting using PON
Digital RoF

- Noise figure independent of fiber length and optical attenuation
- Performance limit depends only on SFP budget
- The chosen SFF budget

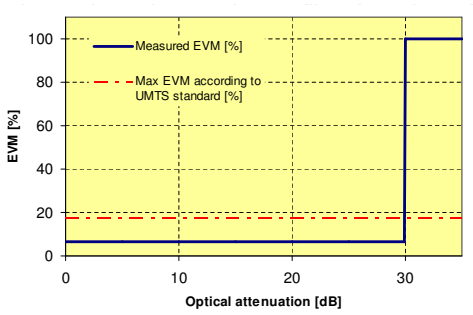

Antenna Remoting using PON
Analog RoF

- The radio signal is transported natively or at an IF over a wavelength
- Stringent Specification on Adjacent Channel Leakage Ratio
  - Need dedicated wavelength
- Some equipment already exist
  - Specific equipment to generate/receive the signal
- No equipment today capable to transmit over PON type B+
  - Requires pt to pt links → need WDM enabled lasers with high linearity
  - Requires a dedicated wavelength window in the PON standard
  - There are some challenges here (see next slide)

Antenna Remoting using PON
Analog RoF -- ACLR

- EVM (Error Vector Magnitude)
  - Well known, is not the issue of the talk…
- ACLR (Adjacent Channel power Leakage Ratio)
  - Power leakage towards neighbour channels (@ +/- 5 & 10 MHz)
  - Warrants not to jam the neighbour channels
    - stringent spec. in the donwlink (figure)

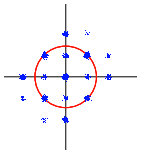

EVM < 17.5%
(QPSK)

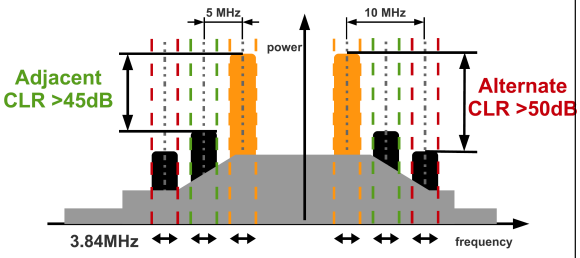

Antenna Remoting using PON
Analog RoF – Required System Architecture

- ACLR driven for downlink
- EVM driven for uplink

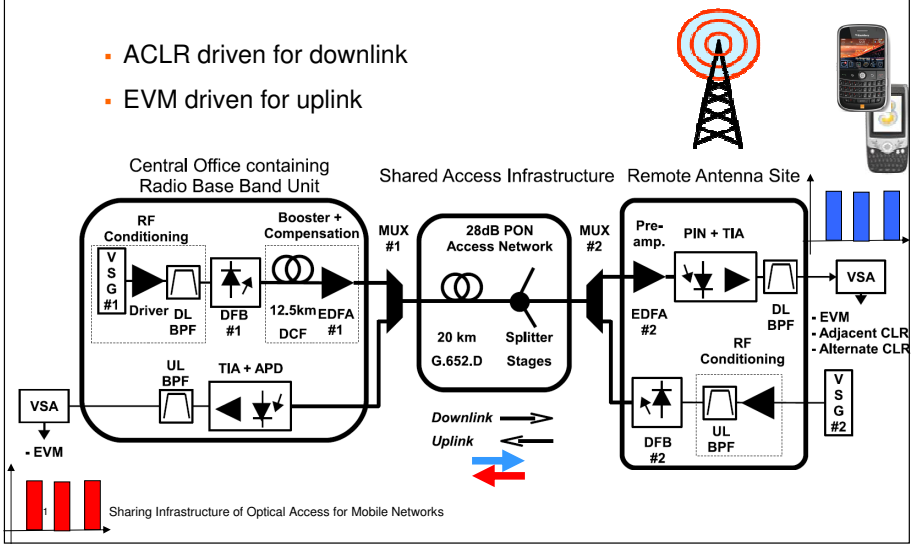

Conclusions
Using PON infrastructures for Mobile Networks?

- The economics are strongly in favor of it:
  - Leverage investments
  - Allow for Mobile Network densification and capacity upgrade
- Backhauling:
  - Already commercially available
  - provides a first – short term – response.
- Antenna remoting:
  - Even larger potential for cost savings
  - Digital: no technical issues
  - Analogue: technical difficulty because of large optical budget

when will optical access infrastructures be ready?

Thank you

This work was supported by the European community in the frame of the ALPHA project

Annex

Mobile Network Context

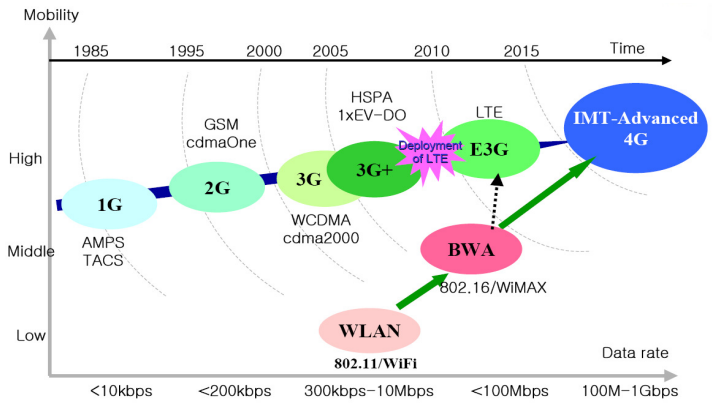

- **GSM**: Global Service for Mobile communications
- **GPRS**: Global Packet Radio Service
- **UMTS**: Universal Mobile Telecommunications System
- **HSPA**: High Speed Packet Access
- **LTE/SAE**: Long Term Evolution/System Architecture Evolution
- **BWA/WiMAX**: Broadband Wireless Access/Worldwide Interoperability for Microwave Access

(Source: H. W. Lee 3GPP2 LTE standardization KRnet 2006)

5 Final downlink architechture

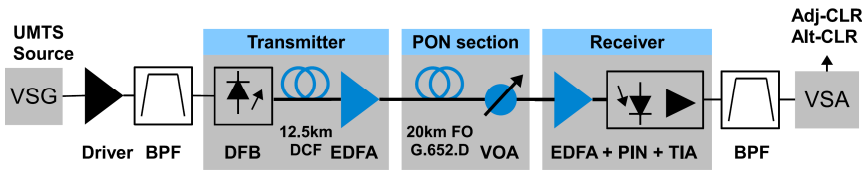

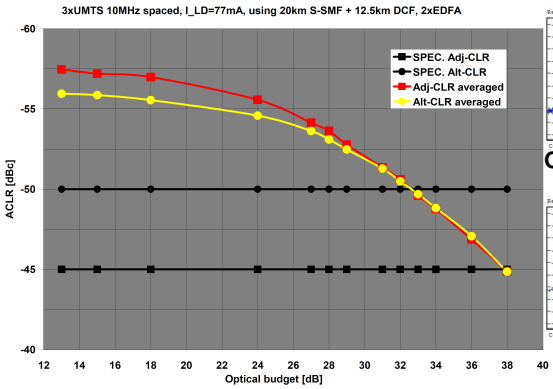

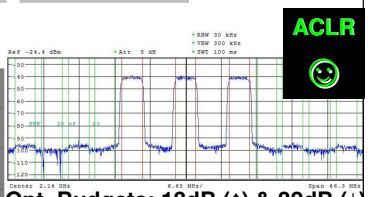

Opt. Budgets: 13dB (↑) & 32dB (↓)

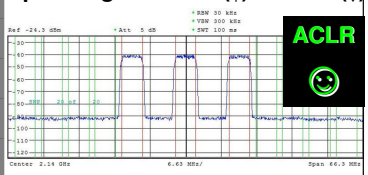

Optical access evolutions and their impact on the metropolitan and home networks

P. Chanclou, Z. Belfqih, B. Charbonnier, T. Duong, F. Frank, N. Genay, M. Huchard, P. Guignard, L. Guillo, B. Landousies, A. Pizzinat, H. Ramanitra, F. Saliou, S. Durel, A. Othmani, P. Urvoas, M. Ouzzif, J. Le Masson
France Telecom Research & Development Division, 2 avenue Pierre Marzin 22307 Lannion, France
philippe.chanclou@orange-ftgroup.com

Abstract : *This paper describes broadband optical access networks evolutions including high speed home interfaces for fixed and mobile services. Technical challenges are also discussed, namely concerning optical extended budget, 10 Gbit/s interfaces as well as the impact of access evolutions on the metropolitan network.*

Introduction

The advantages of employing Passive Optical Network (PON) have been largely recognized. Already standardized G-PONs (Gigabit-capable Passive Optical Networks) are being deployed in many countries since they are a promising technology for cost-effective user-shared system infrastructure. Recent developments in PON technologies offer a solution to operators to increase the splitting ratio or the optical budget dedicated to the reach. These facts enable an access network evolution in the future with an optimum number of central offices with an impact on metropolitan network architectures. Fixed and mobile services could also be merged in the same optical infrastructure in order to optimize systems localization (base station and central office). The low cost of 10Gbit/s interface is also a challenge for the future generation of PON system. Also, if 100Mbits/ or 1Gbit/s interfaces are now feasible for FTTH users, the bottleneck could be the high speed connectivity in home network. In order to deliver such interfaces coming from the access everywhere in the home area, different solutions have been analyzed in terms of easiness and future capability.

Capable architecture evolution of access network

The deployment of an optical budget extension module (G.984.6) [1-3] inside the optical distribution network is one of the attractive solutions to enable the removal of high complexity active devices and reduce the overall access network cost. A first application of budget extension is shown on figure 1. It focuses on the use of extended budget module for a largest customer's eligibility area.

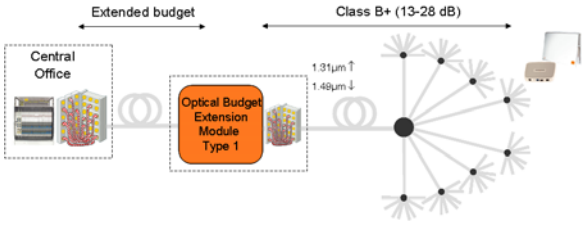

Figure 1: Use of extended budget for a larger eligibility area.

Another scenario (cf. F ig. 2) is to achieve a high efficiency in terms of homes connected per OLT (Optical Line Terminal) PON port. A possible solution, especially for initial roll-out phase, is to improve the PON "filling ratio" by sharing one GPON port between several PON trees but with a maximum of 64 home connected. This scenario is particularly interesting when the take-up rate grows slowly. This scenario offers [4] also a potential reduction of operational works in the optical distribution network because the entire fibre infrastructure is lighted at the initial stage. So we reduce the time for the connection of fitir customer. This solution is shown in figure 2.

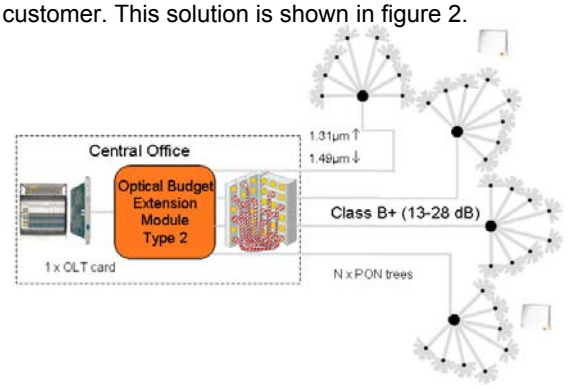

Figure 2: Use of extended budget for increasing splitting ratio.

Of course a solution which can combine both previous benefits could be very useful. Figure 3 shows this scenario in which a remote extender box is used to multiplex "N" PON trees and also to increase the optical reach. In addition, the optical path between the central office and the extender box could be protected. At the central office, the use of time and/or wavelength multiplexer extender module [5] would open a path by multiplexing several G-PON OLT ports. Furthermore this multiplex interface could also be shared between other interface types, as for example point to point Ethernet interfaces dedicated to Digital Subscriber Line Access Multiplexer (DSLAM) collect. This solution would allow to optimize the filling efficiency of OLT ports and to increase the FTTH customer's area eligibility. Optical budget extension modules could be defined as a WDM demarcation device of the future access-metropolitan network of tomorrow.

Authorized licensed use limited to: FRANCE TELECOM. Downloaded on March 31,2010 at 04:20:30 EDT from IEEE Xplore. Restrictions apply.

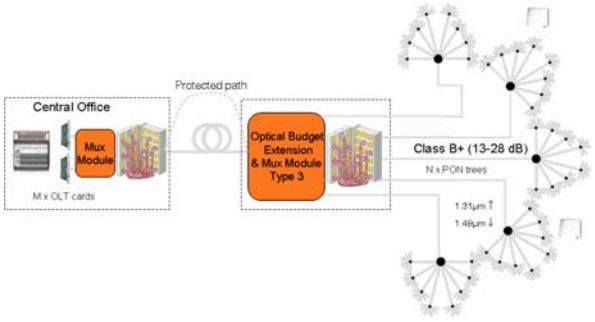

Figure 3: Solution to combine extended budget and multiplexed traffic.

Among different options for offering FTTH, the evolution of solutions to increase the optical budget and to multiplex signals allows a network operator to increase the number of customers accommodated in a GPON system by extending the PON reach, splitting ratio and filling ratio.

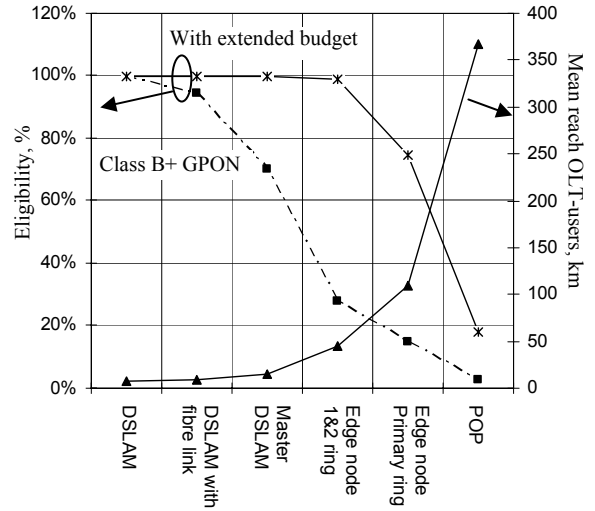

Figure 4: Eligibility and mean reach as a function of the OLT cards localization in the network.

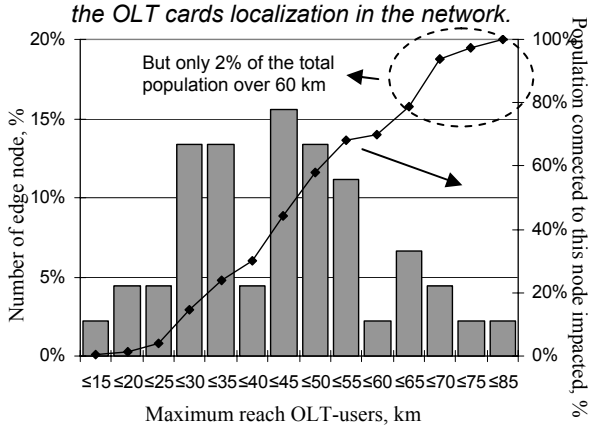

Figure 5: Percentage of OLT sites as a function of maximum reach OLT-users in the case of OLT and edge node co-location.

Central office number optimization

The benefits for operators by adopting solutions providing extended optical budget for GPON can be the reduction of OAM (operation, administration and maintenance) costs and savings due to the OLT location in a reduced number of optical central offices.

We present here, for illustration, some results of an optimization of number of central offices equipped with class B+ GPON OLT required for a roll-out over a large area of 1.4 million mixing high and low population density. Customer's eligibility is a function of the optical budget (with and without extended module) inside the 60km maximum reach. Of course OLT localization has a strong impact on customer's eligibility results. We propose here six scenarios (cf. figure 4) where OLTs are co-localized with DSLAM, DSLAM connected by a fibre link, master DSLAM, metropolitan edge node on the primary and secondary ring, metropolitan edge node on the primary ring only, and POP (Point Of Presence). When extender modules are used, they are sited inside an existing central office. We also illustrated on figure 4 the mean reach between the OLT and the users.

In the particular case where OLT cards are localized only in the metropolitan edge node on the primary and secondary ring, figure 5 presents the evolution of these number of OLT sites (and also percentage of users impacted) as a function of the maximum distance (not the mean) between the node and the user.

Metropolitan and access merger

By increasing the reach of optical access system and by the necessity to ensure service reliability, some metropolitan functionalities will be requested inside extended access network. Typically, a combination of ring and tree could offer superior scalability and low start-up cost with automatic protection path and supervision functions (cf. figure 6). The optical budget extension modules could be passive based on wavelength routing and remote amplification like SARDANA architecture [4] or active based on optical packet switching like ECOFRAME architecture [5].

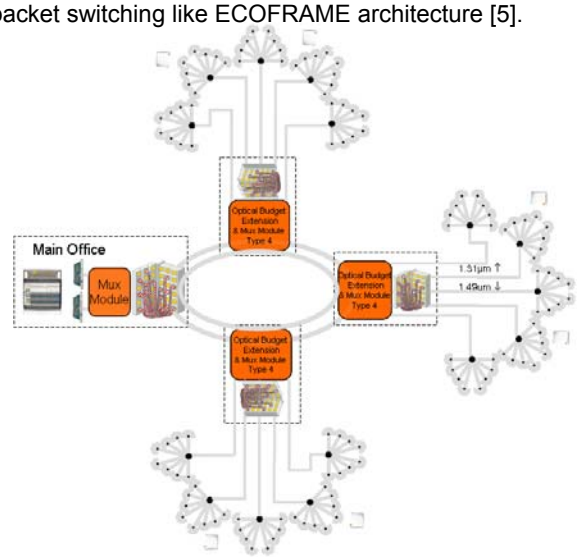

Figure 6: metropolitan and access merger approach.

Authorized licensed use limited to: FRANCE TELECOM. Downloaded on March 31,2010 at 04:20:30 EDT from IEEE Xplore. Restrictions apply.

Convergence of radio and fibre technologies

A new optical fibre infrastructure is deployed for FTTH users. On the other hand, the deployment of radio systems is accelerated due to the explosion of high-speed wireless services, such as 3G mobile phone. An opportunity is present to merge fixed and mobile over a shared fibre network [6]. Three scenarios for sharing fibre infrastructure are discussed hereafter. The backhauling over G-PON traffic is one candidate for transporting traffic between distributed base transceiver station using cell site gateway (CSG) and more centralised nodes like multi aggregation site gateway (MASG) (cf. figure 7-a)). The second scenario, figure 7-b), could be the use by a wavelength overlay of RF signal directly over optical fibre (RoF) between base station and multiple remote radio units. The last scenario (cf. figure 7-c)) could be the use of digital radio over fibre (D-RoF) technology, in which analog radio signals are digitallized. A digital local unit is installed at the basement and is connected to multiple digital remote units using wavelength overlay over the PON infrastructure. The open topics for the future could be the capacity to transmit the D-RoF signal inside the native frame traffic of PON systems and 28 dB optical budget adaptation of RoF systems (cf. ALPHA project [7]).

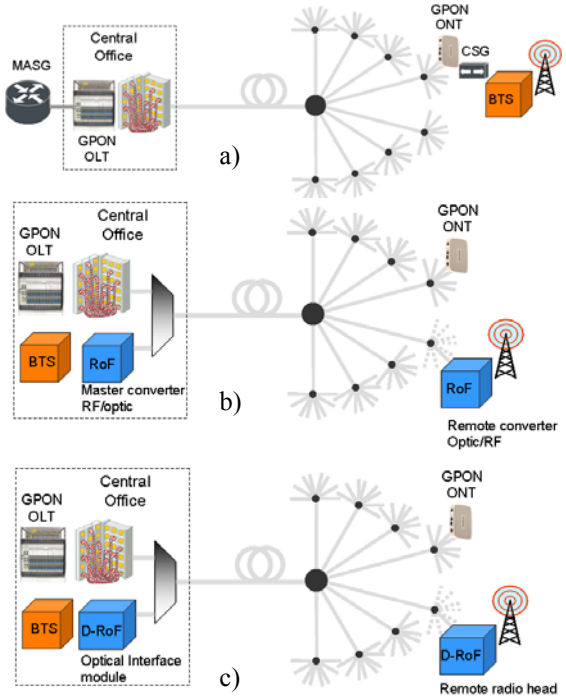

Figure 7: Convergence of radio and fibre technologies

10Gbit/s interfaces for access

If an optical fibre infrastructure based on splitter is deployed for a generation of PON system with 2.5 and 1.25Gbit/s for downstream and upstream respectively, the future generation of system must be compatible with a minimum of CAPEX and OPEX. So next generation system must re-use the optical distribution network and increase the user bandwidth. The low cost and optical infrastructure compatible with 10Gbit/s interface is a challenge for the future generation of PON system.

In order to limit the cost of a solution at 10Gbit/s upstream signal in burst mode, continuous devices must be re-used [8]. Figure 8 illustrates the results obtained by using a photo-receiver stage constituted by APD-TIA photodiode AC coupled to an electrical amplifier and a continuous phase-lock-loop clock recovery at 10.7Gbit/s. We receive burst traffic coming from two directly modulated DFB lasers at 1.3 µm. The burst traffic is acheived by two alternate packets of 4.8 µs with 10.7Gbit/s PRBS sequences at 2^9 and a variable guard time without any optical signal. We also introduce 20 and 60 km of fibre between the receiver and the two lasers. We observe in figure 8 a) and b) the penalty evolution as a function of the guard time and fiber length.

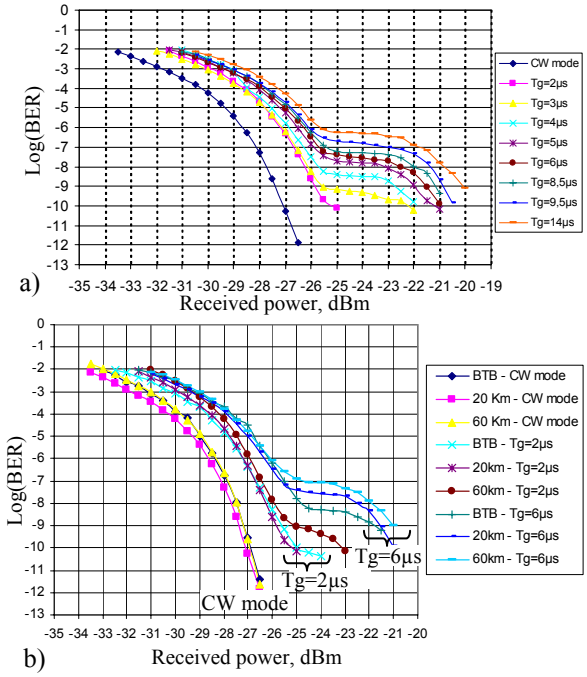

Figure 8: Bit error rate curves of continuous photo–receiver.

Another solution to reduce the cost of 10Gbit/s interface is to re-use 2.5 GHz opto-electronic interface with advanced modulation format [9]. We experimentally demonstrate the feasibility of using Adaptively Modulated Optical OFDM (AMOOFDM) also known as Discrete Multi-tone (DMT) modulation to modulate directly the low bandwidth commercial vertical cavity surface emitting laser (VCSEL) and multimode Fabry-Perot (FP) laser as cost-effective solutions for passive optical network at a high bit rate. Here 10Gbit/s AMOOFDM signal was generated by direct modulation of commercial 2.8 GHz VCSEL, 2.5 GHz multimode FP laser and 2.1 GHz DFB laser at 1550 nm. The receiver used is a 10 GHz avalanche photodiode. Figure 9 illustrates the experimental bit error rate performances of these optical sources.

Authorized licensed use limited to: FRANCE TELECOM. Downloaded on March 31,2010 at 04:20:30 EDT from IEEE Xplore. Restrictions apply.

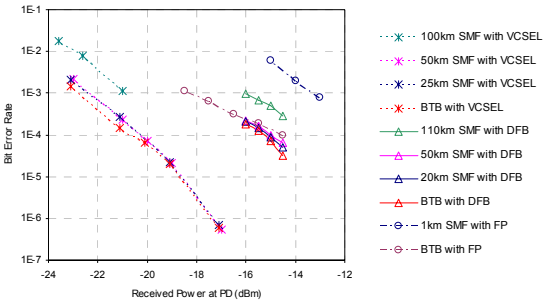

Figure 9: 10Gbit/s transmission performance for direct modulation of VCSEL, FP and DFB lasers

Home networks

In the previous sections we have shown that significant cost reduction will be offered to operators through the deployment of PONs while maintaining the ability to offer Ultra-High Bandwidth connectivity to customers (1Gbit/s). New revenue generating services could be offered/extended/developed to fill the 1Gbit/s pipe to the customer doorway but a pre-requisite is that the end-users have a way to manage, transport and distribute these high speed data flows within their homes into their lounges, home offices and bedrooms. This connectivity media must comply with the requirements of being highly efficient while being easily installable (and even installable by the end-user himself). "No new wire" approaches are being investigated to fulfil these requirements but, if self-installation is achievable, 1Gbit/s guaranteed bandwidth is not yet within reach. The only solution today to guarantee the quality of service for Gbit/s approaching applications is to use Gigabit Ethernet over CAT-5/6 cables. However, then, the self-installation requirement is hard to fulfil as the termination of those cables is not easy to make and the cables must be installed away from power interfering sources. One attractive solution is then to use Step Index Plastic Optical Fibre (SI-POF) whose core diameter (1 mm) is large enough to allow the user to terminate it by simply cutting the end with a sharp knife. An SI-POF cable has only 3 to 4mm of diameter and is very flexible making it ideal for installation in ducts, along a plinth or under a carpet. The data transmission uses visible light which has the added advantage of simplifying the installation and attractiveness of the overall system. Transmission at or around 1Gbps over 50 to 100m of SI-POF has already been demonstrated using a combination of modulation and digital processing techniques [10-12]. We have chosen to use techniques derived from the Power Line Communication and VDSL arena with a combination of Discrete Multi-Tone Modulation and Bit Loading Optimisation algorithm to maximise adaptively the throughput transported in the SI-POF [13]. Using these techniques with a set-up similar to that described in [13] and improved components from Firecomms (650 nm VCSEL and PIN photodiode) we have successfully transmitted 1.5 Gbit/s over 50 m of SI-POF with a BER evaluated to be 1.2×10^{-5} (cf. figure 10). Sampling frequency is set to 1GS/s in the TX side while we used a 2GS/s sampling frequency in the RX side. 1023 independent carriers are used over 500 MHz and, after channel probing, the optimum capacity allocation is found.

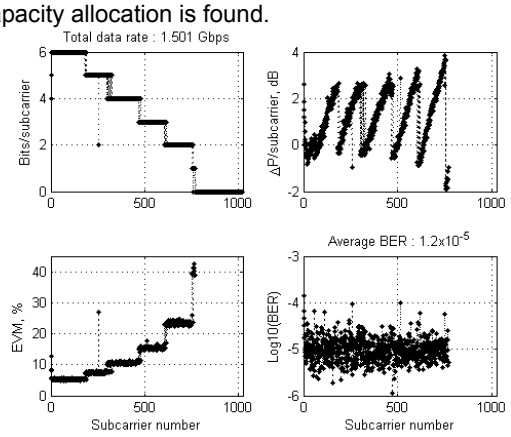

Figure 10: POF transmission results: Optimum bit allocation (top left), power allocation (top right), computed EVM (bottom left) and evaluated BER (bottom right).

Conclusion

We describe a possible evolution of the optical access networks using optical budget extension in order to optimize the number of optical central offices. Convergence of radio and fibre technologies is discussed as well as the evolution of 10Gbit/s optical access interfaces. We also focus this paper on the feasibility of delivering 1 Gbit/s inside the home network over SI-POF with 1 mm core diameter.

Acknowledgments

This work was supported by the EU FP7 ICT SARDANA, POF-PLUS and ALPHA projects. It is also carried out partly in the ANR framework of the AROME, ANTARES, ECOFRAME and INTERACCES projects of the Media&Networks cluster. The authors would also like to thanks B. Capelle, S. del Burgo, M.F. Colinas, J.P. Lanquetin, G. Yvanoff, P. Herbelin, F. Herviou, G. Ivanoff, L. Salaun, R. Crepy, and M.L. De La Rupelle for discussions.

References

1. K.-I. Suzuki et al., OFC 2008, OThL3
2. D. Nesset et al., ECOC 2007, PD3.5
3. N. Suzuki et al., ECOC 2005, Tu1.3.3
4. J. Lazaro et al, OFC2008, OthL2, 2008
5. D. Chiaroni et al, Photonic in Switching 2007
6. M. Suzuki, ECOC2007, 10.6.1., 2007
7. M. Popov, NOC2008
8. Z. Belfqih et al., NOC2008
9. T. Duong et al., ECOC2008, WE.1.F4, 2008
10. S. Randel et al, ECOC2007, Tu5.1.1
11. F. Breyer et al, ECOC2007, Th9.6.6
12. S.C.J Lee et al, OFC2008, OWB3
13. B. Charbonnier et al, ECOC2008, We3.F.5

Authorized licensed use limited to: FRANCE TELECOM. Downloaded on March 31,2010 at 04:20:30 EDT from IEEE Xplore. Restrictions apply.